Supramolecular electrochemistry using cucurbituril-based complexes for analytical and sensing applications

by

Jia Liu
[redacted]

A thesis submitted in fulfilment for the degree of Doctor of Philosophy at University College London (UCL)

June 2023

Declaration

I, Jia Liu, declare that the research displayed in this thesis is my own work. Results obtained by other sources are clearly introduced in acknowledgement.

Abstract

Supramolecular electrochemistry, especially the cucurbit[*n*]uril-based (CB*n*, *n* = 5-8, 10) electrochemistry, has sparked extensive research interests for the combining advantages of complexation-induced unique properties of guest molecules, outstanding features of rigid macrocyclic CB*n* host as well as rich thermodynamic and kinetic information provided by electrochemical techniques. CB*n* perform pronounced binding ability towards a wide range of molecules, giving rise to substantial application potentials, such as reactivity modulation and sensing. Quantitative analysis of binding behaviours between CB*n* and guest molecules can effectively offer instructive guidance to design the host-guest systems better catering for the ending applications, thus being of great interests and importance in supramolecular chemistry area.

Herein, this research started from the investigation of the complexation events between CB7/CB8 host and redox active resazurin (RZ). Interestingly, it has been discovered that the electrochemical activity of RZ can be oppositely modulated upon the complexation with CB7 and CB8, manifesting the effect of the host-guest encapsulation tightness on the reaction activity. In addition to the research regarding reactivity modulation caused by CB*n* complexation, we also explored quantitative analysis for binding behaviours by proposing a rapid and simple electrochemical approach for rapidly estimating binding constants of CB8-methyl viologen (CB8-MV^{2+})-based ternary complexes by uncovering the correlation between their electrochemical characteristics and binding constants. This electrochemical scheme has overcome the shortcomings, such as long experimental period, complicated data analysis, expensive instrument, limited applicability to sparsely soluble guests, *etc*, presented by conventional supramolecular titration methodologies. Furthermore, it is notable that we extended the binding constant estimation applicability boundary from simple buffer solution to complex bio-media, ranging from synthetic urine (SU), human serum (HS), fetal bovine serum (FBS) to animal blood of sheep blood (SB) and horse blood (HB), with the aid of simple CB8-MV^{2+} assay via electrochemical titration measurements. Other than quantitative analysis, the application potentials for supramolecular-based electrochemical sensing have also been explored. A dual-functional assay that can work as either associative binding assay (ABA) or the indicator displacement assay (IDA) was established by employing CB8-MV^{2+} molecular platform, in which the redox active MV^{2+} worked as a sensitive electrochemical reporter. Moreover, included but not limited to simple biologically relevant buffer solution, CB8-MV^{2+} also presented sensing ability for biomolecules, which are of diverse binding affinities and structural conformation in complex bio-media (*e.g.* SU, HS, FBS, SB and HB), with decent sensing properties, *i.e.* down to 10^{-8} M of minimum detectable concentration (MDC) and linear detection range located within physiologically relevant micromolar range. In a nutshell, this research has explored the analytical and sensing applications of CB*n*-based electrochemistry, which is readily to be extended for other applications based on different supramolecular systems.

Impact statement

The modulation of reaction activity upon complexation appeared to be highly attractive in catalysis, analytical chemistry, and synthetic chemistry recently. This research has studied the modulation effect of CB7 and CB8 towards the reaction activity of redox-active resazurin (denoted as $[RZ\text{-}H]^-$ at pH 7) by electrochemistry. It is novel to note that CB7 and CB8 demonstrated opposite modulation effect on the electrochemical reactivity of $[RZ\text{-}H]^-$ in its irreversible reduction process. The opposite modulation of CB7 and CB8 could be presumably due to the different ease of water molecules approaching the reaction centre on RZ resulted from different encapsulation tightness. The observed converse modulation effect of CB*n* is expected to extend to study other redox processes where photo transfer steps are coupled with electron transfer steps, widening the range of investigation on supramolecular modulation.

Binding constants are considered as an important quantitative indicator to offer insights into the molecular interactions between host and guest molecules in supramolecular chemistry. Current methodologies in the estimation of the binding constants of host-guest complexes suffer from a range of inherent limitations such as the expensive instrument, certain solubility of host/guest molecules, long experimental period and complicated data analysis process, and moreover, it is still highly challenging to achieve measurements in biologically most relevant media like serum and blood. This research has first-time proposed a rapid and simple electrochemical scheme for the estimation of binding constants by uncovering a linear correlation between the reduction potential shifts and the isothermal calorimetry (ITC)-measured binding constants of CB8-MV^{2+}-based ternary complexes, allowing for the estimation of binding constants with one-point electrochemical measurement in high-throughput fashion. More surprisingly, this research has enabled binding constant estimation in complex bio-media with the aid of CB8-MV^{2+} assay via electrochemical titration procedures, offering insights into the host-guest interactions in bio-media for in-situ biological research based on supramolecular systems.

Detection for small biologically relevant molecules has attracted and continuously attracted widespread attention. An electrochemical dual-functional sensing assay has been designed based on the self-assembly of CB8 and commercially available MV^{2+} at a low synthetic effort. Particularly, CB8-MV^{2+} can work in two formats, *e.g.* (1) associative binding assay (ABA) and (2) indicator displacement assay (IDA), by taking advantage of environmental sensitive and redox active MV^{2+} and spacious CB8. Gratifying to see that down to 10^{-8} M minimum detectable concentration together with linear detection range in physiologically relevant micromolar range have been achieved by CB8-MV^{2+} assay in diverse complex bio-media (*e.g.* SU, HS, FBS, SB and HB), which is of promising meanings for sensing real samples in practical applications.

Acknowledgements

All works presented here would have not been achieved without the massive support, knowledgeable guidance, powerful encouragement and kindest patience from my principal supervisor, Dr. Tung Chun (John) Lee. I would like to express my incredible appreciation to him. What he has taught me is not limited within the academic research but also extend to the life philosophy. He has shown me how to behave a scientist and a man by kindly treating people, effectively communicating, logically managing daily schedule, and taking family responsibilities. I also would like to gratefully acknowledge my second supervisor, Prof. Ivan Parkin, for his supportive resources. I very much appreciate Prof. Yiming Xie for his generous supports in resources and research guidance during my interruption year in China. Without his support, it would not be possible for me to make use of the interruption period to obtain results.

I also would like to express my gratitude to my research mate in research groups of Dr. Tung Chun (John) Lee and Prof. Yiming Xie for their kind help, specifically, Mr. Alvaro Castillo Bonillo for the synthesis of cucurbit[n]uril products, Dr. Hugues Lambert for the computational simulations, Ms Tabitha Jones for the transmission electron microscopy (TEM) characterization, Dr. Suresh Moorthy for useful advice about the lab general issues.

I wish to express my deepest and heartful gratitude to my family, especially my parents, for their generous financial support, love and care that accompanied me to go through all the downtime during my PhD.

Last, but not least, I also appreciate all the supports from University College London (UCL).

Table of contents

List of publications

1. **Jia Liu**, Hugues Lambert, Yong-Wei Zhang, and Tung-Chun Lee. Rapid estimation of binding constants for cucurbit[8]uril ternary complexes using electrochemistry. *Anal. Chem.*, **2021**, *93*, 4223–4230. (Cover article) ***Chapter 4***
2. **Jia Liu**, Suhang He, Hugues Lambert, Yi-Ming Xie, Tung-Chun Lee. Modulation of electrochemical activity of resazurin by controlling the tightness of host-guest encapsulation in aqueous media (in submission) ***Chapter 3***
3. **Jia Liu**, Tung-Chun Lee. Dual-functional electrochemical biosensing assay using cucurbit[8]uril-methyl viologen host-guest complexes for drug detection in complex bio-media. (in preparation) ***Chapter 5***
4. Weng-I Katherine Chio, **Jia Liu**, Tabitha Jones, Jayakumar Perumal, Dinish U. S., Ivan P. Parkin, Malini Olivo, and Tung-Chun Lee. SERS multiplexing of methylxanthine drug isomers via host-guest size matching and machine learning. *J. Mater. Chem. C*, **2021**, *9*, 12624–12632.
5. Jiaqing Cui, **Jia Liu**, Xing Chen, Jiashen Meng, Shanyue Wei, Tao Wu, Yan Wang, Yiming Xie, Canzhong Lu, and Xingcai Zhang. Ganoderma Lucidum-derived erythrocyte-like sustainable materials. *Carbon*, **2022**, *196*, 70-77.
6. Mingyue Liao, **Jia Liu**, Tao Zuo, Lingyi Meng, Yuqian Yang, Jihuai Wu, Canzhong Lu, Wehai Sun, and Yiming Xie. Defect Passivation through Cyclohexylethylamine Post-treatment for High-Performance and Stable Perovskite Solar Cells. *ACS Appl. Energy Mater.*, **2021**, *4*, 12848-12857.
7. Gemma Davison, Tabitha Jones, **Jia Liu**, Juhwan Kim, Yidan Yin, Doeun Kim, Weng-I Katherine Chio, Ivan P. Parkin, Hyeon-Ho Jeong, Tung-Chun Lee. Computer-Aided Design and Analysis of Spectrally Aligned Hybrid Plasmonic Nanojunctions for SERS Detection of Nucleobases. *Adv. Mater. Technol.* **2023**, 1150, 335-339.
8. Weng-I Katherine Chio, Gemma Davison, Tabitha Jones, **Jia Liu**, Ivan P. Parkin, and Tung-Chun Lee. Quantitative SERS detection of uric acid via formation of precise plasmonic nanojunctions within aggregates of gold nanoparticles and cucurbit[*n*]uril. *J. Vis. Exp.*, **2020**, *164*, DOI: 10.3791/61682.

List of abbreviations

1,3-CHD	1,3-cyclohexadiene
1,4-CHD	1,4-cyclohexadiene
2NP	2-naphthol
ABAs	Associative binding assays
AC	Acridine hydrochloride
ADA	1-adamaintylamine
BR	Britton-Robinson
CB*n*	Cucurbit[*n*]uril
CBs	Cucurbit[*n*]urils
CDs	Cyclodextrins
CE	Counter electrode
CEs	Crown ethers
CEP	Capillary electrophoresis
CHA	Cyclohexane
CHE	Cyclohexene
CXs	Calixarenes
CV	Cyclic voltammetry
DBAs	Direct binding assays
DFT	Density functional theory
DHRS	Dihydro-resorufin
DOSY	Diffusion-ordered spectroscopy
$E_{p,a}$	Anodic peak potential
$E_{p,c}$	Cathodic peak potential
$E_{p/2}$	Half-wave potential
ΔE_p	Peak-to-peak potential splitting

E^0	Standard potential
E_{switch}	Switch potential
E_{sw}	Stair step height
E_{step}	Step size of staircase
ELISA	Enzyme-linked immunosorbent assay
ESI-MS	Electrospray ionization-mass spectroscopy
EXSY	Exchange spectroscopy
FBS	Fetal bovine serum
FIA	Flow-injection analysis
FRET	Fluorescent resonance energy transfer
G1	First guest
G2	Second guest
GS-MS	Gas chromatography-mass spectrometry
HB	Horse blood
HPLC	High-performance liquid chromatography
HPLC-MS	High performance liquid chromatography-mass spectrometry
HS	Human serum
^{1}H NMR	Proton nuclear magnetic resonance
IDAs	Indicator-displacement assays
$I_{p,a}$	Anodic current
$I_{p,c}$	Cathodic current
I_{switch}	Switching current
ITC	Isothermal calorimetry
K	Binding constant
K_{G2}	Binding constant of ternary complex
LoD	Limit of detection

MBBI	Tetramethyl benzobis(imidazolium)
MDAP	2,7-dimethyldiazapyreninum
MDC	Minimum detectable concentration
MDPP	Methylated diazaperoperylenium
MDPT	2,7-dimethyldiazaphenanthrenium
MEM	Memantine hydrochloride
MV^{2+}	Methyl viologen
$MV^{+\bullet}$	Methyl viologen radical
PB	Sodium phosphate buffer
PC	Procaine hydrochloride
PCR	Polymerase chain reaction
PCG	Penicillin G Na
PDDA	Poly(diallyl dimethyl ammonium chloride
POCT	Point-of-care testing
QCM	Quartz crystal microbalance
RE	Reference electrode
RGO	Reduced graphene oxide
RMD	Rimantadine
RS	Resorufin
$[RS-H]^-$	Deprotonated resorufin
RTM	Rivastigmine
$[RZ-H]^-$	Deprotonated resazurin
RZ	Resazurin
SAM	Self-assembled monolayer
SB	Sheep blood
SCE	Saturated calomel electrode

SERS	Surface-enhanced Raman sattering
SIA	Sequential injection analysis
SPR	Surface plasmon resonance
SU	Synthetic urine
SWV	Square wave voltammetry
TR	Tacrine
TYP	Tryptophan
τ	Time for one square wave cycle
UV-vis	Ultraviolet–visible
ΔV	Reduction potential shift
vDW	Van der Wales
WE	Working electrode

List of figures

List of tables

Chapter 1. Introduction and literature review

This Chapter firstly described the motivations of the research and introduced the fundamental working principles of typical electrochemical techniques. Additionally, this Chapter also reviewed the history and current development of a series relevant areas. In the latter part, research objectives and the structure of the thesis were demonstrated.

1.1 Supramolecular hosts

Host molecules with confined cavities have capability of accommodating small guest molecules upon interacting with them via strong covalent bonding or weak non-covalent interactions, such as electrostatic interactions, intermolecular forces and hydrogen bonding. Among a wide range of reported host molecules, supramolecular hosts are macrocyclic hosts, which mainly interact with the guest molecules by non-covalent intermolecular forces. The most popular supramolecular hosts include crown ethers (CEs), calixarenes (CXs), cyclodextrins (CDs) and cucurbit[*n*]urils (CBs).

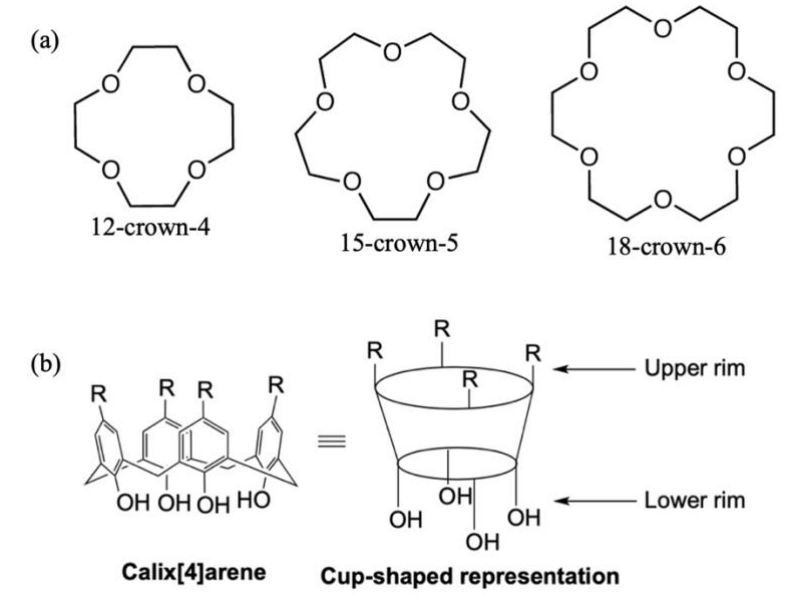

Fig. 1.1 (a) Structures of 12-crown-4, 15-crown-5 and 18-crown-6 [1]. Copyright 1978 Nature Publishing Group. (**b**) Structure of cup-shaped calix[4]arene [2]. Copyright 2000 Royal Society of Chemistry.

Crown ethers (CEs) are an early generation of cyclic hosts, whose discovery and synthesis history can date back to 1967 [3]. CEs consist of repetitive ether units, and the term of 'crown' describes the resembled structure of the complexes formed between CEs and cations. **Fig.1.1a** [1] displays the structures of several typical CEs. The first number in the names of CEs refers to how many atoms located on the ring and the second number in their names specifically refers to the number of oxygen atoms. CEs have capability of forming strong complexes with certain cations by the formation of coordinate bond or hydrogen bond between the oxygen atoms located at the interior of the ring and the cations situated in the inner cavity of CEs. The formed complexes between CEs and cations are amphiphilic [4], *i.e.* the inner section of the complex is hydrophilic while the outer part is hydrophobic, allowing them to serve as catalysts in phase-transfer chemical reactions [5]. Although CEs can be applied for drug delivery after reducing their inherent toxicity [6], further application in biological filed of CEs is still greatly limited by their toxicity [7]. Thus, other macrocyclic hosts candidates that are biological benign present considerably attractive to be explored.

Calixarenes (CXs) are cup-shaped macrocycle compounds that were discovered in the early 1970s. CXs are composed of methylene-bridged phenols with π-basic hydrophobic cavities. **Fig. 1.1b** shows the structure and cup-shaped conformation of calix[4]arene, a typical calixarene derivative, where the number '4' refers to four repetitive units in its ring [8]. Taking advantage of the well-defined hydrophobic cavity, CXs are able to encapsulate a wide range of small guest molecules as host-guest complexes via non-covalent interactions such as π-π and CH-π stacking interactions [2]. Additionally, it is novel to note that the cavity size of CXs is adjustable and the upper and lower rims of CXs are ready to be functionalized by different substituents. As a result, a massive range of CXs derivatives have been designed to form a variety of supramolecular complexes [9] for diverse application purposes including cation recognition [10], cancer chemotherapy [11], fluorescent sensing probes [12], *etc*. However, although CXs are less toxic compared to CEs, one disadvantageous point of CXs needs to be mentioned is that they are practically insoluble in water, making it unpopular in applications in which biological relevant buffer environments are involved. Hence, there is still left space for the discovery and synthesis of other supramolecular hosts with more desired characteristics.

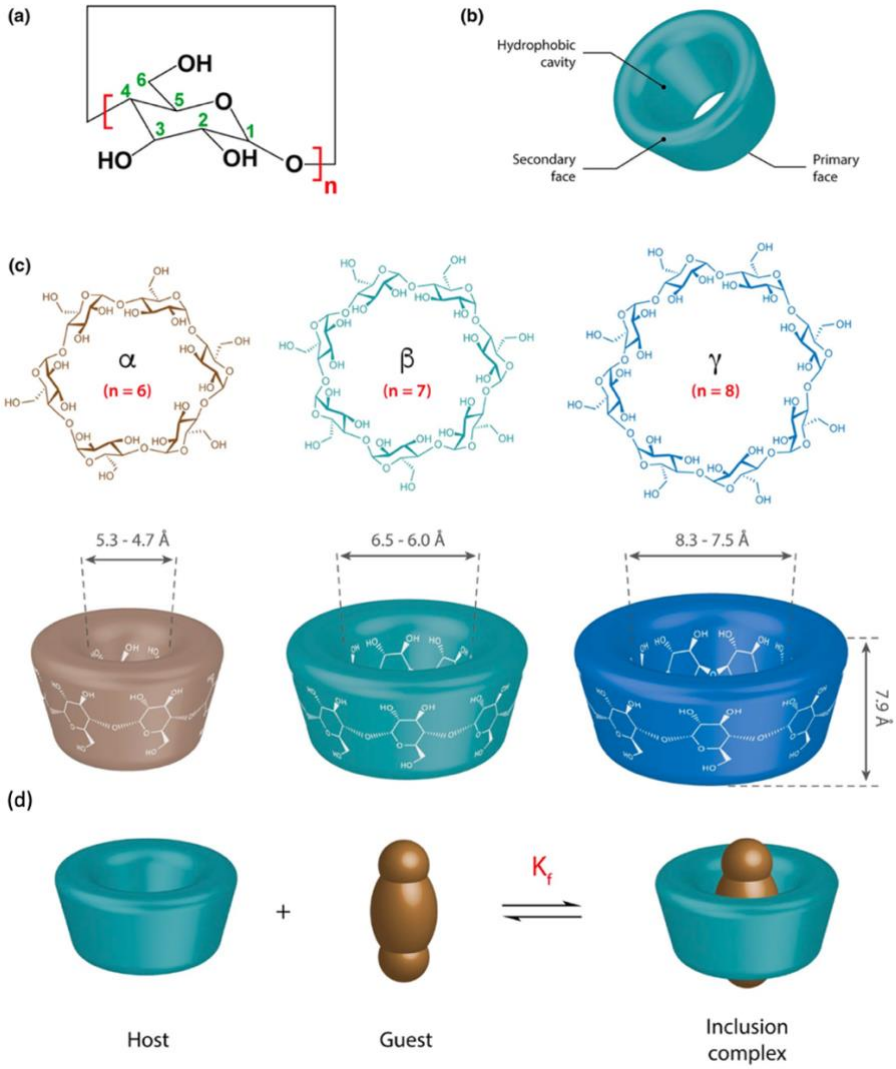

Fig. 1.2 (a) Chemical formula and **(b)** schematic structure of CDs. **(c)** Chemical structure and dimensions of α CD, β CD, and γ CD. **(d)** Schematic representation of the host-guest complexation process between CDs and guest molecules [13]. Copyright 2018 Springer Verlag.

Cyclodextrins (CDs) are a family of synthetic cage supramolecules produced from the enzymatic degradation of starch, one of the most crucial polysaccharides in the world, and it has more than 100 years of history [14]. The truncated-cone-shaped hydrophobic cavity of CDs are composed of several covalently linked glucose units, *i.e.* α-(1,4) linked glucopyranose units, and the cavity shape of CDs is maintained via the hydrogen bonding formed between the hydroxyl groups of neighbouring unites located at the larger rim of the cavity [13]. The cavity of CDs is hydrophobic, with C-H bonds pointing towards the inner cavity. Meanwhile, the outer part of CDs is hydrophilic with the presence of hydroxyl groups, rendering CDs certain water solubilities. According to the number of glucose units included in CDs, they are classified as αCD, βCD and γCD corresponding to six, seven and eight glucose units, respectively (**Fig. 1.2**). The cavity diameter and volume of αCD, βCD and γCD increases sequentially while the cage height of them is identical [15]. Among three homologues of CDs, βCD is the one that has been investigated most extensively due to its most outstanding capability of the formation of inclusion complexes with a substantial range of guest molecules via host-guest interactions. Upon host-guest complexation between CDs and guest molecules (**Fig. 1.2d**), the chemical and physical properties of guest molecules can be modified and thus provide diverse application possibilities. The cytotoxicity of CDs is negligible, attributing their applicability in biological and pharmaceuticals fields. A great deal of research has been directed in the wide range of applications of CDs, including drug delivery [16], molecular recognition [17], food industry [18], environment protection [19], *etc.*

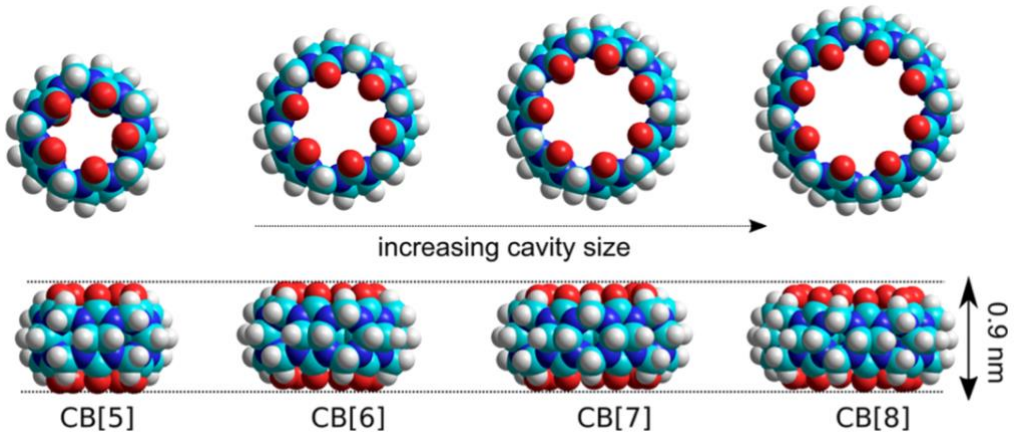

Fig. 1.3 Molecular models of CB*n* (*n* = 5, 6, 7, 8) [20]. Copyright 2018 American Chemical Society.

Cucurbiturils (CBs) are an emerging young generation of synthetic macrocyclic hosts that are attracting particularly widespread attention in the field of supramolecular chemistry. CBs are made up of glycoluril units bridged by methylene, which results in a well-defined, rigid and highly symmetric hydrophobic cavity as well as two identical electronegative carbonyl-lined portals. According to the number of glycoluril units, CBs are named as cucurbit[*n*]uril (CB*n*), where *n* = 5, 6, 7, 8, and 10. Like CDs, the cavity diameter of CBs increases sequentially as the number of glycoluril member while the height keeps unchanged as 0.9 nm (**Fig. 1.3**) [20]. CBs stands out among classic macrocyclic hosts of CEs, CXs and CDs by taking advantages of the unique properties of biological benign nature, ability to form host-guest complexes with stronger binding affinities, higher selectivity as well as specificity towards the shape and charge of guest molecules [21]. Detail discusssion about the fundamental properties and the host-guest chemistry of CB*n* can be found in the *Chapter 1.4* and *1.5*. With unique features of CBs, CBs display manifold application potentials, such as molecular recognition, surface-enhanced Raman spectroscopy (SERS)-based sensing, molecular

machines and switches, supramolecular catalysis, drug delivery, environmental and analytical chemistry, *etc* [22-25].

1.2 History and synthesis of CBs

A white and amorphous condensation product of glycoluril and formaldehyde was obtained in concentrated hydrochloric acid solution by Behrend's group in 1905, which is a very first predecessor of CBs and known as Behrend polymer [26]. Until 1981, the constitution of this condensation product was characterized by Mock *et al* when they revisited Behrend's experiments and reports [27]. Mock and co-workers successfully crystalized a hydrated macrocycle consisting of six glycoluril units and twelve methylene bridges, which was named as CB6 due to the resemblance between its structure and the pumpkin, and the number '6' refers to the number of glucoluril units contained in the compound [27-29]. Indeed, the obtained CB6 by Mock *et al* in this work was not pure and was a mixture of other CB analogues, and the isolation and X-ray characterization of CB*n* homologues (CB5, CB7 and CB8) were achieved until 2000 by Kim and co-workers [30]. Within the following 2 years, Day *et al* identified the interlocked complex of CB5⊂CB10 [31], paving for the presence of CB5 and CB10. With the presence of CB5, CB7 and CB8 in addition of CB6 at the beginning of new millennium, research interests regarding CB*n* chemistry grew up at a remarkable rate, which is witnessed by numerous articles and reviews were published over the decade past 2000 [32], indicating that CB*n* is a new generation of research focus in supramolecular chemistry after CXs.

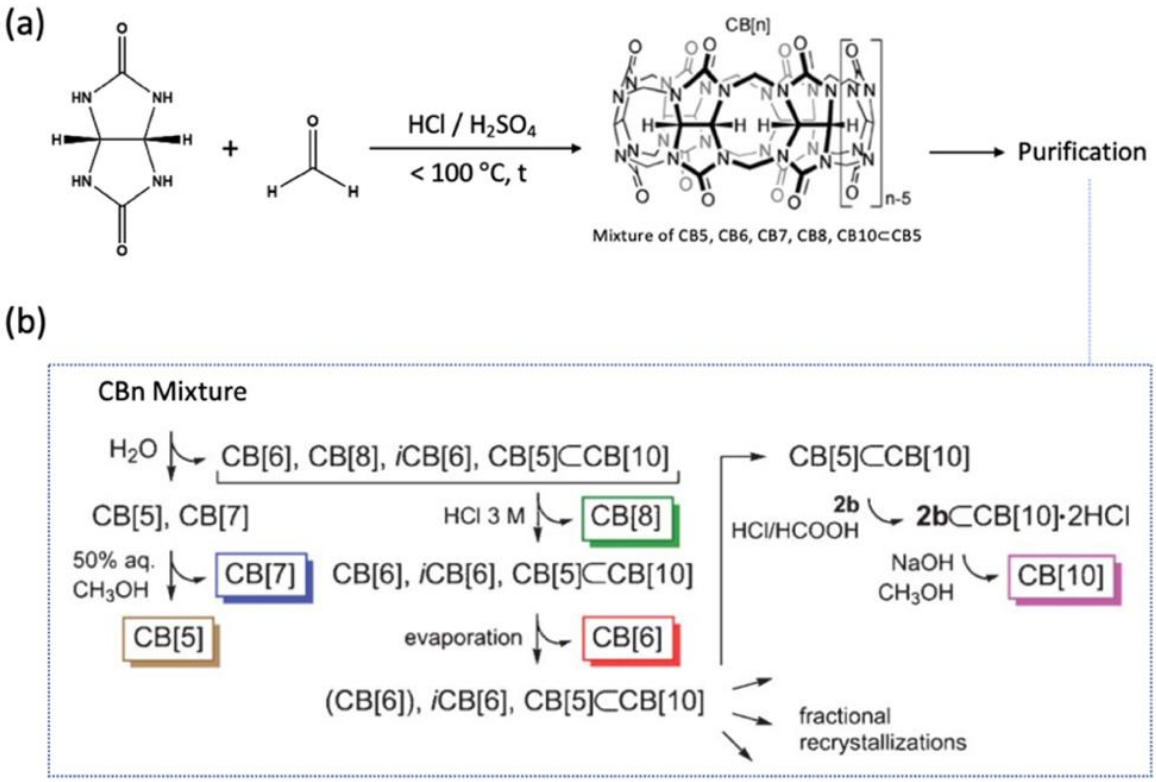

Fig. 1.4 (a) Synthesis and **(b)** general purification procedures of CB*n* mixture, where 2b is 1,12-dodecanediamine. Reproduced with the permission from ref. [32] and ref. [33]. Copyright 2009, 2012 Royal Society of Chemistry.

The precise fabrication protocol, isolation strategy as well as the reaction mechanism of CB*n* were thoroughly investigated by Isaacs and co-workers [33-35]. The general fabrication

of CB*n* mixtures starts from the reaction between glycoluril and formaldehyde in concentrated acidic condition as illustrated in **Fig. 1.4a** [33]. CB*n* (*n* = 5-8) mixture can be obtained by evaporation and precipitation in water and methanol after heating the solution up to 80-100 °C during10-100 hours; CB6 is the major constituent of the obtained CB*n* mixture, and there are still trace amount of CB5⊂CB10, inverted CB6 (*i*CB6) and other oligomers. To isolate CB*n* mixture into pure CB6, CB7 and CB8, the CB*n* mixture can be purified following procedures proposed by Isaacs *et al* [35], which is mainly based on the differential solubility of each component in water, water/methanol, and diluted HCl as displayed in **Fig. 1.4b**. In detail, CB5 and CB7 can be isolated from the raw CB*n* mixture by dissolving the raw CB*n* mixture in water and 50% methanol solution sequentially. The precipitate content of the aqueous solution of raw CB*n* mixture after centrifuging is the mixture of CB6, CB8, *i*CB6 and CB5⊂CB10, from which CB8 can be purified from the mixture with 3M of HCl. CB6 can be then obtained via the evaporation of the left mixture. CB5 and CB10 can be obtained by displacing the CB5 from CB5⊂CB10 via the competitive binding of the commercially available 1,12-diaminododecane at acidic condition and the left 1,12-diaminododecane can be removed via washing with NaOH/methanol solution [32,33,36].

1.3 Basic properties of CBs

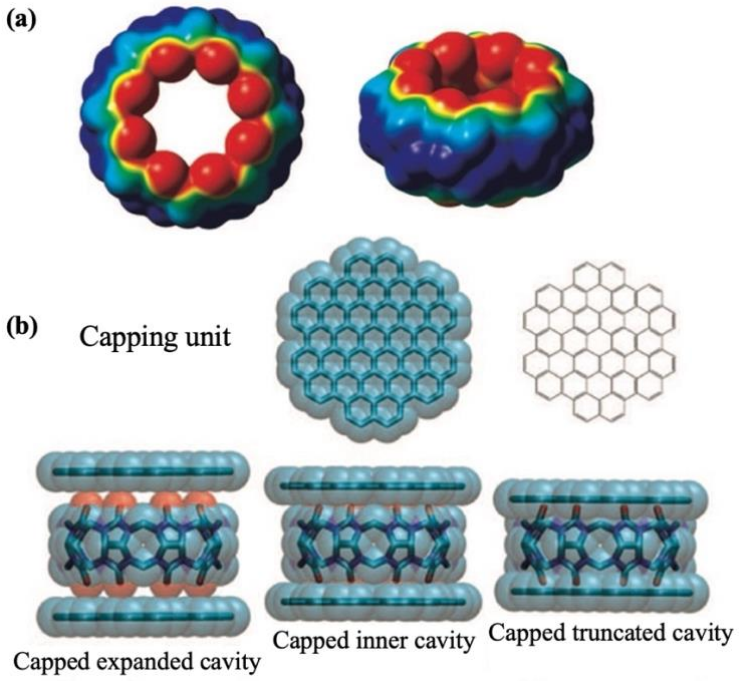

Fig. 1.5 (a) Electrostatic potential map (top and side view) of CB8 [21]. The red zone represents the electron-rich region, and the blue zone represents electron-deficient region. Copyright 2011 Wiley-VCH. **(b)** Three different types of CB*n* cavities with two identical graphene-like capping [21]. Copyright 2011 Wiley-VCH.

CB*n* (*n* = 5-8, 10) are a family of rigid macrocycles consisting of n glycoluril units. Two identical rims of CB*n* are carbonyl lined and electronegatively charged, which are visualized by the electrostatic potential map obtained by the Nau group [21]. As shown in **Fig. 1.5a**, the electron density of CB*n* portals is rich in the presence of carbonyl oxygens, rationalizing the outstanding performance of CB*n* as cation receptors; on the other hand, the electron density on the equatorial phase of CB*n* are deficient because neither lone electron pairs nor bonds point towards the inside cavity of CB*n*. The electron density of the interior cavity

bears little information for the hydrophobic cavity of CB*n*. The effective hydrophobicity of CB*n* cavity is determined by the polarity, which was estimated by several polarity-sensitive probes [37]. It was found that the inner cavity of CB*n* is less polar than water, indicating that the inner cavity of CB*n* is hydrophobic in essence.

All CB*n* homologues have identical height of 9.1 Å, while their cavity diameter, portal diameter and outer diameter increase along the homologous CB*n* family [21,33]. The exact values of these structural parameters for CB*n* (*n* = 5-8, 10) are displayed in **Table 1.1**. The portal diameter of *CBn* is smaller than its cavity diameter, rendering it strict size selectivity towards guest molecules. The cavity volume of CB*n* were computationally calculated by introducing two identical blocking lids to 'seal' the open portal of CB*n* in computed models, and according to different degrees of capping, three different types of cavity volume, *e.g.* expanded cavity, truncated cavity and inner cavity, were estimated for each CB*n* (**Fig. 1.5b**, **Table. 1.2**). Comparing three types of computed cavity volume of CB*n* with X-ray and crystallographic data, the most useful value to determine the effective cavity space for binding interactions is the inner cavity value. It is worth noting that the inner cavity volume of CB6, CB7 and CB8 are comparable to that of αCD, βCD and γCD, respectively, while the binding features of CDs are distinct from CBs. Interestingly, the water solubility of CB*n* is fairly desire; specially, the solubility of CB*n* with odd number of glycoluril unit (CB5, CB7) have better water solubility, *i.e.* 20-30 mM, than CB*n* which have even number of glycoluril unit (CB6, CB8 and CB10) [31].

Table 1.1 Structural parameters of CB*n* (*n* = 5-8, 10) [30,33]. Copyright 2000 American Chemical Society, 2009 Royal Society of Chemistry.

Parameters (Å)	CB5	CB6	CB7	CB8	CB10
Cavity diameter	4.4	5.8	7.3	8.8	11.3-12.4
Portal diameter	2.4	3.9	5.4	6.9	9.5-10.6
Outer diameter	13.1	14.4	16.0	17.5	20.0
Height			9.1		

Table 1.2 Estimated cavity volumes of CB*n* (*n*=5-8, 10) [21]. Copyright 2011 Wiley-VCH.

	Estimated cavity volume (Å^3)		
Cavity type	Expanded	Truncated	Inner
CB5	81	51	68
CB6	164	93	142
CB7	282	158	242
CB8	479	263	367
CB10	901	494	691

Cavity volumes of CB*n* cannot completely reveal their effective binding capacities because it is preferable to leave a specific void room to maximize the entropy after encapsulating guest molecules. Packing coefficient, defined as the volume ration between the guest molecule and the inner cavity of host molecule, is utilized as an effective indicator to

predict the binding affinity between host and guest. Surprisingly, the rule of '55% of PC' in solution proposed by Rebek *et al* was found to be the optimum packing coefficient giving the highest binding affinity of host-guest complex [38]. The underlying reason of such 55% packing coefficient rule is that 45% void space left in the cavity render certain mobility freedom for both host and guest molecule while a higher packing coefficient would at the expanse of such mobility freedom. Of course, the number of 55% is not extremely strict and a certain degree of shifts in packing coefficient is tolerated with a resulting depressed binding constant [39]. Referring to the optimum 55% packing coefficient and the inner cavity volume of CB*n*, the number of water molecules stay inside CB*n* cavity was estimated in the range of 1 to 20 using X-ray characterization and molecular dynamics simulations (**Table. 1.3**) [21,40].

Table 1.3 Number of water molecules inside inner cavity of CB*n* (*n* = 5-8, 10) [21]. Copyright 2011 Wiley-VCH.

	Number of water molecules in inner cavity	
	X-ray	Molecular dynamics simulations
CB5	1-2	2
CB6	3-4	4
CB7		7
CB8	11-12	10
CB10		20

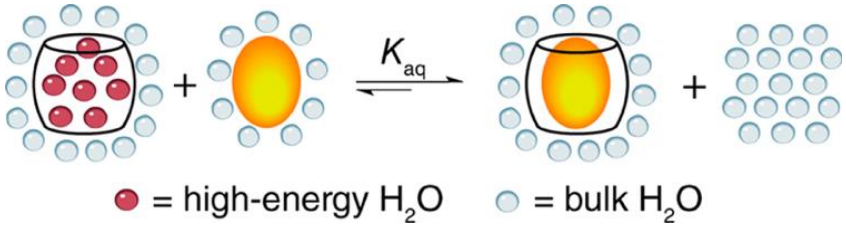

Fig. 1.6 The release of high-energy water molecules of CB*n* upon complexation with guest molecules [41]. Copyright 2012 American Chemical Society.

Water molecules confined in a microenvironment are remarkably distinct from the bulk water molecules [42-44], which are called 'high-energy water molecules' because such confinement is neither enthalpically nor entropically favourable. The convergence of molecular dynamics simulations and experimental results obtained by Alfonso and co-workers [41,45] reveals that the release of these included high-energy water molecules from CB*n* cavities works as the major driving force when CB*n* binds to neutrally charged guest molecules in aqueous solutions. The removal of included water molecules upon complexation provides CB*n* entropic gain, which accordingly results in strong binding affinities for CB*n* towards uncharged guest molecules (**Fig. 1.6**). It is worth mentioning that the interactions between confined water molecules in the cases of small CB homologues, *e.g.* CB5, CB6 and CB7, are significantly less favourable with respect to bulk water molecules since their small cavities limited the formation of hydrogen bonds and do not allow hydrogen bonds to arrange into a more energetically stable network as indicated by the H-bond count and $E(H_2O)$ in **Table. 1.4** [41,45]. Conversely, CB8, a larger homologue of CB*n*, enables the internal water molecules to optimize their hydrogen bonds networks to a similar structure with bulk water molecules, giving rise to a comparable value of $E(H_2O)$ with bulk phase (**Table. 1.4**). Overall, the energy of one single CB*n* confined water molecule decreases as the cavity size increases because the formation of stable hydrogen

bond networks is favoured by larger cavities, while on the other hand, the number of confined water molecules increase as the cavity size [21,41,45]. Combing these two counterbalancing factors, CB7 appears to be the one offering the strongest binding affinities for neutral guest molecules with respect to other CB*n* homologues by perfectly compromise these two factors to reach maximum energy gain.

Table 1.4 The number of hydrogen bond and energy regarding the release of confined hight-water molecules of CB*n* (*n* = 5-8, 10) [21]. Copyright 2011 Wiley-VCH.

	H-bond count	$E(H_2O)$ (kJ/mol)	ΔE(all) (kJ/mol)
Bulk water	2.54	79±15.2	
CB5	0.99	63.2±14	-41.6±28.8
CB6	1.31	64.4±11	-51.5±29.0
CB7	2.01	74.4±11.3	-102.4±31.3
CB8	2.55	81.8±12.5	-66.2±10.7

$E(H_2O)$ represents to the average potential energy loss with the removal of one single water molecule from CB*n* cavity; ΔE(all) represents the potential energy difference when removing all confined water molecules and transferring the bulk aqueous solution.

1.4 Host-guest chemistry of CBs

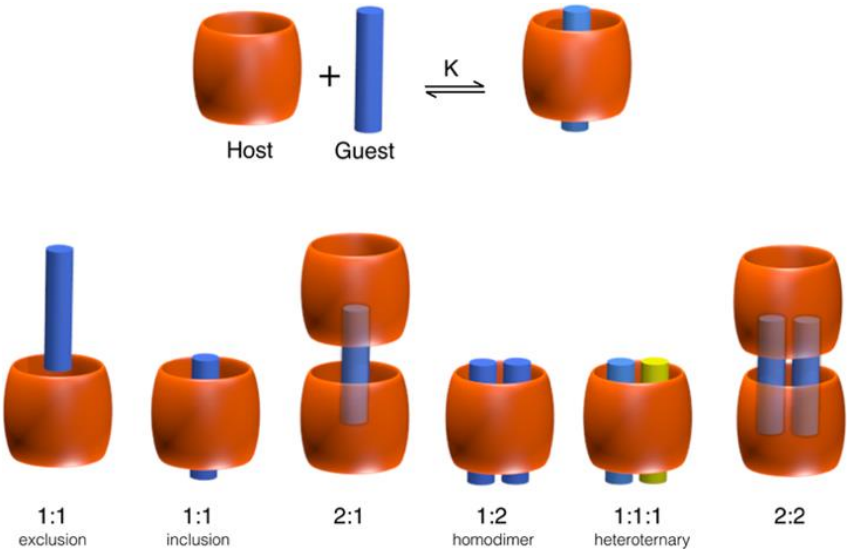

Fig. 1.7 CB*n*-based inclusion and exclusion complexes with different stoichiometries [20]. Copyright 2015 American Chemical Society.

The fundamental behind diverse application potentials of CBs including but not limited to sensing [46-49], drug delivery [50-54], catalysis [55,56], molecular machines [57], materials design [58,59], is host-guest chemistry of CBs, and interestingly, the physical, chemical and/or biological properties of encapsulated guests tend to be modified upon the complexation. The first complexation behaviour for CBs was reported by Mock *et al* in 1983 [60]; specifically, the formation of host-guest complexes between CB6 and alkylammonium and alkyl diammonium ions were studied. Loads of investigations have been executed to gain comprehensive understanding about the driving force for the formation of host-guest complexes of CB*n*.

Considering about the driving force for the formation of CB*n*-based host-guest complexes, several different effects have been proposed. When CB*n* work as a cation binder, the ion-diploe interactions and/or the formation of hydrogen bond between positively charged guests, such as guest possess ammonium groups, and the electronegatively charged carbonyl rims of CB*n* play a determinant role. When guest is neutrally charged, the hydrophobic effect that describes the entropic gain upon the release of confined high-energy water molecules after encapsulating guests mainly drives the formation of CB*n*-based inclusion complexes. No matter whether the guest is charged, size complementary effect (empirical 55% packing coefficient rule) is of particular importance in determining the binding affinities of CB*n*-based complexes.

Table 1.5 Binding constants (logK_a) of complexes between CB*n* and cations [61]. Copyright 2019 Royal Society of Chemistry.

	CB5	CB6	CB7	CB8
$NH4^+$	2.59	3.79	2.82	
Li^+	2.02	2.41	2.34	1.69
Na^+	3.94	3/89	3.41	2.49
K^+	4.73	3.81	3.46	2.66
Rb^+	3.22	4.30	3.43	2.64
Cs^+	2.61	5.31	3.50	2.55
Ag^+		3.87	3.54	2.32
Mg^{2+}	2.50	3.57	3.24	2.72
Ca^{2+}	2.64	4.22	4.25	3.31
Sr^{2+}	5.16	4.91	4.79	3.63
Ba^{2+}	6.44	5.29	5.28	3.95
Ni^{2+}	2.73	2.59	3.50	2.73
Cu^{2+}		2.88	3.75	2.86
Zn^{2+}		2.45	3.40	2.67
Al^{3+}		3.81	2.90	2.90
Fe^{3+}	3.66	5.17	4.18	3.00
Yb^{3+}	3.71	3.50	4.42	3.44
La^{3+}	4.17	4.16	5.28	3.76

As for the stoichiometry of CB*n*-based host-guest complexes, there are several different conditions as demonstrated in **Fig. 1.7**, among which 1:1 is the most typical ratio for binary complexes in the cases of smaller CB*n* homologues (*n* = 5-7). For CB8, apart from 1:1 host-guest complex, it is able to accommodate two guest molecules simultaneously by leveraging its spacious cavity and depending on the kind of the included two guest molecules, they are

defined as homo- and hetero-ternary complex, corresponding to the 1:2 and 1:1:1 ratio respectively in **Fig. 1.7**.

For CB5, the smallest homologue of CB family, the formation of 1:1 binary host-guest complexes and corresponding binding affinities with inorganic cations, including transition metal, ammonium, monovalent alkali, divalent alkaline and trivalent ions in aqueous solution have been investigated, which were also achievable by other larger CB members. The corresponding binding constants are summarized in **Table 1.5** [61-63]. Additionally, CB5 was also reported to be capability to encapsulate neutral gas molecules (N_2 and O_2) and organic molecules (methanol and acetonitrile) in gas phase [64].

For another small homologue of CB, CB6 is the first fabricated and most abundant CB species. Other than the cations demonstrated in **Table 1.5**, it has been reported that CB6 can form 1:1 binary inclusion complex with aliphatic alcohols, aromatic compounds, different kinds of amines, and surprisingly, an ultrahigh binding affinity of 10^{10} M^{-1} is achieved by spermine [20,65]. Additionally, CB6 is also able to encapsulate cations mentioned in the case of CB5 and the corresponding binding affinities are generally slightly stronger than that of CB5 (**Table 1.5**) [61,66]. Other than these inclusion complexes, it is reported that CB6 can also form exclusion complexes with a group of molecules like pyrene and peptide [20].

For the larger CB homologue of CB7, its cavity is spacious enough to accommodate simple three-dimensional guests other than chain molecules and small gas molecules, and thereby the variety of guest molecules is much more diverse and the corresponding binding affinities are generally higher with respect to CB5 and CB6 [20]. Adamantylamine, ferrocene and cobaltocene derivatives (**Fig. 1.8a**) are found as typical strong binders for CB7, offering impressively high binding constants, *e.g.* 7.2×10^{17} M^{-1} of CB7-diamantane diammonium [67-73]. Such favourable binding constants is on account of the desired entropic gain via complete removal of confined high-energy water molecules from the cavity as well as the excellent size and shape matching effect. Taking ferrocene as an example, which was first proposed by Kim and Kaifer in 2003 [70], its perfect size matching is visually illustrated by its DFT-optimized molecular model **Fig. 1.8b**. The strong binding strength reached in the case of CB7 is comparable to [71,72] or even exceed [73] the strongest non-covalent interactions explored in the case of nature biotin-avidin pair. In addition to spacious cavity of CB7, its outstanding water solubility of around 30 mM promise its promising applicability in aqueous biologically relevant environment via its strong binding with drug molecules, proteins, aminos, peptides.

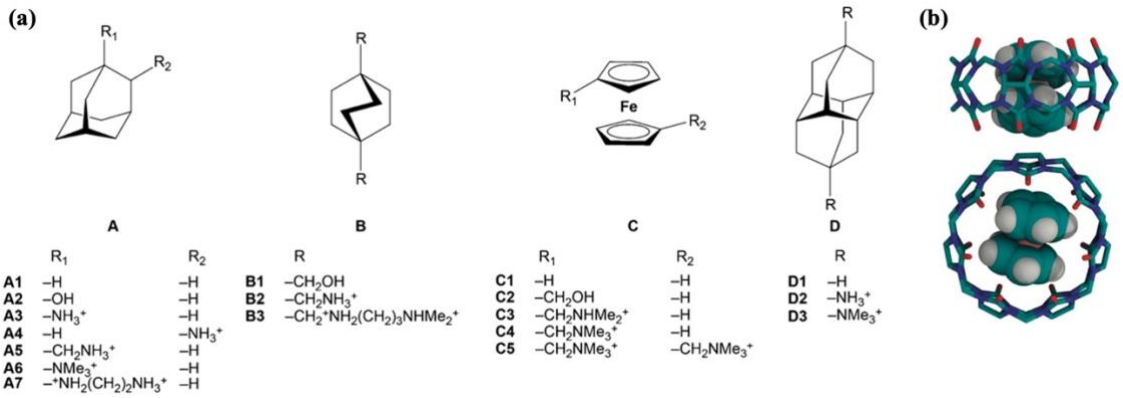

Fig. 1.8 (a) Chemical structures of strong guest molecules for CB7 [28,69]. Copyright 2015 Royal Society of Chemistry, 2005 American Chemical Society. **(b)** The optimized molecular model of CB7-ferrocene complex [68]. Copyright 2003 American Chemical Society.

For CB8, whose cavity size is comparable to γCD and 1.7 times larger than that of CB7, demonstrates a comparable host-guest chemistry fundamentals and relatively more kinds of host-guest binding possibilities in comparison with other smaller CB members. Firstly, like other smaller CB homologues, CB8 is also amendable for the formation of simple 1:1 binary complex with both planar and relatively bulker guests. Strong binders like bulky adamantane and ferrocene derivatives for CB7 (**Fig .1.8b**) can also be tightly encapsulated by CB8, giving a generally slightly weaker binding constants with respect to CB7 [71,72].

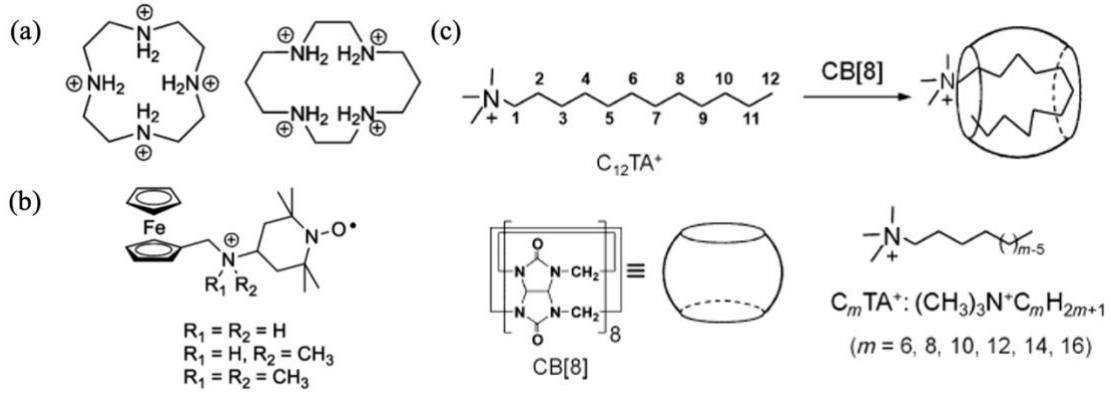

Fig. 1.9 Chemical structures of **(a)** two macrocyclic molecules that can be encapsulated by CB8 and **(b)** molecules possess two binding sites that can preferentially bind with CB8 [74,75]. Copyright 2002, 2011 Royal Society of Chemistry. **(c)** Conformational change of an aliphatic chain upon complexation with CB8 [76]. Copyright 2011 Wiley-VCH.

Apart from these simple three-dimensional guest molecules, CB8 cavity is even spacious enough to accommodate larger macrocycles as guests (**Fig. 1.9a**), allowing for the formation of a macrocycle-macrocycle complex [74]. Moreover, it is interesting to note that CB8 can induce conformational change of included guests on account of the large cavity width. For example, Kim and co-workers found that aliphatic chain tends to exist as U-shape conformation within CB8 cavity in order to be fully encapsulated (**Fig. 1.9c**) [76]. Although such U-shape folding will lead to an entropic penalty, the significant enthalpic gain from the van der Waals interactions between the hydrophobic cavity and chain can overcompensate it in this instance. Additionally, the inclusion of nitroxide derivatives by CB8 has been investigated recently by researchers [75,77-82]. When one molecule possesses two binding sites of ferrocene and nitroxide simultaneously, such as the chemical structures shown in **Fig. 1.9b**, CB8 perform differential complexation towards them. The inclusion preference of CB8 towards these two binding blocks is dependent on the methylation degree of the nitrogen. When R1 = R2 = H, CB8 mainly includes the ferrocene residue while when the hydrogen on nitrogen is displaced by methyl side chain, the tempo block tends to be encapsulated inside CB8 as well, and surprisingly, when two of hydrogen atoms on nitrogen are entirely displaced by methyl group, the inclusion of tempo unit appears to be clearly predominant in comparison to the ferrocene residue [75].

Apart from simple 1:1 binary complexation, CB8 presents uniquely in its ability to encapsulate two guest molecules simultaneously. Depending on the kinds of two included guest molecules, the obtained ternary complex is classified as homo- and hetero-ternary complex. The formation of a wide range of CB8-based hetero-ternary complexes with doubly charged viologen derivatives as the first guest (G1) and aromatic molecules like tryptophan, dopamine, 2-naphthol, phenol, 1,6-dihydroxynaphthalene, 1,5-dihydroxynaphthalene, 2,3-dihydroxynaphthalene, 2,7-dihydroxynaphthalene, pyrocatechol, 4-chlorophenol, 4-cyanophenol, 2-methoxyphenol, tryptophan derivatives, *etc*, as the second guest (G2) has been identified [83-86]. The binding constants corresponding to the second binding behaviours were

exploited in detail by isothermal calorimetry (ITC) and electrospray ionization mass spectroscopy (ESI-MS), and desire correlation was found between the values obtained in solution and gaseous condition [87]. In addition to these hetero-ternary complexes, homo-ternary complexes of a variety of guests such as neutral red [88], anthracene derivatives [89,90], 9-aminoacridinium [91], *N*-phenylpiperazine [92], coumarin [93], have been reported (**Fig .1. 10a**). In an analogous fashion, radical cations can also dimerize inside CB8 cavity as homo-ternary complexes. For instance, the dimerization of methyl viologen radical ($MV^{+\bullet}$) after undergoing one-electron electrochemical reduction is a typical example that has been studied by the Kim group and the Kaifer group (**Fig. 1.10b**) [67,94-96]. The ability of radical dimerization inside CB8 cavity offers an exceptional electrochemical reduction property to inclusion complex of CB8-methyl viologen (CB8-MV^{2+}). Generally, the reduction potential tends to negatively shift upon complexation with CB*n*, for example, the reduction peak of CB7-MV^{2+} is more negative than that of free MV^{2+}, which is rationalized by the preferential binding of CB7 towards more positively charged species of MV^{2+} via ion-dipole interactions. On the contrary, the reduction of MV^{2+} is favoured upon CB8 encapsulation, which is attributed to the stronger binding of CB8 with the dimerized one-electron reduced intermediate $MV^{+\bullet}$. Such opposite shift of MV^{2+} reduction potential in the presence of CB7 and CB8 is illustrated in the electrochemical results in **Fig. 1.11**.

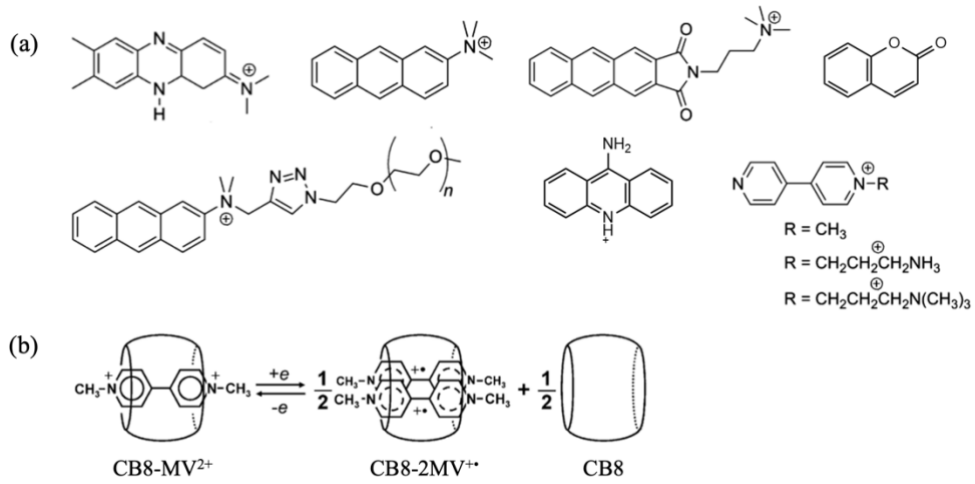

Fig. 1.10 (a) Chemical structures of selective guests that can form homo-ternary complex with CB8 [76]. Copyright 2011 Wiley-VCH. **(b)** Dimerization process within CB8 cavity upon MV^{2+} reduction [94]. Copyright 2002 Royal Society of Chemistry.

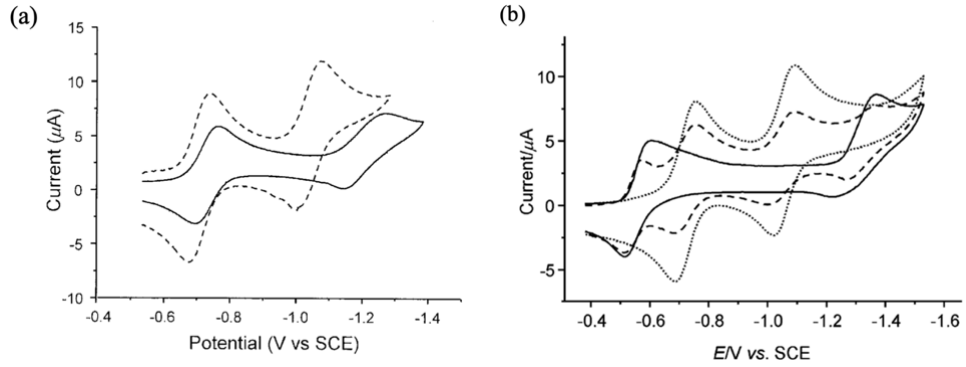

Fig. 1.11 Cyclic voltammograms of **(a)** 0.5mM MV^{2+} in the absence (dashed line) and presence of 3 equivalents of CB7 (solid line), and **(b)** 0.5mM MV^{2+} in the absence (dotted line) and presence of 0.25 (dashed line) and 1 equivalent of CB8 (solid line) [94,96]. Copyright 2002 Royal

Society of Chemistry, 2002 Proceedings of the National Academy of Sciences of the United States of America (PNAS).

Other than inclusion complexes, CB*n* can also form exclusion complexes with guest molecules through host-guest interactions. For example, a large guest molecule of fullerene[60] was found to be able to form a 1:2 exclusion complex with large CB8 (**Fig. 1.12**) [97].

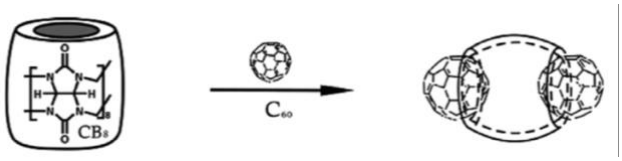

Fig. 1.12 The formation of 2:1 exclusion supramolecular complex between fullerene[60] and CB8 [97]. Copyright 2006 Elsevier.

1.5 Basics of electrochemistry

Electrochemistry is a powerful tool to investigate the electron-transfer involved reactions of redox active molecules. It is mainly to probe the process undergoing at the interface between the electrode and the liquid phase containing target redox analyte and conductive electrolyte. At this interface, a special layer of charging called 'electrical double layer' is formed, consisting of two parallel planes. The first layer is a compact layer that is composed of ions adsorbed on the electrode surface resulting from the chemical interactions, and the second layer is diffuse layer that is made of free ions that move in the liquid phase [98,99]. Under the applied external potential in electrochemical measurements, the capacitance current tends to be present due to the charging and/or discharging of the double layer, which tends to interfere the investigations for the target electrochemical reactions, and thus, such capacitance current needs to be depressed or isolated. The current that is intended to monitor is the faradaic current, which is associated with the reduction and/or oxidation reactions of the target redox active species happening at the surface of the working electrode (WE).

$$E = E^0 + \frac{RT}{nF} ln \frac{(Ox)}{(Red)} \qquad (1.1)$$

Thermodynamic data determines whether the reaction takes place spontaneously and kinetic data describes the reaction rate. In terms of thermodynamics, Nernst equation (**eq. 1.1**) proposed by Walther Nernst allows for the calculation of the reduction potential referring to the standard potential (E^0) of a species and the estimation of the relative reducibility of the target species [100,101], where R is the universal gas constant; T is the temperature; n is the number of electrons; F is the Faraday's constant; (Ox) and (Red) are the concentration of oxidant and reductant, respectively. In terms of kinetics, the overall rate for an electrochemical reaction is determinant by the slowest step among electrode reactions and mass transport processes. There are three types of mass transport in an electrochemical reaction, *i.e.* diffusion, migration, and convection, among which the diffusion mode depending on the concentration gradient between the electrode surface and the bulk solution is the mostly involved one. If the rate of the reaction is fully diffusion-controlled, then the reaction is completely reversible process.

Three-electrode setup consisting of reference electrode (RE), counter electrode (CE) and working electrode (WE) is the most typically utilized arrangement in electrochemical measurements. The most popular REs includes Ag/AgCl and saturated calomel electrode (SCE), and the most popular CE is platinum wire/plate; for WE, disc electrodes with well-defined electrode surface area are widely utilized, such as Au disc, Pt disc and glassy carbon electrodes. The sweeping potential is the potential applying between WE and RE, and the

recorded current is the current flowing from WE to CE. The liquid phase measured is the solution contains the target redox active species and conductive electrolyte like salt solution or buffer solution.

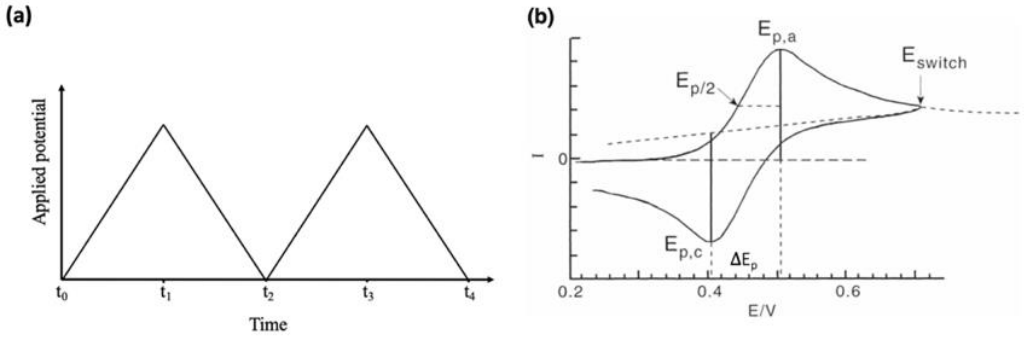

Fig. 1.13 (a) Potential waveform and **(b)** characteristic parameters of CV [102]. Copyright 2010 Springer.

Among diverse electrochemical methodologies, cyclic voltammetry (CV) is the most typical and frequently utilized transient technique since it can provide rich information to understanding the kinetics and thermodynamics of the reaction [102-107]. The potential waveform in cyclic voltammetry (CV) is linearly cycled versus time, and the current of the redox species responding to the linearly cycled potential is recorded as cyclic voltammogram (**Fig. 1.13a**). Several setting parameters, including scan rate, initial and final potential, step size, equilibrium time and maximum current, are of importance to obtain the CV curve with characteristic and information-rich profile. When the involved electron transfer process is reversible and the redox species can diffuse freely, the plot for peak current against the square root of the scan rate is in linear shape.

Characteristic parameters in CV are labelled in **Fig. 1.13b.** $E_{p,a}$ and $E_{p,c}$ are the peak potentials corresponding to the anodic reaction and cathodic reaction, respectively; the half-wave potential ($E_{p/2}$) is defined as the potential where the current is half of the corresponding peak current; the switch potential (E_{switch}) is the potential at which the scanning direction switch from forward to backward. It is worth to note that when the reaction is fully reversible, the half-wave potential is often in accordance with the mean value of peak potentials, which is calculated as $1/2(E_{p,a} + E_{p,c})$. Current at $E_{p,a}$, $E_{p,c}$ and E_{switch} are defined as anodic current ($I_{p,a}$), cathodic current ($I_{p,c}$) and switching current (I_{switch}). The peak-to-peak separation between anodic and cathodic peaks defined as ΔE_p, which is utilized as an indicator for the reversibility of the electrochemical reactions. The theoretically expected value of ΔE_p is 57 mV at 298 K for a completely reversible reaction; as ΔE_p closer to the theoretical value, the reaction is predicted as more reversible.

Other than CV, square wave voltammetry (SWV) is an electrochemical technique that attracted increasing attention recently due to its high sensitivity. The applied external potential in SWV is the sum of a square wave and staircase potential as shown in the waveform in **Fig. 1.14a** [108-111]. The current at stationary WE with the potential pulsed forward and backward at a fixed frequency. The pulse direction is the same as the step of staircase and the reverse pulse starts in the middle way of the staircase step. Key parameters and timing relationships in SWV are shown in **Fig. 1.14b**. In detail, τ is the time for one square wave cycle; frequency is the reciprocal of τ; E_{sw} is the height of the stair step; E_{step} is the step size of staircase; peak-to-peak amplitude is 2 times of E_{sw}, and scan rate of SWV is equal to the ratio of E_{step} and τ, *i.e.* E_{step} times frequency. In SWV, the current is sampled at the end of forward and reverse of each pulse such as i_1 and i_2 and the difference between two current values is plotted against applied

potential as SWV curve. The charging of double layer is depressed by such current sampling mode, *i.e.* postponing the current recording to the end of each pulse, and thus, peaks observed in SWV is confined to faradaic processes. Hence, the peak current in SWV is directly proportional to the concentration of redox active species. Additional to the high sensitivity of SWV benefiting from the discrimination of capacitance current, the much faster scan rate offered by SWV compared to other differential pulse methodologies allow rapid measurements in the scale of seconds.

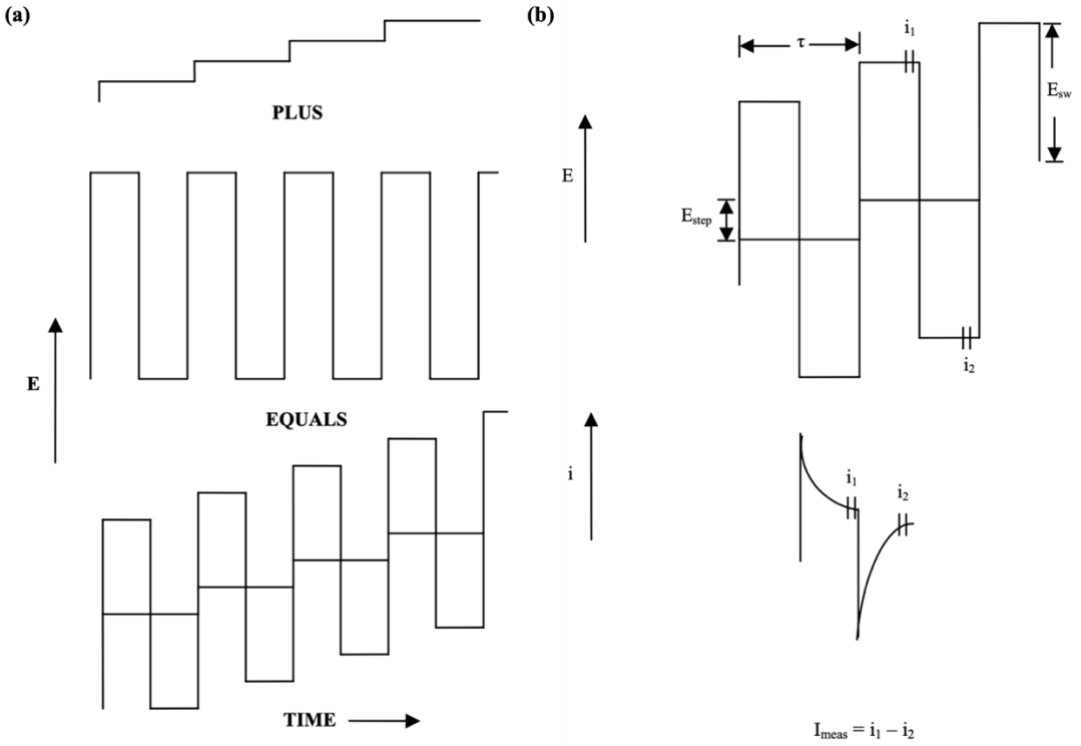

Fig. 1.14 (a) Potential waveform of SWV. **(b)** Timing relationships and key parameters in SWV [108]. Copyright 1985 American Chemical Society.

1.6 Supramolecular electrochemistry

The inclusion of a variety of redox-active guest molecules by supramolecular hosts have been widely investigated and their redox behaviours tend to be modified upon the complexation. Based on this, a wide range of electrochemical sensors and electrochemically controlled molecular machines have been developed, and promising progresses in the field of electroanalytical chemistry have been promoted [112-118]. Among diverse supramolecular hosts, CDs and CBs present most popular in electrochemical sensing. For sake of improved sensitivity and selectivity of electrochemical sensor, electrodes are often modified and functionalized by special materials.

Taking advantage of the hydrophobic inner cavity and hydrophilic exterior, CDs perform certain binding selectivity towards guest molecules and desired applicability as well as stability in aqueous-based systems. In the area of CDs-based electrochemical sensor, CDs modified carbon materials such as graphene, graphene oxide, reduced graphene oxide and multi-walled nanotube, are prevailing [112,114-119]. One application route of such CDs functionalized nanohybrid is to directly serve as the sensing matrix to capture the specific target analytes presenting in electrolyte [120]. For example, a non-enzymatic sensing matrix of βCD functionalized graphene was fabricated for cholesterol sensing, where βCD provides sensor with high selectively upon host-guest complexation and graphene offers great conductivity to

the electrode [120]. As demonstrated in **Fig. 1.15a**, methylene blue was employed as the redox active indicator to be captured by βCD as βCD-methylene blue complex, which is ready to be displaced by the target sensing molecule (cholesterol) via competitive complexation behaviour. With the addition of cholesterol into the cell containing βCD-methylene blue, the electrochemical behaviour of βCD-methylene blue showed responding changes, *i.e.* the peak potential of βCD-methylene blue shifted positively with the increasing amount of cholesterol. The relationship between the amount of cholesterol and the peak potential shift of βCD-methylene blue in the presence of cholesterol was uncovered, enabling the quantitative detection of cholesterol.

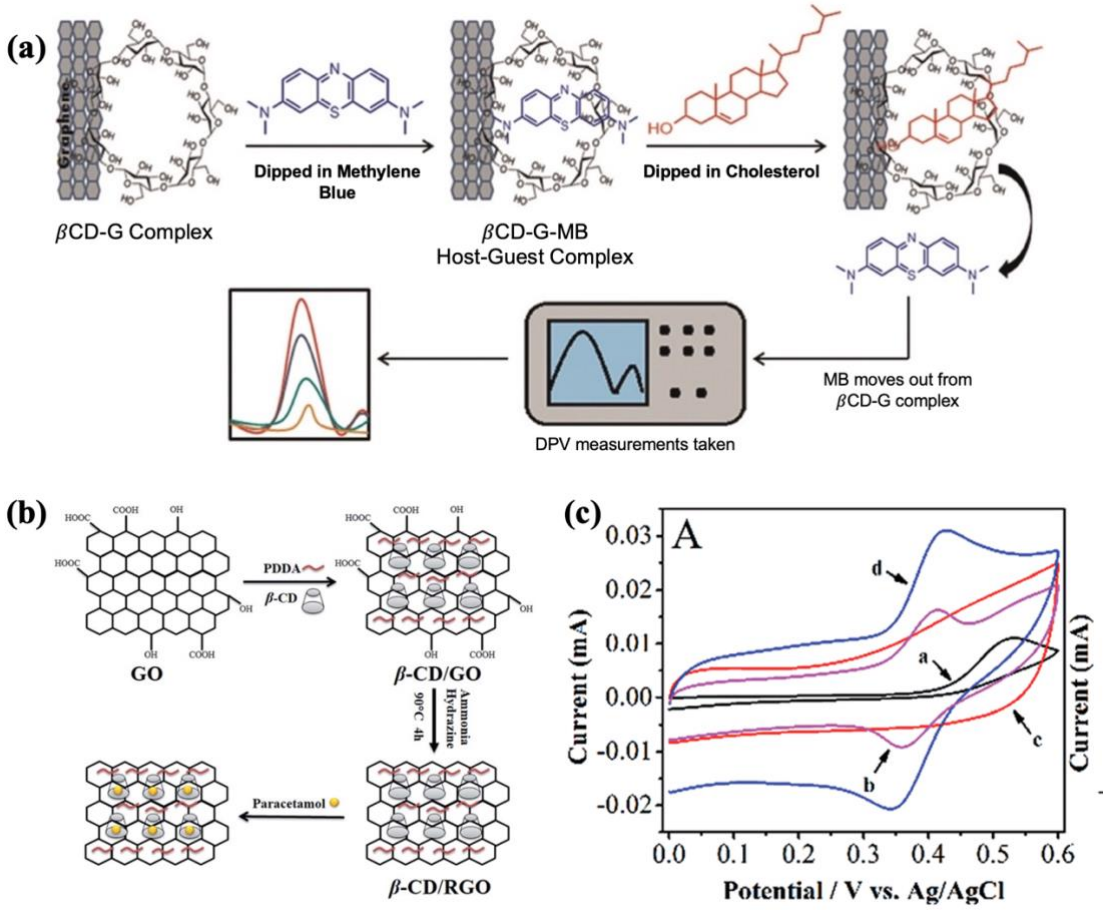

Fig. 1.15 (a) βCD functionalized graphene as sensing matrix for cholesterol sensing [120]. Copyright 2015 Elsevier. **(b)** The fabrication route of βCD functionalized reduced graphene oxide (βCD/RGO) for paracetamol sensing. PDDA = Poly(diallyl dimethyl ammonium chloride). **(c)** Cyclic voltammograms of 0.1 mM paracetamol measured by a: bare glassy carbon electrode, b: RGO, d: βCD/RGO, and cyclic voltammogram of electrolyte without paracetamol by βCD/RGO [121]. Copyright 2015 Elsevier.

Alternatively, instead of directly working as sensing matrix, CDs functionalized carbon materials can be utilized to modify the commercially available working electrode to enhance the detection sensitivity compared to that of pristine electrode [120-122]. For instance, the reduced graphene oxide (RGO) was modified by βCD as βCD/RGO and utilized as the working electrode for electrochemical sensing of paracetamol (**Fig.1.15b**) [121]. As indicated by **Fig.1.15c**, only one irreversible oxidation peak of paracetamol can be observed with bare glassy carbon electrode; however, a pair of redox peaks can be observed when utilizing RGO or βCD/RGO as working electrode. Compared to RGO, the redox peak intensity of βCD/RGO

was further enhanced because only single-layer surface adsorption of paracetamol works in the case of RGO while in the presence of βCD, combined of host-guest complexation and the surface envelope adsorption are achievable. In a nutshell, the design of CDs-based sensing materials offering desired sensitivity as well as selectivity is mainly dependent on the host-guest complexation ability of CDs host.

With the aid of well-defined hydrophobic cavity and two opening carbonyl-lined electronegative portals, CBs exhibit selective complexation abilities towards a variety of target molecules to modify their physical, chemical, or electrochemical properties, thereby imparting promising application potentials such as the electroanalytical application [25,67,94-97,123], the design of electrochemical sensor [25,124-128] and electrochemically controlled molecular machines [129-133]. As for electroanalytical application, the electrochemical behaviours of redox active analyte are modulated by the CBs complexation. The changes in electrochemical behaviours of MV^{2+} and ferrocene in the presence of CB7/CB8 are precedent examples for CBs as analytical platform and have been deeply investigated by the Kim group and the Kaifer group [67,94-97]. The detail introduction regarding these systems have been discussed in *Chapter 1.5* and it is unnecessary to be repeated here again. As for the CBs-based electrochemical sensors, the predominant working route is the modification of electrode by immobilizing CBs on the surface of electrode [124-128]. For example, CB8 was immobilized on glassy carbon electrode by PVC or Nafion for electrochemical detection of dopamine [125]. Upon CB8 modification of bare glassy carbon electrode, the selectivity and limit of detection (LoD) for dopamine were highly improved by taking advantage of the selective host-guest complexation between CB8 and target dopamine.

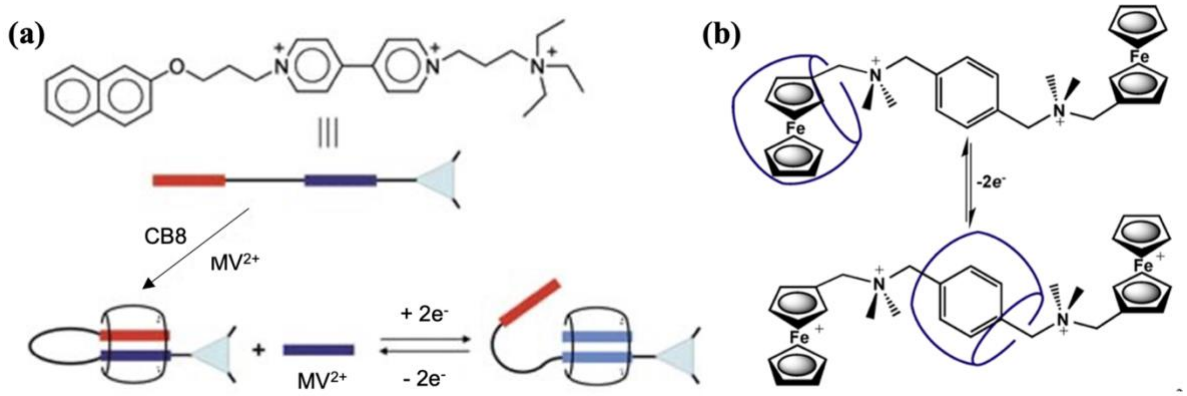

Fig. 1.16 (a) The formation and unlock of a molecular loop driven by electrochemical redox process with the aid of CB8 and MV^{2+} [129]. Copyright 2005 Wiley-VCH. **(b)** Electrochemically switchable pseudoproteases formed by CB7 and an axle compound [130]. Copyright 2014 American Chemical Society.

Other than electrochemical sensor, molecular motions can be triggered by electrochemical approach in the presence of CBs. For instance, an electrochemical redox process triggered molecular loop was fabricated by Kim *et al* [129]. As illustrated in **Fig. 1.16a**. the guest molecule possessing two binding moieties (naphthalen-2-yloxy and viologen) bind with CB8 as stable 1:1 complex by bending the bridge between two binding moieties as a molecular loop. Interestingly, with the addition of MV^{2+}, upon one-electron reduced MV^{2+} and the viologen unit on the guest molecule, the molecular loop was unlocked. The MV^{2+} here works like a key to unlock the molecular loop formed by the host-guest complexation of CB8. Leveraging the differential binding preference of CBs towards different binding sites of one specific guest molecule before and after reduction or oxidation process, molecular wheels have also been designed [130]. For example, switchable pseudoproteases were designed by CB7 and

an axle compound consisting of three binding sites, *e.g.* two ferrocenyl-methylammonium terminates and one central diammonium-1,4-xylylene unit (**Fig.1.16b**). In the presence of 1 equivalent of CB7, one of the ferrocenyl terminate are preferably encapsulated by CB7 and the exchange of CB7 between two identical ferrocenyl binding sites is relatively slow. Upon the electrochemical oxidation of two ferrocenyl units, CB7 move from the ferrocenyl units to the central diammonium-1,4-xylylene moiety, in which CB7 resembles a molecular wheel reversibly sliding through the axle compound under the electrochemical controlling. In summary, by taking advantage of the preferential and selective binding ability of CBs towards guest molecules, a wide range of application potentials in the field of electrochemistry have been explored.

1.7 Basics of binding constants

Generally, the formation of a complex between host and guest molecule is a crucial process in supramolecular chemistry. Selectivity in the complexation, which is related to the molecular recognition specificity, can be assessed by the ratio of binding constants of complexes formed between host and different target analytes. Binding constant is a basic criterion for quantitative analysis of the host-guest interactions. The terms of binding constant, association constant, equilibrium constant and stability constant are synonymous and represented as *K* in this thesis. A common way to determine the binding constant is based on a binding equilibrium model as illustrated by **eq. 1.2** and **eq. 1.3**.

$$a \cdot \mathrm{H} + b \cdot \mathrm{G} \rightleftharpoons \mathrm{C} \qquad (1.2)$$

$$K = \frac{[\mathrm{C}]}{[\mathrm{H}]^a[\mathrm{G}]^b} \qquad (1.3)$$

where H is host; G is guest; C is the complex of $H_a \cdot G_a$; *a* and *b* are the stoichiometry; *K* is the binding constant; $[\mathrm{H}]$, $[\mathrm{G}]$ and $[\mathrm{C}]$ are the concentrations of host, guest and complex, respectively, at equilibrium.

Binding constant (*K*) is regarded as a criterion for the assessment of the dynamic host-guest complexation event. Thus, thermodynamic parameters, including enthalpy (*H*), entropy (*S*), and Gibbs free energy (*G*), present as more suitable criteria to express the molecular recognition abilities of supramolecular systems. As described in **eq. 1.4** and **eq. 1.5**, it can be found that thermodynamic parameters are related to each other. The relationship between binding constant (*K*) and these thermodynamic parameters can be derived from the **eq. 1.4** and **eq. 1.5** as **eq. 1.6**, which is the van't Hoff equation [134,135].

$$\Delta G = -RT \ln K \qquad (1.4)$$

$$\Delta G = \Delta H - T\Delta S \qquad (1.5)$$

$$\ln K = -\frac{\Delta H}{R} \cdot \frac{1}{T} + \frac{\Delta S}{R} \qquad (1.6)$$

1.8 Current binding constants determination methods

Binding constant is a crucial indicator to quantitatively estimate the intermolecular interactions between host and guest in supramolecular chemistry, and the ratio of binding constants can be a criterion for the molecular sensing selectivity of supramolecular system,

which can provide instructional information guiding the design of host-guest systems catering for different applications. Manifold methodologies for the determination of binding constants have been proposed, such as quartz crystal microbalance (QCM), surface plasmon resonance (SPR), electrospray ionization mass spectrometry (ESI-MS), capillary electrophoresis (CEP) and supramolecular titration approaches. Investigations regarding molecular interactions between large biomolecules, such as protein, antibody, antigen, DNA, RNA, enzyme substrate, enzyme, *etc*, have been widely performed; however, the study for binding constant estimation for small molecules, *e.g.* molecules with molecular weight around 10^2 to 10^3 Dalton, are relatively limited, which are yet common to see in host-guest complexes applied for sensing, such as detection of pharmaceutical molecules [136], illicit drug molecules, environmental pollutants [137], explosives [48] *etc*. Hence, it is of certain necessities to further explore the quantitative analysis of non-covalent interactions between small molecules.

QCM and SPR are techniques based on the substrate working in solid phase for studying molecular interactions, which mainly measuring mass changes caused by molecular interactions; in particular, QCM mainly measures the change in resonance frequency of quartz crystal, while SPR primarily measures changes of the surface plasmon resonance angle [138-141]. Although QCM is more affordable than SPR, its application range is limited by its complicated quantitative interpretation of frequency change, especially the viscoelastic factor, indicating that one needs to be more careful when analysing QCM responses for large molecular applications [139]. SPR is able to provide a real-time monitoring of non-covalent biomolecular interactions with desired sensitivity; however, information regarding binding stoichiometry is not available in SPR measurements and the protein immobilization process is sometimes delicate when studying interactions between proteins and ligands [140,141]. The ESI-MS is another technique that has been developed to quantitively analyse the non-covalent molecular interactions, which can not only work for biomolecules like proteins, peptides, DNA duplex, metabolites, and nucleic acids but also for macrocyclic host-guest complexes like CEs-based and CDs-based inclusion complexes [142-146]. As known, the mass spectrometer is measuring the ratio of mass and charge of ions in vacuum, and among diverse methods to ionize the analyte molecule, electrospray ionization (ESI) is relatively mild, allowing the structure of complex to almost keep unchanged when transferring from solution phase to gas phase. The binding constant of the target analyte complex is estimated by monitoring the intensity change of a reference complex with known binding strength after adding a host or guest molecule included in the target complex. CEP, a method for the determination of the binding constants, is booming in recent decades, offering manifold advantages including short measurement period, small analyte consumption, simplicity, *etc* [147-149]. However, several intrinsic limitations of CEP cannot be totally ignored. For example, its application scope is mainly limited to the charged specie involved system in specific solvent, *e.g.* ion-ligand in polar solvents like H_2O and a few organic solvents; namely, it is hard for the estimation of the binding associations between neutral molecules.

Supramolecular titration approaches are the most popular methodologies for evaluating the binding affinities of host-guest complexes, in which the change of a specific physical property such as the heat transfer in isothermal titration calorimetry (ITC), absorption peak in ultraviolet–visible (UV-vis) spectroscopy, fluorescence intensity in fluorescence spectroscopy, and chemical changes in proton nuclear magnetic resonance (^{1}H NMR) during the binding interactions is measured.

ITC is one of the most routinely utilized techniques to accurately measure binding constants [150-153]. With the stepwise addition of titrant into the stock solution of host or guest, the binding reactions take place, accompanied by a heat transfer and temperature change. What

measured by ITC is the released or absorbed heat that is used to maintain the temperature of the reaction cell unchanged during the titration (**Fig. 1.17**).

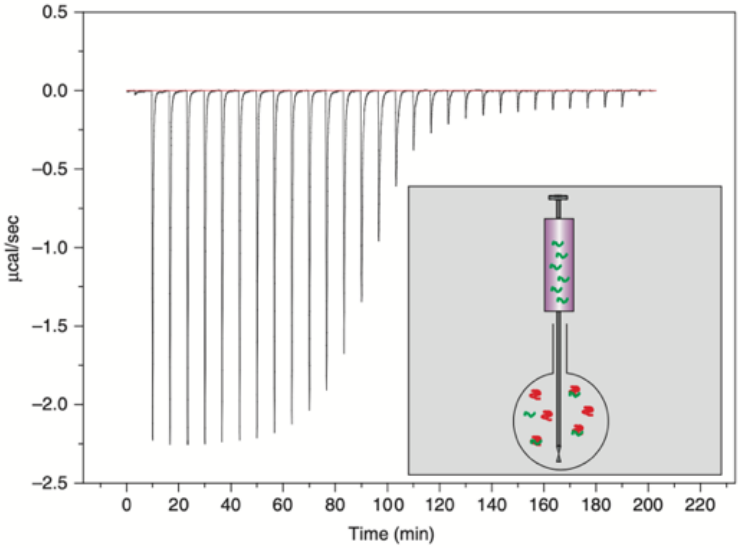

Fig. 1.17 A typical ITC experiment result, where the y-axis is the energy changing rate to maintain the temperature difference between the reaction cell and reference cell constant during the titration. The heat corresponding to each titration can be calculated from the area under each peak. Inset: ITC reaction cell [150]. Copyright 2001 Elsevier.

Spectroscopic-based titration techniques such as UV-vis [154-158] and fluorescence [159-166] are also of wide interests for quantitative analysis of the binding behaviours. In the case of UV-vis titrations, the absorption peak increases or decreases correspondingly with the successive injection of the host (or guest) into the cell containing guest (or host) with a fixed concentration. **Fig. 1.18a** is an example UV-vis titration spectra for the determination of the binding strength between CB7 and m-phenylenediamine [71]. The concentration of guest molecule was kept at 44 μM with the stepwise addition of CB7 until its concentration achieved 4.7 equivalents. With the UV-vis titration spectra, the intensity of the characteristic absorbance at 231 nm was extracted and plotted against the concentration of the CB7. The binding constant of CB7-m-phenylenediamine was obtained as (80700$\pm$6000) M^{-1} by fitting this data into a 1:1 binding model. **Fig. 1.18b** is an example for fluorescence titration in binding constant determination. With the addition of CB8 into the MPDP guest solution with a specific concentration, the characteristic emission peak intensity of MPFP increases correspondingly. The obtained titration curve indicates the binding affinity between CB8 and MPDP is highly strong, *e.g.* (3.89$\pm$0.99) $\times$ 10^{12} M^{-1} with 1:1 binding stoichiometry.

Other than spectroscopic techniques, ^{1}H NMR titration is also a common titration method to provide the thermodynamic information regarding the molecular association-disassociation processes such as the binding constants of complexes formed between cations and macrocyclic hosts [167-174]. It is worth to note that NMR is not only able to study the thermodynamic aspect of the binding behaviours but also enable the kinetic investigation with the aid of time-resolved mode of NMR like diffusion-ordered spectroscopy (DOSY) and exchange spectroscopy (EXSY) [173]. **Fig. 1.18c** displays an example of ^{1}H NMR titration for binding constant determination between cryptand host (*o*-Me_2-1.1.1) and cationic guest (Na^+). Specifically, upon the addition of Na^+, the characteristic chemical shift of *o*-Me_2-1.1.1 host located around 1.38 ppm downshifted gradually due to the formation of the complex, and the plot between the peak shifting magnitude and the concentration of Na^+ was fitted by a well-documented model to estimate the corresponding binding constant.

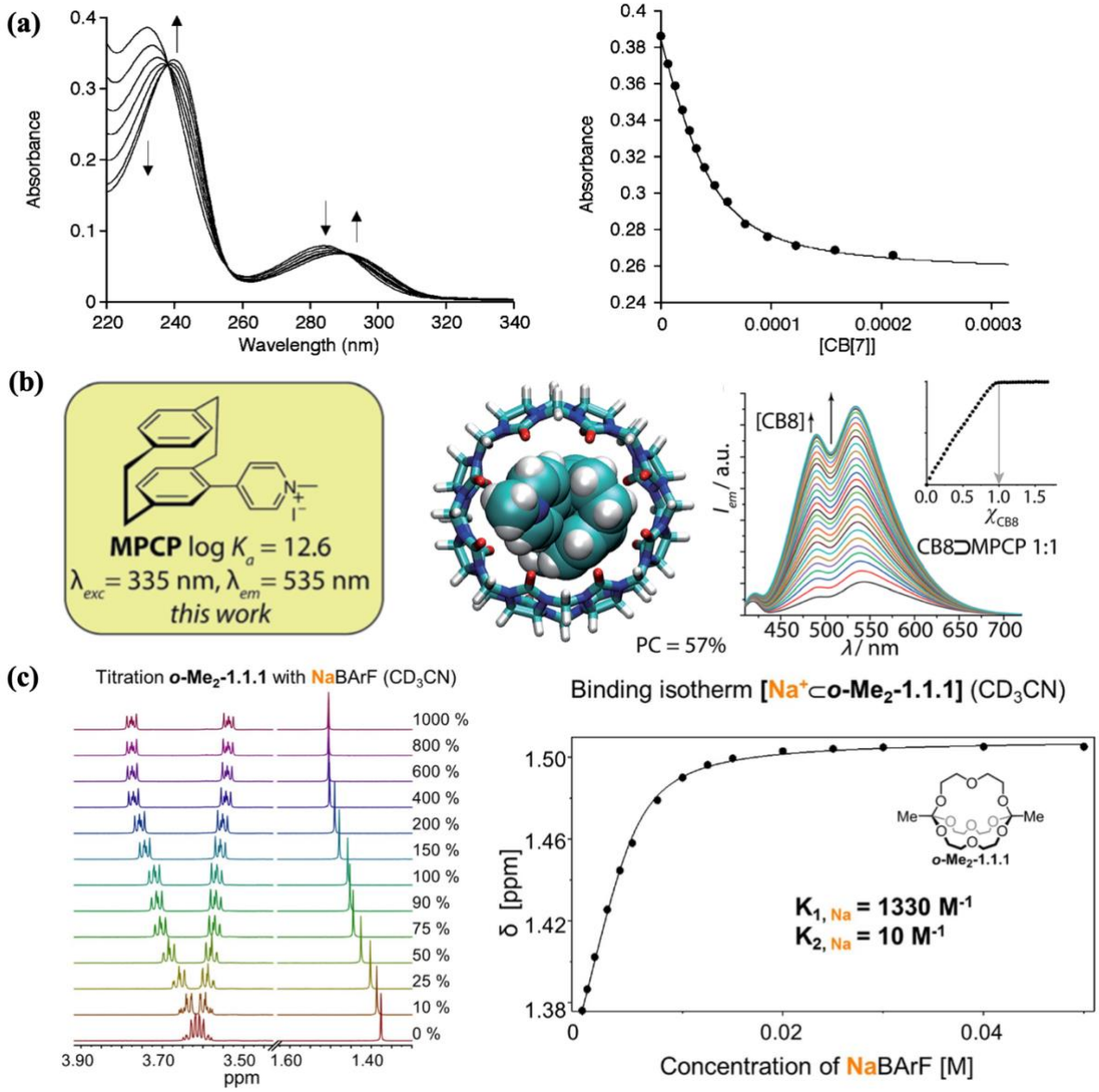

Fig. 1.18 (a) UV-vis titration spectra of m-phenylenediamine with the successive addition of CB7. Scatter: the change of characteristic peak absorbance plotted against the concentration of added CB7. Solid line: the curve obtained by fitting the scatters with a 1:1 binding model [71]. Copyright 2005 American Chemical Society. **(b)** The chemical structure of MPCP guest molecule**,** DFT-optimized molecular model of CB8-MPCP complex and fluorescence titration spectra of MPCP with the successive addition of CB8. Inset: Job plot for the determination of binding stoichiometry [159]. Copyright 2019 Royal Society of Chemistry. **(c)** The ^{1}H NMR titration spectra of *o*-Me2-1.1.1 host with the stepwise addition of Na^+ and the binding curve of the complex formed between *o*-Me2-1.1.1 and Na^+ [173]. Inset: The chemical structure of the *o*-Me2-1.1.1 host. Copyright 2015 MDPI.

In summary, diverse supramolecular titration approaches are indeed effective methodologies for the determination of binding constants and loads of studies in the area of supramolecular chemistry have employed these titration approaches to obtain quantitative information regarding the complexes. However, these titration methods inevitably suffer some inherent limitations, including the long experimental period, multiple repeated titration steps, complicated data analysis procedure, limited application scope towards analyte that is hard to

prepare solution with accurate concentration. Hence, there is still space left for further development in the field of quantitative analysis of binding to overcome or mitigate these shortcomings.

From the viewpoint of the media where the binding constant is determined, current conventional supramolecular titration measurements are strictly limited to simple buffer solution, leaving in-situ binding constant determination in complex bio-media, such as urine, serum and even animal blood, largely unexplored. This is due to the multiple substances present in bio-media are likely to interplay with supramolecular hosts and cause interferent signals that can largely shield the target characteristic peak. Nevertheless, a large portion of practical application scenarios, such as in-situ biosensing based on supramolecular assays, is performed in complex bio-media, for which the binding constant estimated in simple buffer solution cannot give exact and accurate information regarding in-situ binding behaviours. Hence, protocol which is capable of estimating binding constant in complex biologically relevant media presents significantly attractive.

1.8 Current supramolecular-based sensing methods

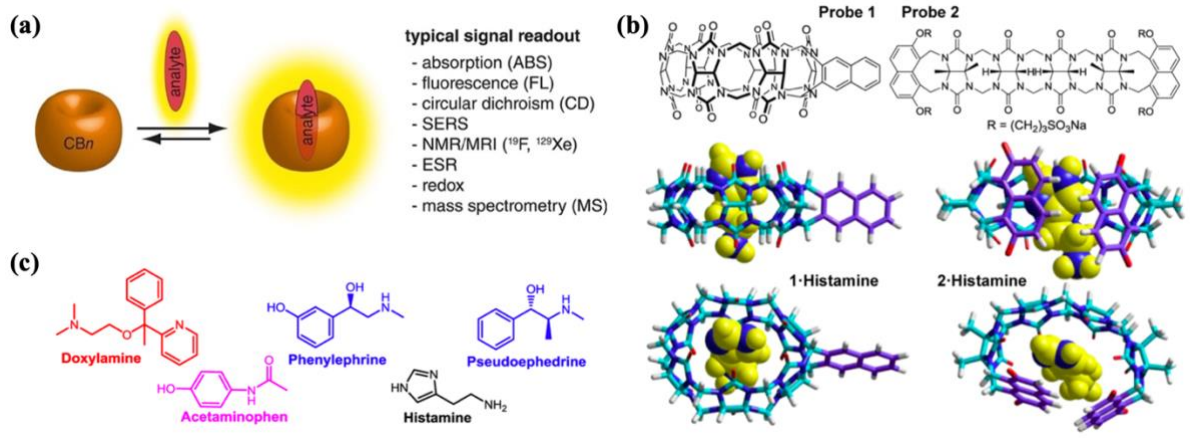

Fig. 1.19 (a) Working principle of direct binding assays (DBAs) [175]. Copyright 2018 Wiley-VCH. **(b)** Two CB-based direct binding assays for the detection of drug molecules. **(c)** Chemical structures of target drug molecules [176]. Copyright 2013 American Chemical Society.

Plenty of analytical techniques have been developed for molecular detections catering for either scientific meanings or practical applications. With the aid of supramolecular hosts, the detection sensitivity and selectivity can be simultaneously enhanced, and thereby supramolecular-based sensing techniques have sparked widespread interests in molecular detection field. Generally, sensing assays based on the capture of the target analyte molecules by supramolecular hosts especially CBs are classified into three types: (1) direct binding assays (DBAs); (2) associative binding assays (ABAs); (3) indicator displacement assays (IDAs).

Direct binding assays (DBAs) refer to the assays that can generate fingerprint signals responding to the capture of the target analyte onto the supramolecular assays (see the working principle of CBs-based DBAs in **Fig. 1.19a** [175-177]). Generally, there are two detection routes of DBAS. One route is that the target analyte molecule itself can generate detectable fingerprint signals and can be altered upon complexation. For example, the redox active molecules like viologen derivatives and ferrocene derivatives can be detected by CBs-based DBAs using electrochemical technique since their electrochemical behaviours present responsive towards CBs complexation. The other detection route of DBAs is that the supramolecular receptor is modified by a detectable indicator like a dye molecule to produce responsive signals. This route is relatively more widely utilized in molecular sensing field with respect to the previously

described one. Isaacs and co-workers designed two DBAs based on naphthene fluorophore functionalized CB6 and acyclic CB6 receptor, respectively, for the detection of pharmaceutical amines (**Fig. 1.19b**) [176]. The fluorescent intensity of these two DBAs is quenched or amplified upon the capture of the pharmaceutical amines shown in **Fig. 1.19c** [176]. The analyte-induced quenching or amplification of fluorescent intensity of these two DBAs is caused the interplay among geometry, binding mode as well as binging strength. For instance, when the target drug molecule contains pyridine units, the fluorescence of DBAs will be quenched upon binding, and nitro group is also a functional group that is known to quench the fluorescence of the DBAs. On the other hand, if there is no functional unit in the target molecule, the fluorescence of the DBAs tends to be amplified, which could be rationalized by the increased rigidity of DBAs upon complexation with the target molecule. The binding affinities are thus relative to the magnitude of the amplification of the fluorescence and would provide indicative information for the molecular detections. Although the general performance of DBAs is pronounced from both quantitative and qualitative perspectives, the design and fabrication of DBAs are generally complicated. The functionalization of supramolecular receptor requires complicated fabrication steps limited its application potentials to an extent, leaving interests for the development of simple molecular detection assays.

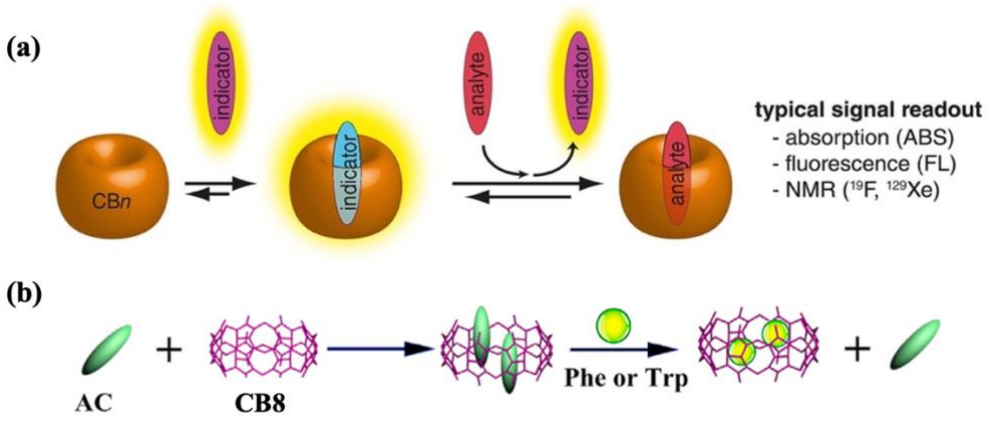

Fig. 1.20 (a) Working principle of indicator displacement assays (IDAs) [175]. Copyright 2018 Wiley-VCH. **(b)** The CB8-2AC based fluorescent IDA for amino acids recognition [165]. Copyright 2020 Elsevier.

Indicator displacement assays (IDAs) refer to the assays constructed by the encapsulation of an active indicator inside the supramolecular host and the indicator in IDAs is displaced by the analyte molecule via a competitive binding to generate a responsive signal [161-166,175,178-188]. The presence of IDAs enables the detection for molecules which are photophysical transparent and hard to be detected. Taking account of the working principle of IDAs, the binding constants between the host and indicator needs to be suitably selected, *i.e.* strong enough to form complex with host but less strong than the one of the target analytes with host. Meanwhile, the photophysical characteristics like the UV-vis absorption, fluorescent emission and NMR chemical shift, of the indicator are required to be distinctly different when it exist in its complexed and free form. Among diverse of supramolecular hosts, CBs stand out to construct the IDAs due to its desired binding capabilities and affinities towards a wide range of molecules. **Fig. 1.20a** demonstrates the general working principle of CBs-based IDAs. Loads of fluorescent CBs-based IDAs have been designed for molecular detection and the Nau group contributed predominantly to this filed. For example, Nau and co-workers have proposed a CB6 and dye indicator formed IDA for the detection of hydrocarbon gases, including alkanes, alkenes and acetylene [186]. Gaseous analytes were dissolved as saturated aqueous solutions to

be detected by CB6-dye IDA. In the presence of different gaseous analytes, the fluorescent of dye molecule was displaced to different magnitudes, giving rise to distinguishable quenching in the emission intensity of the dye indicator. Aino acids detection by the IDA based on CB8 and acridine hydrochloride fluorophore has been proposed by Xiao and co-workers [165]. The strong fluorescent acridine hydrochloride (AC) was found to form 1:2 inclusion complex with CB8, and its fluorescence intensity was largely quenched when upon the complexation, thus allowing the complex between CB8 and acridine hydrochloride to work as an IDA. In the presence of amino acids like phenylalanine and tryptophan, two AC molecules were displaced out of CB8 cavity and 1:2 inclusion complex between CB8 and the amino acid were formed instead, generating a responsive amplified fluorescence from the displaced free AC (**Fig.1.20b**).

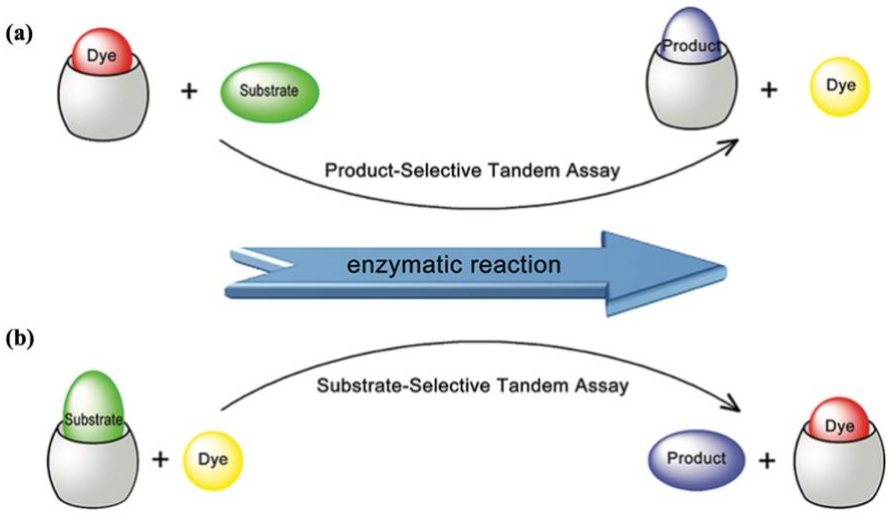

Fig. 1.21 The working principle of the IDA-based label-free enzyme assay [188]. Copyright 2009 American Chemical Society.

Apart from the simple molecule recognition, label-free enzyme sensing has also been achieved with the aid of supramolecular-based IDAs. A series of supramolecular tandem assay for the monitor of enzymatic reactions have been proposed by the Nau group [162, 181,187-189]. The concept of the label-free enzyme assay was inspired and developed based on the establishment of IDAs. The general working principle is based on the competitive binding between the indicator, enzymatic substrate, and the product of the enzymatic reaction (**Fig. 1.21**) and the accompanied photophysical changes of the indicator. In this case, the indicator needs to be selected more carefully, *i.e.* the binding constant between the indicator and supramolecular host should fall in the window defined by the complexes formed by the substrate and product of the enzymatic reaction. When the binding constant between supramolecular host and dye is stronger than that of enzymatic substrate but weaker than that of the product produced by the enzymatic reaction, supramolecular host preferably forms inclusion complex with dye indicator before the enzymatic reaction, while as the enzymatic reaction proceeding, the encapsulated dye molecule is displaced out of the cavity by the product of enzymatic reaction. This type of supramolecular enzyme assay can be regarded as the product-selective assay (**Fig. 1.21a**). On the other hand, the assay works as substrate-selective when the binding constants with the supramolecular host rank as substrate > dye indicator > the product of enzymatic reaction (**Fig. 1.21b)**. For example, the decarboxylase reactions of amino acids including lysine, histidine, arginine and ornithine were continuously monitored by the product-selective enzyme assay constructed by CB7 and fluorophore dapoxyl; in detail, the fluorescence of CB7 complexed dapoxyl is considerably stronger than uncomplexed dapoxyl. The dapoxyl was

displaced out of CB7 cavity by the amine products generated by the decarboxylation of amino acids, giving rise to the quenched fluorescence intensity [162].

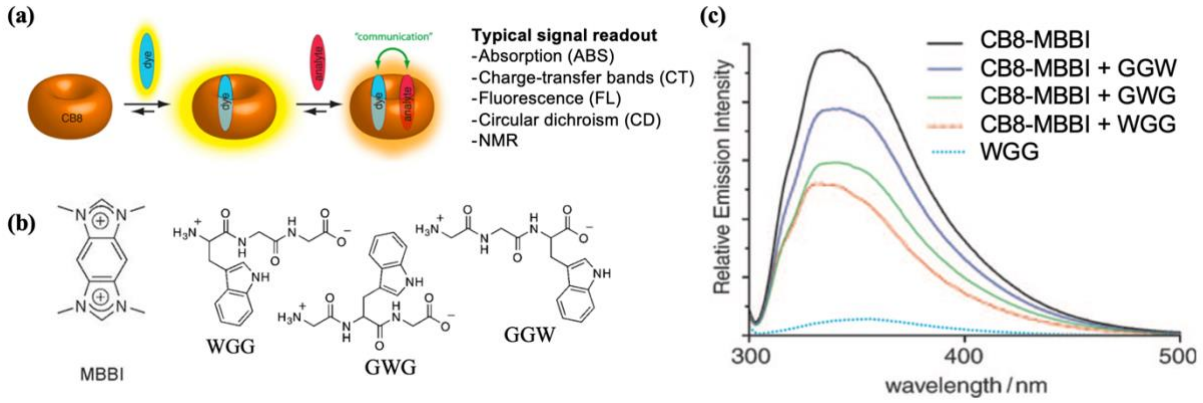

Fig. 1.22 (a) Working principle of associative binding assays (ABAs) [175]. Copyright 2018 Wiley-VCH. **(b)** Chemical structures of fluorescent MBBI dye and three different tripeptides: Trp-Glt-Gly (WGG), Gly-Trp-Gly (GWG) and Gly-Gly-Trp (GGW). **(c)** The fluorescent spectra of CB8-MBBI ABA in the absence and presence of three different peptides demonstrated in **(b)** and the fluorescent spectrum of free WGG [190]. Copyright 2010 Wiley-VCH.

Like IDAs, associative binding assays (ABAs) also based on the supramolecular pre-encapsulated indicator system, but instead of displacing the indicator out of the host cavity, the space left in the supramolecular receptor is still enough for the capture of the analyte molecule as ternary complexes to produce responsive signals [175,176,188,191-193]. Among CBs homologues, sensing strategy of ABAs mainly relies on CB8, whose cavity size is large enough to encapsulate two guest molecules, *e.g.* one indicator and one target analyte molecule, simultaneously. The general working principle of CB8-based ABAs is illustrated in **Fig. 1.22a**, where the inherently fluorescent dye molecule is accommodated by CB8 prior to the molecular detection to generate a responsive change in its fluorescent fingerprints towards the binding with the target analyte molecule. The interactions between the first and second guest molecules inside CB8, such as the charge-transfer between the electron-deficient cations and electron-rich aromatic guests, affording the unique properties which is beneficial for sensing of ABAs. Among diverse measuring techniques, spectroscopic methods, *e.g.* fluorescence and UV-vis spectroscopy, are most popular in ABAs. A series of different dye molecules like methylated diazaperoperylenium (MDPP), 2,7-dimethyldiazapyreninum (MDAP), 2,7-dimethyldiazaphenanthrenium (MDPT), tetramethyl benzobis(imidazolium) (MBBI) have been designed and fabricated to be readily assembly with CB8 as ABAs for molecular sensing [189,190,193,194]. For example, the self-assembled fluorescent ABA, CB8-MBBI, was proposed by Scherman and co-workers for the detection of tripeptides [190]. As shown in **Fig. 1.22b**, the fluorescence emission of CB8-MBBI ABA was quenched in the presence of tripeptides, and the magnitude of quenching is correlated to the binding constants between the peptides and CB8-MBBI, *i.e.* the stronger the binding between the tripeptide and CB8-MBBI, the larger the quenching magnitude of CB8-MBBI. Basically, the ABAs is akin to DBAs, but ABAs are easier to construct because no covalent functionalization step for inert supramolecular receptor is needed in ABAs. Moreover, the ABAs format perform the potential to differentiate different target analytes by the clearly distinguishable signals relying on the communications between the pre-encapsulated indicator and the target analyte inside CB8. However, in the case of IDAs, the signals generated by different analytes would be the same, *e.g.* change of fluorescent intensity. For example, the peptides can be distinguished from the tryptophan containing

molecules by CB8-MDPP ABA using spectroscopic spectra [85,189]. Furthermore, in comparison to IDAs, indicator displacement processes via competitive binding with analytes are not included in ABAs, thereby reducing the energy loss and enhancing the detection sensitivity of ABAs.

Although diverse supramolecular-based sensing assays have been developed, most of them can only work in single format, *e.g.* either as DBA or ABA or IDA, sensing assay that can integrate two working formats in one is still rare because the assay is normally designed based on one specific working theory, for example, IDAs are often established by designing a specific indicator molecules for strong target analyte molecules, while ABAs are often constructed with a reporter molecule possessing planar structural conformation together with a moderate binding affinity. Moreover, in concern with real-case applications, in-situ sensing in biologically relevant media, such as urine, serum and even animal blood, is of vast interests, especially in the case of point-of-care applications. Hence, simple design of supramolecular-based assay to be able to work as a multifunctional assay for in-situ biosensing in complex bio-media is of practical meanings to be explored.

1.9 Current biosensors for drug detection

Detection of small drug molecules are of particular interests for therapeutic and clinical applications and numerous sensing assays have been designed for drug molecular detection based on different principles, which nevertheless suffer from certain limitations from different perspectives. Sensors for biological, pharmaceutical and clinical applications are often required to be of high sensitivity, specificity, selectivity as well as matrix tolerance when operating in physiologically relevant matrices, *e.g.* urine, serum and blood. This section reviewed the existing sensors for the detection of small drug molecules which have been investigated in *Chapter 5*.

1.9.1 Adamantylamine detection

Adamantylamine (ADA), also known as amantadine, is a drug molecule used for the treatment of Parkinson disease and influenza in animals and human beings [195]. The mean daily dose of ADA and therapeutically relevant mean plasma concentration of ADA in humans were reported as 135.1±62.3 mg/day and 812.5±839.5 ng/ml (range, 91 – 4400 ng/ml), respectively [196]. Overdosing of ADA can result in a series of harmful effects in humans, *e.g.* drug resistance and neurotoxicity, which are likely to be related to jitteriness, anxiety, nightmares, and hallucinations [197]. Hence, an effective sensing assay for quantitative detection of ADA in physiologically biofluids is of certain clinical importance to avoid excessive use of ADA.

Diverse sensing strategies for ADA detection have been developed with the aid of different techniques, including electrochemistry [198,199], chromatography [195,200,201], NMR [202], immunology [203,204] and spectroscopy [205-211] The Lai group has proposed a competitive immunochromatographic assay for detection of amantadine in chicken muscle [212], achieving a limit of detection (LoD) of 1.80 ng/mL and a linear detection range from 2.5 ng/mL to 25 ng/mL. This study can only perform semi-quantitative analysis of ADA and appear to be limited for quantitative determination of ADA concentration. An electrochemical sensor was developed based on methylene blue (MB)/ β -cyclodextrin (β CD)/poly(N-acetylaniline) electrode by Hao *et al* [198]. The sensing signals were produced upon competitive host-guest complexation between ADA and MB with βCD immobilized on the electrode surface. This assay offers LoD of 0.09 mM in BR buffer, appearing not to be sensitive enough for clinically relevant applications. The Biederemann group has developed a fluorescent sensing assay for ADA detection based on the covalent CB7-indicator dye conjugates, which demonstrated desirable resistance to dilution and salt effects in biologically relevant buffered saline and even

in real urine [207]. The proposed sensor enabled selective and quantitative sensing of ADA in human urine and saline media, which could find future use in establish diagnostic laboratories or point-of-care testing (POCT). However, it should be noted that the design and establish of such CB7-dye conjugates as indicator displacement assay (IDA) for ADA quantitative determination required profound knowledge about supramolecular systems and certain chemical synthetic efforts, and moreover, the application in serum and blood media has not been explored by this assay [207].

1.9.2 Memantine detection

Memantine (MEM) is a drug utilized for the treatment of moderate-to-severe Alzheimer's disease, and the maximal therapeutically relevant plasma concentration of memantine in human was reported to be around 1 μM [213]. Excessive using of MEM may lead to convulsions or serious side effects on patient's hear and breathing. Sensing assays for MEM detection are virtually absent in the literature. MEM cannot be directly monitored by spectrophotometric technique as it has tricyclic saturated ring structure and does not have adequate light absorption. Sensing methodologies for MEM in physiologically relevant matrices, such as human plasma [214], rat plasma [215] and urine [216] have been published by using high-performance liquid chromatographic (HPLC). However, pre-column derivatization step was required in all these literatures [214-216]. Sinn *et al*. proposed a CB8-dye based indicator displacement fluorescent assay, allowing for in-situ MEM detection in blood serum [159]. Considering the ultra-strong binding between CB8 and MEM, a new dye molecule, *e.g.* methyl-pyridinium-paracyclophan, whose binding affinity with CB8 is significantly high (log$K$ = 12.59 in DI water), has been designed and fabricated as indicator in this paper to achieve the sensing of MEM. According to the present research regarding MEM detection in biofluids, it is still demanding to develop a simple and effective methodology without the need of complicated pre-treatment steps and chemical synthetic procedures.

1.9.3 Rimantadine detection

Rimantadine (RMD) is an oral antiviral drug utilized to prevent or treat influenzavirus A infections in humans. It has been reported that the safety dose of RMD is 3 mg/kg/day in human, and the corresponding steady-state peak serum concentration of RMD was measured as 100 to 574 ng/ml and time to achieve peak concentration ranged from 2.5 to 6.0 h after the doses [217]. The unwanted adverse effects caused by overdosing of RMD appear to be more serious in elderly patients, including dizziness, vomiting, stomach pain, anxiety, nausea, *etc*, therefore additional caution is required for elderly people [218]. Hence, quantitative determination of RMD in plasma to adjust the dose regime and prevent overdosing is of clinical importance. Several literatures have been published regarding RMD investigation in animal food, chicken muscle, rat plasma and human plasma [219-222], involved with liquid chromatographic technique requiring multiple pre-treatment steps, such as pre-column derivatization and sample clean-up procedures, resulting in complicated sensing procedures. Thus, simple method for quantitative analysis of RMD in biofluids still needs further exploring.

1.9.4 Procaine hydrochloride detection

Procaine hydrochloride (PC) is a salt form of procaine with local anaesthetic and antiarrhythmic properties. It is normally utilized in dental operation to nub the area around the tooth and is also for pain reduction caused by intramuscular injection of penicillin. When it is used as local anaesthetics for human, its dosage ranged from 600 to 1000 mg [223]. The systemic analgesia can be achieved in humans after injection of 100 to 800 mg of PC [223]. Respiratory failure and cardiac arrest can arise from the overdosing PC. Diverse methodologies have been developed for quantitative detection of PC, including electrochemistry [224], gas

chromatography-mass spectrometry (GS-MS) [225], surface-enhanced Raman spectroscopy (SERS) [226,227], chemiluminescence [228], spectrophotometry [229], colorimetry [230] and high-performance liquid chromatography (HPLC) [231]. Nevertheless, most of precedent research are limited the detection media to water, acidic, or buffer solution, molecular recognition of PC in complex biologically relevant matrices like urine and serum, which are common to be involved in clinical applications, have been rarely reported. Ohshima *et al*. has developed a sensing strategy for PC in human plasma and urine by GS-MS, which requires solid-state extraction procedure and measured the recovery rates of PC spiked sample but not directly determined extract concentration of PC [225]. Therefore, an effective scheme for quantitative determination of PC in clinically relevant bio-matrices remains attractive to be explored.

1.9.5 Tryptophan detection

Tryptophan (TYP) is a type of essential amino acid in humans, working for normal growth in infants. TYP also works as a building block in body's proteins, and a precursor to neurotransmitters, hormone melatonin and vitamin B3 [232]. The normal concentration range of in human plasma is 50–100 μM [232]. It has been reported that the abnormal blood levels of TYP can cause schizophrenia and autism [233], and the excessive TYP can give rise to various metabolites, some of which may inhibit the decomposition of histamine. Thus, facile way to quantitatively detect TYP is in vast need in the fields of clinical medicine, food and livestock feed. Diverse schemes for TYP detection in bio-media have been designed so far, including fluorescence [234,235], electrochemistry [233,236], high-performance liquid chromatography (HPLC) [237], gas chromatography-mass spectrometry (GS-MS) [238], surface-enhanced Raman spectroscopy (SERS) [239], *etc*. Some of these measurements, *e.g.* HPLC [237] and GS-MS [238], require elaborate and expensive instruments, multiple kinds of regents, complicated sample preparation steps, pre-treatment procedures, resulting in limitations in their real applications. Some of measurements are involved with sophisticated molecular design and laborious fabrication steps, such as dye molecule for fluorescent sensors [234,235] and chemically modified working electrode for electrochemical sensors [233,236]. Hence, a simple procedure for TYP detection in complex biologically relevant matrices with desired sensing performance is demanding, especially for practical applications, *e.g.* clinical and diagnostic detection.

1.9.6 Tacrine detection

Tacrine (TR) has been clinically utilized for treatment and management of Alzheimer's disease by acting as acetylcholinesterase inhibitor to prolong its activity and enhancing its concentration in cerebral cortex. As studied, a mean average steady-state concentration in plasma ranging from 1.1 to 30 ng/ml was obtained with doses ranging from 40 to 160 mg of tacrine daily [239]. Side effects of TR occur frequently, and its blood concentration is valuable in predicting the development of the side effects and its measurement may optimize the dosage of the drug [240]. A certain number of studies have been implemented for TR detection [241-243]; nevertheless, more research was made for monitoring the inhibition and activation of acetylcholinesterase [244-247]. Aparico *et al*. developed a spectrofluorimetric determination strategy for TR, allowing for a detection range of 1 – 70 ng/mL in aqueous buffer solution [242]. The Guo group has proposed a colorimetric methodology for TR detection based on molybdenum dichalcogenides nanoparticles as peroxidase mimetics [243]. The presence of acetylcholinesterase inhibitor TR could be detected by the decrease in the amount of thiocholine generated by the hydrolysis of acetylthiocholine chloride catalysed by acetylcholinesterase [243]. Although, this scheme uncovered a relationship between the observed signal and the concentration of TR, multiple reaction processes, such as the the oxidation of 3,30,5,50-tetrametylbenzidine and the hydrolysis of acetylthiocholine chloride, were involved, making the sensing route complicated and may produce accumulative error in the result. In

terms of acetylcholinesterase monitoring, colorimetric technique was utilized most widely [244-247]. For example, the Chen group has established an acetylcholinesterase assay using oxidase-like activity of 2D palladium square nanoplates growing on reduced graphene oxide [244]; the Luo group has established an enzyme colorimetric cellulose membrane bioactivity strip for sensing and screening of acetylcholinesterase inhibitors [245]; the Lu group has developed a colorimetric detection method using Pt nanoparticles and N-doped graphene as nano-enzymes [246]. All these studies were involved enzyme catalysed reactions, which could result in slow and complicated sensing procedure. Therefore, a straightforward, simple, facile, rapid detection scheme for TR in biologically matrices is still in great needs.

1.10 Motivations

Supramolecular electrochemistry has attracted and keeps attracting extensive interest in diverse fields, such as reaction activity modulation [67], molecular detection [46-49], dynamic molecular machines [76,129,131,133], catalysis [248,249], *etc*, by taking advantage of the combination of unique properties provided by host-guest interactions and rich thermodynamic and kinetic information obtained by electrochemical techniques.

Binding constant is an important indicator to quantitatively determine the strength of host-guest interactions in the field of supramolecular chemistry, effectively providing instructive guidance to design supramolecular systems catering for different applications [134]. However, the existing methodologies for binding constant determination suffer from inherent shortcomings, including loads of repeated experimental steps, specific solubility requirements for analytes, complicated data analysis procedures, and required bulky instruments, *etc* [135]. Furthermore, binding constant estimation in complex physiologically relevant media (*e.g.* urine, serum and blood) remains extremely challenging and unexplored. Hence, approach that can determine binding constants either rapidly in high-throughput fashion or in complex bio-media appears considerably attractive.

Sensitive and selective molecular detection based on supramolecular chemistry have been and are continuously of extensive research interests due to its outstanding sensing properties and promising practical meanings, such as environment pollutant monitoring [25], drug molecules sensing [47,164,191,194,250], explosives detection [46] and so on. Although multiple supramolecular-based sensing assays have been designed, biosensing in physiologically most relevant media, such as urine, serum and even animal blood is still largely limited because the complex mixture of substances presented in these media can cause strong interferent signals and undergo competitive binding with target analytes. Thus, designing a powerful sensing assay providing desired sensing features, wide applicability, simple measuring equipment and workability in complex physiologically relevant media is of both scientific and practical meanings. Moreover, modulation of reactivity is also of interests in the field of supramolecular electrochemistry, while the precedent studies are mainly limited to viologen-derived and ferrocene-derived redox active species, leaving a space to be further investigated.

Herein, electrochemical properties of tens of inclusion complexes were measured to explore the correlation between their binding constants and electrochemical features and the potential of rapid binding constant estimation. In addition, electrochemical titration measurements based on supramolecular assay were performed to uncover new possibilities of binding constant estimation as well as biosensing in complex matrices. In concern with electroanalytical application, reaction modulation effect of supramolecular host was studied to widen the current application scope of supramolecular-based reactivity modulation.

1.11 Research objectives

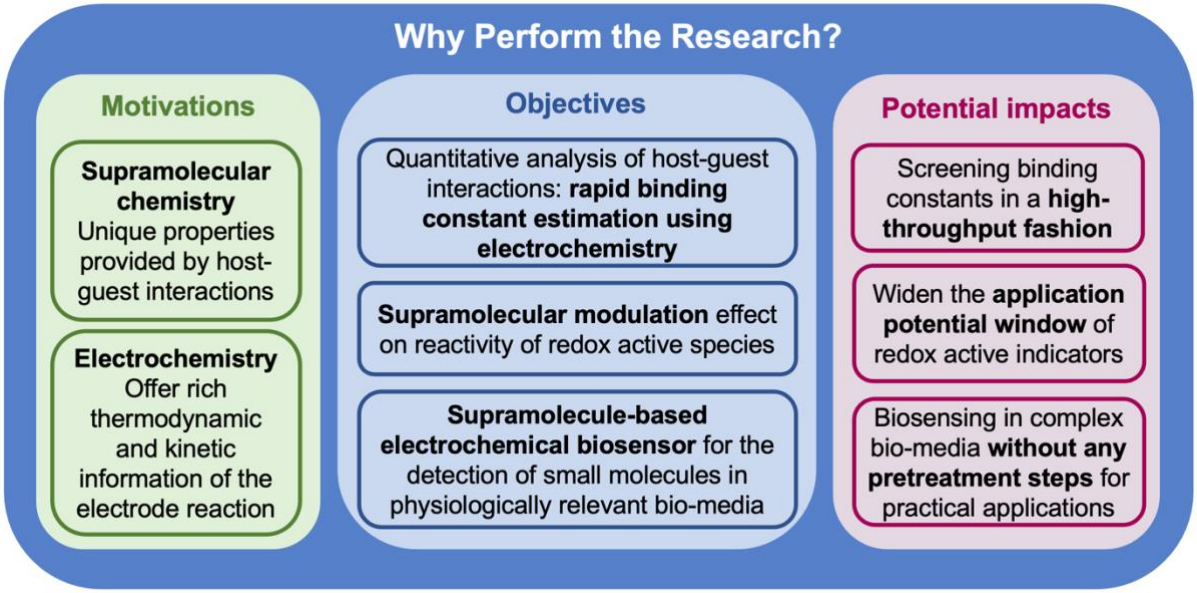

Fig. 1.23 Research motivations, objectives and potential impacts.

As illustrated in **Fig. 1.23**, this research was motivated by the promising application potentials of supramolecular chemistry and information-rich data set of electrochemistry to combine these two disciplines as supramolecular electrochemistry for new application possibilities in the fields of analytical chemistry and electrochemical (bio)sensing. The major objectives of this research are listed as below:

- To investigate the host-guest complexation processes qualitatively and quantitatively between CB*n* and a wide range of guest molecules via experimental and computational approaches, such as target analytes and electrochemical active probes.
- To monitor how complexation will influence electrochemical properties of redox active guest molecule via electrochemical techniques.
- To develop rapid electrochemical strategy for quantitative analysis of host-guest interactions, allowing for screening host-guest complexes based on binding constant in a high-throughput fashion.
- To explore bio-sensing and binding constant determination application potentials in complex bio-media of host-guest system by designing electrochemical assay based on CB8 and redox active probe.

1.12 Thesis structure

Chapter 1 summarized the research motivations, hypotheses, and objectives after reviewing precedent development and current stage of a series of relevant fields, including the supramolecular hosts, synthesis methodologies and fundamental properties of CBs, host-guest chemistry, basics of typical electrochemical techniques, supramolecular-based electrochemistry, basics of binding constants, current binding constants determination methods, current biosensors for drug detection, and supramolecular-based molecular detection.

Chapter 2 introduced all materials, equipment, parameters for measurements as well as the sample preparation protocols involved in this research. Meanwhile, Chapter 2 also provided detail descriptions regarding the computational simulations for the optimization of molecular models of free guest molecules and inclusion host-guest complexes.

Chapter 3 explored how electrochemical reactivity of a redox probe, *e.g.* resazurin ($[RZ\text{-}H]^{-}$), can be modulated by changing the subtle microenvironment around it via host-guest

complexation with CB*n* (*n* = 7, 8) hosts of different sizes. In particular, the irreversible reduction process of RZ was found to be oppositely modulated in the presence of 1 equivalent of CB7 and CB8. This opposite modulation was hypothesised to be due to the different cavity sizes and tightness of host-guest encapsulation in the cases of CB7 and CB8. The explored activity modulation abilities of rigid CB7 and CB8 hosts would spark the investigations of supramolecular modulation for other redox processes.

Inspired by the findings in *Chapter 3*, *Chapter 4* investigated the electrochemical reactivity modulation of a pre-encapsulated redox probe, *e.g.* MV^{2+}, inside a CB8 cavity via further complexation with a second guest molecule (G2). Notably, we have uncovered fundamental correlation between the reactivity and the host-guest binding constant of G2, which allows us to rapidly determine binding constants of unseen G2 via a single electrochemical measurement. The mechanistic investigations based on the convergence of experimental results and computational simulations suggested that the correlation is resulted from the dynamic host-guest association/disassociation events taking place after the electron transfer step in electrochemical reduction. In addition to the soluble G2 molecules, the estimation of binding constants for G2 with poor aqueous solubilities such as organic hydrocarbons were also tested by this electrochemical scheme.

Based on the supramolecular electrochemical system developed in *Chapter 4*, *Chapter 5* exploited its potential application in ultrasensitive quantification of drugs in complex bio-media, and binding constant determination in situ. Specifically, CB8 and redox active MV^{2+} were employed as the supramolecular host and electrochemical reporter, respectively. The spacious cavity of CB8 that allows for simultaneous accommodation of two molecules and the clearly distinguishable electrochemical behaviours of complexed and uncomplexed MV^{2+} enabled self-assembly CB8-MV^{2+} to perform in a dual-functional fashion, *i.e.* CB8-MV^{2+} can either work as an associative binding assay (ABA) by the formation of CB8-MV^{2+}-based ternary complexes with analyte molecule or served as an indicator displacement assay (IDA) for analytes which can strongly bind with CB8. This assay showed extensive applicability in detecting diverse spectroscopically silent and electrochemically inactive biomolecules in complex bio-media, ranging from synthetic urine, serum to animal blood, and more surprisingly, the binding constants of corresponding CB8-based complexes can be simultaneously estimated.

Chapter 6 concluded the research outcomes and discussed potential following-up work that can be done to promote the further development in the aera of supramolecular electrochemistry.

Chapter 2. Materials and methods

2.1 Materials

CB7 and CB8 were synthesized and purified by members of the Lee group, and the corresponding protocol was described in *Chapter 1.3*. All other chemicals were at analytical grade and used directly after received without any further treatments. Methyl viologen dichloride hydrate (98%), sodium phosphate monobasic dihydrate, procaine hydrochloride, penicillin G sodium salt, indole, 2-naphthol, 6-methoxy-2-naphthol, 2,3-dihydroxynaphthalene, 2,7-dihydroxynaphthalene, 1,5-dihydroxynaphthalene, 1,6-dihydroxynaphthalene, 2-chlorophenol, 3-chlorophenol, 4-chlorophenol, tryptophan, phenol, sesamol,2-methoxyphenol, pyrocatechol, 4-bromophenol, 4-fluorophenol, 3-methoxyphenol, resorcinol, 40methoxyphenol, hydroquinone, 4-cyanophenol, 2-hydroxybenzoitirle, phloroglucinol, urea, citric acid, uric acid, creatinine and albumin were purchased from Sigma Aldrich (America). Potassium chloride was ordered from Emsure. Sodium chloride was bought from VWR (America). β-cyclodextrin (βCD), γ-cyclodextrin (γCD), 1-adamantylamine and sodium phosphate dibasic heptahydrate, resazurin, boric acid and phosphoric acid were bought from Aladdin. 1,7-dihydroxynaphthalene and sodium phosphate dibasic heptahydrate were obtained from Alfa Aesar (UK) and Fisher Scientific (America), respectively. Tacrine was obtained from Bidepharm (China). Acetic acid and sodium hydroxide were bought from SCR (China). Resorufin was ordered from TCl company (China). Rivastigmine and rimantadine were purchased from Generon supplier (UK). Memantine hydrochloride was purchased from Stratech Scientific Ltd (UK).

2.2 Synthesis and purification of CB7 and CB8

CB7 and the mixture of CB6 and CB8 were synthesized and purified by Mr. Alvaro Castillo Bonillo. CB8 was isolated from the mixture by me.

All fabrication and purification steps were performed according to the procedure proposed by Isaacs as illustrated in *Chapter 1.3* [33,34]. In detail, CB*n* mixture was fabricated via the reaction between glycoluril and paraformaldehyde in the ice-cold concentrated HCl solution. The mixture was heated at 80 ºC for 5 hours and then heated up to 100 ºC for 14 hours.

The obtained mixture was cooled down to the room temperature and evaporated to a minimum volume to form slurry for purification. The slurry was poured into distilled water with 1:4 volume ratio and the **Crop 1** contained CB5-8, CB10 was collected via filtration.

Crop 1 was stirring in a backer of water with volume ratio of 1/10 and filtrated to collect the **Mixture 1** of CB6, CB8, CB10. The supernatant was then poured into methanol to obtain **Mixture 2** of CB5, CB7 by filtration.

CB8 was obtained by stirring **Mixture 1** in a backer with 3 M HCl and filtration. This step was repeated for at least 4 times to ensure CB6 and CB10 are removed thoroughly. Then, pure CB8 was acquired via recrystallization in warm concentrated HCl and dried in the ambient environment with a porous parafilm covered.

To eliminate potential CB6 residues in **Mixture 2**, it was dissolved in H_2O and poured into methanol until the pH of solution reaches pH >5. CB7 solid was isolated by stirring the resultant solution in 1:1 methanol: H_2O and filtration. Pure CB7 was obtained by dissolving the isolated CB7 into water and recrystallization by slow acetone addition.

The purity of the obtained CB7 and CB8 sample was checked by performing ^{1}H NMR tests periodically after purification steps. If the obtained CB7 and CB8 are not pure enough,

purification procedures described in the previous two paragraphs will be repeated until the purity meet the requirement.

2.3 Electrolyte preparation

50 mL of 6.25 mM phosphate buffer (PB) solution (pH 7) was obtained by mixing 38 mL of sodium phosphate dibasic heptahydrate ($Na_2HPO_4 \cdot 7H_2O$) stock solution and 12 mL sodium phosphate monobasic dihydrate ($NaH_2PO_4 \cdot 2H_2O$) stock solution. In detail, 1419.6 mg of $Na_2HPO_4 \cdot 7H_2O$ and 1199.8 mg of $NaH_2PO_4 \cdot 2H_2O$ powder were dissolved into 50 mL distilled water, respectively, as concentrated stock solution. 2.5 mL of the obtained two concentrated stock solution were diluted to 50 mL by distilled water as stock solutions to be utilized for 6.25 mM PB solution prepration.

Britton-Robinson (BR) buffer (pH 7) was prepared with 0.04 M boric acid, 0.04 M phosphoric acid, 0.04 M acetic acid and 0.2 M NaOH. Specific amount of 0.2 M NaOH was added into the 0.04 M acidic mixture (boric acid, phosphoric acid and acetic acid) until the pH of the solution reaching 7, which was measured by pH meter.

Synthetic urine was prepared by adding 500 mg of urea, 260 mg of NaCl, 240 mg of NaH_2PO_4, 225 mg of KCl, 40 mg of creatinine, 20 mg of citric acid, 8 mg of uric acid and 2.5 mg of albumin into 50 mL distilled water.

Fetal bovine serum (FBS) and human serum (HS) were bought from Sigma Aldrich. Defibrinated sheep blood (SB) and horse blood (HS) were purchased from Fisher Scientific. FBS, HS, SB and HB were used as obtained for electrochemical measurements without any additional treatments such as deproteinization.

2.4 ^{1}H NMR spectroscopy

All ^{1}H NMR spectra were recorded by Bruker Avance III 400 MHz instrument at room temperature. All samples for ^{1}H NMR measurement were prepared at 1 mM in deuterium oxide (D_2O) unless stated otherwise. ^{1}H NMR tubes were cleaned by ethanol, isopropanol, acetone and distilled water for 3 times with the aid of ultrasonic bath and dried in vacuum oven prior to the new measurement to ensure no residues from previous sample was left in the tubes.

2.5 Computational simulations

Computational simulations were performed to obtain the insights into the complexation between host and guest molecules. The binding energy of a host-guest complex was calculated by the energy obtained at the same level of theory.

2.5.1 Optimization of molecular models

Molecular models of free guest molecules and their corresponding host-guest inclusion complexes formed with CB*n* were optimized by MMFF94 in Chem3D before the full density functional theory (DFT) minimization at wB97XD/6-31G* and CPCM/wB97XD/6-31G* level of theory using Gaussian 09. CPCM implicit water model was utilized to appropriate the solvation effects presented in electrochemical measurements which were carried out in aqueous condition.

2.5.2 Ab initio molecular dynamics

All experiments introduced in this section were done by Dr. Hugues Lambert. CP2K software was employed for the PM6-D3 semiempirical DFT model with time step of 1 fs in vacuum [251,252]. Systems were held for 10 ps to equilibrate with a CSVR thermostat within the NVT block with a time constant and temperature of 100 fs and 300 K, respectively. The

thermostat was removed after the equilibration, and then the system transmitted for 30 ps within the NVT block.

The charge and multiplicity for $MV^{+\bullet}$-involved and MV^{2+}-involved complexes were set as 1, 2 and 2,1, respectively. The entropy and energy were obtained from 30 ps trajectories for the ternary complexes studied in *Chapter 4*. The conservation of energy from the trajectory was improved by utilizing ASPC extrapolation approach [253]. The average energy for each sample was collected from the average value of the potential energy for the sample at every 10 times step. With the spectrally differentiate evaluating of entropy, the configurational entropy for each sample was obtained. All configurations obtained by trajectory were RMSD aligned with Open Babel before computing the power spectrum of the Cartesian coordinates of the atoms, which was finally utilized for the integration of the configurational entropy value [254]. To calculate the Gibbs free energy, the translational and rotational entropy were computed using Gaussian 16.

2.6 UV-visible spectroscopy

UV-vis absorption spectra in *Chapter 3* were collected by an Ocean Optics Flame spectrophotometer at room temperature. The cuvette with 1 cm of path and DH-mini light source were utilized for all measurements. Integration time, scans to average and boxcar width were set as 10 ms, 300 and 3, respectively in all measurements. Samples in *Chapter 3* for Job's plots measurements and pK_a titration were prepared in 2 mM PB solution (pH 7) and BR buffer, respectively.

2.7 Fluorescence spectroscopy

Fluorescence titration spectra were recorded by an Ocean Optics Flame spectrophotometer with 533-nm LED (1.96 mW) as excitation using cuvette with 1 cm of path to contain samples at room temperature. 5 s of integration time, 3 of scans to average and 10 of boxcar width were utilized for all measurements. Titration experiments were performed by successively dropping small amount of host solution into the guest stock solution, whose concentration was kept almost unchanged over the entire titration. 2 mM of PB solution (pH 7) was utilized as the solvent for sample preparation.

2.8 Electrochemical measurements

All cyclic voltammetry (CV) and square wave voltammetry (SWV) measurements discussed were carried out on Gamry Interface 1010E potentiostat. All measurements were performed using a three-electrode setup in a 50 mL electrochemical cell, consisting of (1) WE: glassy carbon electrode (GCE, d = 3 mm) in *Chapter 3* or gold disk working electrode (d = 2 mm) in *Chapter 4* and *Chapter 5*, (2) RE: leakless Ag/AgCl electrode (d = 5 mm) and (3) CE: platinum plate counter electrode (6.5 × 6.5 mm). All of electrodes were immersed into aqueous electrolyte and connected to the Potentiostat. Samples for electrochemical measurements were prepared by dissolving specific amount of the target analytes in 30 mL of electrolyte solution in 50 mL centrifuge tube, which were put in ultrasonic bath for hours before transferred to the electrochemical cell for measurements. Prior to each measurement, the sample solution was purged with nitrogen gas for more than 10 minutes to remove the dissolved oxygen in the solution.

Electrochemical measurements in *Chapter 3* were done in Britton-Robinson (BR) buffer solution at pH of 7.0. BR buffer solution was prepared by adjusting the pH of 0.04 M solution of boric acid, acetic acid, and phosphoric acid by 0.2 M NaOH.

6.25 mM sodium phosphate buffer (PB) solution at pH of 7.0 were utilized as the electrolyte for electrochemical measurements discussed in *Chapter 4* and *Chapter 5*, which was prepared with sodium phosphate monobasic dihydrate and sodium phosphate dibasic heptahydrate.

2.8.1 Cyclic voltammetry

All CV curves demonstrated in *Chapter 3* were recorded by sweeping the potential from 300 mV to -400 mV for 5 cycles at scan rate of 10 mV/s with step size of 1 mV.

All CV curves displayed in *Chapter 4* were obtained by cycling the potential from -200 mV to -800 mV for 5 cycles at various scan rates of 10, 20, 50 or 100 mV/s with step size of 2 mV.

2.8.2 Square wave voltammetry

All SWV measurements were performed by setting pulse size and frequency as 25 mV and 5 Hz, respectively. Equilibrium time was set as 15 s in all cases. The exact step size and potential range were introduced separately as followings.

In *Chapter 3*, SWV curves were collected with the potential ranging from 300 mV to -400 mV with 1 mV of step size.

In *Chapter 4*, SWV experiments discussed were performed by sweeping the potential from 0 mV to -800 mV with 2 mV of step size.

In *Chapter 5*, all SWV titration measurements were collected by sweeping the potential from -200 mV to -700 mV with 2 mV of step size. Parameters for SWV measurements to determine the binding constants of ternary complexes were the same as that in *Chapter 4*.

Chapter 3. Modulation of electrochemical activity of resazurin by controlling the tightness of host-guest encapsulation in aqueous media

This Chapter investigated the formation of host-guest complexes between resazurin (RZ) and a series of synthetic receptors, including cucurbit[7]uril (CB7), cucurbit[8]uril (CB8), β-cyclodexitrin (βCD) and γ-cyclodextrin (γCD) from both qualitative and quantitative perspectives by ^{1}H NMR spectroscopy, UV-vis titration and computational simulations. Gratifying to find that a reverse modulation effect on the electrochemical reactivity of resazurin (in deprotonated form of [RZ-H]$^-$ at neutral pH) was achieved upon the complexation with rigid CB7 and CB8, which was rationalized by the fact that different cavity volume that can either facilitate or disfavour water molecules to approach the reaction centre on [RZ-H]$^-$ for reduction. Nevertheless, unlike CB7 and CB8, no similar modulation effect has been observed in the case of βCD and γCD although their cavity sizes are comparable to that of CB7 and CB8, respectively, highlighting the importance of cavity rigidity of host.

3.1 Introduction

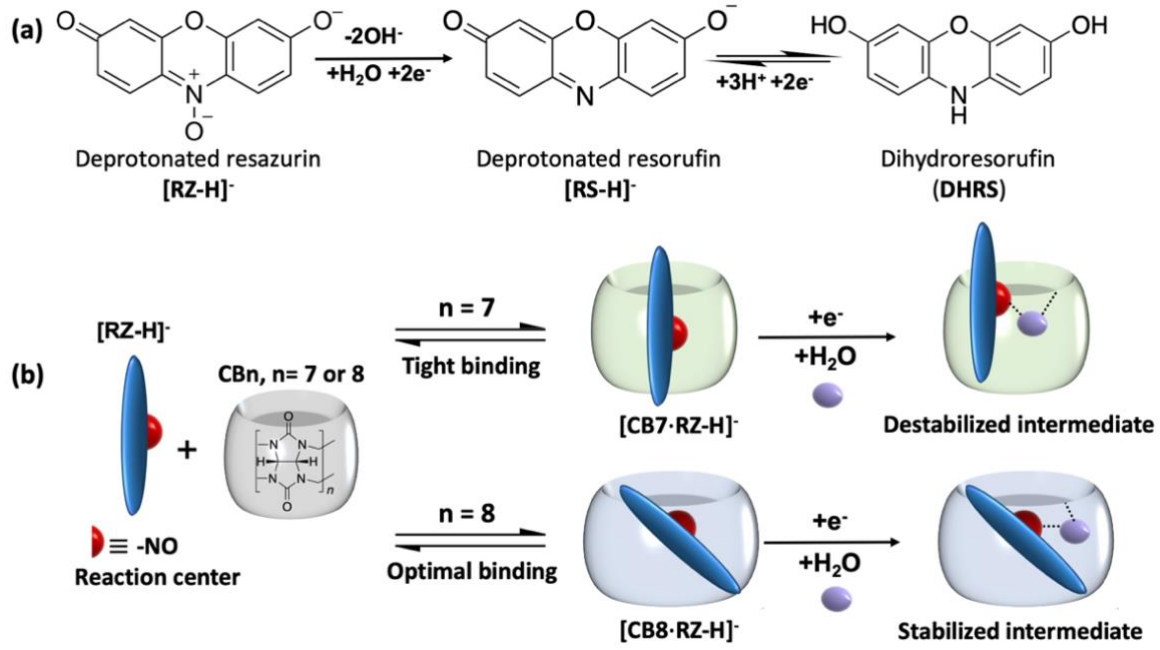

Fig. 3.1 (a) The two-step reduction processes of deprotonated resazurin ([RZ-H]$^-$) at neutral pH (7.0). **(b)** Schematic representation of the complexation between [RZ-H]$^-$ and CB7/CB8 with different binding tightness and the corresponding intermediate generated upon reduction.

Resazurin (RZ) is a weak fluorescent dye molecule that is biologically compatible and redox active, thus being extensively applied in trace detection in biological field, such as determining cell cytotoxicity [255,256], investigating bacteria contamination [257], studying cell proliferation [258,259], testing antibiotic susceptibility [260]. What render RZ numerous applications in biologically trace sensing is its changes in visible colour and fluorescent intensity happened in the course of two-step reduction process, *i.e.* the weak fluorescent purple RZ can be irreversibly reduced to strong fluorescent pink resorufin (RS), and then a non-fluorescent transparent dihydro-resorufin (DHRS) can be generated via a followed reversible reduction process (**Fig. 3.1a**) [261]. On account of the importance of the redox property for RZ to be utilized in practical applications, the modulation of its reduction reactivity, which has not yet been explored, is thus of great meaning.

CB*n* (*n* = 5-8, 10) are a family of synthetic macrocycles consisting of electronegative carbonyl-lined portals and hydrophobic well-defined cavities, enabling superior binding strength and selectivity via ion-dipole interaction and hydrophobic effect for host-guest complexation compared to the analogous synthetic receptor of cyclodextrins (CDs). Hence, the application potentials of CB*n* have been extensively exploited, such as explosive and crime detection [46,136,250], food safety inspection [262], environmental pollutants monitoring [208], drug delivery [53] and so on.

Among CB*n* homologues, CB7 and CB8 are most prevalent in aqueous-based scenarios, such as electrochemical measurement cell and biologically relevant system, due to their desire water solubility and biocompatibility [67,94,95,117,263,264]. It has been explored that the reactivity of redox active guest can be modulated upon complexation by taking advantage of the different microenvironment inside cavity of CB*n* compared to the bulk solution. For example, The Kaifer group and the Kim group have proposed that the electrochemical behaviours of MV^{2+} can be modulated upon complexation with CB7 and CB8 [94,95,117,263]. In detail, the formation of CB7-MV^{2+} can de-activate the reduction of MV^{2+} due to the preferable stabilization of CB7 for more positively charged MV^{2+} than the reduction product. On the hand, the first reversible electrochemical reduction process of MV^{2+} was found to be activated when it binds to CB8, which is attributed to the formation of stable 1:2 complex between CB8 and the reduction intermediate of MV^{2+}. Nevertheless, the activation based on such dimerization requires the generation of highly polarizable aromatic intermediate radical (*e.g.* $MV^{+\bullet}$), which is quite rare. As a result, the precedent research regarding CB*n*-based modulation effect on the electrochemical reactivity is mainly limited to viologen derived molecules.

Herein, the host-guest complexation between RZ and a variety of hosts, including CB7, CB8, βCD and γCD, were investigated and compared. Quantitative analysis of the binding behaviours of complexes were done by fluorescent and UV-vis spectroscopies, and was visually supported by energy-minimized molecular models obtained by computational simulations. Gratifying to note that a reverse modulation effect on RZ (in its deprotonated form in neutral pH, annotated as $[RZ\text{-}H]^-$) was discovered upon complexation with CB7 and CB8, *i.e.* CB7 demonstrated de-activation effect on the irreversible reduction process of $[RZ\text{-}H]^-$ while CB8 active it. Nevertheless, no significant modulation effect was observed in the cases of flexible βCD and γCD hosts, indicating the pronounced role of cavity rigidity in modulation. The reverse modulation effect of CB7 and CB8 was evidenced by the opposite reduction peak potential shift observed by cyclic voltammetry (CV) and square wave voltammetry (SWV), *i.e.* the reduction peak potential of $[RZ\text{-}H]^-$ negatively shifted by -54 mV when it binds to CB7 while positively shifted by +37 mV in the presence of CB8 observed by CV. According to computational simulations, the supramolecular modulation could be rooted from the ease for water molecules to approach the reaction centre on $[RZ\text{-}H]^-$, *e.g.* the -NO group, as illustrated in **Fig. 3.1b**. The proposed reverse modulation effect on electrochemical reactivity of guest molecule based on the binding tightness is expected to open up a pathway in the area of supramolecular electrochemistry for the investigation of other proton transfer involved electrochemical processes.

3.2 Complexation between $[RZ\text{-}H]^-$ and CB7/CB8

After qualitatively determining the formation of complex between RZ and CB7/CB8, the quantitative analysis regarding their thermodynamic stability represented by binding constants were achieved via fluorescence titration experiments. Fluorescence spectra of RZ in 2 mM PB solution at neutral pH, where RZ mainly exists in the deprotonated form ($[RZ\text{-}H]^-$, $pK_{a,RZ}$ = 5.76, **Fig. 3.2**) and at which we later observed the most effective modulation effects in electrochemistry, upon successive addition of CB7/CB8 were recorded and the major

emission peak at 583 nm was suppressed upon complexation (**Fig. 3.3 a-b**). It is noted that the observed spectral depression with addition of CB is not owing to the p*K*a shift effect of CB as evidenced by the pK_a titration in **Fig. 3.2**. The binding constant of [CB7•RZ-H]$^-$ and [CB7•RZ-H]$^-$ were determined as 2.38×10^8 M^{-1} and 3.16×10^5 M^{-1}, respectively, by fitting the Fluorescence titration results into 1:1 fitting model. To confirm the binding stoichiometry of between [RZ-H]$^-$ and CB7/CB8, Job plots of [CB7•RZ-H]$^-$ and [CB8·RZ-H]$^-$ were obtained by continuous variation method, *i.e.* performing UV-vis experiments at fixed concentration sum of [RZ-H]$^-$ and CB7/CB8 (**Fig. 3.4a-b**). As depicted in **Fig. 3.4c-d**, the maximum value appeared when the percentage of host (CB7 and CB8) was 0.5, verifying that the ratios between CB7/CB8 host and [RZ-H]$^-$ guest in complex are 1:1.

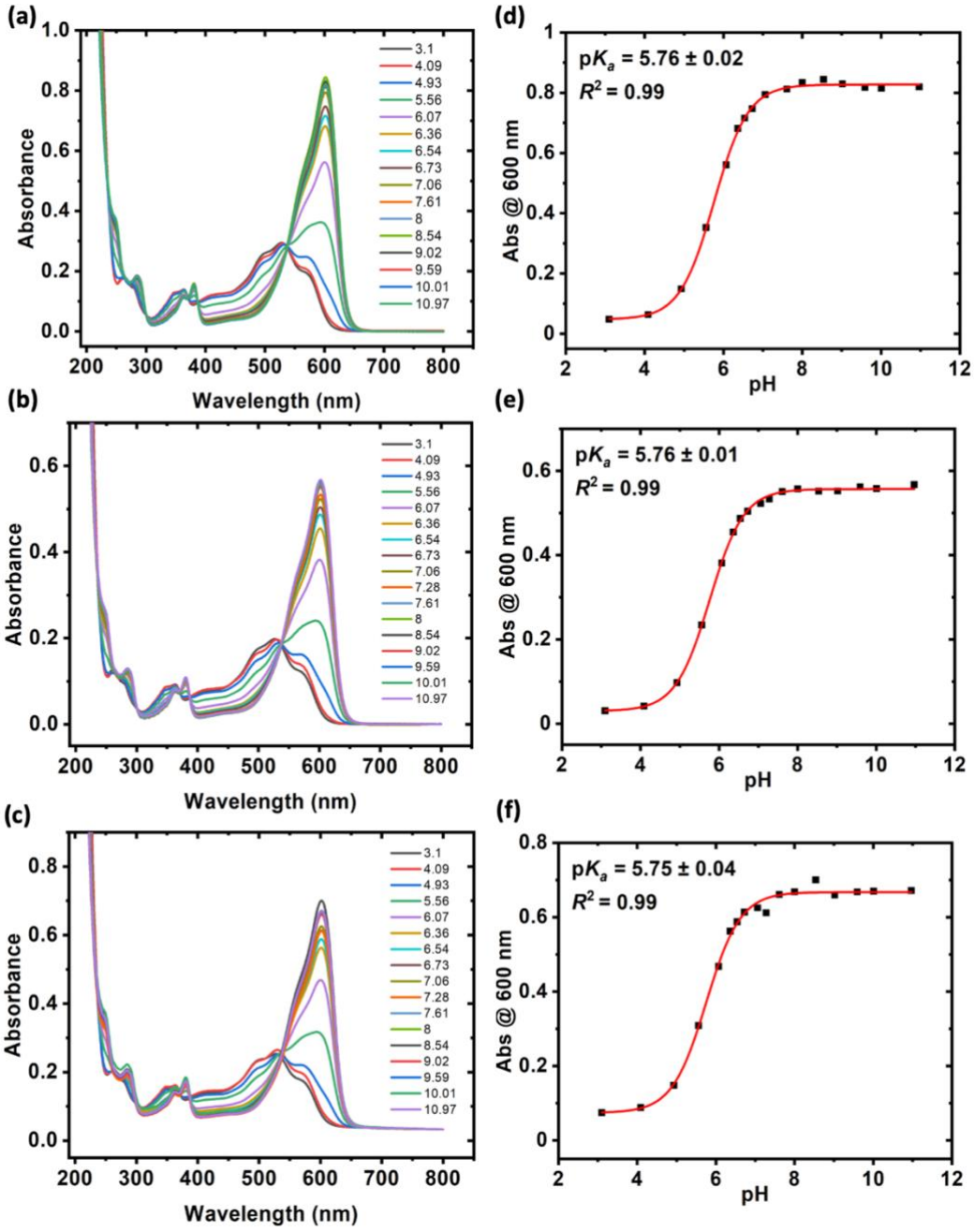

Fig. 3.2 UV-vis spectra of 20 μM **(a)** RZ, **(b)** [CB7·RZ]$^-$ and **(c)** [CB8·RZ]$^-$ in BR buffer solution at a variety of pH values. pK_a titration results of **(d)** RZ, **(e)** [CB7·RZ]$^-$ and **(f)** [CB8·RZ]$^-$.

Interestingly, host-guest complexation between CB*n* and negatively charged species are rare in literatures, predominantly due to the electrostatic repulsion from electron-rich carbonyl-lined portal of CB*n*. The encapsulation of [RZ-H]$^-$ by CB7/CB8 could be mainly driven by hydrophobic effects (classical and non-classical, in which the classical and non-classical hydrophobic effect refer to the entropy gain and enthalpy gain, respectively, from release of water molecules locked on hydrophobic molecular surfaces upon binding) [41,265] and dispersion interactions while the negatively charged phenoxide group is situated at the terminal position of the molecular skeleton, which is far away from the portal region of CB*n* and therefore suffer minimized repulsion. This hypothesis can be supported by the optimized molecular models of complexes (**Fig. 3.3c-d**) and the investigation of complexation-induced p*K*a shift effect, which is indicative of the host-guest electrostatic interactions.

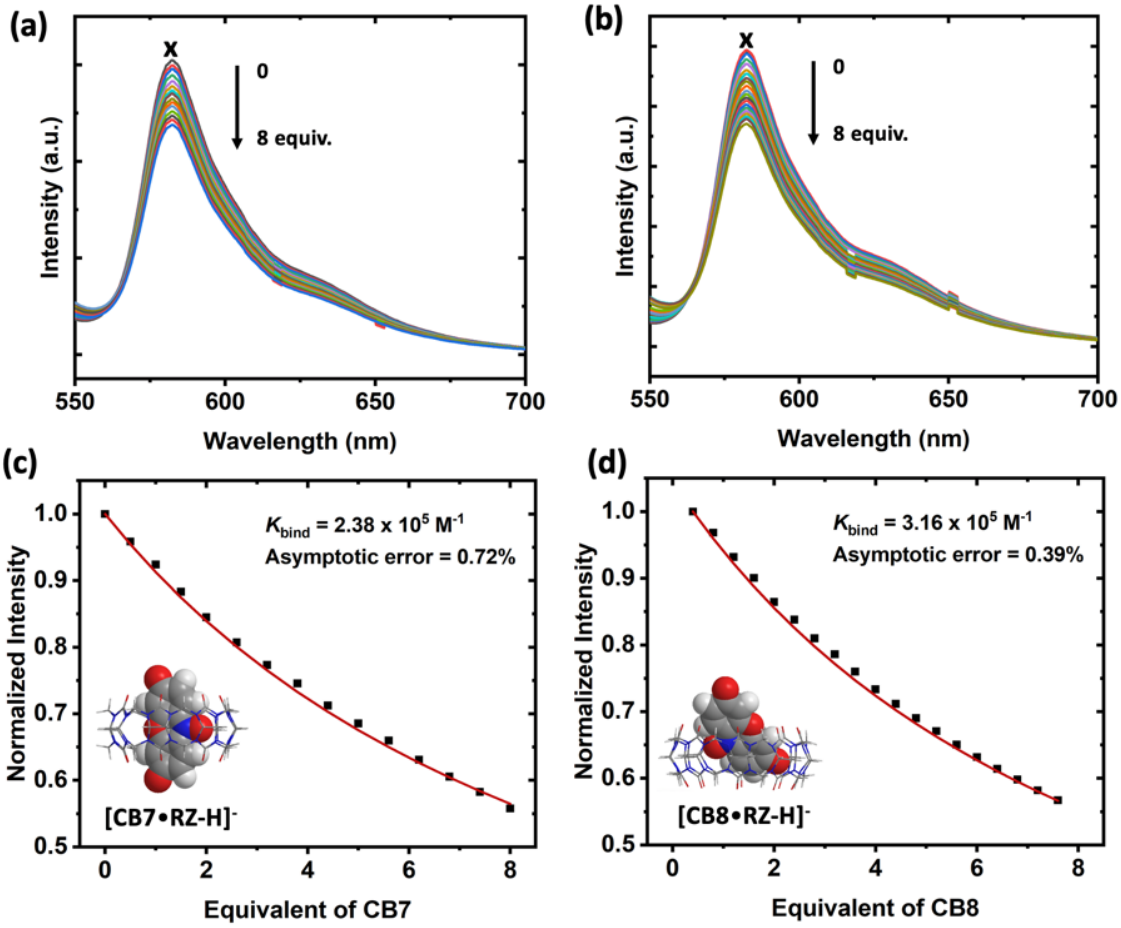

Fig. 3.3 Fluorescence titration spectra obtained by successively adding 4 μM of **(a)** CB7 and **(b)** CB8 into 0.2 μM of [RZ-H]$^-$ (solvent: 2 mM PB; pH = 7.0). Estimation of binding constants of **(c)** [CB7·RZ-H]$^-$ and **(d)** [CB8·RZ-H]$^-$ by fitting the normalized intensities at 583 nm during titration into 1:1 binding model. Inset: energy-minimized molecular model of [CB7·RZ-H]$^-$ and [CB8·RZ-H]$^-$ at CPCM/wB97XD/6-31G* level of theory, where CPCM implicit water model was utilized to simulate the solvent effects in aqueous-based electrochemical measurements.

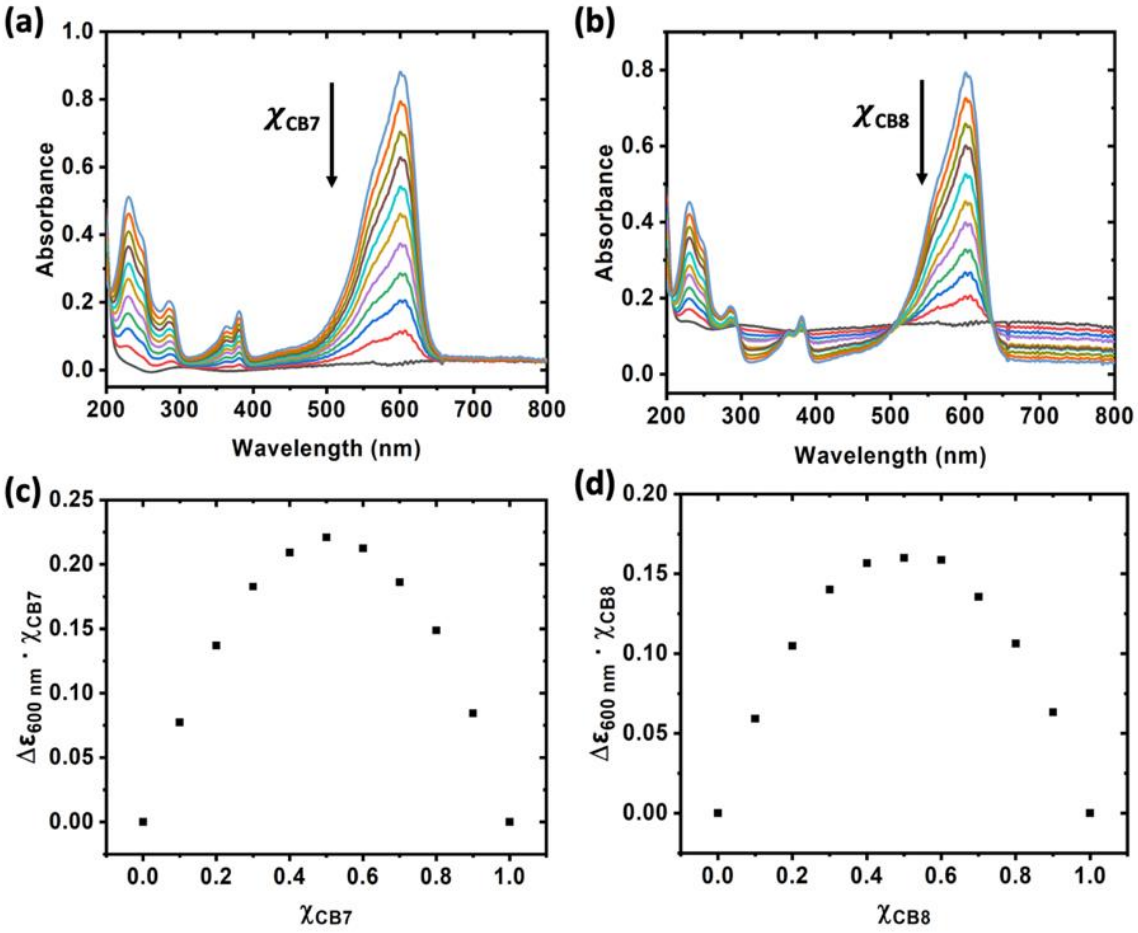

Fig. 3.4 UV-vis titration spectra obtained by fixing the concentration sum of $[RZ\text{-}H]^-$ and host = **(a)** CB7, **(b)** CB8 at 20 μM (solvent: 2 mM PB solution; pH = 7.0). Job plots of **(c)** $[CB7{\cdot}RZ\text{-}H]^-$ and **(d)** $[CB8{\cdot}RZ\text{-}H]^-$ extracted from titration spectra in **(a)** and **(b)**.

3.3 Modulation effects of CB7 and CB8 on electrochemical activity of $[RZ\text{-}H]^-$

The electrochemical properties of $[RZ\text{-}H]^-$ in absence and presence of 1 equimolar of CB7 and CB8 were then measured using cyclic voltammetry (CV) and square wave voltammetry (SWV) after confirming the formation of $[CB7{\cdot}RZ\text{-}H]^-$ and $[CB8{\cdot}RZ\text{-}H]^-$ complexes. As illustrated in **Fig. 3.1a**, $[RZ\text{-}H]^-$ can undergo two consecutive reduction processes, in which deprotonated RZ ($[RS\text{-}H]^-$) is generated via the first irreversible (*R1*) reduction at pH 7 and then it can be further reversibly reduced to neutral DHRS. Characteristic reduction properties of $[RZ\text{-}H]^-$ shown by black curve in **Fig. 3.5a, c** observed by CV and SWV are consistent with what reported in literature [266]. In particular, the reduction potential of *R1* are 5 mV and 14 mV vs Ag/AgCl reference electrode observed in CV. The peak-to-peak splitting of *R2* reversible redox peak pair in CV is around 44 mV (**Fig. 3.5a)**, which is comparable to the typical value of 57 mV at 298 K [267] for completely reversible redox active species, implying that the second reversible reduction process of $[RZ\text{-}H]^-$ is kinetically fast.

The peak-to-peak splitting value of *R2* redox pair was widened in the presence of CB7/CB8 (**Fig. 3.5a**), suggesting a slower diffusion kinetics of bulky complexes ($[CB7{\cdot}RZ\text{-}H]^-$ and $[CB8{\cdot}RZ\text{-}H]^-$) with respect to free $[RZ\text{-}H]^-$. In addition, cathodic peaks were distorted, and the anodic peak was greatly enlarged in the presence of CB7/CB8, which could be attributed to the increasingly pronounced precipitation of the reduction products caused by the

slower diffusion of bulky complexes [268]. Meanwhile, when electron transfer step is coupled by host-guest complexation process, distortions in cathodic curves is likely to appear [269].

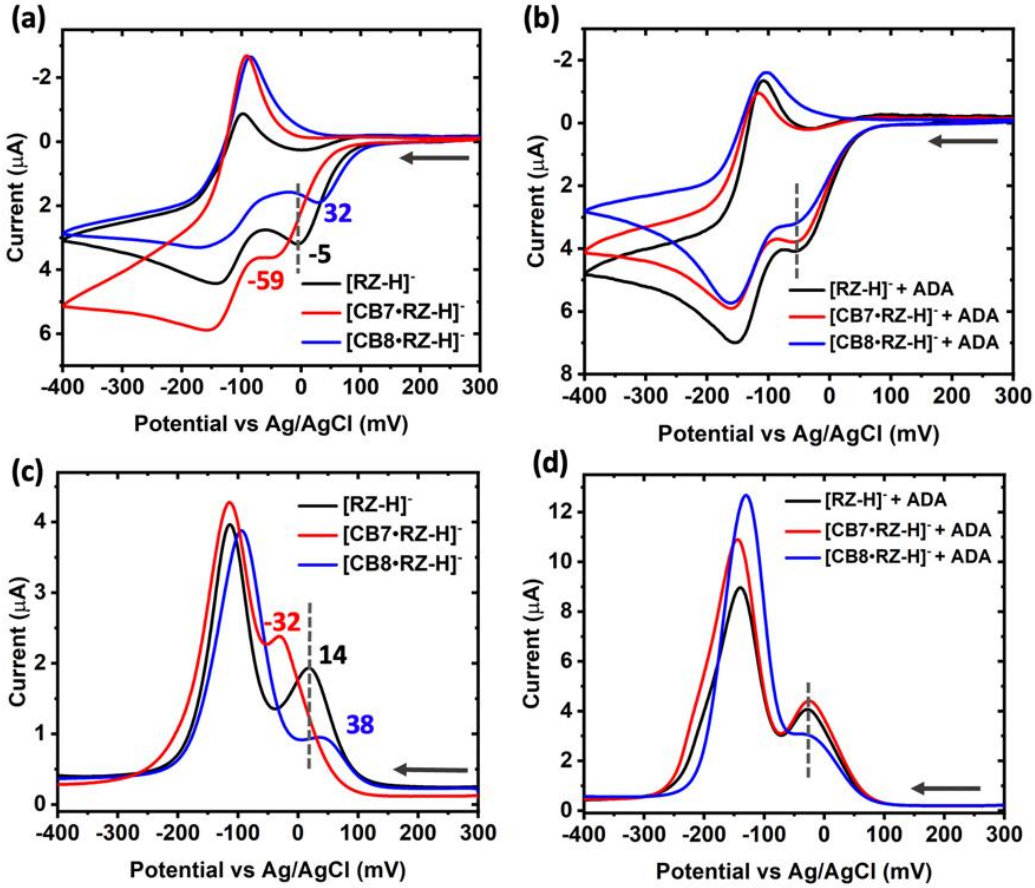

Fig. 3.5 Cyclic voltammograms of $[RZ\text{-}H]^-$, $[CB7{\cdot}RZ\text{-}H]^-$ and $[CB8{\cdot}RZ\text{-}H]^-$ **(a)** in absence and **(b)** presence of 3 equivalents of 1-adamantylamine (ADA). Square wave voltammograms of $[RZ\text{-}H]^-$, $[CB7{\cdot}RZ\text{-}H]^-$ and $[CB8{\cdot}RZ\text{-}H]^-$ **(c)** in absence and **(d)** presence of 3 equivalents of ADA. Arrows indicate the potential sweeping direction. Electrolyte: BR buffer (pH 7). Scan rate: 10 mV/s. Frequency: 5 Hz. Pulse size: 25 mV. Step size: 1 mV.

It is notably to see that peak potential corresponding to *R1* of $[RZ\text{-}H]^-$ were shifted to opposite direction upon complexation with CB7/CB8 (**Fig. 3.5a, c**), *i.e.* $\Delta V_{R1,\,CB7}$ = -54 mV and $\Delta V_{R1,\,CB8}$ = +37 mV in CV, and $\Delta V_{R1,\,CB7}$ = -56 mV and $\Delta V_{R1,\,CB8}$ = +24 mV in SWV at pH 7, revealing that *R1* of $[RZ\text{-}H]^-$ was facilitated after being encapsulated by CB8 but became less favourable when complexing with CB7. The magnitude of reduction potential shift observed here is comparable to the one reported in typical CB7-MV^{2+} (*e.g.* ΔV = -30 mV) system reported by the Kaifer group [67].

Although the electrochemical behaviours of $[RZ\text{-}H]^-$ is known to be sensitive [266,270] pH change cannot be the reason for the observed opposite peak potential shift effect caused by CB7 and CB8, because the pH of sample in electrochemical cell was adjusted again after adding CB7/CB8 prior to the tests and BR buffer solution was utilized to maintain pH at 7.0 throughout the entire electrochemical measurement. Additionally, supramolecular pK_a shift effect can also not be the leading reason for the observed opposite modulation since no pronounced pK_a shift effect was observed in the cases of CB7 and CB8 for $[RZ\text{-}H]^-$ (**Fig. 3.2**). With this discussion and observation, the modulation of redox activity of $[RZ\text{-}H]^-$ upon complexation with CB7/CB8 was not resulted from the change in protonation state of $[RZ\text{-}H]^-$, and thereby

implying that it could be caused by the change in microenvironment around $[RZ\text{-}H]^-$ after complexation.

As a control experiment, 1-adamantylamine (ADA), is composed of an adamantane skeleton with an amino group substituted at one of the four methyne sites. ADA is a well-known strong guest for both CB7 and CB8 with reported binding constants of $K_{CB7\text{-}ADA} = 4.23 \times 10^{12}\ M^{-1}$ and $K_{CB8\text{-}ADA} = 8.19 \times 10^{8}\ M^{-1}$ [71], thus having been employed to displace the encapsulated $[RZ\text{-}H]^-$ out of CB7/CB8 cavity to investigate whether the reduction peak shift phenomenon is indeed related to the supramolecular encapsulation of $[RZ\text{-}H]^-$. Gratifying to see that the reduction peak potential of *R1* shifted back to almost the same position of free $[RZ\text{-}H]^-$ after adding 3 equivalents of ADA into $[CB7{\cdot}RZ\text{-}H]^-$ and $[CB8{\cdot}RZ\text{-}H]^-$ system (**Fig. 3.5b, d**), confirming that the modulation effects on the electrochemical reduction reactivity are indeed from the complexation.

Note that there is a systematic shift towards the negative direction in the reduction peak potential of *R1* when 3 equivalents of $AdNH_2$ are present. For instance, the *R1* peak potential shifted from –5 mV to –54 mV in the CV (**Fig. 3.5a,b**). The observed systematic shift can be rationalized by the formation of a self-assembled monolayer (SAM) of ADA on the surface of the GCE, which was facilitated by hydrophobic interactions between the adamantyl moiety and the mildly hydrophobic glassy carbon surface. The resulting SAM can hinder electron transfer from the electrode to resazurin, resulting in the systematic shift in reduction potential. Furthermore, the excess cationic $Ad\text{-}NH_3^+$ can interact with the anionic $[RZ\text{-}H]^-$ in the system, contributing to the observed potential shift. The tiny differences in reduction potential between free $[RZ\text{-}H]^-$ (–54 mV), $[CB7{\bullet}RZ\text{-}H]^-$ (–53 mV) and $[CB8{\bullet}RZ\text{-}H]^-$ (–55 mV) in **Fig. 3.5b** can be due to the incomplete displacement of $[RZ\text{-}H]^-$ from the CB7/8 cavities since host-guest displacement is a dynamic process. Nevertheless, these differences are considered slight and within the range of methodological error.

3.4 Complexation between $[RZ\text{-}H]^-$ and βCD/γCD

To gain further understanding of the role of CB cavity play for the modulation mechanism, we then employed synthetic hosts of β-cyclodextrin (βCD) and γ-cyclodextrin (γCD) to perform measurements. βCD and γCD are known to be analogous hosts of CB7 and CB8 with comparable cavity volume, and thus the packing coefficient of their complexes with $[RZ\text{-}H]^-$ should be similar. However, βCD and γCD cavities are more flexible and less rigid compared to that of CB7 and CB8, thus being readily utilized to investigate the role of the encapsulation tightness in activity modulation.

The complexation between $[RZ\text{-}H]^-$ and βCD/γCD was confirmed by fluorescence spectroscopy (**Fig. 3.6**) and UV-vis spectroscopy (**Fig. 3.7**). Quantitative analysis regarding the interaction strength between $[RZ\text{-}H]^-$ guest and βCD/ γCD hosts were achieved via fluorescence titration. Upon the stepwise addition of βCD/ γCD into $[RZ\text{-}H]^-$ solution (in 2 mM PB solution, pH 7), the main emission peak of $[RZ\text{-}H]^-$ at 583 nm was depressed accordingly (**Fig. 3.6a-b**). The binding constants of $[\beta CD{\cdot}RZ\text{-}H]^-$ and $[\gamma CD{\cdot}RZ\text{-}H]^-$ complexes were estimated as $2.86 \times 10^5\ M^{-1}$ and $3.05 \times 10^5\ M^{-1}$ by fitting the fluorescence titration data into 1:1 binding model (**Fig. 3.6c-d**). The 1:1 binding ratio was further confirmed by continuous variation method, *i.e.* measuring UV-vis spectra with a various percentage of host (βCD/ γCD) at a fixed concentration sum of host and guest (**Fig. 3.7a-b**). As indicated by the maximum points appear at 0.5 in Job plots (**Fig. 3.7c-d)**, the binding stoichiometry of $[\beta CD{\cdot}RZ\text{-}H]^-$ and $[\gamma CD{\cdot}RZ\text{-}H]^-$ complexes are indeed 1:1.

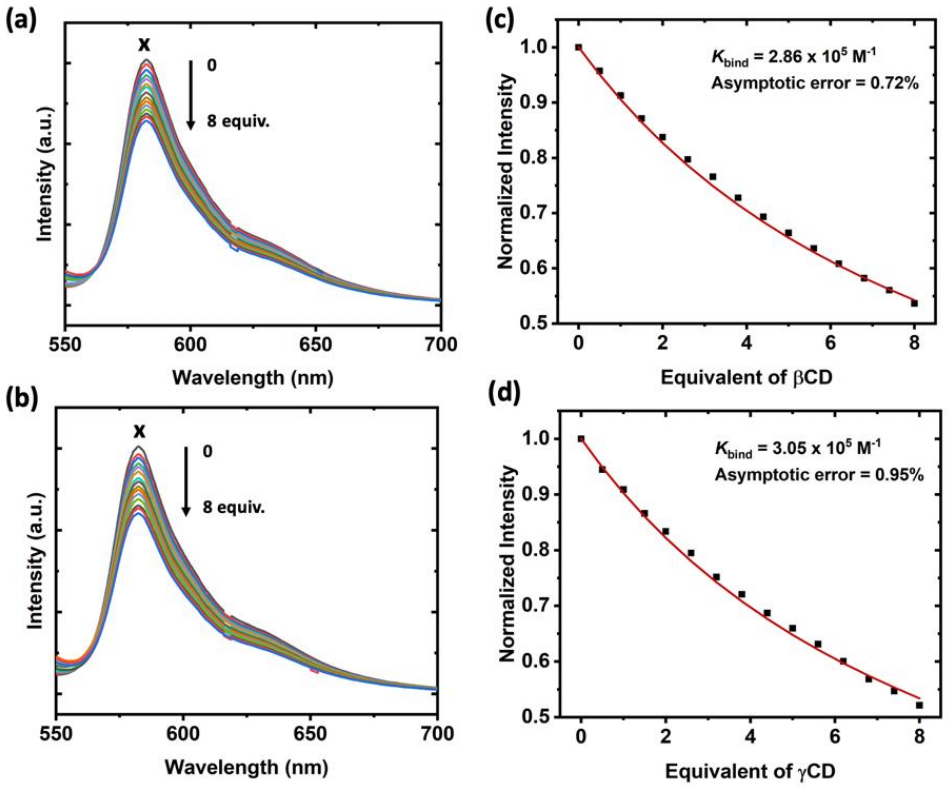

Fig. 3.6 Fluorescence titration spectra obtained by adding by successively adding **(a)** βCD and **(b)** γCD into 0.2 μM of [RZ-H]$^-$ (solvent: 2 mM PB solution; pH = 7.0). Excitation: 533-nm LED (1.96 mW). Estimation of binding constants of **(c)** [βCD·RZ-H]$^-$ and **(d)** [γCD·RZ-H]$^-$ by fitting the titration results into 1:1 binding model.

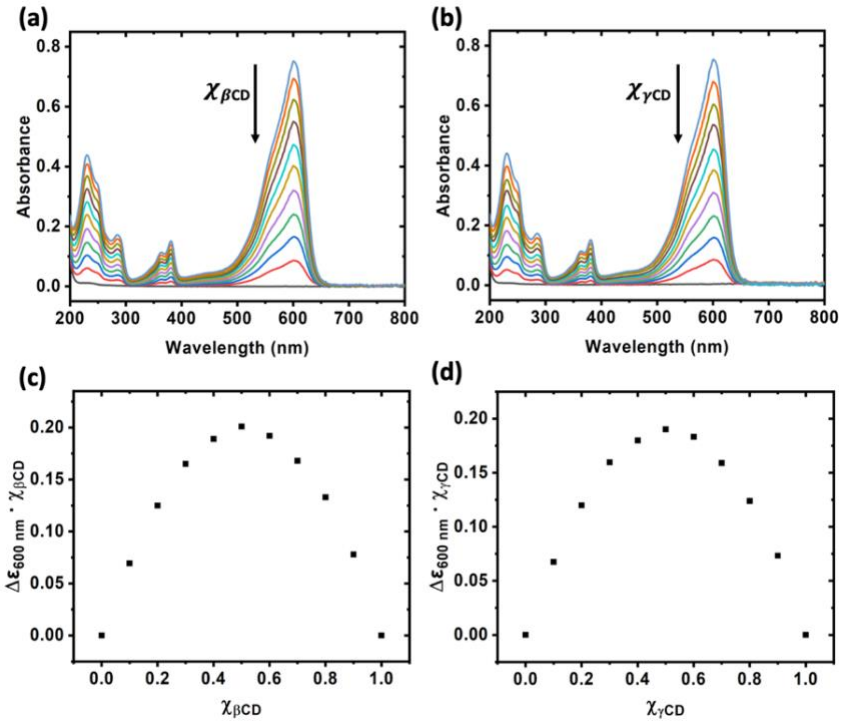

Fig. 3.7 UV-vis titration spectra obtained by fixing the concentration of [RZ-H]$^-$ and host = **(a)** βCD, **(b)** γCD at 20 μM (solvent: 2 mM PB solution; pH = 7.0). Job plots of **(c)** [βCD·RZ-H]$^-$ and **(d)** [γCD·RZ-H]$^-$ extracted from titration spectra in **(a)** and **(b)**.

3.5 Modulation effects of βCD and γCD on electrochemical activity of [RZ-H]$^-$

The modulation effect of βCD and γCD on electrochemical reactivity of [RZ-H]$^-$ were monitored after confirming the formation of [βCD·RZ-H]$^-$ and [γCD·RZ-H]$^-$ complexes. CV and SWV tests of [RZ-H]$^-$ in the presence of 1 equivalent of βCD and γCD were recorded at the identical conditions and parameters as those utilized in the cased of CB7 and CB8. Unlike CB7/CB8, no obvious reduction potential shift of [RZ-H]$^-$, *e.g.* < 10 mV, were achieved by βCD and γCD (**Fig. 3.7**), suggesting that there is no significant reactivity modulation effect on the reduction of [RZ-H]$^-$ offered by complexation with βCD and γCD although their binding affinities are comparable to that of CB7 and CB8 (**Fig. 3.6**). This could be presumably due to the fact that the cavity of βCD/γCD is more flexible than that of CB7/CB8, thus the microenvironment around βCD/ γCD-encapsulated [RZ-H]$^-$ is closer to the bulk solution than CB7/CB8, highlighting the key role of rigid and well-defined cavity as well as corresponding tight binding in modulating the redox activity of [RZ-H]$^-$.

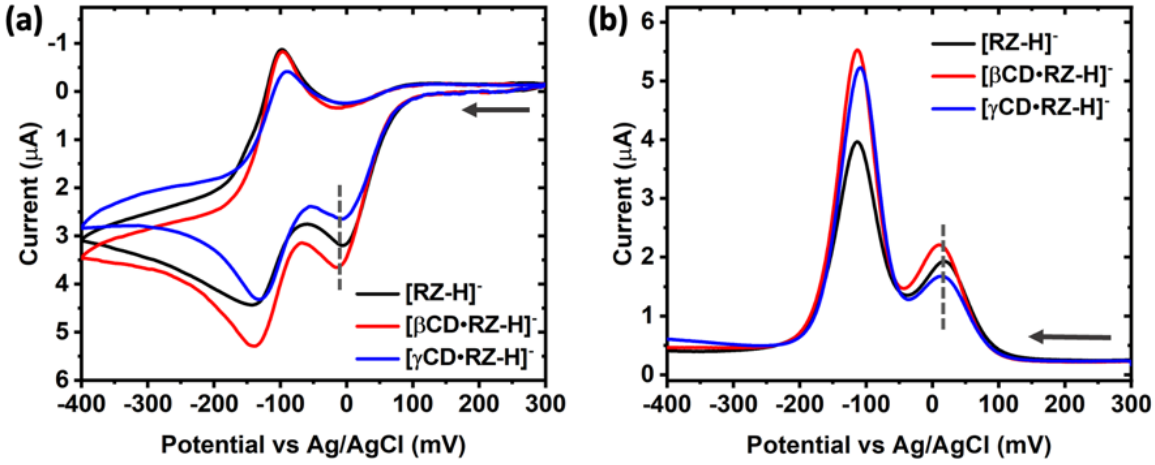

Fig. 3.8 (a) Cyclic voltammograms and **(b)** square wave voltammograms of [RZ-H]$^-$, [βCD·RZ-H]$^-$ and [γCD·RZ-H]$^-$. Frequency: 5 Hz. Step size: 1 mV. Electrolyte: BR buffer (pH 7).

3.6 Mechanistic analysis

Closer mechanistic inspection regarding the opposite modulation effects observed in the case of CB7 and CB8 was done in detail in this section. As depicted in **Fig. 3.1a**, protonation of -NO group (reaction centre), which was mediated by water molecules, and cascades of electron transfer were involved in irreversible *R1* process of [RZ-H]$^-$ [266]. We therefore built hypothesis that the opposite reactivity modulation effect on [RZ-H]$^-$ by CB7/CB8 could be related to the accessibility of water molecules to the CB7/CB8-included reaction centre (**Fig. 3.1b**). In particular, the reaction centre of [RZ-H]$^-$ was located deep inside cavity no matter it was encapsulated by CB7 or CB8, as indicated by the binding geometric information predicted in DFT optimized molecular models (**Fig. 3.3c-d**). To verify this hypothesis, we computed the van der Waals volume of [RZ-H]$^-$ using HyperChem and Spartan and determined its packing coefficient within CB7 and CB8, respectively (**Table 3.1**). Initially, attempted to analyze the binding modes of [RZ-H]$^-$ with CB7 and CB8 using NMR by the shifting of chemical shifts; however, the immediate formation of a precipitate upon mixing the guest and host solutions resulted in a solid complex state that was unsuitable for liquid NMR analysis. As an alternative, we optimized the complexation modes using DFT calculations (**Fig. 3.3c-d**). Our observation indicates that, [RZ-H]$^-$ resides partially in the cavity rather than being fully encapsulated in both CB7 and CB8. This illustrates the considerably large packing coefficient observed for

$[RZ\text{-}H]^-$ in relation to both the expanded and inner cavity volumes of CB7. In the case of CB8, the PC generally falls in a region that is highly conducive to the occurrence of complexation, *i.e.* the Rebek's rule [38], which predicts the most favorable binding at 55% packing coefficient with regard to the inner cavity volume because 45% empty cavity space guarantee certain mobility freedom for host and guest and a higher packing coefficient is likely to at the expanse of such mobility freedom. Certainly, the number of 55% is not extremely strict and a certain degree of shifts in packing coefficient is acceptable with a resulting depressed binding constant [39]. Notably, the reaction center of $[RZ\text{-}H]^-$ is deeply immersed in both host cavities.

Table 3.1 Molecular volume, packing coefficients and binding constants of $[CB7{\bullet}RZ\text{-}H]^-$ and $[CB8{\bullet}RZ\text{-}H]^-$ with/without one H_2O molecule included.

	Volume	Packing coefficient (%)	
		CB7	CB8
$[RZ\text{-}H]^-$	179.8[a]	64 (74)[a]	38 (49)[a]
	206.29[b]	73 (85)[b]	43 (56)[b]
$[RZ\text{-}H]^- + H_2O$	196.98[a]	70 (81)[a]	41 (54)[a]
	225.64[b]	80 (93)[b]	47 (61)[b]

[a] Calculated by HyperChem 8.0.10.
[b] Calculated by Spartan 20 Parallel Suite.
Packing coefficient were calculated based on the expanded (inner) cavity volume of CB7 and CB8 reported by the Nau group [21].

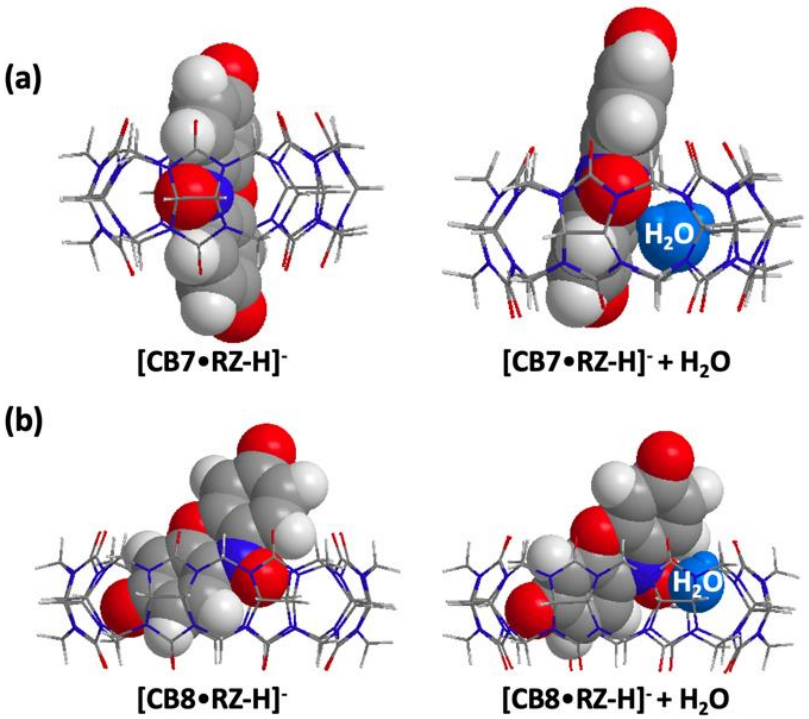

Fig. 3.9 Optimized molecular models of **(a)** $[CB7{\cdot}RZ\text{-}H]^-$ and **(b)** $[CB8{\cdot}RZ\text{-}H]^-$ with/without one water molecule near -NO group (reaction centre) of $[RZ\text{-}H]^-$.

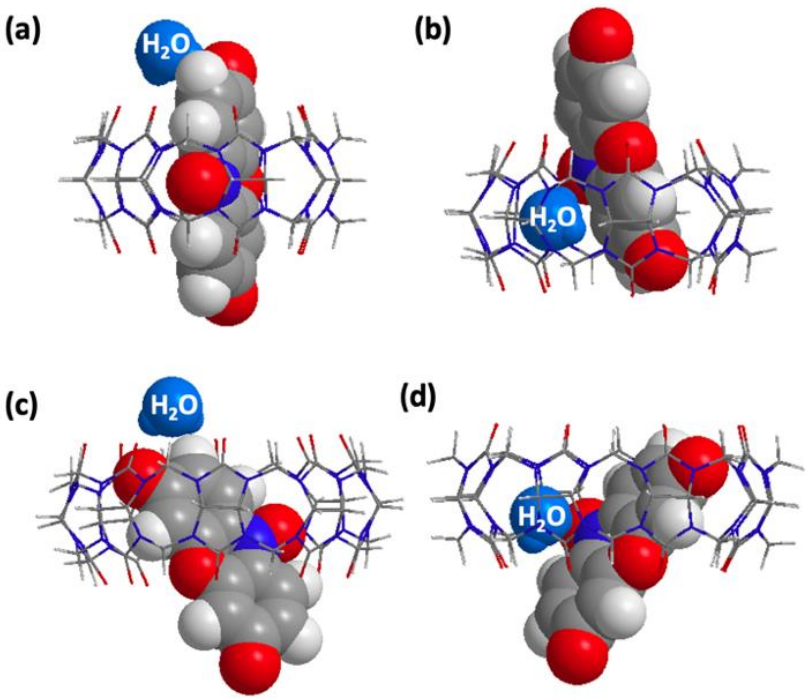

Fig. 3.10 Optimized molecular models of $[CB7{\cdot}RZ\text{-}H{+}e]^{2-}$ with one water molecule near **(a)** O^-, **(b)** -NO reaction centre. Energy-minimized molecular models of $[CB8{\cdot}RZ\text{-}H{+}e]^{2-}$ with one water molecule near **(c)** O^-, **(d)** -NO reaction centre.

Table 3.2 Optimized energies of free $[RZ\text{-}H{+}e]^{2-}$, $[CB7{\bullet}RZ\text{-}H{+}e]^{2-}$ and $[CB8{\bullet}RZ\text{-}H{+}e]^{2-}$ interacting with one water molecule computed at CPCM/wB97XD/6-31G* level of theory, where CPCM implicit water model was utilized to simulate the solvent effects in aqueous-based electrochemical measurements.

	Position of H_2O	Optimized Energy (kcal/mol)	ΔE (kcal/mol)
$[RZ\text{-}H{+}e]^{2-} + H_2O$	Near $-O^-$	E_O = -560269.7699	+2.7
	Near -NO	E_N = -560267.0987	
$[CB7{\bullet}RZ\text{-}H{+}e]^{2-} + H_2O$	Near $-O^-$	E_O = -3202902.01	+6.8
	Near -NO	E_N = -3202895.236	
$[CB8{\bullet}RZ\text{-}H{+}e]^{2-} + H_2O$	Near $-O^-$	E_O = -3580409.198	-4.2
	Near -NO	E_N = -3580413.347	

$[RZ\text{-}H{+}e]^{2-}$ represents one-electron reduced intermediate formed by $[RZ\text{-}H]^-$
E_O = Optimized energy when H_2O is located near $-O^-$ of $[RZ\text{-}H{+}e]^{2-}$;
E_N = Optimized energy when H_2O is located near -NO of $[RZ\text{-}H{+}e]^{2-}$;
$\Delta E = E_N - E_O$.
Note that the optimized energy in the table is based on the total electronic energy of the system modelled by DFT, without thermal corrections. No entropic term is included in these optimized energy values, and they can be roughly considered as enthalpy but are not exactly the same as conventional enthalpy.

The binding between $[RZ\text{-}H]^-$ and CB7 is snug owing to its smaller cavity volume compared to CB8, while the introduction of a water molecule adjacent to reaction centre will partially displace $[RZ\text{-}H]^-$ from CB7 cavity in the cases of $[CB7{\cdot}RZ\text{-}H]^-$ and $[CB7{\cdot}RZ\text{-}H{+}e]^{2-}$, as shown by their corresponding optimized molecular models in **Fig. 3.9a** and **3.10b**. The partial displacement of $[RZ\text{-}H]^-$ is likely to weaken the host-guest interactions, therefore giving rise to a destabilized reaction intermediate in the proton transfer step. On the other hand, when $[RZ\text{-}H]^-$ binds to larger CB8, the binding geometry of $[CB8{\cdot}RZ\text{-}H]^-$ and its one-electron reduced intermediate $[CB8{\cdot}RZ\text{-}H{+}e]^{2-}$ are less prone to the introduction of a water molecule around the reaction centre of $[RZ\text{-}H]^-$ (**Fig. 3.9b** and **3.10d**), indicating the pre-organization effects of CB8 on $[CB8{\cdot}RZ\text{-}H]^-$ and $[CB8{\cdot}RZ\text{-}H{+}e]^{2-}$ play an effective role to encapsulate and stabilize the introduced water molecular in the step of proton transfer. The pre-organization effects offered by CB8 is also likely to make entropic contribution to the activation of *R1* process of $[RZ\text{-}H]^-$.

To gain semi-quantitative knowledge about the above hypothesis, we computed energy values of the optimized molecular models of one-electron intermediates with one encapsulated water molecule either near the $-O^-$ or -NO group (**Fig. 3.10** and **Table 3.2**). In the case of free $[RZ\text{-}H{+}e]^{2-}$, the system was slightly destabilized by +2.7 kcal/mol with water molecule moving from $-O^-$ to -NO reaction centre. Notably, such energy increase was enlarged to +6.8 kcal/mol in the case of $[CB7{\cdot}RZ\text{-}H]^-$, suggesting the process for water molecule to arrive -NO reaction centre became less energetically favourable with respect to its free form; however, the energy difference was reversely reduced to -4.2 kcal/mol in the case of $[CB8{\cdot}RZ\text{-}H]^-$, implying that it became more energetically favourable for water molecule to approach -NO reaction centre, in agreement with the hypothesis.

3.7 Conclusions

We qualitatively and quantitively investigated the host-guest complexation between $[RZ\text{-}H]^-$ and different synthetic hosts including CB7, CB8, βCD and γCD by ^{1}H NMR, fluorescence spectroscopy, UV-vis spectroscopy as well as computational simulations. Gratifying to note that an opposite modulation effect on $[RZ\text{-}H]^-$ electrochemical reactivity was achieved upon complexation with rigid hosts, *e.g.* CB7 and CB8. Such modulation effect can be rationalized by the binding tightness that determines the ease for water molecules to approach the encapsulated -NO reaction centre of $[RZ\text{-}H]^-$ in the step of proton transfer. Nevertheless, it is interesting to note that the analogous hosts of βCD and γCD do not display effective modulation effect although their binding affinities with $[RZ\text{-}H]^-$ are comparable to that of CB7/CB8, highlighting the crucial role of the rigidity of cavity.

The investigated supramolecular modulation effect on the electrochemical activity of encapsulated $[RZ\text{-}H]^-$ achieved the research objective regarding cucurbiturils-based complexes applications in the field of analytical chemistry. The proposed approach is expected to be extended to other redox reactions that include proton transfer process and encourage us to gain knowledge about and better design nano-confined chemical systems. In addition, it is inspired that we can extend the supramolecular modulation study from one host-one guest complex to one host-two guests complexes which consist of one pre-encapsulated first guest molecule and one subsequently encapsulated second guest, such as CB8-MV^{2+}-G2 ternary complexes.

Chapter 4. Rapid estimation of binding constants for cucurbit[8]uril ternary complexes using electrochemistry

This chapter is published as a cover article in *Analytical Chemistry* (https://dx.doi.org/10.1021/acs.analchem.0c04887).

This Chapter reported a facile methodology for the estimation of binding constants of cucurbit[8]uril-methyl viologen-based hetero-ternary complexes (CB8-MV^{2+}-G2) with the aid of electrochemistry, readily providing instructive information in designing supramolecular-based materials for specific application, such as drug delivery, selective sensing, *etc*. In particular, a linear correlation with $R^2 > 0.85$ between isothermal colorimetry (ITC) determined binding constants and the cyclic voltametric- and square wave voltametric-measured reduction potential shift of twenty-five reference CB8-MV^{2+}-G2 complexes with respect to CB8-MV^{2+} was discovered. The estimation of binding constants of an unknown CB8-MV^{2+}-based hetero-ternary complex can be achieved by one-point electrochemical measurement within 10 min (~ 5 h in ITC) following our proposed electrochemical scheme, allowing for screening in high-throughput fashion. Moreover, high precision (± 0.03) and practical accuracy (± 0.32) in binding constants (represented as $\log K_{G2}$) have been displayed by our electrochemical scheme. Mechanistic investigation based on experimental and computational results suggests that the linear correlation is rooted from the host-guest exchange behaviours taking place after the electron-transfer process. As a proof-of-concept application, the binding constants of a group of six-membered cyclic hydrocarbons, which are hard to be measured by conventional titration methodologies due to their high volatility and sparse solubility, were estimated with our electrochemical scheme.

4.1 Introduction

The noncovalent interactions between host and guest play a key role in designing supramolecular-based materials for manifold end applications, such as, selective molecular detection [46-48,175,271], drug delivery and controlled releasing [20,58,272,273], supramolecular functionalized nanomaterials [49,274-279], molecular catalysis [28,248,249], reaction activation or inhibition [280,281], single-molecule conductance [282] *etc*, and thus the quantitative analysis of them are of great importance in supramolecular chemistry. Binding constant is a widely accepted indicator giving a quantitative index to the interaction strength of supramolecular complexes. Supramolecular titration methodologies are the most common routes for the estimation of binding constants, which rely on the change of specific physical property with the successive addition of guest solution into host solution or vice versa. In particular, the normally utilized physical property and the corresponding characterization techniques include absorbance in UV-vis spectroscopy, heat transfer in ITC, chemical shifts in NMR, emission intensity in fluorescence spectroscopy [283]. Although ITC has been continuously regarded as the gold standard for the estimation of binding constants, especially for interactions between large biomolecules, while it suffers from some intrinsic defects of titration experiments, such as the tedious experimental steps, expensive and bulky instrument, complicated data analysis, specific requirement of the solubility of the analyte and the limited applicability for sparsely soluble analytes. Apart from supramolecular titration methodologies, other substrate-based methodologies such as surface plasmon resonance (SPR) and quartz crystal microbalance (QCM) for quantitative measuring the molecule interactions in supramolecular complexes have also been explored; however, these methodologies demonstrate limited applicability towards small molecules, such as molecules with molecular weight around 10^2 Dalton, and predominantly work for the biomolecules with big molecular weight (~ 10^5 Dalton), *e.g.* proteins and antibodies [138,139].

CB*n* (*n* = 5-8, 10) are a young generation of supramolecular hosts possessing rigid and hydrophobic cavity as well as carbonyl-bridged and electronegatively charged rims. Positively charged guests can interact with the electron-rich portal of CB*n* via ion-diploe interactions and/or the hydrogen bonding, rendering CB*n* a strong receptor for cationic guests. Neutrally charged guests can take advantage of the hydrophobic effect of CB*n* cavity to obtain entropic gain upon releasing high-energy water molecules via complexation, thereby being able to form strong complex with CB*n* as well. Other than the capability of giving high binding affinities in the cases of a wide range of guest molecules, the millimolar aqueous solubility of CB*n* allows its application in biologically relevant aqueous environment, where the electrochemical measurements are generally carried out.

Among CB*n* homologues, CB8 stands out due to its spacious cavity offering unique ability to simultaneously encapsulate two guest molecules, especially two π-conjugated molecules. According to the type of two guest molecules, CB8-based ternary complexes are classified into homo- and hetero-ternary complexes [21,30,84,193,284,285]. Specifically, redox active, electron-deficient and dicationic methyl viologen (MV^{2+}) is a typical first guest for CB8 to form 1:1:1 heterogeny complexes with a wide range of second guest molecules (G2) which possess aromatic motif, for which the hydrophobic effects along with the charge-transfer interactions between two guest molecules jointly serve as driving force [84,87,94,284]. It is novel to note that the reduction potential peak of MV^{2+} can be shifted upon the complexation with CB7/CB8, which can be rationalized by electrostatic stabilization and dimerization of intermediate radical inside CB8 cavity, respectively. Thus, MV^{2+} is ready to serve as a redox reporter for investigation of host-guest complex using electrochemistry. However, the correlation between the binding affinities of a range of G2 with CB8-MV^{2+} and their corresponding responsive electrochemical profiles has not been explored prior to our research [269].

Herein, a rapid and simple electrochemical approach for the estimation of the binding constants of CB8-MV^{2+}-based ternary complexes (K_{G2} in **Fig. 4.1**) has been reported. The precision of logK_{G2} obtained by our approach is approximated to be $\pm$0.03, and the accuracy is estimated to be within a practical range of $\pm$0.32. The binding constant (K_{G2}) of an unknown analyte can be estimated by one-point experiment in less than 10 min, which is significantly faster than the conventional titration experiments (around 5 h for ITC), thus allowing for the high-throughput estimation of binding constants. Specifically, twenty-five molecules, whose K_{G2} have been measured by ITC were selected as the reference G2 for the formation of CB8-MV^{2+}-G2 ternary complexes [87]. The reduction potential values of all twenty-five CB8-MV^{2+}-G2 ternary complexes were measured by cyclic voltammetry (CV) and square wave voltammetry (SWV) to extract the shift of their reduction potential with respect to CB8-MV^{2+} binary complex (ΔV_{G2} in **Fig. 4.3**). Remarkably, a linear correlation with $R^2 > 0.8$ between the potential shift of CB8-MV^{2+}-G2 ternary complexes (ΔV_{G2}) and ITC-determined binding constants (logK_{G2}) was uncovered. The underlying mechanism leading to such linear correlation was elucidated by the combined results from experiments and computational simulations. It is revealed that this correlation is originated from the dynamic exchange events of host and guest after the electron transfer step in reduction process. To prove the concept, the applicability of the proposed scheme towards a group of volatile and sparsely miscible/soluble organic cyclic hydrocarbons was checked by estimating their binding constants logK_{G2} with the linear regression corelation, whose binding constants are otherwise hardly obtained by conventional titration methodologies.

4.2 Complexation and electrochemistry of CB8-MV^{2+} and CB8-MV^{2+}-G2

The formation of CB8-MV^{2+} and CB8-MV^{2+}-G2 complexes were illustrated in **Fig. 4.1a**; in detail, 1:1 binary complex of CB8-MV^{2+} was formed via the ion-dipole interactions between positively charged MV^{2+} and electronegative portals of CB8, and then 1:1:1 CB8-MV^{2+}-G2 complex was formed by introducing 1 equivalent of G2 into CB8-MV^{2+} solution with the driving force from hydrophobic effect of G2 and the charge-transfer interactions between electron-deficient MV^{2+} and G2 inside CB8 cavity. The formation of complexes was confirmed by ^{1}H NMR. Taking 2-naphthol (2NP) as an example G2, the corresponding ^{1}H NMR spectra are shown in **Fig. 4.1b**, which is consistent with previous reported results [78]. The chemical shifts of pyridinium protons on MV^{2+} was upshifted in the presence of 1 equivalent of CB8 due to the shielding effect of CB8, suggesting the formation of CB8-MV^{2+} binary complex. With the addition of 1 equivalent of 2NP, the chemical shifts corresponding to pyridinium protons of MV^{2+} were further upshifted and widened with respect to CB8-MV^{2+}, indicating that the formation of CB8-MV^{2+}-2NP ternary complex.

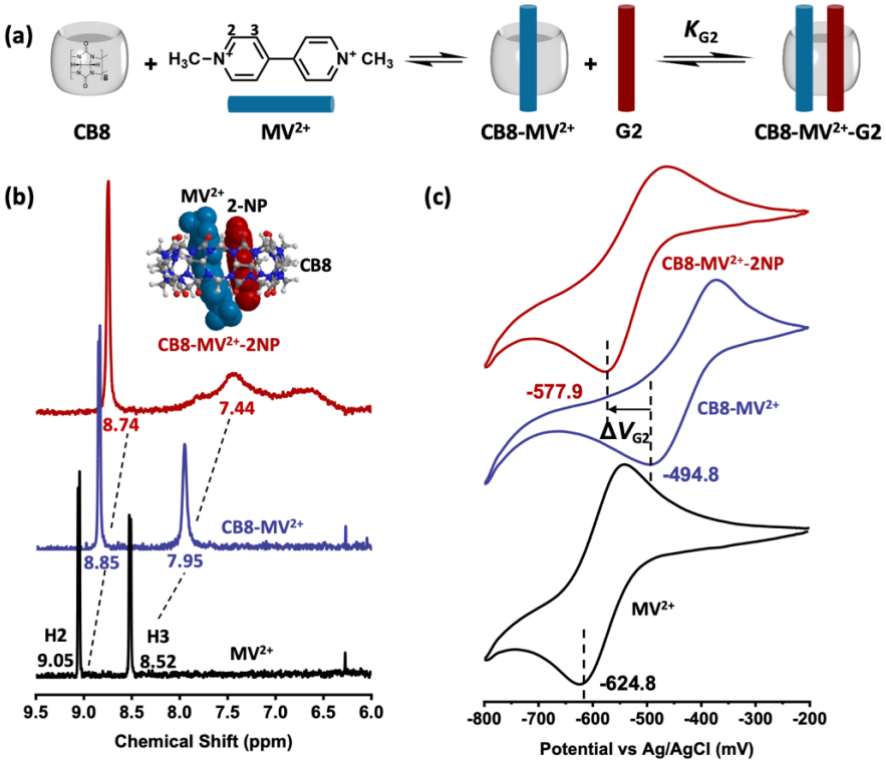

Fig. 4.1 (a) Self-assembly process of CB8-MV^{2+} binary complex and CB8-MV^{2+}-2 naphthol (CB8-MV^{2+}-2NP) ternary complex. K_{G2} is the binding constant between G2 and CB8-MV^{2+}. **(b)** ^{1}H NMR spectra of MV^{2+}, CB8-$MV^{2+}$and CB8-MV^{2+}-2NP. Inset: energy-optimized molecular model of CB8-MV^{2+}-2NP obtained at CPCM/wB97XD/6- 31G* level of theory, where CPCM implicit water model was utilized to simulate the solvent effects in aqueous-based electrochemical measurements. **(c)** Cyclic voltammograms of MV^{2+}, CB8-$MV^{2+}$and CB8-MV^{2+}-2NP. ΔV_{G2} is defined as the absolute value of the difference between the reduction potential of CB8-$MV^{2+}$and CB8-MV^{2+}-G2.

As known, CB8 is a strong cationic receptor with its electron-rich rims, and consequently, the metal ions presented in the electrolyte would compete with MV^{2+} to bind with CB8. Thus, it is of importance to choose a properly compromising concentration of electrolyte at which a desired conductivity can be given and the binding between metal ions in electrolyte with CB8 is not too strong to interfere the investigation of the binding between CB8

and target analyte of MV^{2+}. CV and SWV measurements of MV^{2+}, CB8-MV^{2+} and CB8-MV^{2+}-2NP were carried out in different concentrations of PB solution at pH of 7.0 (**Fig. 4.2**). The reversible reduction of free MV^{2+} is a fast process with respect to complexes and its redox peaks slightly increased as the increasing concentration of electrolyte by taking advantage of the enhanced conductivity (**Fig. 4.2a, d**). Nevertheless, dynamic host-guest association and disassociation behaviours are involved in the cases of CB8-MV^{2+} and CB8-MV^{2+}-2NP complexes. As illustrated in the CV and SWV curves of CB8-MV^{2+} (**Fig. 4.2b-c**) and CB8-MV^{2+}-2NP (**Fig. 4.2e-f**), peak corresponding to free MV^{2+} started to appear when the concentration of electrolyte was higher than 20 mM, suggesting that the stability of CB8-MV^{2+} and CB8-MV^{2+}-2NP complexes were reduced by the competitive binding of concentrated Na^{+} in electrolyte. Meanwhile, the reduction peak strength ratio between $MV^{2+}$and CB8-MV^{2+} or CB8-MV^{2+}-2NP complex decreased significantly with the increasing electrolyte concentration. Additionally, the peak corresponding to CB8-MV^{2+}-2NP completely disappeared when the concentration of electrolyte achieved 100 mM, indicating that the stability of CB8-MV^{2+}-2NP is more susceptible to the concentration of electrolyte with respect to that of CB8-MV^{2+}. The representative colour resulted from the charge-transfer interactions between $MV^{2+}$and 2NP in the case of CB8-MV^{2+}-2NP decayed greatly as the electrolyte concentration increased (**Fig. 4.2g**). Taking both conductivity and complex stability into account, 6.25 mM of PB solution was thus chosen as the electrolyte utilized for all electrochemical measurements displayed in this Chapter.

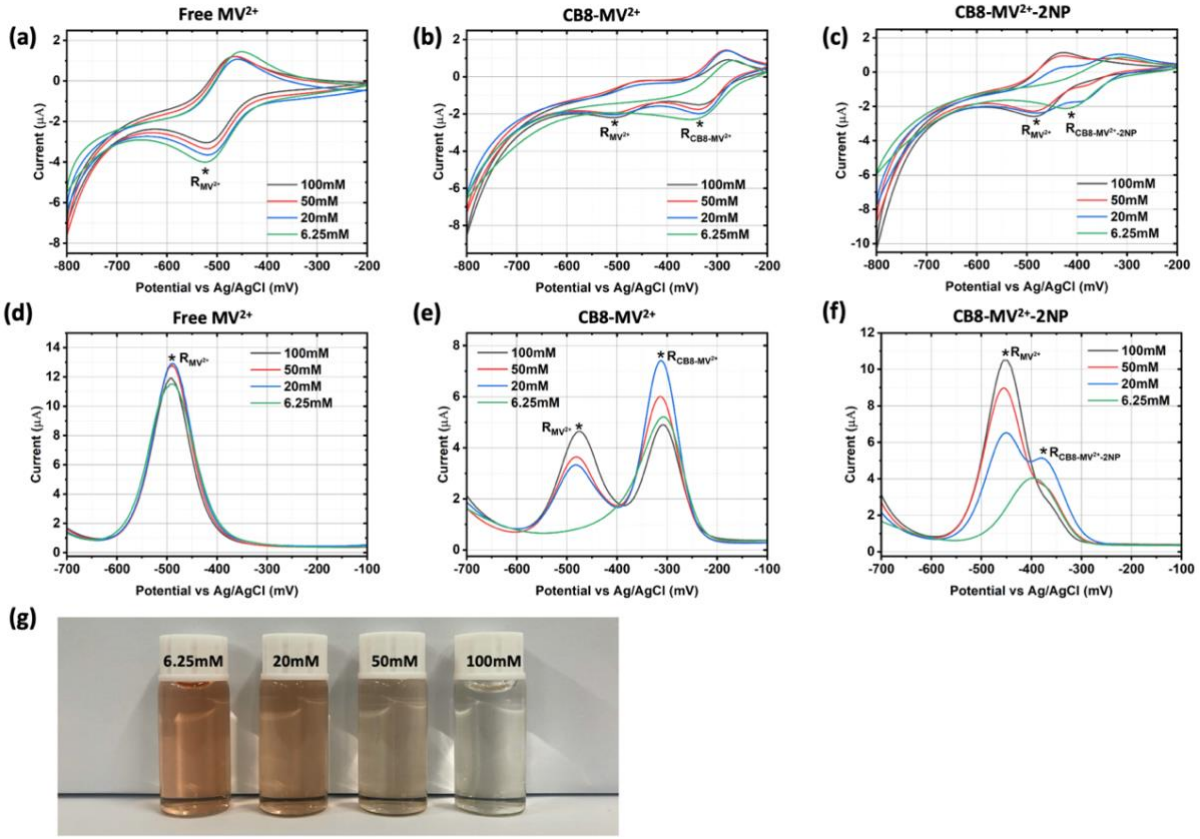

Fig. 4.2 Cyclic voltammograms of **(a)** 1 mM free MV^{2+}, **(b)** 1 mM 1:1 CB8-MV^{2+} and **(c)** 1 mM 1:1:1 CB8-MV^{2+}-2NP in different concentrations (6.25, 20, 50 and 100 mM) of PB solution (pH 7) at scan rate of 10 mV/s. Square wave voltammograms of **(d)** 1 mM free MV^{2+}, **(e)** 1 mM 1:1 CB8-MV^{2+} and **(f)** 1 mM 1:1:1 CB8-MV^{2+}-2NP in different concentrations (6.25, 20, 50 and 100 mM) of PB solution (pH 7) at frequency and step size of 5 Hz and 2 mV,

respectively. **(g)** Photo of 1mM CB8-MV^{2+}-2NP samples prepared in PB solution (pH 7) at different concentrations of 6.25, 20, 50 and 100 mM.

The electrochemical characteristics of MV^{2+}, CB8-MV^{2+} and CB8-MV^{2+}-2NP were investigated by cyclic voltammetry (**Fig. 4.1c**). It has been widely studied that dicationic MV^{2+} can experience two consecutive reversible reduction steps, generating $MV^{+\bullet}$ radical and neutral MV^0, respectively [67,94]. The first reversible reduction process, *i.e.* from dicationic MV^{2+} to $MV^{+\bullet}$ radical process, was mainly discussed here in this Chapter. The reduction potential of 1 mM MV^{2+} was measured as -624.8 mV versus Ag/AgCl reference electrode at scan rate of 10 mV/s by cyclic voltammetry. After introducing 1 equivalent of CB8 into 1 mM of MV^{2+}, the reduction peak was positively shifted by 130 mV to -494.8 mV under the same measuring parameters of CV, replying that the reduction of CB8 encapsulated MV^{2+} is easier than its free form. Such positive shift of MV^{2+} reduction peak in the presence of CB8 is consistent with what Kim and co-workers have reported. Such positive shift can be rationalized by the reversible dimerization of the reduction product $MV^{+\bullet}$ inside CB8 cavity as stable 1:2 CB8-$2MV^{+\bullet}$ complex [94].

It is interesting to note that after adding 1 equimolar of 2NP into 1:1 CB8-MV^{2+}, the reduction peak was shifted back towards the negative direction to -577.9 mV (**Fig. 4.1c**), indicating that the formation of CB8-MV^{2+}-2NP ternary complex hindered the reduction process. Additionally, it was found that the magnitude of reduction potential shift (ΔV_{2NP}) showed an asymptotic growth with increasing equivalence of 2NP until it reached one (**Fig. 4.3**). Thus, 1 equivalent of G2 was applied in all other electrochemical experiments of ternary complexes in this Chapter. Provided the reduction of CB8-MV^{2+}-2NP would end as 1:2 stable complex CB8-$2MV^{+\bullet}$ and free 2NP, its entire reduction process could be regarded as an electrochemically driven dissociation of CB8-MV^{2+}-2NP ternary complex. Therefore, it can be hypothesized that the hindrance magnitude to the electrochemical reduction of CB8-MV^{2+}-2NP reflecting by the potential shift ΔV_{2NP} in **Fig. 4.1c** would correlate to its thermodynamic stability represented by its binding constant K_{2NP}, and MV^{2+} would work as an efficacious redox indicator to estimate the binding constant (K_{G2}) of a particular CB8-MV^{2+}-G2 ternary complex rapidly and simply.

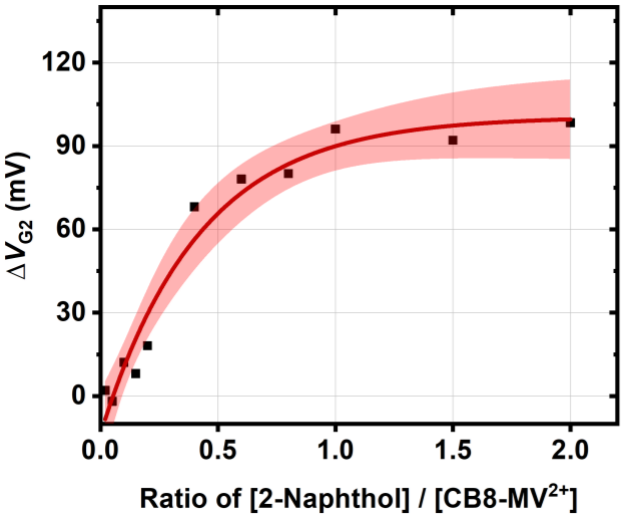

Fig. 4.3 Plot of potential peak shift (ΔV_{G2}) of CB8-MV^{2+} with the addition of different amount of 2NP against the ratio of 2NP/CB8-MV^{2+}.

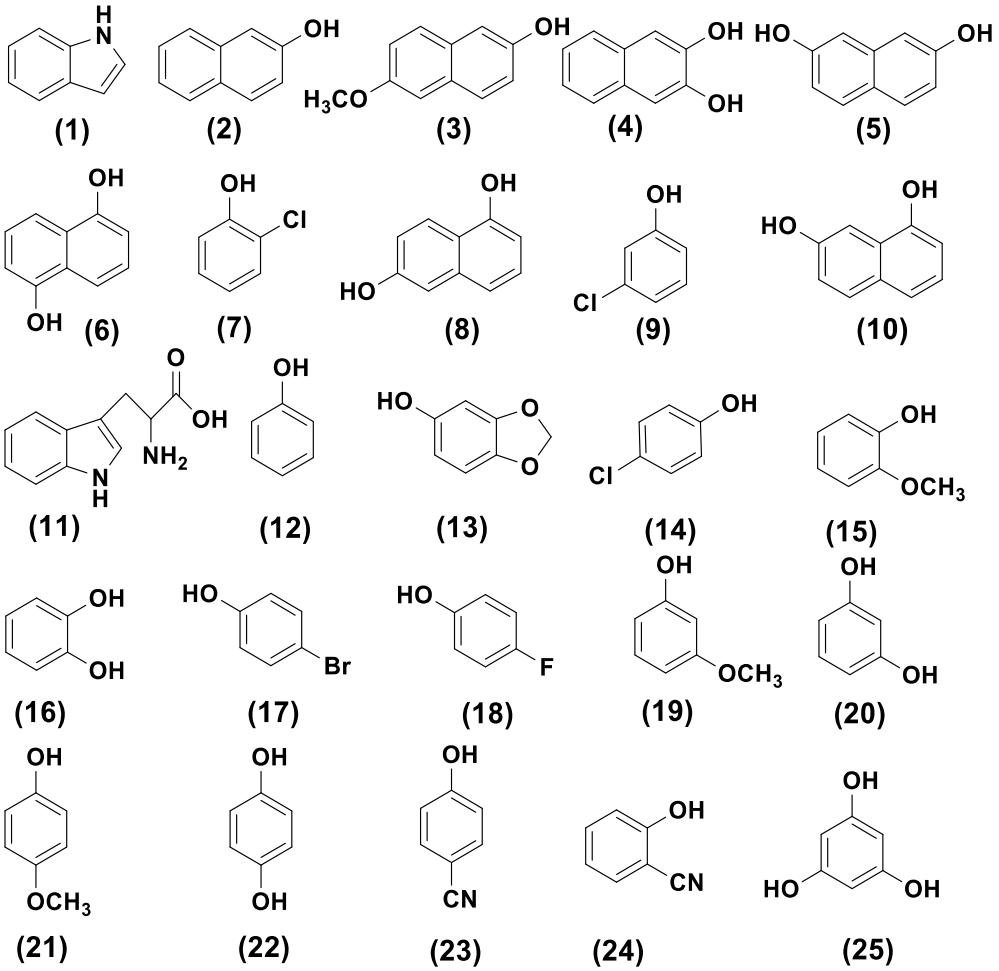

Fig. 4.4 Chemical structures of reference second guests for CB8-MV^{2+}-G2 in decreasing order of ITC-determined K_{G2} [87].

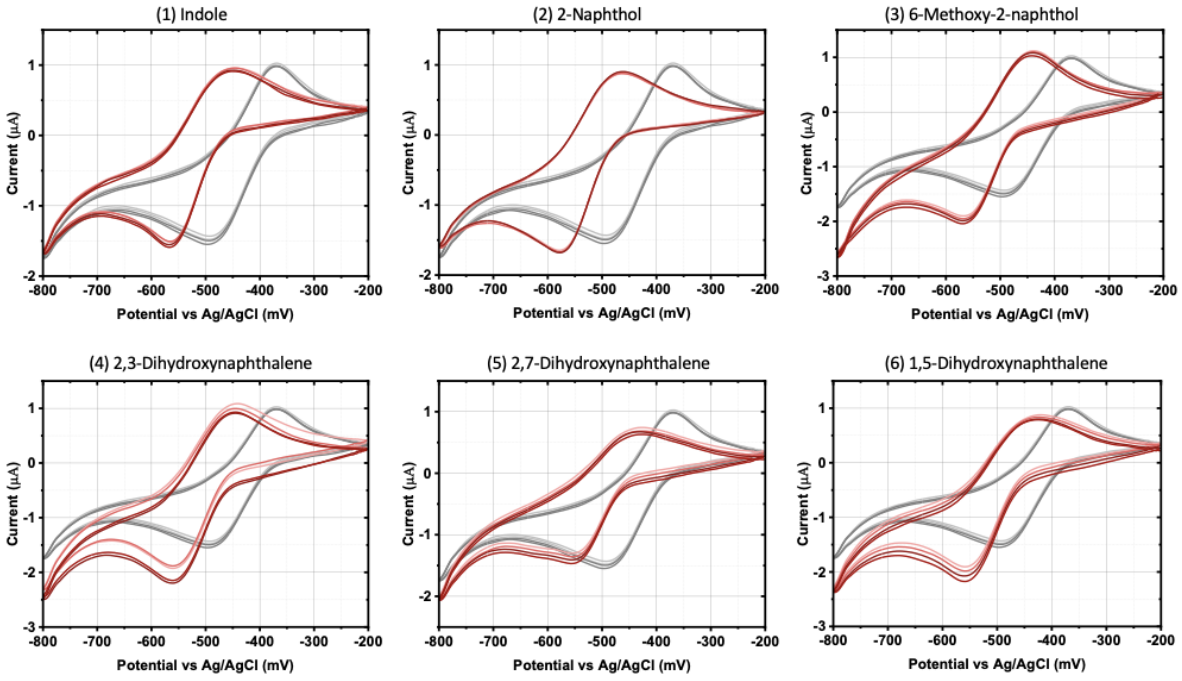

Continued on the next page

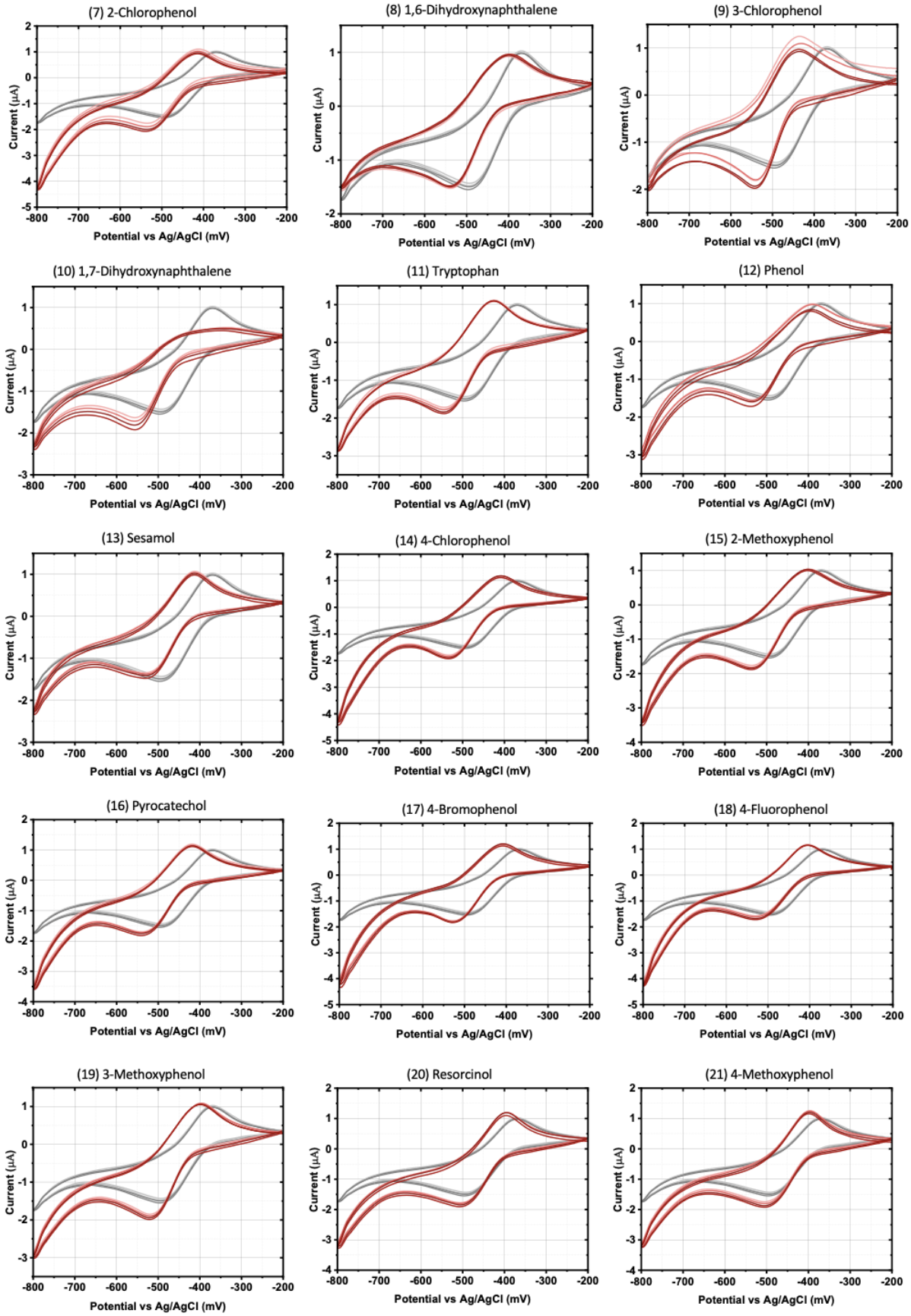

Continued on the next page

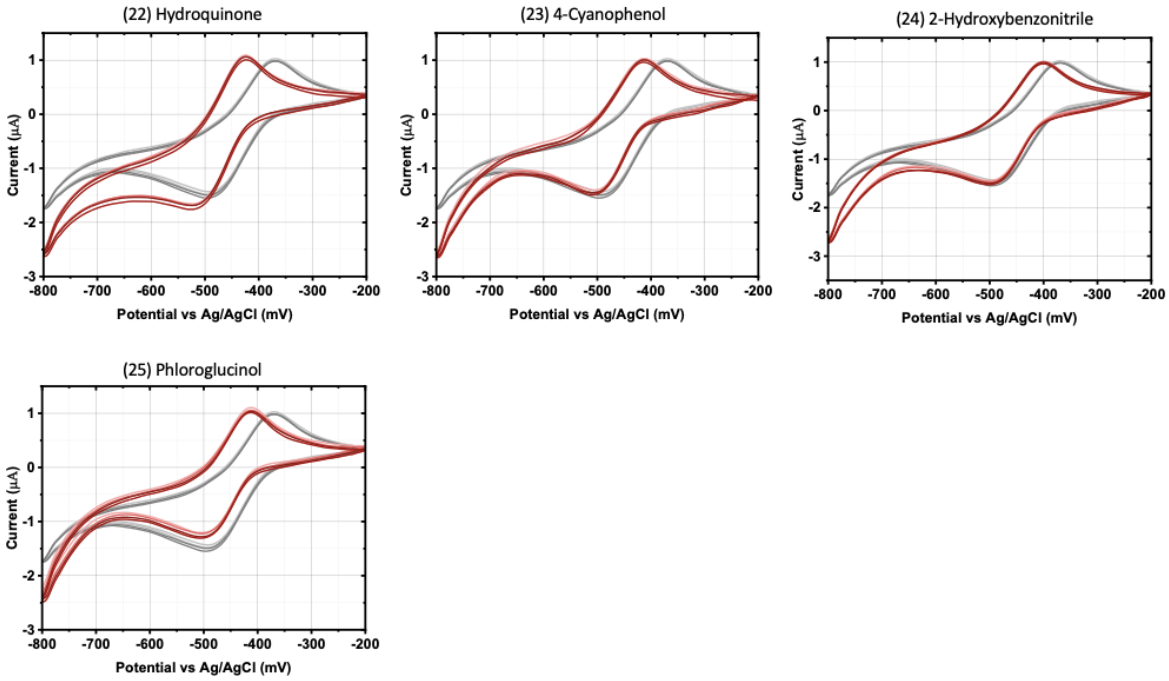

Fig. 4.5 Twenty-five overlaid cyclic voltammograms of CB8-MV^{2+} (grey line) and CB8-MV^{2+}-G2 (red line) obtained by cycling potential from -200 mV to -800 mV for 5 cycles at scan rate of 10 mV/s using Au disk and leakless Ag/AgCl as WE and RE, respectively. Electrolyte: 6.25 mM PB solution (pH 7). The name of G2 was labelled on the top of each plot.

To prove the assumptions proposed above, the reduction potential shift (ΔV_{G2}) of twenty-five reference CB8-MV^{2+}-G2 ternary complexes with respect to CB8-MV^{2+} were electrochemically measured by CV and SWV as shown in **Fig. 4.5** and **Fig. 4.6**, respectively. To reduce the inconsistency for the correlation with ITC measured data, the electrolyte condition in electrochemical measurements was chosen the same as that used in ITC [78]. Chemical structures of corresponding twenty-five G2 molecules were demonstrated in **Fig. 4.4** in decreasing order of their documented binding constants (K_{G2}) measured by ITC [78].

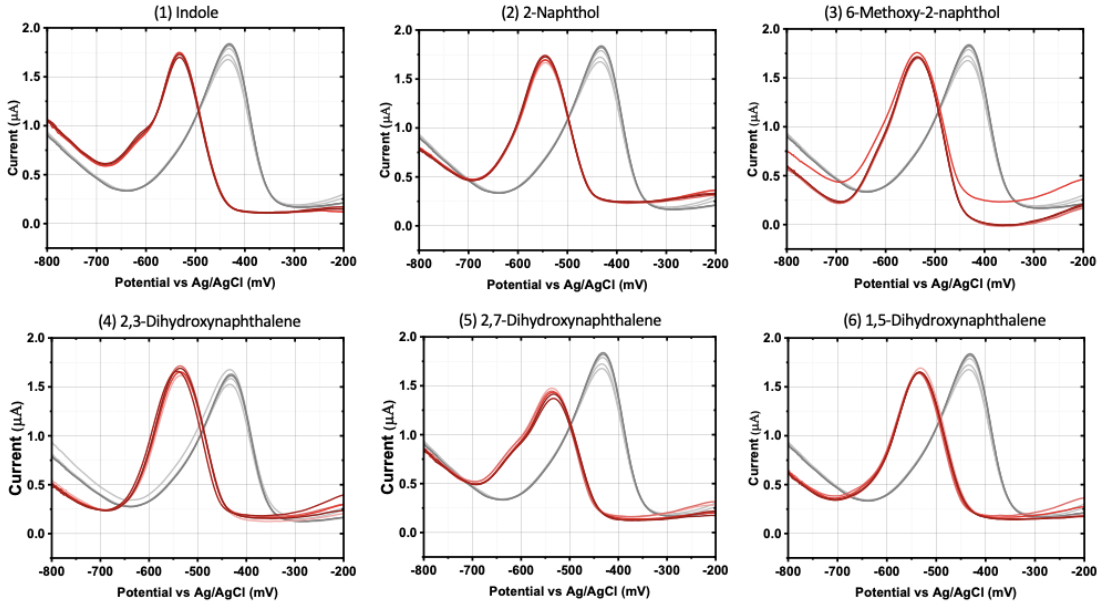

Continued on the next page

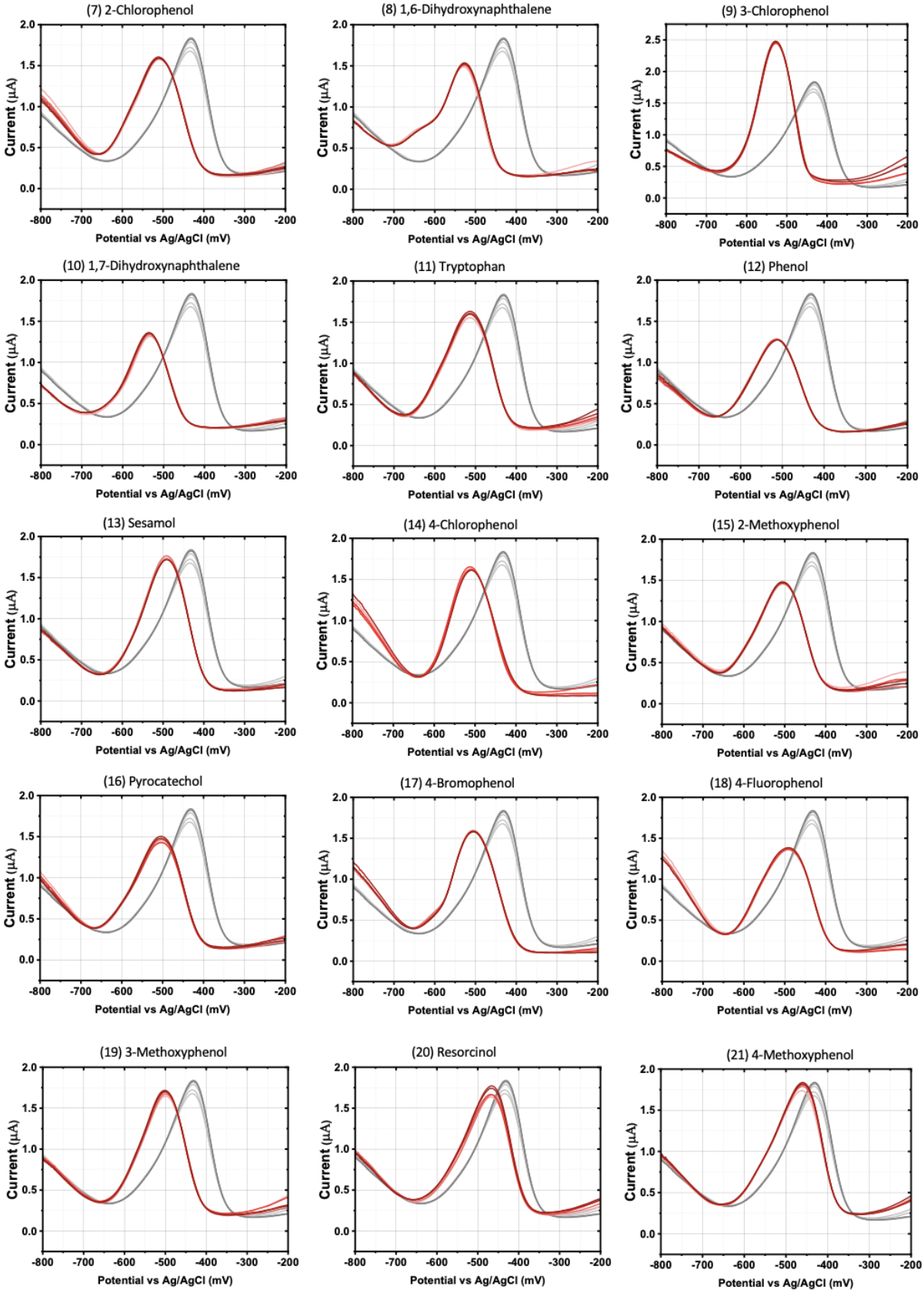

Continued on the next page

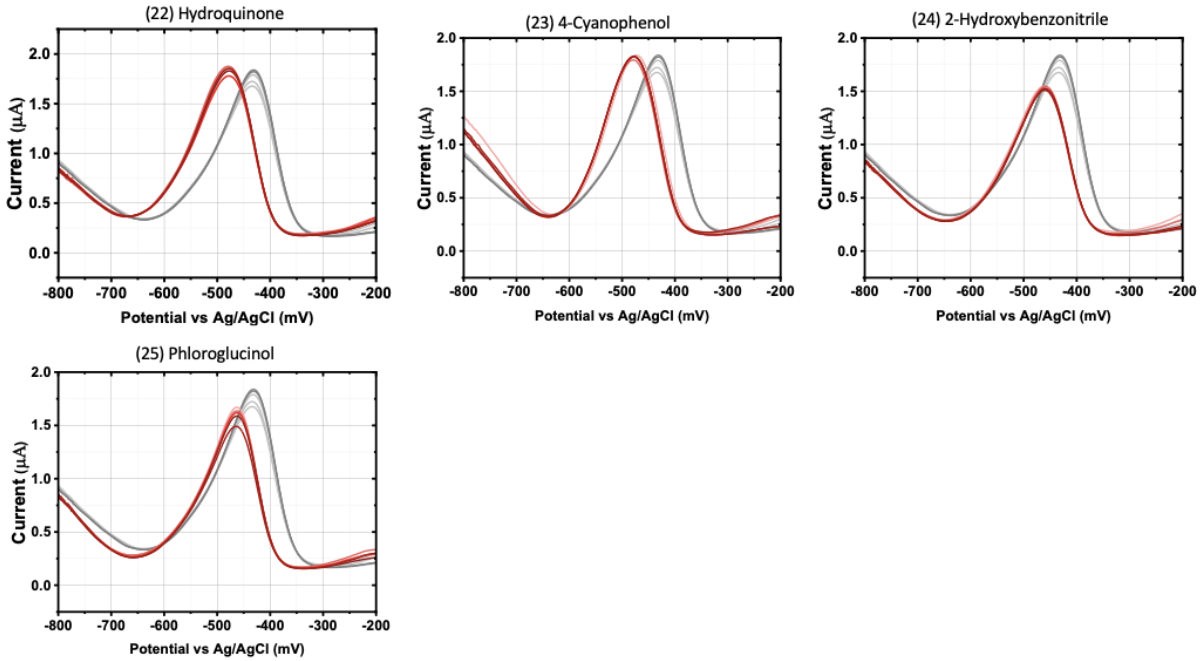

Fig. 4.6 Twenty-five overlaid square wave voltammograms of CB8-MV^{2+} (grey line) and CB8-MV^{2+}-G2 (red line) obtained by setting the initial and end voltage as -200 mV and 800 mV, respectively. Each CB8-MV^{2+}-G2 was measured for 5 times. WE: Au disk. RE: leakless Ag/AgCl. Electrolyte: 6.25 mM PB solution (pH 7). The name of G2 was labelled on the top of each plot.

4.3 Correlation between the reduction potential shift of CB8-MV^{2+}-G2 and the ITC binding constants

The reduction potential shift values (ΔV_{G2}) of twenty-five CB8-MV^{2+}-G2 reference ternary complexes were obtained by CV and SWV and plotted against their corresponding reported $\log K_{G2}$ obtained by ITC. **Fig. 4.7a-b** were plotted by assuming ITC obtained binding constants to be true values to remove the methodological error for correlation with our electrochemical results; **Fig. 4.7c-d** took the ITC experimental error into account for reference. It is notably to discover that a simple linear regression relationship was fitted between ITC determined $\log K_{G2}$ and electrochemically measured ΔV_{G2} for twenty-five CB8-MV^{2+}-G2 reference ternary complexes with desired R^2 values of 0.85 and 0.82 in CV and SWV, respectively. The regular residual was found to be distributed narrowly at the centre of zero with a relatively small peak width (**Fig. 4.8a,d**), consistent with the linear fitting observed between percentiles and regular residual (**Fig. 4.8b,e**), and there was no trending bias in variance through the overall range of fitted $\log K_{G2}$ when regular residual was plotted against fitted $\log K_{G2}$ (**Fig. 4.8c,f**). These residual analysis of the linear fitting between ITC determined $\log K_{G2}$ and electrochemically measured ΔV_{G2} support the appropriateness of the applied fitting model. The R^2 values of the fitting between $\log K_{G2}$ and CV measured ΔV_{G2} were found to be decreased as the scan rate of cyclic voltammetry increased, indicating that the slower the scan rate, the more the host-guest exchange involved system approached its steady state (**Fig. 4.9**). The changing trending of R^2 with the scan rate is in line with the fact that unlike half-wave potentials, CV peak potentials are not of thermodynamic meanings, and therefore a slow scan rate is important to ensure the data credibility. The slope of empirical linear fitting regression plots corresponding to CV (**Fig. 4.7a,c**) and SWV (**Fig. 4.7b,d**) appear to be the same, suggesting a good consistency between two electrochemical measuring techniques. The mildly larger intercept in CV fitting with respect to that in SWV could be rationalized by the larger

potential shift observed in SWV resulted from the minor contribution from the anodic peak to the overall SWV curve (**Fig. 4.10**).

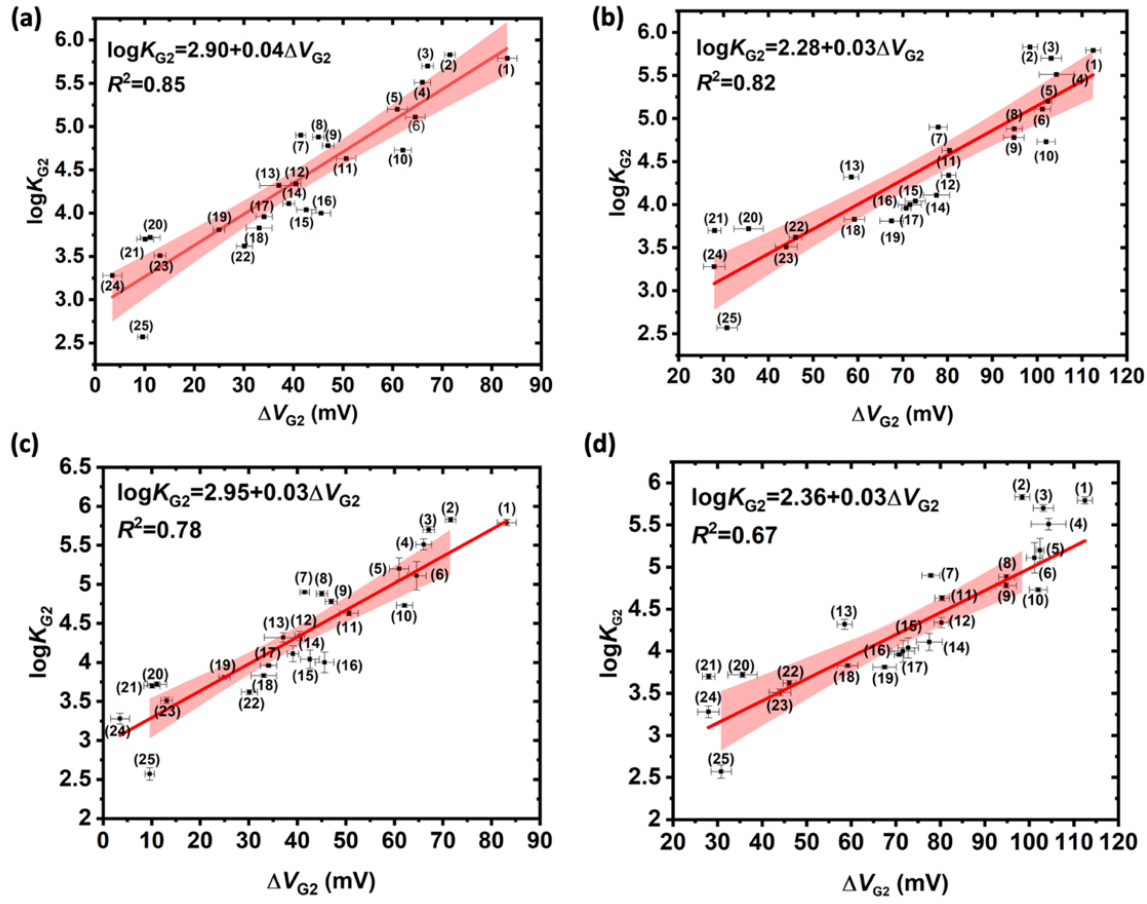

Fig. 4.7 Linear regression curves of ITC-determined logK_{G2} against the reduction potential shift ΔV_{G2} of twenty-five CB8-MV^{2+}-G2 reference ternary complexes measured by CV **(a)** without and **(c)** with experimental error of ITC. Linear regression curves of ITC-determined logK_{G2} against the reduction potential shift ΔV_{G2} measured by SWV **(b)** without and **(d)** with experimental error of ITC. The number labelled adjacent each data point corresponds to the chemical structures in **Fig. 3.4**. Regression function and corresponding R^2 are demonstrated at the upper-left corner. Red line is the linear regression curve and pink band is the 95% confidence range. The regression function is inherently empirical. There are boundary conditions for the accrual correlation when (i) logK_{G2} is approaching '+infinity', ΔV_{G2} is close to 0, and when (ii) logK_{G2} is approaching '−infinity', ΔV_{G2} appears to be a constant. Thus, the correlation curve should not be linear over the entire range.

Leveraging the obtained correlation between ITC determined logK_{G2} and CV/SWV measured ΔV_{G2} shown in **Fig. 4.7**, the logK_{G2} of an unknown G2 is allowed to be rapidly estimated with ΔV_{G2} obtained by one-point CV or SWV test within 10 min, eliminating the requirement of the multiple measuring steps in conventional supramolecular titration methodologies. The accuracy of CV- and SWV-based scheme for the estimation of logK_{G2} were assessed from the root mean squared deviation of ITC determined logK_{G2} from the linear regression equation as ±0.32 and ±0.35, respectively, with the assumption of regarding ITC determined logK_{G2} as true values, which is enough for the purposes of high-throughput screening and sorting logK_{G2} of a series of unknow G2. The precision of CV- and SWV-based scheme stemmed from twenty-five reference ternary complexes were estimated as 0.06 and

0.03, respectively, by taking account of the standard deviation of the ΔV_{G2} in five repeated measurements, which were comparable to that of ITC measurements.

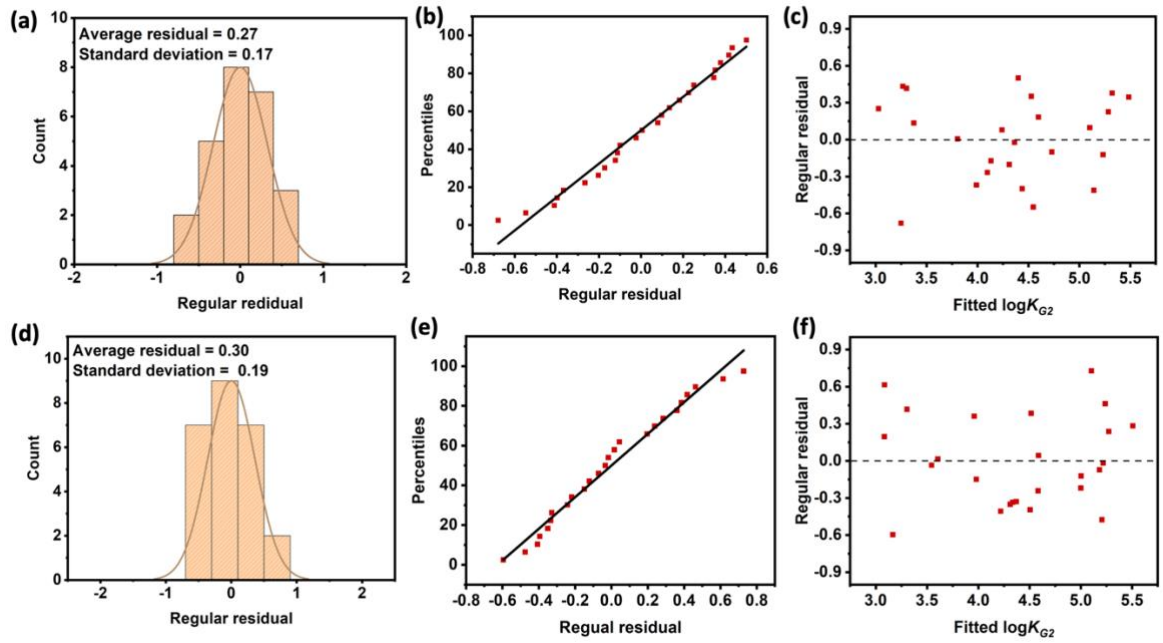

Fig. 4.8 The normal distribution of regular residual corresponding to the correlation fitting of **(a)** CV and **(d)** SWV obtained results. The relationship between percentiles and regular residual corresponding to the correlation fitting of **(b)** CV and **(e)** SWV obtained results. The plots of regular residual against the fitted logK_{G2} corresponding to the correlation fitting of **(c)** CV and **(f)** SWV obtained results.

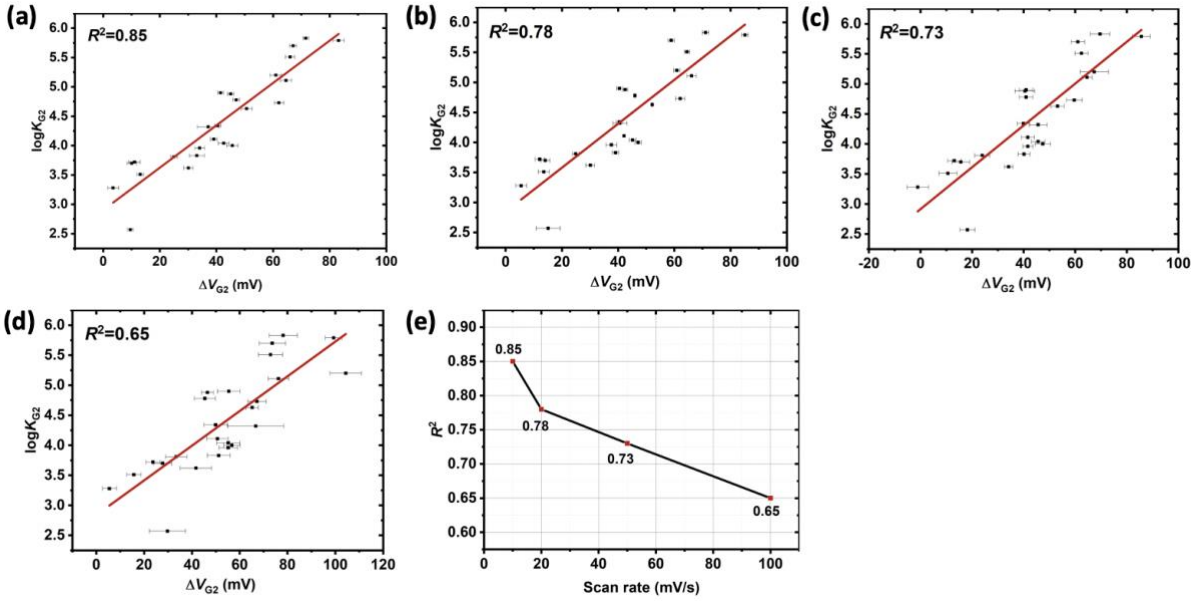

Fig. 4.9 R^2 of linear fitting between ITC determined logK_{G2} and CV measured ΔV_{G2} at scan rate of **(a)** 10 mV/s, **(b)** 20 mV/s, **(c)** 50 mV/s, and **(d)** 100 mV/s. **(e)** The changing trend of R^2 against the scan rate in CV measurements.

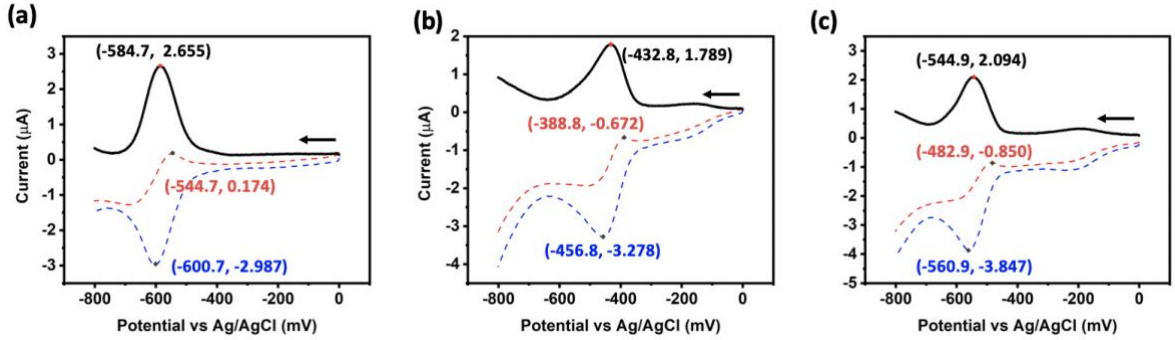

Fig. 4.10 Overall SWV curve (black), cathodic curve (blue), and anodic curve (red) of (a) free MV^{2+} **(b)** CB8-MV^{2+} and **(c)** CB8-MV^{2+}-2NP.

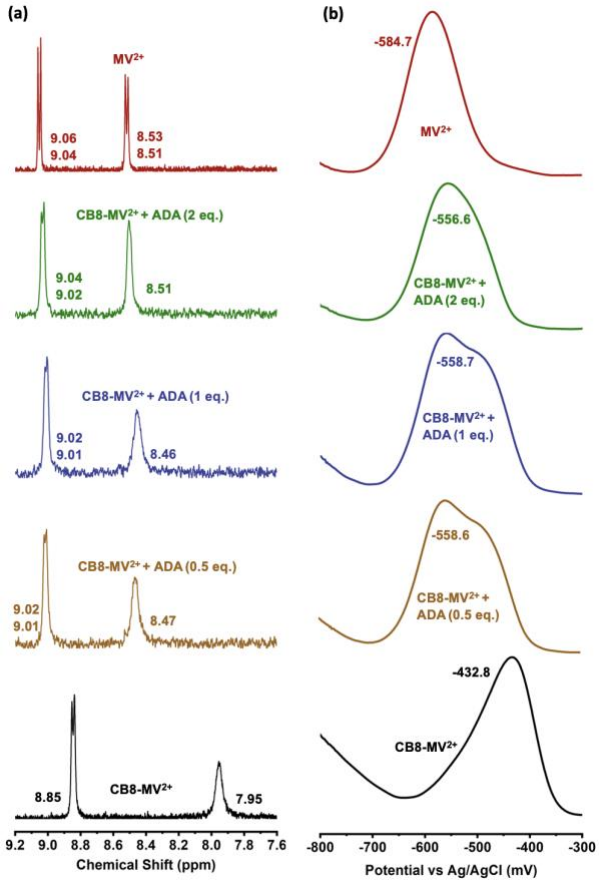

Fig. 4.11(a) ^{1}H NMR spectra and **(b)** corresponding SWV curves of free MV^{2+} and CB8-MV^{2+} in absence and presence of 0.5, 1 and 2 equivalents of 1-adamaintylamine (ADA).

When encountering bulky G2 molecules, it is of great importance to determine whether it is capable of forming ternary complex with CB8-MV^{2+} prior to the estimation of its corresponding binding constant. It is common to see bulky guests like 1-adamaintylamine (ADA) tends to replace the MV^{2+} out of CB8 cavity, resulting in free MV^{2+} and binary complex of CB8-ADA, which could be incorrectly recognized as the formation of ternary complex and thus giving rise to the false-positive value of binding constant in some conventional supramolecular titration protocols such as UV-vis titration experiments. Here, with the aid of sensitive electrochemical techniques, the events of formation of ternary complex and replacement of MV^{2+} can be clearly distinguished from each other. For example, taking ADA as an example bulky analyte, a convolution of reduction peaks corresponding to free MV^{2+} and

CB8-MV^{2+} was observed in the presence of ADA, implying the displacement of MV^{2+} by ADA rather than the formation of CB8-MV^{2+}-ADA took place (**Fig. 4.11b**), consistent with the corresponding ^{1}H NMR spectra (**Fig. 4.11a**). The convolution of peaks in SWV curves caused by the displacement of bulky guests can be easily discovered by human eyes, thereby reducing the probability of false-positive binding constants.

4.4 Electrochemical mechanism analysis

To study the electrochemical mechanism underlying the redox reaction processes of complexes, detail insights into the electrochemical data were performed. We assume the predominate existing form of redox active indicator MV^{2+} is complexed form in CB8-MV^{2+}-G2 sample prior to the redox reaction, and the electron transfer process directly takes place at the interface between the electrode and CB8-MV^{2+}-G2 solution. The first assumption receives support from the generally strong binding affinities of CB8-based ternary complexes [20], and moreover, both CV and SWV are highly sensitive to the occurrence of free form of MV^{2+} (**Fig. 4.12**), but we did not observe the reduction peak corresponding to free MV^{2+} in CB8-MV^{2+}-G2 cases. The second assumption is supported by the fact of fast electron transfer kinetics in the case of free MV^{2+} as well as the reported efficient charge transfer process taking place in the CB7-complexed MV^{2+} [263]. Thus, we ascribe the electrochemical mechanism of free MV^{2+} reduction process observed in CV and SWV to be E_rC_r mechanism [286], referring to a reversible electron transfer process (**eq. 4.1**) followed by a reversible chemical reaction, *i.e.* the host-guest exchange in our case (**eq. 4.2**).

$$[\text{CB8-MV}^{2+}\text{-G2}] + e^- \rightleftharpoons [\text{CB8-MV}^{+\bullet}\text{-G2}] \quad (4.1)$$

$$[\text{CB8-MV}^{+\bullet}\text{-G2}] \rightleftharpoons 1/2[\text{CB8-2MV}^{+\bullet}] + 1/2\text{CB8} + \text{G2} \quad (4.2)$$

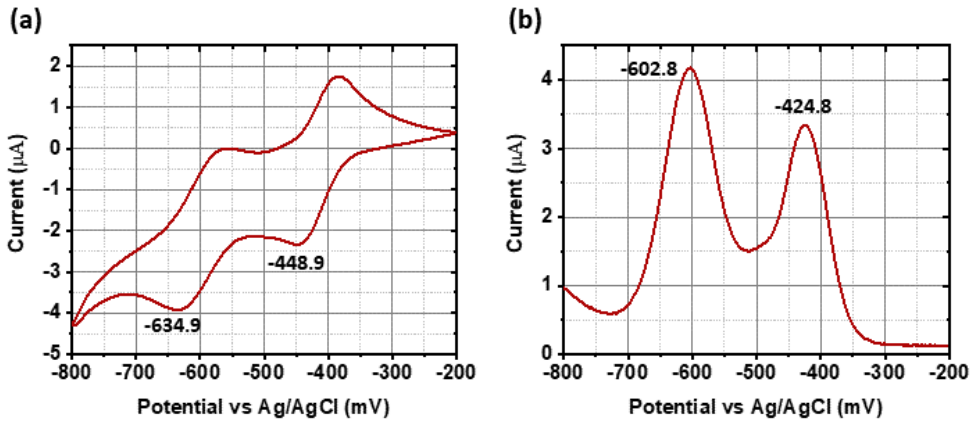

Fig. 4.12 (a) CV and **(b)** SWV curve of the sample containing 1 mM of CB8 and 2 mM MV^{2+} in 6.25 mM PB solution (pH 7).

Detail insights into the CV curves obtained at scan rate of 10 mV/s indicates that the ratio between anodic peak current $i_{a,p}$ and cathodic peak current $i_{c,p}$ of CB8-MV^{2+} complex ($i_{a,p}/i_{c,p}$ = 1.32) is larger than that of free MV^{2+} ($i_{a,p}/i_{c,p}$ = 1.07), which could be rationalized by the accumulation of the redox couple of $MV^{2+}/MV^{+\bullet}$ at the surface of gold working electrode upon complexation with CB8 [46,287]. It is reported that theoretical maximum value of peak current ratio $i_{a,p}/i_{c,p}$ is 1. The larger than 1 peak current observed in the reduction of MV^{2+} and CB8-MV^{2+} could result from the over-estimation of the cathodic peak current at the switching potential $(i_{s,p})_0$ in the utilized Nicholson method (**eq. 4.3**) due to the onset of the hydrogen evolution process taking place at the switching potential (**Fig. 4.13**).

$$i_{a,p}/i_{c,p} = (i_{a,p})_0/(i_{c,p})_0 + 0.485\times(i_{s,p})_0/(i_{c,p})_0 + 0.086 \quad (4.3)$$

where $i_{a,p}$ and $i_{c,p}$ are the anodic and cathodic peak current with a proper baseline; $(i_{a,p})_0$ and $(i_{c,p})_0$ are the experimentally obtained anodic and cathodic peak current; $(i_{s,p})_0$ is the experimentally obtained current at the switching potential.

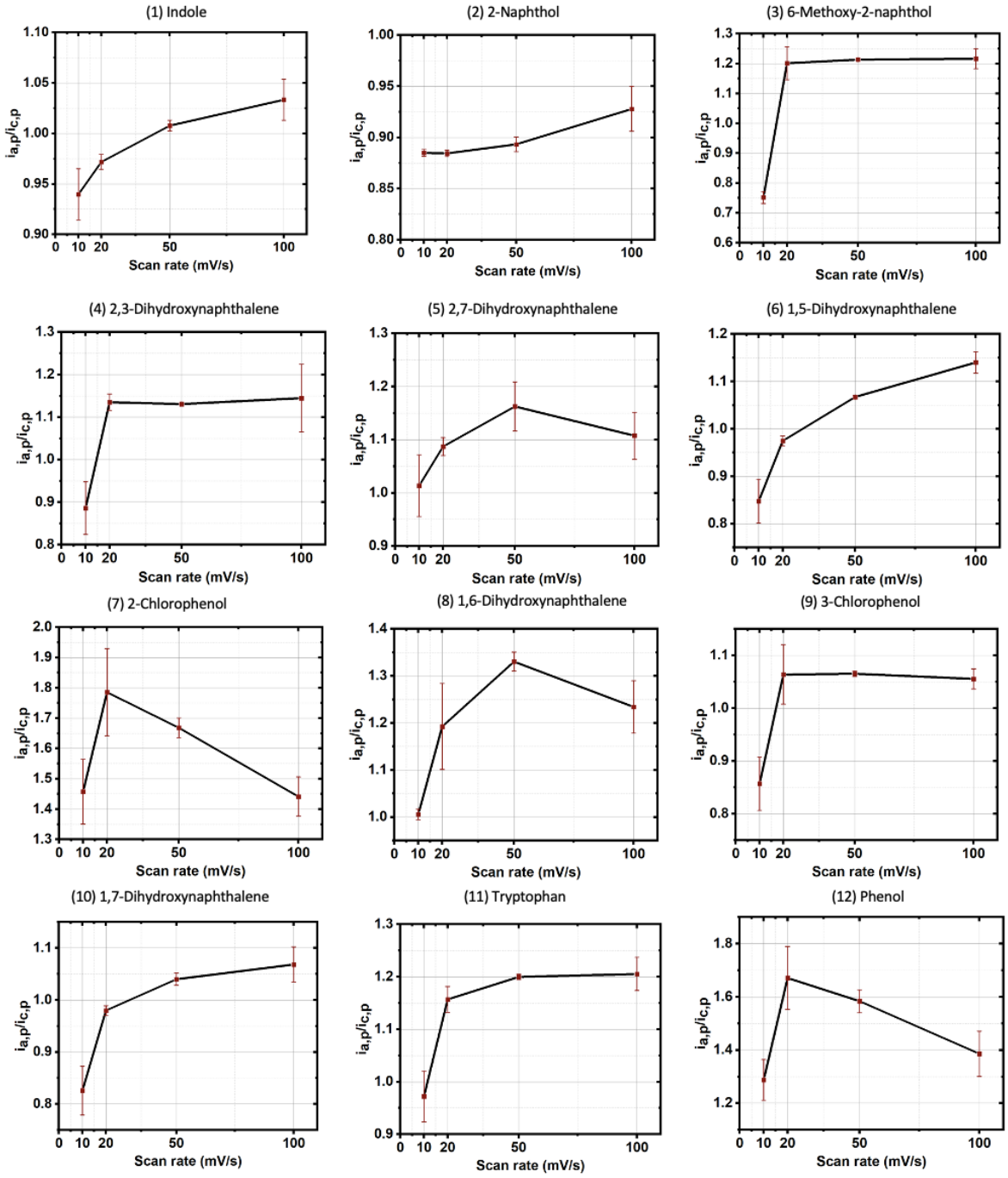

Continued on the next page

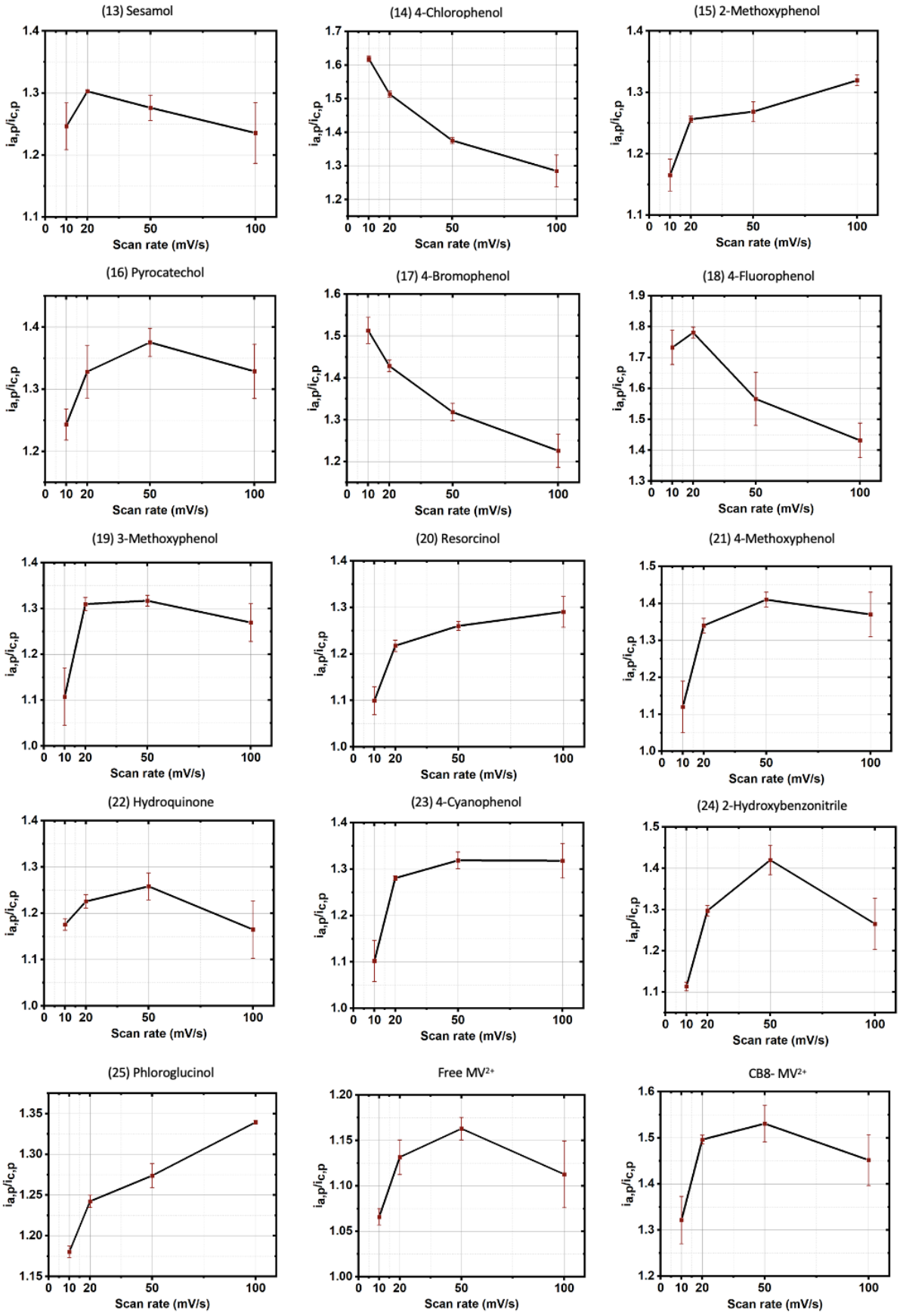

Fig. 4.13 Plots of peak current ratio between anodic peak current and cathodic current calculated using Nicholson method against the scan rate in CV measurements for twenty-five

reference CB8-MV^{2+}-G2 ternary complexes, CB8-MV^{2+} and MV^{2+}. The corresponding G2 is labelled at top of each plot.

In addition, the peak-to-peak potential splitting (ΔE_p) of CV curves measured at 10 mV/s in the cases of free MV^{2+}, CB8-MV^{2+} and CB8-MV^{2+}-G2 reference ternary complexes were investigated and compared. It was observed that the ΔE_p value of free MV^{2+} (83 mV) is the smallest with respect to CB8-MV^{2+} (125 mV) and CB8-MV^{2+}-G2 (92 to 217 mV) complexes, revealing the reversibility of the reduction of free MV^{2+} is higher than that of its complexed form, *e.g.* CB8-MV^{2+} and CB8-MV^{2+}-G2 complexes. This could be attributed to the fact that the reverse anodic reaction was kinetically hindered by the CB8 complexation, in line with the reported formation of stable 1:2 CB8-$2MV^{+\bullet}$ complex during the redox reaction (**eq. 4.2**).

Further inspection can be obtained by analysing the effect of scan rate on the peak current ratio ($i_{a,p}/i_{c,p}$) and peak-to-peak potential splitting values in cyclic voltametric results (ΔE_p). It is interesting to note that a general increasing trend of $i_{a,p}/i_{c,p}$ was observed in most of CB8-MV^{2+}-G2 ternary complexes as scan rate increased from 10 mV/s to 100 mV/s (**Fig. 4.13**), and meanwhile it was found that in all cases, including free MV^{2+}, CB8-MV^{2+} and CB8-MV^{2+}-G2 ternary complexes, ΔE_p increased with the increasing scan rate (**Fig. 4.14**). These findings suggest that the involved homogeneous chemical reaction is an irreversible process, *i.e.* the overall electrochemical mechanism is E_rC_i mechanism. This seemingly controversial observation stresses the exceptional kinetic stability of 1:2 CB8-$2MV^{+\bullet}$ complex that makes the rate of reverse reaction in **eq. 4.2** considerably slow with respect to the timescale in CV measurements and makes the homogeneous chemical reaction in **eq. 4.2**, *i.e.* the host-guest exchange process, seemingly irreversible.

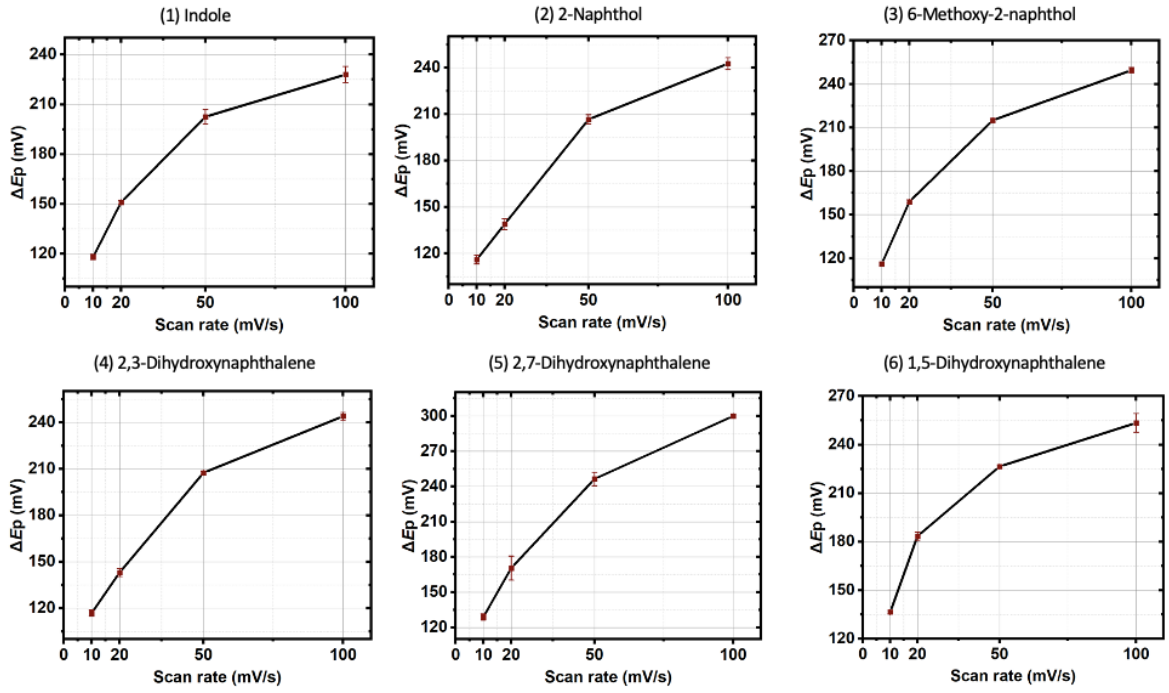

Continued on the next page

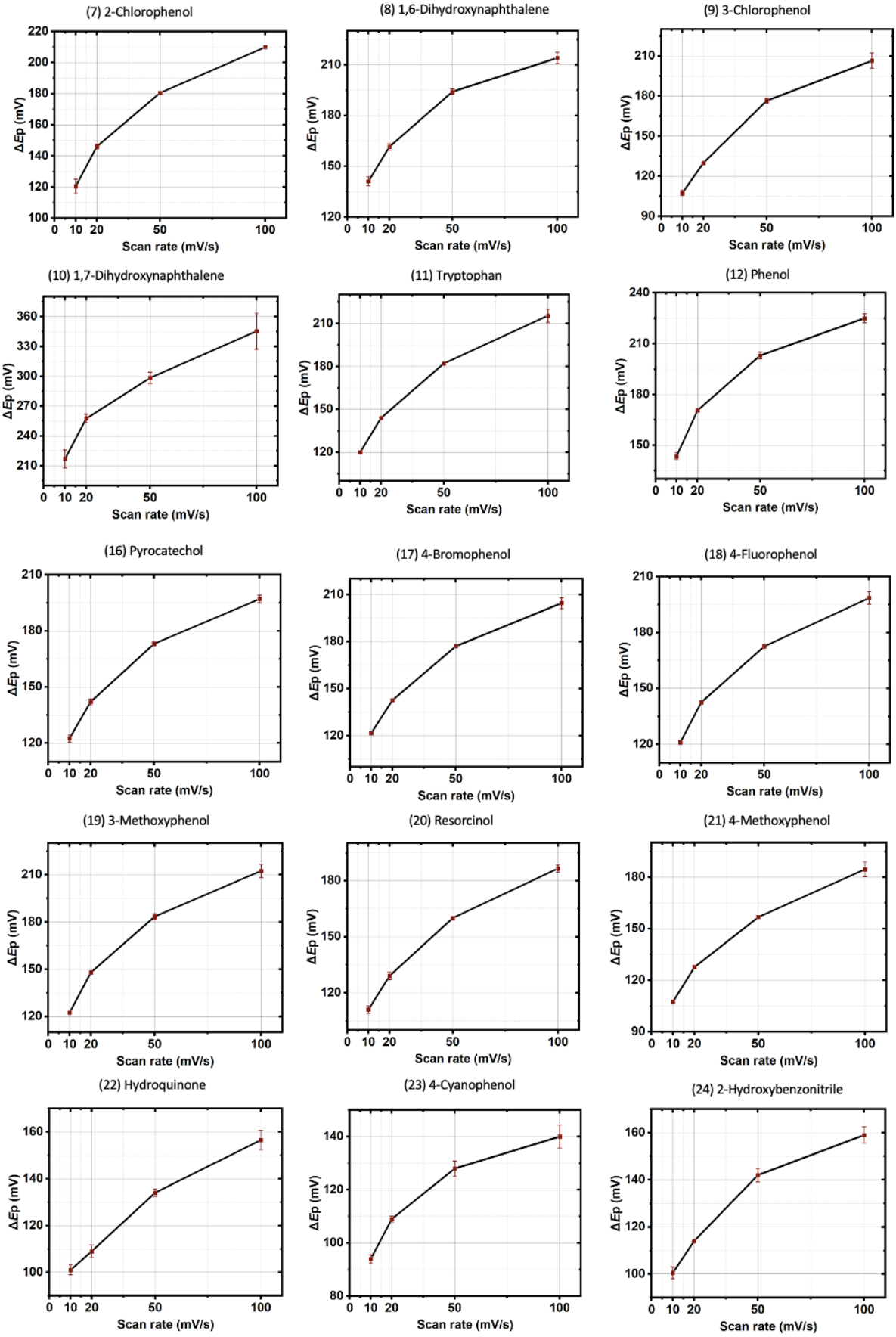

Continued on the next page

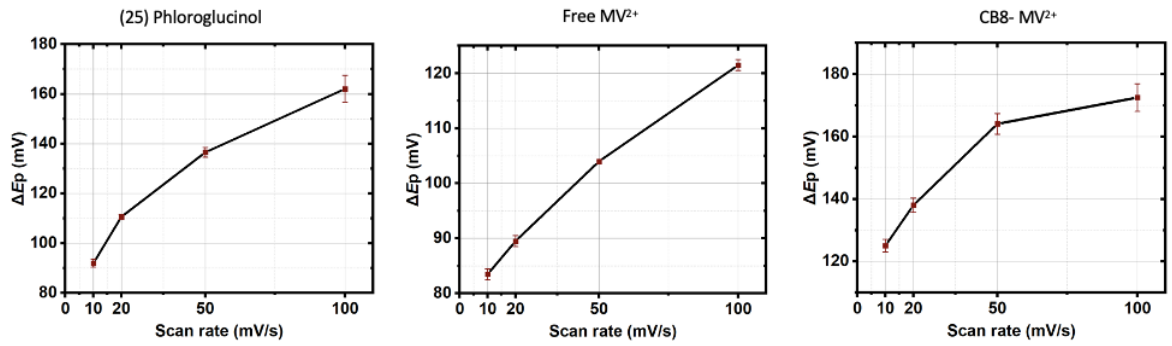

Fig. 4.14 Plots of peak-to-peak potential splitting against scan rate in CV measurements for twenty-five reference CB8-MV^{2+}-G2 ternary complexes, CB8-MV^{2+} and MV^{2+}. The corresponding G2 is labelled at top of each plot.

Additionally, it is noted that in the cases of strong CB8-MV^{2+}-G2 ternary complexes, *i.e.* K_{G2} is high, the shape of their CV curves demonstrated a high dependence on the scan rate. In detail, a small hump appeared in the negative side with respect to the main anodic peak at higher scan rates these strong CB8-MV^{2+}-G2 ternary complexes, such as CB8-MV^{2+}-indole and CB8-MV^{2+}-2NP (**Fig. 4.15**). The appeared minor hump could be resulted from the direct oxidation of CB8-$MV^{+\bullet}$-G2 rather than the kinetically stable CB8-$2MV^{+\bullet}$, suggesting that the G2 which can work as a strong binder is likely to compete with the formation of stable CB8-$2MV^{+\bullet}$ by forming CB8-$MV^{+\bullet}$-G2. Meanwhile, the kinetics of host-guest exchange processes of these strong G2 are generally slower with respect to that of weak G2, whose CV curves present highly symmetric without the appearance of minor hump over the whole range of scan rate from 10 mV/s to 100 mV/s. It is worth mentioning that the comprehensive analysis regarding the electrochemical mechanism could be more complicated if taking account of the interplay between diverse redox active species during the dynamic interconversion and is out of the scope of our present study.

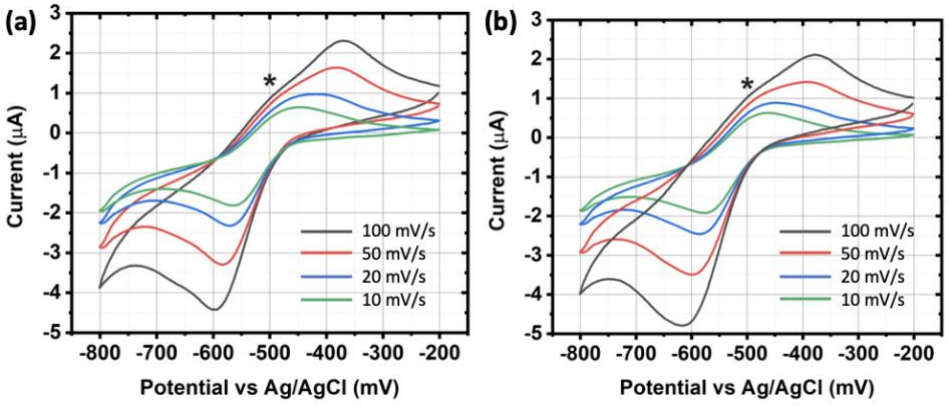

Fig. 4.15 Cyclic voltammograms of **(a)** CB8-MV^{2+}-indole, and **(b)** CB8-MV^{2+}-2NP obtained at different scan rates. The asterisk marks the minor hump.

4.5 Mechanistic investigation based on computational simulations

Clarification: modelling in this section were performed by my colleague, Dr. Hugues Lambert.

To quantitively understand the origin attributing to the linear correlation of the ITC determined binding constants logK_{G2} with the electrochemically measured potential shift ΔV_{G2} of CB8-MV^{2+}-G2 ternary complexes, computational simulations based on density functional

theory (DFT) were performed. MMFF94 was utilized to minimize the molecular models of ternary complexes first prior to the DFT optimization at wB97XD/6-31G* and CPCM/wB97XD/6-31G* level of theory, where CPCM implicit water model was utilized to simulate the solvent effects in aqueous-based electrochemical measurements. The dispersion corrected DFT functional wB97XD was employed to precisely assess the van der Waals interactions which tend to significantly contribute to the binding strength of the host-guest complexes. Specifically, the energy change upon the reduction processes, *e.g.* steps in **eq. 4.1, 4.4 and 4.5**, was computed with the DFT optimized molecular models. Nevertheless, no correlation between the computed energy change of CB8-MV^{2+}-G2 ternary complexes and the ITC determined logK_{G2} was discovered (**Fig. 4.16**). As indicated by **Fig. 4.16a-b**, the correlation between ITC determined logK_{G2} and ΔV_{G2} is unlikely to be rooted from the redox step (**eq. 4.5**) but could stem from host-guest exchange process (**eq. 4.2**) taking place after the reduction. **Eq. 4.5** describes the full redox reaction of CB8-MV^{2+}-G2 ternary complex taking both anodic and cathodic half-reaction into account, which ensures the electronic conservation of the equation. In addition, as suggested by the lack of correlation in **Fig. 4.16c-d**, the solvation effects, which was not considered in the calculation for **Fig. 4.16c-d**, tend to significantly influence the binding constants of CB8-MV^{2+}-G2 ternary complex in aqueous environment.

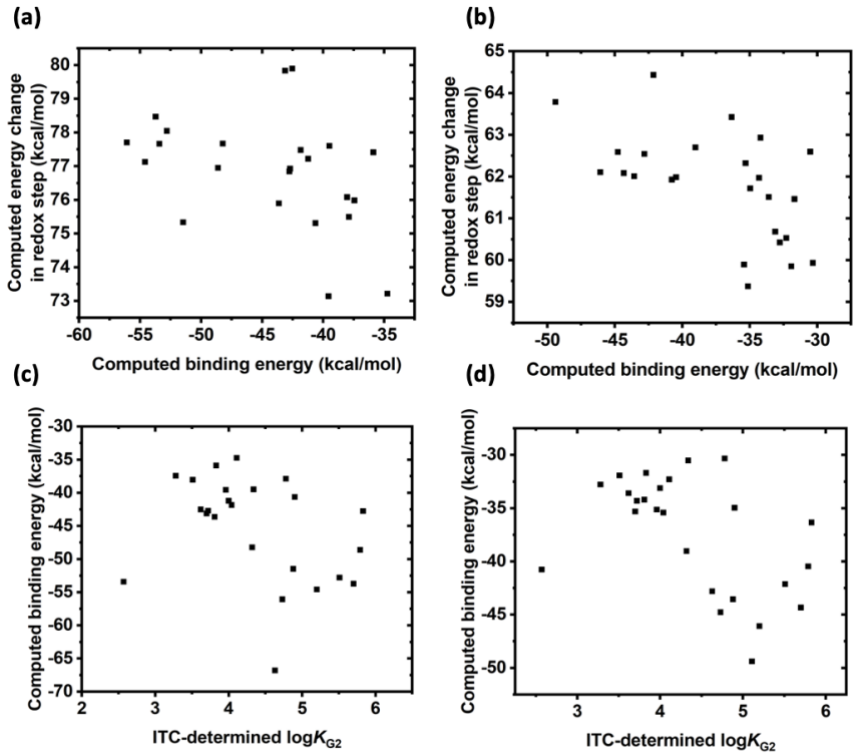

Fig. 4.16 (a-b) Scatter plots of computed energy change in **eq. 4.5** against the computed binding energy of CB8-MV^{2+}-G2 calculated by **eq. 4.4**. **(c-d)** The computed binding energy of CB8-MV^{2+}-G2 calculated by **eq. 4.4** against the ITC determined logK_{G2}. The computational simulations for **(a)** and **(c)** were performed at wB97XD/6-31G* level of theory, and for **(b)** and **(d)** were performed at CPCM/wB97XD/6-31G* level of theory, where CPCM implicit water model was utilized to simulate the solvent effects in aqueous-based electrochemical measurements.

$$[\text{CB8-MV}^{2+}] + \text{G2} \rightleftharpoons [\text{CB8-MV}^{2+}\text{-G2}] \quad (4.4)$$

$$[\text{CB8-MV}^{2+}\text{-G2}] + 3/2\text{H}_2\text{O} \rightleftharpoons [\text{CB8-MV}^{+\bullet}\text{-G2}] + 1/4\text{O}_2\ (\text{triplet}) + \text{H}_3\text{O}^+ \quad (4.5)$$

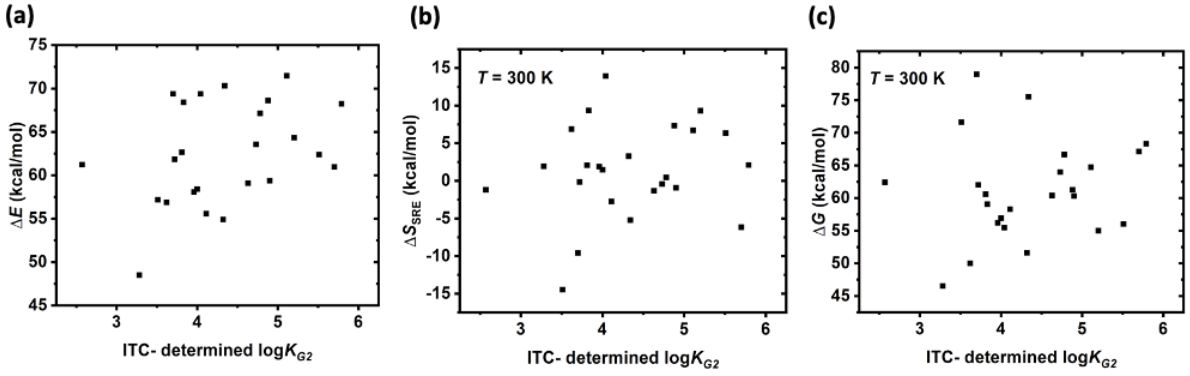

Fig. 4.17 Scatter plot of **(a)** the computed energy changes (ΔE) in step of **eq. 3.5** at 300 K, **(b)** the configurational entropy changes in the reduction of [CB8-MV^{2+}-G2] to [CB8-$MV^{+\bullet}$-G2] (ΔS) at 300 K, and **(c)** the Gibbs free energy changes (ΔG) against the logK_{G2} determined by ITC. The energy values of redox reaction involved species were obtained by time-averaged the energy over 30 ps trajectories in vacuum condition at the PM6D3 level of theory. The configurational entropy values were obtained utilizing the Spectrally Resolved Estimation of the entropy with the 30 ps trajectories. The Gibbs free energy were calculated using the computed enthalpy and entropy values taking the oxidation of H_2O into account for electronic conservation (**eq. 4.5**).

CB*n* cavities are expected to have a complicated energy landscape which cannot be completely represented with the energies and structures of a local minimum, ab initio molecular dynamics at the PM6-D3 level of theory was thus utilized for further inspection, while no satisfying correlation was found either (**Fig. 4.17**). Specifically, the energy and the configurational entropy changes in the reduction process were computed using the time-averaged energies and the spectrally resolved estimation, respectively, based on 30 ps trajectories [254]. It was found that the changing magnitude of configurational entropy can be larger than 10 kcal/mol at 300 K, which cannot be neglected. Nevertheless, there is no symmetric trend in configurational entropy change against the ITC determined logK_{G2} either (**Fig. 4.17b**). Similarly, no obvious trend was observed in the energy changes over the reduction of ternary complexes while their range is wider than that of wB97XD optimization (**Fig. 4.17a**). Again, no desired correlation was obtained between the free Gibbs energy changes upon reduction and the ITC determined logK_{G2}, making the standard redox potential of CB-MV^{2+} cannot be directly modulated by the encapsulation of G2.

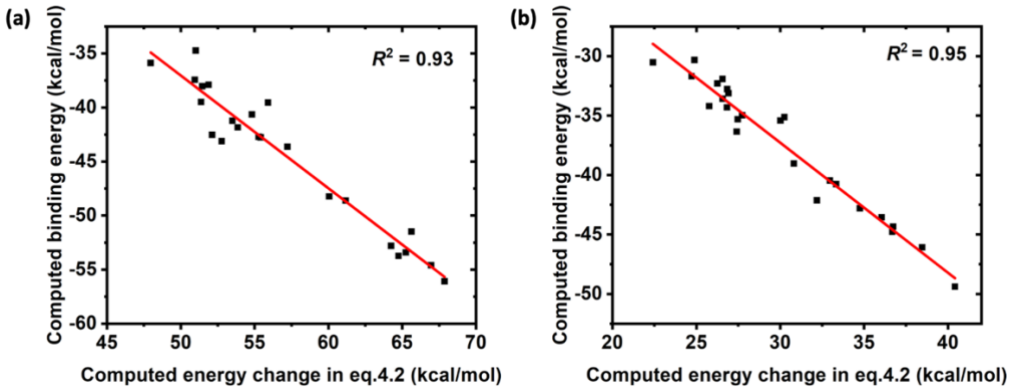

Fig. 4.18 Linear fitting of computed binding energy in **eq. 4.4** against the computed energy change in host-guest exchange process (**eq. 4.2**) using the energy obtained at **(a)** wB97XD/6-

31G* and **(b)** CPCM/wB97XD/6-31G* level of theory, where CPCM implicit water model was utilized to simulate the solvent effects in aqueous-based electrochemical measurements. Note that the optimized energy utilized for the calculation of binding energy and energy change in **eq. 4.2** is based on the total electronic energy of the system modelled by DFT, without thermal corrections. No entropic term is included in these optimized energy values, and they can be roughly considered as enthalpy but are not exactly the same as the conventional enthalpy.

The above computational results suggest that the theory underlying the correlation between ITC determined logK_{G2} and ΔV_{G2} is unlikely to be related to the redox step in **eq. 4.5** but more likely to come from the subsequent host-guest exchange events in **eq. 4.2**, which can be regarded as an electrochemically induced supramolecular dissociation process. Indeed, the reported potential shift in the case of CB8-MV^{2+} is rationalized by the host-guest exchange of CB8-2$MV^{+\bullet}$ instead of the relative stability of the redox species. Therefore, the measured ΔV_{G2} demonstrates the overall difference of free energy in **eq. 4.1** and **4.2**, in line with the proposed E_rC_r mechanism. It is satisfactory to find that the computed energy change in the process of **eq. 4.2** demonstrated a linear fitting (R^2 = 0.95) with the computed binding energy of a CB8-MV^{2+}-G2 ternary complex calculated by the optimized energy obtained at CPCM/wB97XD/6-31G* level of theory (**Fig. 4.18**), implying that the G2 which can strongly bind to CB8-MV^{2+} can also be a strong guest for CB8-$MV^{+\bullet}$. Thus, the electrochemical reduction process of CB8-MV^{2+}-G2 ternary complex will only provide a competitive binding route for CB8-2$MV^{+\bullet}$ as CB8-$MV^{+\bullet}$-G2 but not interfere the relative binding constants within a range of G2.

According to the Nernst Equation (**eq. 4.6**), the observed reductio potential E is dependent on the E_0, which is related to the ΔG_0 and the concentration ratio of [Red]/[Ox] of a specific redox couple (**eq. 4.7**). In the case of CB8-MV^{2+}, the formation of kinetically stable CB8-2$MV^{+\bullet}$ attributes to its favoured reduction process compared to free MV^{2+}, and the consumption of active reduced CB8-$MV^{+\bullet}$ via the formation of less active CB8-2$MV^{+\bullet}$ would result in a positively shifted reduction potential [94]. Here, we propose that the binding constant of G2 with CB8-MV^{2+} regulates the ease of the formation of CB8-2$MV^{+\bullet}$. A G2 with stronger binding constant could hinder the formation of CB8-2$MV^{+\bullet}$ to a greater extent, thereby pushing the reduction potential of the corresponding CB8-MV^{2+}-G2 to a closer position as the free MV^{2+}.

$$E = E_0 - \frac{RT}{nF}\ln\frac{[\mathrm{Red}]}{[\mathrm{Ox}]} \qquad (4.6)$$

$$\Delta G_0 = -nFE_0 \qquad (4.7)$$

where E is the reduction potential at specific temperature T; E_0 is the standard reduction potential; n is the number of electrons involved in redox reaction; F is the Farady constant; [Red] and [Ox] are the concentration of reduced and oxidized species; ΔG_0 is the standard free Gibbs energy change of the redox reaction.

4.6 Proof-of-concept application

To explore the applicability of our proposed electrochemical scheme, we investigated the binding constants of a group of cyclic hydrocarbons as candidate G2 to form ternary complexes with CB8-MV^{2+}, including cyclohexane (CHA), cyclohexene (CHE), 1,3-cyclohexadiene (1,3-CHD), 1,4-cyclohexadiene (1,4-CHD), and benzene, which are known to be volatile and sparingly soluble in aqueous solution, thus making it imperial to prepare their sample solution with accurate concentration for conventional titration methodologies. In our case, their 1:1:1 CB8-MV^{2+}-G2 samples of these cyclic hydrocarbons were prepared by adding excessive amount of cyclic hydrocarbons into 1:1 CB8-MV^{2+}-solution. As indicated by the titration result of 2NP (**Fig. 4.3**), the potential shift (ΔV_{G2}) will not increase further when the

equivalent of 2NP is larger than 1, and thus the excessive G2 is less likely to cause unexpected effect on the ΔV_{G2}.

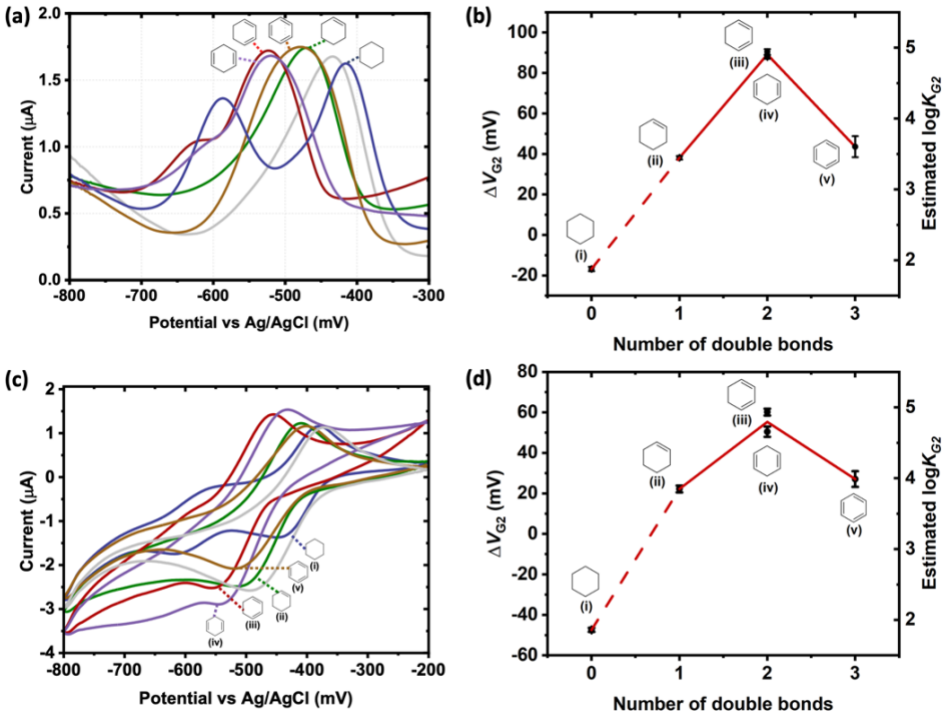

Fig. 4.19 (a) SWV and **(c)** CV curves of CB8-MV^{2+} (grey line) and CB8-MV^{2+}-G2 complexes, where G2 = CHA (blue line), CHE (green line), 1,3-CHD (red line), 1,4-CHD (purple line), and benzene (brown line). The chemical structures of G2 are demonstrated near the corresponding curve. **(b)** SWV and **(d)** CV measured ΔV_{G2} and the estimated $\log K_{G2}$ of CB8-MV^{2+}-G2 complexes plotted against the number of double bonds in G2. The chemical structures of G2 are demonstrated near the corresponding data point.

As expected, certain potential shifts (ΔV_{G2}) of CB8-MV^{2+} were observed in the presence of cyclic hydrocarbons as G2 in both SWV and CV modes (**Fig. 4.19a,c**), and then their corresponding $\log K_{G2}$ were estimated using ΔV_{G2} based on the correlation equations displayed in **Fig. 4.7a-b**, and except CHA, the estimated $\log K_{G2}$ of all other four cyclic hydrocarbons G2 were within the range from 3.5 to 5.0, which is at the similar level as the reported binding constants of other G2 with similar structures [20]. The potential shift values (ΔV_{G2}) as well as the estimated binding constants ($\log K_{G2}$) of these cyclic hydrocarbons G2 were plotted against the number of double bonds in their structures (**Fig. 4.7c-d**). It was suggested that except for benzene, ΔV_{G2} and $\log K_{G2}$ demonstrated an increasing trend with the number of double bonds in G2's structures, which could be rationalized by the enhancing van der Waals and charge-transfer interactions with MV^{2+} upon increasing number of π electrons. The double bonds cannot freely rotate like single bonds, thus rendering G2 less flexibility and reduced entropic penalty upon complexation. The declined binding constant ($\log K_{G2}$) in the case of benzene could be attributed to its higher aqueous solubility with respect to other four cyclic hydrocarbons G2, which disfavoured its complexation from the viewpoint of solvation effect [87].

Interestingly, in the presence of CHA, two reduction peaks were observed in CB8-MV^{2+}, whose peak potential were located at -586.8 mV and -415.6 mV, respectively (**Fig. 4.20**), and the former one could be from the free MV^{2+} by comparing their reduction peak potentials. The presence of free MV^{2+} peak was probably resulted from the formation of 1:1 CB8-CHA

complex or the precipitation of CB8. Therefore, although the size and the hydrophobicity of CHA present proper for the formation of ternary complex with CB8-MV^{2+}, our electrochemical results suggested a weak or even no binding between CHA and CB8-MV^{2+}, consistent with the lack of double bonds and higher molecular flexibility of CHA. As for the reduction peak located at -415.6 mV of CB8-MV^{2+} in the presence of CHA (**Fig. 4.20**), it could be either from the CB8-MV^{2+} (-466.7 mV) or resulted from the CB8-MV^{2+}-CHA complex with the corresponding estimated logK_{G2} of around 1.8 if it formed. The formation or lack of formation of the ternary complex between these six-membered cyclic hydrocarbons and CB8-MV^{2+} were characterized by ^{1}H NMR (**Fig. 4.21**).

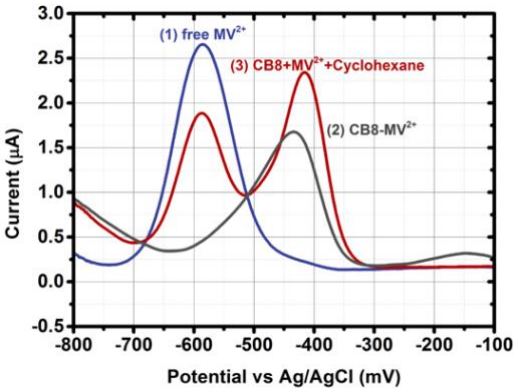

Fig. 4.20 Overlaid SWV curves of free MV^{2+}, CB8-MV^{2+} and CB8-MV^{2+}-CHA.

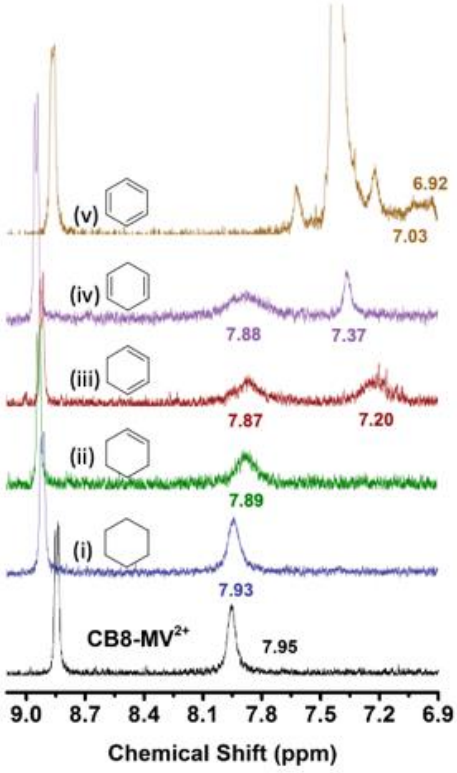

Fig. 4.21 ^{1}H NMR spectra of CB8-MV^{2+} and CB8-MV^{2+} in presence of (i) CHA, (ii) CHE, (iii) 1,3-CHD, (iv) 1,4-CHD and (v) benzene.

4.7 Conclusions

We propose a rapid and simple electrochemical scheme for the estimation of binding constants of CB8-MV^{2+}-based ternary complexes by uncovering a linear correlation (R^2 = 0.85)

between the electrochemical measured potential shifts (ΔV_{G2}) of a given CB8-MV^{2+}-G2 ternary complex and their corresponding reported binding constants ($\log K_{G2}$) determined by ITC, allowing for the desired practical accuracy and high precision of ± 0.32 and ± 0.03 in the estimated $\log K_{G2}$ of an unknown G2, respectively. The whole experiment process following our electrochemical scheme can be finished within 10 min, which is considerably faster than that of the concentration titration methodologies such as hour-scale in ITC. Mechanistic insights with the convergence of experimental and computational results suggest that the linear correlation is rooted from the dynamic host-guest exchange and rearrangement events taking place after the electron transfer step in reduction reaction. It is notably to note that we figure out the applicability and robustness of our proposed electrochemical scheme by studying the binding constants of the ternary complexes formed between a group of six-membered cyclic hydrocarbons and CB8-MV^{2+}, which are hardly determined by conventional titration methodologies otherwise on account of their great volatility and low water solubility. In addition, the information rich electrochemical results enable the monitoring of the different states of the redox active species (MV^{2+}) and lower the possibility of false-positive estimation of binding constants. This electrochemical-based scheme is expected to be expanded to investigating other redox active probe involved host-guest complexes and brings new possibilities of screening and determining binding constants in high-throughput fashion to design supramolecular systems for diverse applications.

Chapter 5. Dual-functional Electrochemical Biosensing Assay using Cucurbit[8]uril-methyl viologen Host-guest Complexes for Small Biomolecule Detection in Complex Bio-media

This Chapter proposed a smart but simple design of an electrochemical assay based on simple self-assembly of commercially available cucurbit[8]uril (CB8) and redox active methyl viologen (MV^{2+}) at a low synthetic effort. Gratifying to find that CB8-MV^{2+} assay integrates multiple functions into one, including (1) associative binding assay (ABA), (2) indicator displacement assay (IDA) as well as (3) real-time monitoring of continuous process. Notably, new possibilities of biosensing and binding constants estimation in biologically most relevant complex matrices, *e.g.* urine, serum and even animal blood, have been achieved by CB8-MV^{2+} electrochemical assay, which has been rarely or even never been reported yet. Down to 10^{-8} M of minimum detectable concentration (MDC) towards a wide range of small biomolecules, such as drugs and amino acid, were achieved in buffer solution, and 10^{-6} M MDC was achieved in bio-media, such as whole human serum, fetal bovine serum and diluted blood, which is at the same level as the therapeutically relevant concentrations of these drug molecules. At the same time, CB8-MV^{2+} electrochemical assay offered the linear detection ranges located within physiologically relevant micromolar range no matter it worked as IDA or ABA. Additionally, CB8-MV^{2+} electrochemical assay also demonstrates capability of real-time monitoring of continuous drug injection process, inspiring its further application in real-time investigations of drug loading and releasing events.

5.1 Introduction

In the field of biosensing, kinds of sensors have been developed for the detection of big biomolecules with molecular weight around 10^5 Dalton, such as antigens. These sensors can offer high specificity and low limit of detection (LoD) by taking advantages of specific biological reactions between biomolecular receptors (*e.g.* antibody, aptamer, enzyme subtract, nucleic acid, DNA, RNA, aptamer and protein) and target analytes by employing techniques related to the biochemically amplification of targets, such as polymerase chain reaction (PCR). However, research regarding quantitative determination of small drug molecules (*e.g.* molecular weight is around 10^2 Dalton) are relatively limited.

Detecting small drug molecules in biologically most relevant media, such as urine, serum and even animal blood, are of great meanings and importance for pharmaceutical and clinical applications. Nevertheless, it is still highly challenging for current sensing assays to achieve this as the complex substances presented in bio-media could either cause strong background signals to shield the target characteristic signals for sensing or interact with probe molecules to interfere the target signal producing events. Some sensing strategies for molecular detection in biological and pharmaceutical fields have been designed with the aid of conventional techniques as reviewed in *Chapter 1.9*, such as chromatography [288-291], but most of them suffer from inherent shortcomings like unsatisfactory minimum detectable concentration, complicated sensing protocols, expensive and bulky equipment, low reproducibility, *etc*.

Supramolecule-based biosensors stand out for the detection of small biomolecules by taking advantages of their improved selectivity and specificity upon the non-covalent interactions between host and guest molecules. Among diverse artificial supramolecular receptors, CB*n* is of particular interest due to its wide binding capability towards a broad range of guest molecules with relatively strong binding affinities (10^3 to 10^{12} M^{-1}) in biologically relevant aqueous environment [93,292-294]. Moreover, leveraging the spacious cavity of CB8, in

addition to 1:1 host-guest binary complexes, it can form ternary complexes by encapsulating two guest molecules simultaneously, thereby offering more possibilities for the design of the supramolecular-based sensing assays. Generally, according to the working mechanism, CB8-based sensing assays can be classified into three types [161,175], including (1) direct binding assays (DBAs), (2) associative binding assays (ABAs) and (3) indicator displacement assays (IDAs). DBAs refer to the assays that can directly generate responsive signals to be detected upon binding with the target analyte molecules. Thus, CB*n* often needs to be chemically modified by active probe molecules, like fluorophores [159,176,177]. ABAs are the assays based on spacious CB8 and sensitive reporter guest molecule (*e.g.* dye molecules), which can detect the target analyte via the measurable signals responding to the capture of the target analyte as ternary complex [85,161,189,191]. IDAs are the assays which rely on the competitive binding between the pre-complexed indicator and the target analyte. The pre-complexed environment-sensitive indicator is expected to be displaced by the analyte molecule upon the formation of strongly binding complex, and the specific property of the indicator, *e.g.* fluorescent intensity, is ready to be altered upon the displacement [161-163,175,178,183]. Although kinds of supramolecular-based sensing assays have been developed but most of them are only able to work in one of these three working mechanisms, and meanwhile some complicated fabrication steps are required, thereby resulting in a limited application range [85,161-163,175,176,178,183,189,191].

In the field of supramolecular chemistry, binding constant is a crucial indicator to quantitatively analyse the host-guest interactions and offer guidance on the design of supramolecular systems. Binding constant ratio can be utilized to assess the selectivity of molecular sensing towards analytes, offering information for the design of the supramolecular-based sensors. There are thus multiple supramolecular titration methodologies developed for the estimation of binding constants, mainly including UV-vis spectroscopy titration, fluorescence spectroscopy titration, ^{1}H NMR titration, and isothermal titration calorimetry (ITC). Nevertheless, it is not viable for these techniques to work in complex bio-media, thus leaving impossible for in-situ binding constant determination.

Herein, a simple yet powerful electrochemical assay has been established via the self-assembly of CB8 and redox active indicator of MV^{2+}, eliminating the need of chemical modification steps. Supramolecular-based electrochemical assay CB8-MV^{2+} integrates multiple functions into one, including being an IDA and an ABA for biosensing, and a molecular platform for binding constants determination with the aid of electrochemical titration (*e.g.* SWV titration) approach. In particular, down to 10^{-8} M of minimum detectable concentration, together with a physiologically relevant micromolar linear detection range, have been achieved by CB8-MV^{2+} assay in both of its IDA and ABA mode, which can be further optimized by simply adjusting the concentration of CB8-MV^{2+}, for a wide range of small biomolecules detection, including Parkinson's drug adamantylamine (ADA), Alzheimer's drug memantine (MEM) and antiviral drug rimantadine (RMD), local anaesthetic drug procaine (PC), Alzheimer's drug tacrine (TR) and amino acid tryptophan (TYP). Notably, CB8-MV^{2+} assay exhibited excellent interference tolerance ability and performed biosensing capability in complex bio-media, ranging from simple buffer solution, synthetic urine (SU) to fetal bovine serum (FBS) and human serum (HS) and even to animal blood, maintaining desired sensing properties. More surprisingly, CB8-MV^{2+} assay established advanced development in binding constant determination with the aid of SWV titration experimental approach, allowing for the in-situ binding constant estimation in biologically most relevant environment, such as SU, HS, FBS, sheep blood (SB) and horse blood (HB). New possibilities of biosensing and binding constant estimation in complex bio-media demonstrated by CB8-MV^{2+} electrochemical assay open new venue for the design and application of supramolecular-based biosensing assays.

5.2 Establishment of CB8-MV^{2+} electrochemical assay

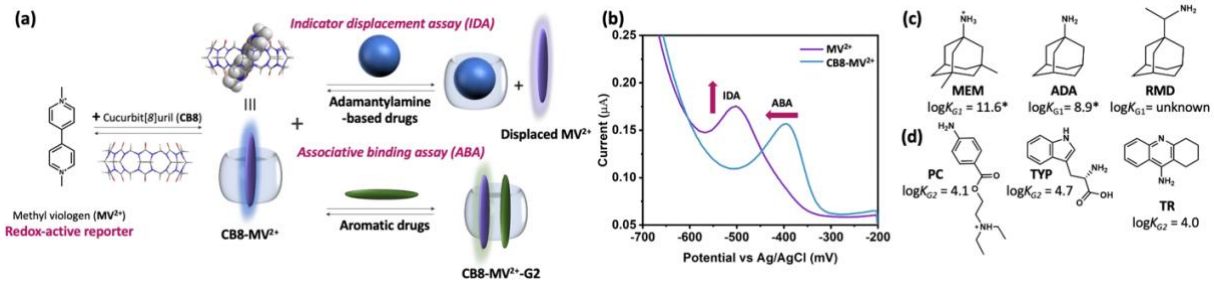

Fig. 5.1 (a) Schematic representation of two working formats of CB8-MV^{2+} assay. **(b)** Representative SWV responsive signals correspond to two working modes of CB8-MV^{2+} assay. Structures of biomolecules detected by CB8-MV^{2+} via **(c)** indicator displacement assay (IDA) and **(d)** associative binding assay (ABA) formats. Asterisk (*) indicates values refer to reference [71]. Note that the selection of target drug molecules in this work is based on three criteria: (1) commercially available, (2) desired aqueous solubility for stock solution preparation, and (3) specific geometry that is either bulky to displace MV^{2+} out of CB8 cavity or planar to form ternary complex with CB8-MV^{2+}.

CB*n* (*n* = 5-8, 10) is a young generation of synthetic receptors possessing a series of impressive properties, for example, the electron-rich carbonyl lined portals render them strong binding towards cationic guest molecules upon the ion-dipole interactions; the well-defined cavities offer them superior binding selectivity upon size complementary effect; the hydrophobicity of inner cavity enable the release of encapsulated high energy water molecules upon encapsulation of guest molecules, especially for neutral guest molecules. CB8 stands out among CB*n* homologues owing to its spacious cavity which can accommodate two guest molecules at the same time, giving rise to ternary complexes (**Fig. 5.1a**). Redox active MV^{2+} is a typical guest for CB8 to form 1:1 binary complex with binding constant of 8.1×10^5 M^{-1} [20] and its reduction potential can be significantly shifted towards positive direction upon complexation with CB8 as found in *Chapter 4*, making it easy to discriminate the reduction peak of MV^{2+} in its free form from complexed form in the case of CB8-MV^{2+}, as indicated by SWV curves in **Fig. 5.1b**. Thus, when MV^{2+} is displaced out of CB8 cavity by strong guest molecules, which normally have 3D and relatively bulky chemical structures (**Fig. 5.1c**), such as ADA derivatives [71,295,196], the newly appearance and responsive increase of free MV^{2+} reduction peak ($\Delta I_{MV2+|MV+\bullet}$) can serve as indicative signals for sensing of strong guest molecules by employing CB8-MV^{2+} as IDA (**Fig. 5.1a-b**). Additionally, as investigated in *Chapter 4* [269], the reduction peak potential of CB8-MV^{2+} exhibits negative potential shift responding to the encapsulation of second guest (G2) molecules, which are normally in planar conformation and possess aromatic motif (**Fig. 5.1d**), and the peak potential shift amount ($\Delta V_{G2} = |E_{CB8\text{-}MV2+\text{-}G2} - E_{CB8\text{-}MV2+}|$) is quantitatively related to the concentration of G2, thereby enabling CB8-MV^{2+} to work as an ABA for sensing as well (**Fig. 5.1a-b**). Hence, by taking advantage of powerful and sensitive indicator MV^{2+}, which can translate the binding events of analytes into readable signals, CB8-MV^{2+} electrochemical assay can work in two formats of IDA and ABA for biosensing with the aid of powerful SWV measurement technique.

5.3 Complexation between biomolecules and CB8-MV^{2+} electrochemical assay

5.3.1 Complexation between strong guest molecules and CB8

The strong binding of between ADA-derived molecules and CB8 have been thoroughly investigated by researchers, and the binding constants of CB8-MEM and CB8-ADA were reported as 10^{11} M^{-1} and 10^8 M^{-1}, respectively (**Fig. 5.1c**) [71,72,295]. Although the binding affinity

of CB8-RMD has not been reported yet, RMD can be confidently considered as a strong guest for CB8 with its comparable molecular structure as ADA and MEM.

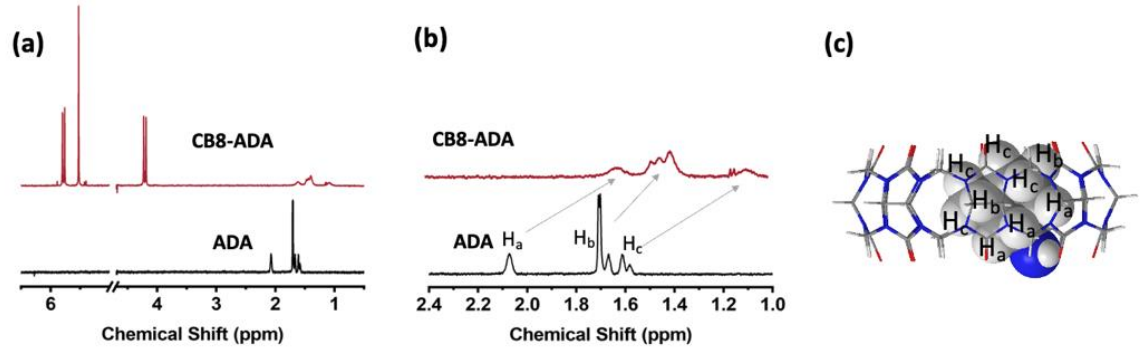

Fig. 5.2 (a) ^{1}H NMR spectra and **(b)** zoom-in ^{1}H NMR spectra of ADA and 1:1 CB8-admantylamine (ADA) complex in D_2O. **(c)** DFT optimized molecular model of CB8-ADA.

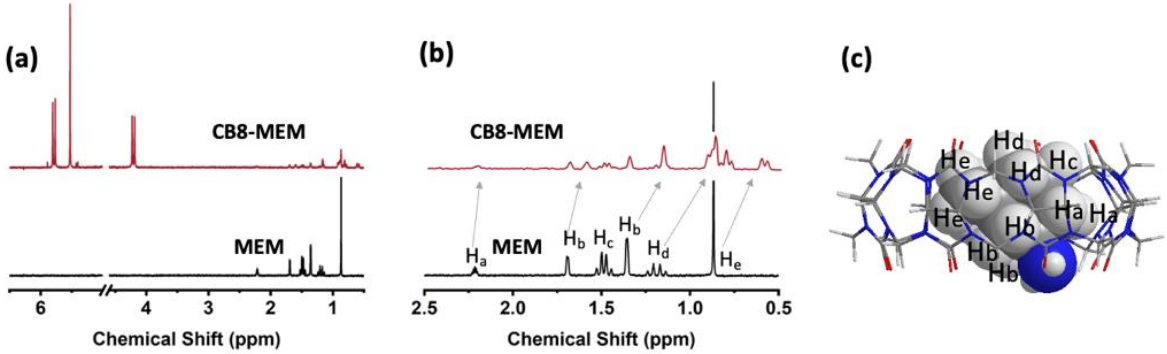

Fig. 5.3 (a) ^{1}H NMR spectra and **(b)** zoom-in ^{1}H NMR spectra of memantine (MEM) and 1:1 CB8-MEM complex in D_2O. **(c)** DFT optimized molecular model of CB8-MEM.

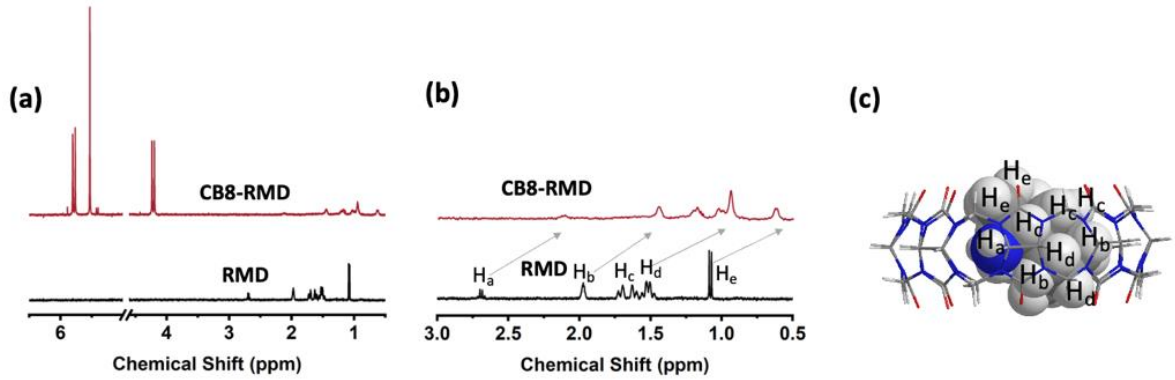

Fig. 5.4 (a) ^{1}H NMR spectra and **(b)** zoom-in ^{1}H NMR spectra of rimantadine (RMD) and 1:1 CB8-RMD complex in D_2O. **(c)** DFT optimized molecular model of CB8-RMD.

5.3.2 Complexation between second guest molecules and CB8-MV^{2+}

To figure out whether CB8-MV^{2+} can effectively work as ABA for biosensing, drugs of PC and TR and amino acid TYP with aromatic motif, which can facilitate the charge transfer interactions with encapsulated MV^{2+} inside CB8 cavity, were employed as sample analytes. The complexation between these analytes and CB8-MV^{2+} were verified experimentally and

computationally. In particular, the chemical shifts of H_a and H_b on PC were significantly upshifted and widened in the presence of 1 equimolar of CB8-MV^{2+} (**Fig. 5.5b**), indicating an increasing shielding effect imposed on these two protons on PC. The increasing shielding effect suggests that H_a and H_b are located inside CB8 inner cavity, in line with the conformation shown in the corresponding DFT-minimized molecular model of CB8-MV^{2+}-PC ternary complex (**Fig. 5.5c**). Nevertheless, protons of H_c and H_d on PC displayed downfield shift with the addition of 1 equivalent of CB8-MV^{2+} (**Fig. 5.5b**), implying that these two protons were not positioned deep inside CB8 cavity, which were specified as the outer portal region of CB8 by DFT-optimized molecular model of CB8-MV^{2+}-PC in **Fig. 5.5c**. Similarly, whether TR drug and TYP amino acid can form ternary complex with CB8-MV^{2+} were verified by ^{1}H NMR and computational simulations as well. All chemical shifts of protons on TR were shifted towards the upfield region in the presence of CB8-MV^{2+} (**Fig. 5.6a**), indicating that the formation of inclusion complex of CB8-MV^{2+}-TR, as shown in **Fig. 5.6b**. As for amino acid TYP, chemical shifts of H_a and H_b were mildly shifted to the upfield upon the addition of 1 equimolar of CB8-MV^{2+} (**Fig. 5.7b**), replying that these protons are located near the portal of the CB8, consistent with the observation in DFT-optimized molecular model of CB8-MV^{2+}-TYP in **Fig. 5.7c**.

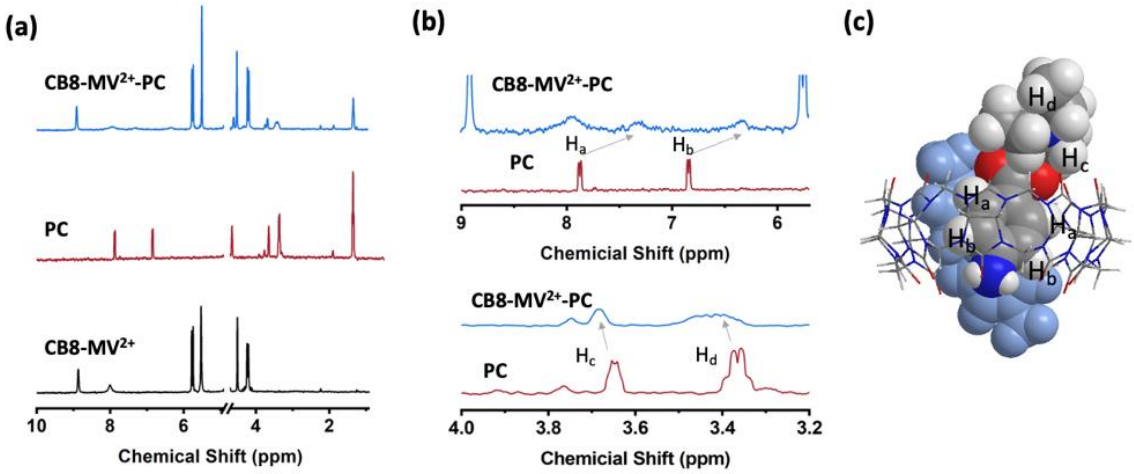

Fig. 5.5 (a) ^{1}H NMR spectra and **(b)** zoom-in ^{1}H NMR spectra of 1:1 CB8-MV^{2+}, procaine hydrochloride (PC) and 1:1:1 CB8-MV^{2+}-PC complex in D_2O. **(c)** DFT optimized molecular model of CB8-MV^{2+}-PC. Blue block represents MV^{2+}.

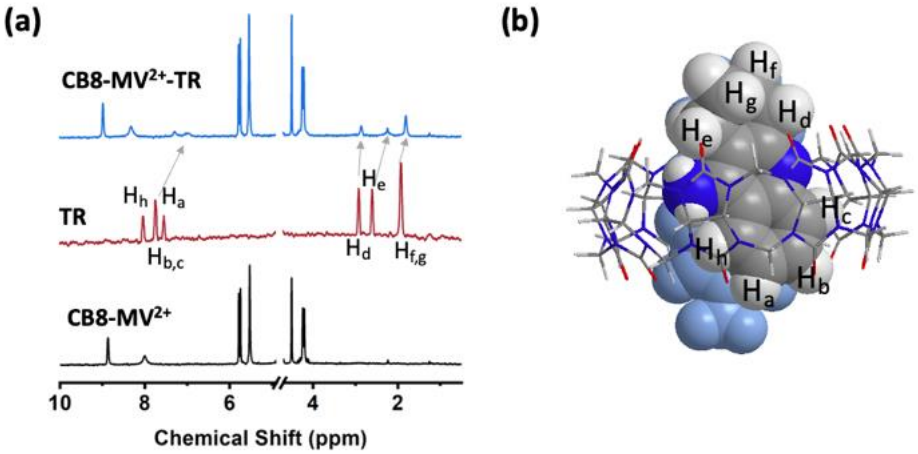

Fig. 5.6 (a) ^{1}H NMR spectra of 1:1 CB8-MV^{2+}, tacrine (TR) and 1:1:1 CB8-MV^{2+}-TR complex in D_2O. **(b)** DFT optimized molecular model of CB8-MV^{2+}-TR. Blue block represents MV^{2+}.

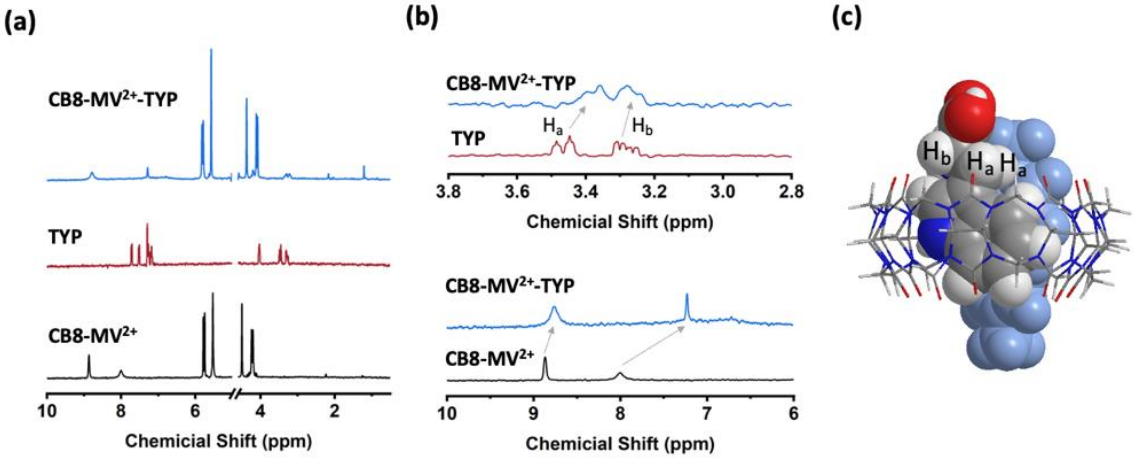

Fig. 5.7 (a) ^{1}H NMR spectra and **(b)** zoom-in ^{1}H NMR spectra of 1:1 CB8-MV^{2+}, tryptophan (TYP) and 1:1:1 CB8-MV^{2+}-TYP complex in D_2O. **(c)** DFT optimized molecular model of CB8-MV^{2+}-TYP. Blue block represents MV^{2+}.

After qualitatively confirming the complexation of PC, TR and TYP with CB8-MV^{2+}, quantitative estimation of the binding constants (K_{G2}) of CB8-MV^{2+}-G2 (G2 = PC, TR and TYP) were investigated following the rapid electrochemical approach proposed in *Chapter 4* [269]. Specifically, the reduction potential shift (ΔV_{G2}) values were obtained by taking SWV measurements of 1 mM of CB8-MV^{2+} and 1 mM of CB8-MV^{2+}-G2 (G2 = PC, TYP and TR) with identical experimental conditions as that utilized in *Chapter 4* (**Fig. 5.8**). Then, logK_{G2} of CB8-MV^{2+}-G2 (G2= PC, TR and TYP) were calculated as 4.1, 4.7, and 4.0, respectively (**Fig. 5.8**), using the correlation equation displayed in **Fig. 4.7b**.

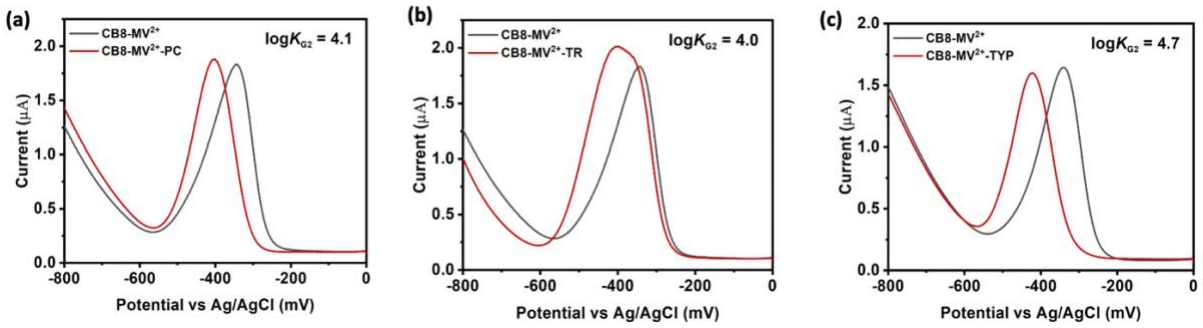

Fig. 5.8 SWV curves of 1 mM of CB8-MV^{2+} in absence (grey line) and presence (red line) of 1 equimolar of G2 = **(a)** procaine hydrochloride (PC), **(b)** tacrine (TR) and **(c)** tryptophan (TYP) for the estimation of their binding constants (logK_{G2}) utilizing the correlation proposed in **Fig. 4.7b** in *Chapter 4* [269].

5.4 Biosensing based on CB8-MV^{2+} electrochemical assay

5.4.1 CB8-MV^{2+} works as indicator displacement assay (IDA)

As discussed in *Chapter 5.1*, the responsive signals detected by IDA are generated by the displacement of indicator out of supramolecular host cavity upon the competitive binding of analytes [297]. The selectivity of IDAs towards analyte molecules is typically in terms of the geometry, charge and hydrophobicity of the analyte, resulting in a limited specificity of IDAs compared to sensing assays constructed using biomolecular receptors, such as antibodies, aptamers, enzyme substrates, *etc*, as the inherent specificity of non-covalent competitive binding interactions is weaker than that of biomolecular interactions. On the other hand, IDAs

can offer attractive advantages for molecular detection. For instance, IDAs do not require the indicator covalently linked to the host, making diverse indicator molecules can be employed for one host molecule to establish various sensing assays targeting for different analytes [298]. Moreover, IDAs are operative in both organic solvents and aqueous media, allowing for electrochemical measurements in physiologically relevant biofluids. In addition, IDAs enable the detection of analytes which cannot generate characteristic signals by themselves, *e.g.* electrochemical inactive and spectroscopic transparent molecules [299]. Finally, for physiologically relevant biofluids where naturally consist of concentrated interferent substances like protein and salts, direct-binding assay (DBA) cannot work well due to the undesirable complexation from interferent; however, IDA holds the promise for sensing in these complex biofluids. Hence, IDAs keeps attracting widespread attention as a powerful molecular detection tool, especially for biosensing in complicated bio-media.

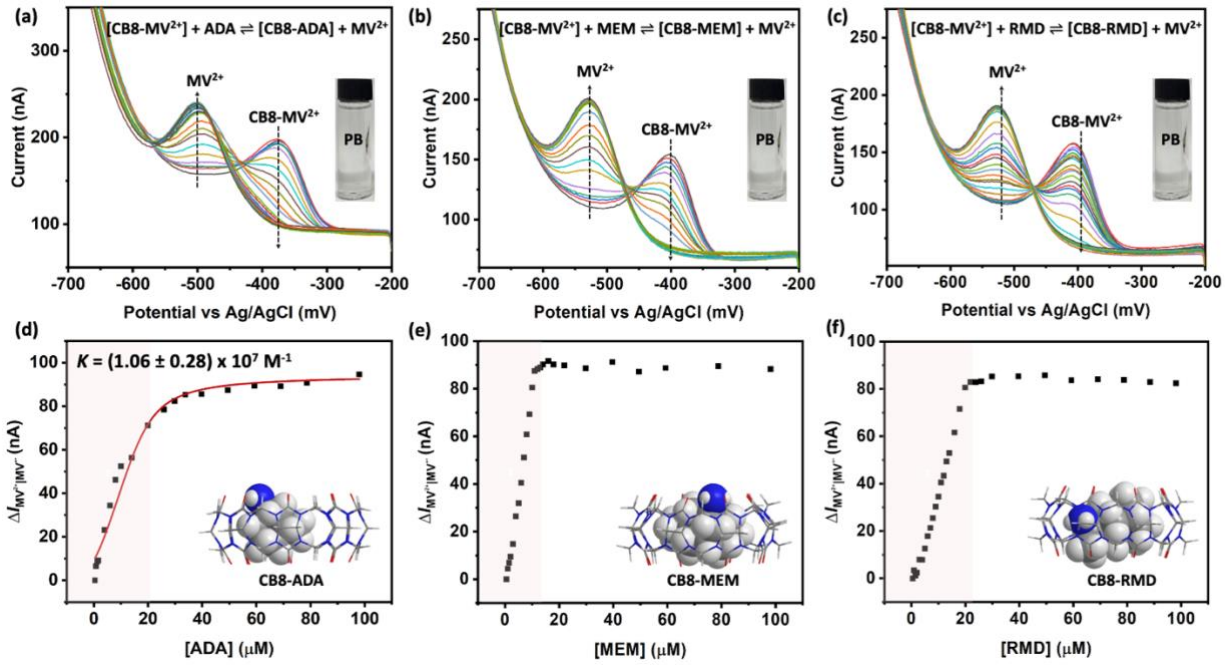

Fig. 5.9 SWV curves recorded with stepwise addition of **(a)** adamantylamine (ADA), **(b)** memantine (MEM) and **(c)** rimantadine (RMD) into 20 μM of CB8-MV^{2+} in 6.25 mM PB solution (pH 7). Scatter plots of $MV^{2+}/MV^{+\bullet}$ reduction peak current change ($\Delta I_{MV2+|MV+\bullet}$) over the titration against the concentration of **(d)** ADA, **(e)** MEM and **(f)** RMD. Insets are the energy-minimized molecular models of **(d)** CB8-ADA, **(e)** CB8-MEM and **(f)** CB8-RMD optimized at CPCM/wB97XD/6-31G* level of theory, where CPCM implicit water model was utilized to simulate the solvent effects in aqueous-based electrochemical measurements. Light pink shadow represents the linear detection range.

As illustrated in **Fig. 5.1a-b**, CB8-MV^{2+} is expected to work as an electrochemical active IDA for biomolecular sensing by using the appearance and the increase amount of displaced MV^{2+} reduction peak, which is generated by the competitive binding from target analyte, as the indicative signals. Here, we employed ADA, MEM and RMD as example analytes, whose complexation have been studied in *Chapter 5.3*. Pulse voltammetry technique, SWV, was chosen as our measuring tool, which can separate faradic current and provide quick measuring rate, increased sensitivity, and peak current strength. SWV titration measurements were performed by successively adding target analytes (*e.g.* ADA, MEM and RMD) into CB8-MV^{2+} as a fixed concentration of 20 μM. Based on the findings in *Chapter 4* [269], we utilized 6.25 mM PB solution (pH 7), in which the shape of CB8-MV^{2+} electrochemical curve is sharp,

as our starting electrolyte. Upon stepwise addition of target analytes, the peak corresponding to $MV^{2+}/MV^{+\bullet}$ reduction increased accordingly (**Fig. 5.9a-c**). The relationship between the increase amount in $MV^{2+}/MV^{+\bullet}$ reduction peak ($\Delta I_{MV2+|MV+\bullet}$) and the concentration of added analyte is exponential, as can be seen in the scatter plots in **Fig. 5.9d-f**. Moreover, it is noted that the peak intensity of displaced MV^{2+} and CB8-MV^{2+} stopped changing after the adding amount of the analyte reached the maximum equivalent determined by the starting concentration of CB8-MV^{2+} assay (*e.g.* 20 μM in this case), subjecting to the mass conservation law. Gratifying to see that the minimum detectable concentration has been achieved down to sub-micromolar level, *ca.* 0.5 μM, by 20 μM of CB8-MV^{2+} IDA, which is comparable to 0.8 μM achieved by high-performance liquid chromatographic (HPLC) for RMD detection [219] and lower than 0.09 mM achieved by electrochemical sensing using modified electrode for the detection of ADA [198]. Furthermore, linear detection range within micromolar range, where is physiologically relevant and of predominant interests for practical biosensing, has also been accomplished by 20 μM of CB8-MV^{2+} IDA (as indicated by the light pink shadow in **Fig. 5.9d-f**).

In addition to biosensing, it is surprising that CB8-MV^{2+} also demonstrated the ability to estimate the binding constant. Taking ADA as an example, its binding constant was determined as $(1.06 \pm 0.28) \times 10^7$ M^{-1} (**Fig. 5.9d**) in 6.25 mM PB solution (pH 7) by fitting the SWV titration results into 'one host-one guest-one competitor' model developed by the Nau group. Needs to mention that the sharp turning titration curves of MEM and RMD (**Fig. 5.9e-f**) resulted from the ultra-high binding affinities exceed the application scope of current available fitting model, thereby leaving their binding constant values blank. Despite this limitation, it is still quite novel for one simple CB8-MV^{2+} assay to simultaneously perform biosensing and binding constants estimation functions with the aid of SWV titration approach.

5.4.2 CB8-MV^{2+} works as associative binding assay (ABA)

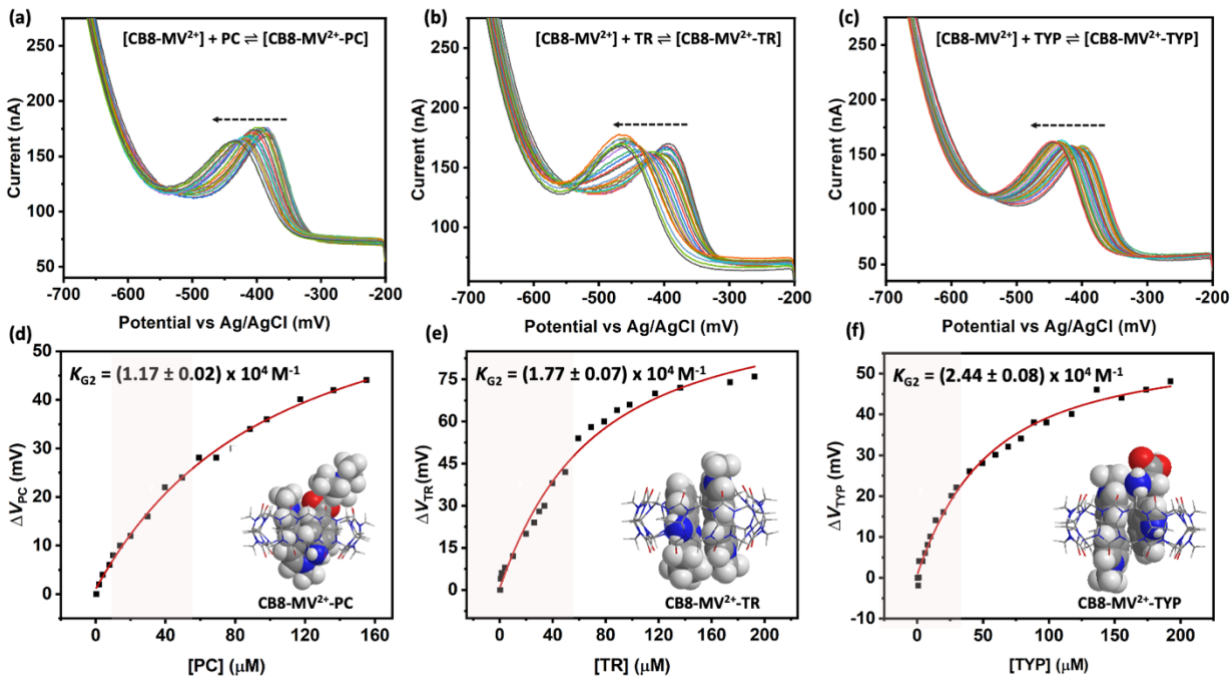

Fig. 5.10 SWV curves recorded with stepwise addition of **(a)** procaine hydrochloride (PC), **(b)** tacrine (TR) and **(c)** tryptophan (TYP) into 20 μM of CB8-MV^{2+} in 6.25 mM PB solution (pH 7). Scatter plots of reduction peak potential shift (ΔV_{G2}) over the titration against the concentration of **(d)** PC, **(e)** TR and **(f)** TYP. Insets are the energy-minimized molecular models

of **(d)** CB8-MV^{2+}-PC, **(e)** CB8-MV^{2+}-TR and **(f)** CB8-MV^{2+}-TYP optimized at CPCM/wB97XD/6-31G* level of theory, where CPCM implicit water model was utilized to simulate the solvent effects in aqueous-based electrochemical measurements. Light pink shadow represents the linear detection range.

In addition to IDA, CB-MV^{2+} also presents ability to serve as ABA by using the reduction peak potential shift of CB8-MV^{2+} as responsive signal for biosensing as depicted in **Fig. 5.1b**. Taking biomolecules with planar conformation, such as PC, TR and TYP, as examples analytes, SWV titration measurements were carried out to study whether CB-MV^{2+} can work in ABA format. As observed in the SWV titration curves (**Fig. 5.10a-c**), the reduction peak of CB8-MV^{2+} gradually shifted towards negative potential region, responding to the successive addition of the analyte. In analogy to the observation in IDA, the reduction peak potential shift (ΔV_{G2}) is exponentially related to the concentration of analyte (*e.g.* PC, TR and TYP) (**Fig. 5.10d-f**). Moreover, micromolar minimum detectable concentration (MDC) as well as linear detection range have also been achieved by CB8-MV^{2+} ABA, for example, the MDC of PC is around 1.0 μM, which is comparable to that of electrochemical sensor based on nanotube film coated electrode [199] and gas chromatography mass spectrometry (GS-MC) [225]. Notably, the binding constants of PC, TR and TYP with CB8-MV^{2+} were successfully estimated by fitting their SWV titration results into 'one host-one guest' model from the Nau group, in which CB8-MV^{2+} is regarded as a whole host for G2. The obtained binding constants (K_{G2}) of CB8-MV^{2+}-PC, CB8-MV^{2+}-TR and CB8-MV^{2+}-TYP are $(1.17 \pm 0.02) \times 10^4$ M^{-1}, $(1.77 \pm 0.07) \times 10^4$ M^{-1}, $(2.44 \pm 0.08) \times 10^4$ M^{-1} (**Fig. 5.10d-f**), consistent with the ones estimated by our reported rapid electrochemical scheme [269] (**Fig. 5.8**). This consistency between two approaches confirmed the reliability of SWV titration methodology in binding constant estimation.

With these findings, it is credible that CB8-MV^{2+} electrochemical assay is muti-functional, *i.e.* CB8-MV^{2+} is capable of integrating sensing and binding constant into one in both dual formats of IDA and ABA.

5.4.3 Optimization of minimum detectable concentration

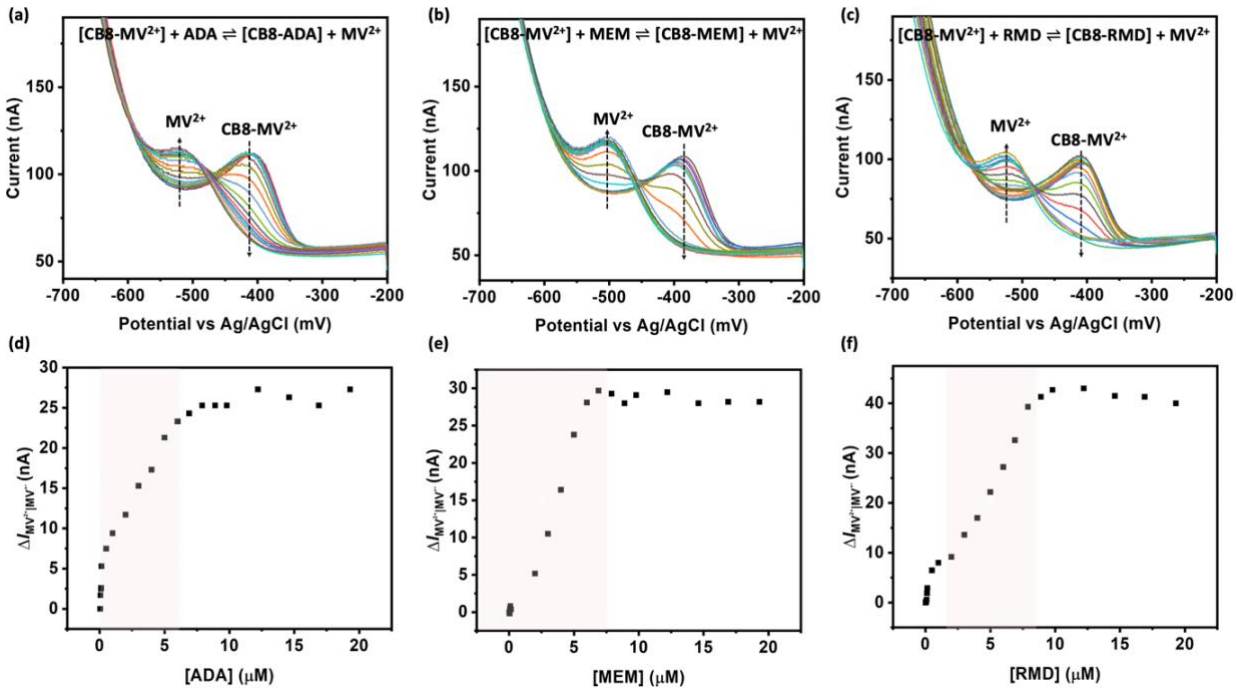

Fig. 5.11 SWV curves recorded with stepwise addition of **(a)** adamantylamine (ADA), **(b)**

memantine (MEM) and **(c)** rimantadine (RMD) into 10 μM of CB8-MV^{2+} in 6.25 mM PB solution (pH 7). Scatter plots of $MV^{2+}/MV^{+\bullet}$ reduction peak current change ($\Delta I_{MV2+|MV+\bullet}$) against the concentration of **(d)** ADA, **(e)** MEM and **(f)** RMD. Light pink shadow represents the linear detection range.

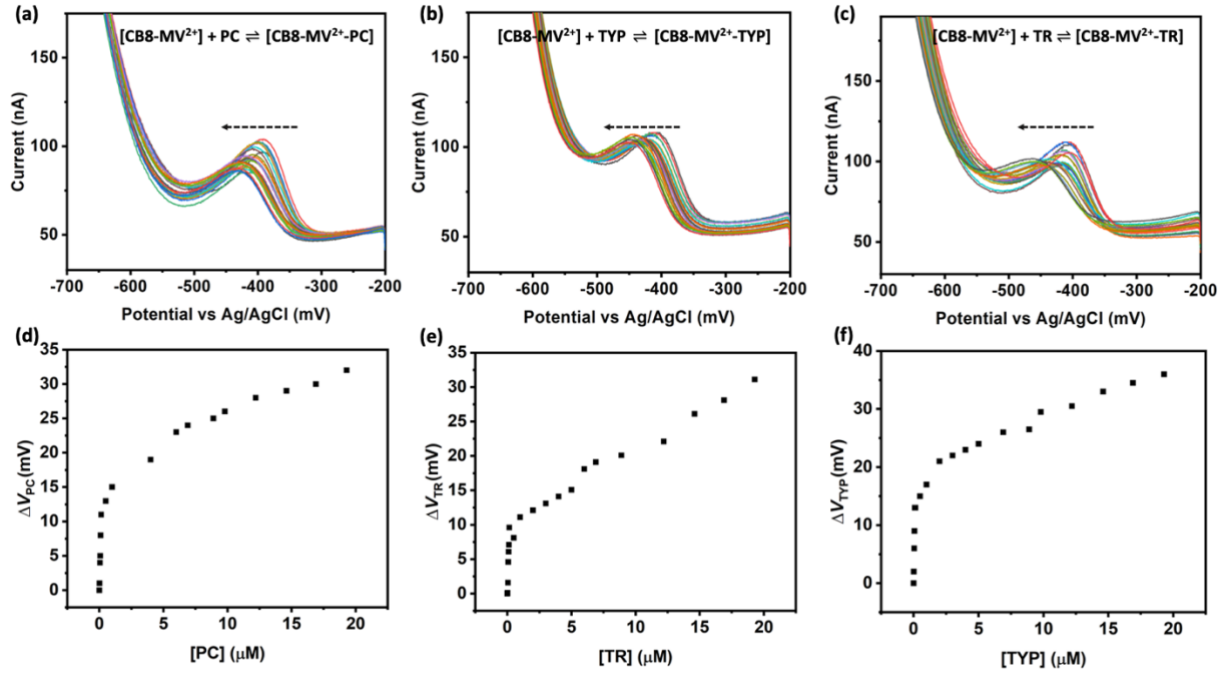

Fig. 5.12 SWV curves recorded with stepwise addition of **(a)** procaine hydrochloride (PC), **(b)** tacrine (TR) and **(c)** tryptophan (TYP) into 10 μM of CB8-MV^{2+} in 6.25 mM PB solution (pH 7). Scatter plots of reduction peak potential shift (ΔV_{G2}) against the concentration of **(d)** PC, **(e)** TR and **(f)** TYP.

Gratifying to note that the minimum detectable concentration (MDC) of CB8-MV^{2+} electrochemical assay can be easily optimized upon adjusting its concentration, thereby better catering for different sensing requirements. We optimized the minimum detectable concentration by one order of magnitude by decreasing the concentration of CB8-MV^{2+} from 20 μM to 10 μM regardless of whether CB8-MV^{2+} worked as IDA for ADA, MEM and RMD sensing (**Fig. 5.11**) or ABA for PC, TR and TYP sensing (**Fig. 5.12**). For example, the MDC for ADA and PC was optimized to 0.07 μM and 0.02 μM, respectively. The adjustable minimum detectable concentration is of great and extensive interest for practical applications.

Table 5.1 summarized the minimum detectable concentration and corresponding linear detection range of example small biomolecules achieved by CB8-MV^{2+} via its IDA and ABA working formats at concentrations of 20 μM and 10 μM in PB solution (pH 7), as well as the therapeutically relevant plasma concentration of these target biomolecules. As can be seen, minimum detectable concentration can be optimized by two orders of magnitude by simply decreasing the concentration of CB8-MV^{2+} from 20 μM to 10 μM, and at the same time, the corresponding linear detection range was also shifted to a lower concentration region by around 15 micromolar. Such observation confirmed the adjustability of minimum detectable concentration as well as linear detection range of CB8-MV^{2+} electrochemical assay, making it can better cater for specific requirements in practical applications.

It can be seen that the micromolar minimum detectable concentration (MDC) of these six analytes achieved by 20 μM CB8-MV^{2+} dual-functional assay is at the same level as their corresponding therapeutically relevant plasma concentration range (**Table 5.1**), indicating that

the CB8-MV^{2+} electrochemical assay can meet the therapeutic requirement for practical sensing in pharmaceutical and clinical field.

Table 5.1 Minimum detectable concentration and linear detection range of example bio-analytes achieved by 10 μM (20 μM) CB8-MV^{2+} in PB solution (pH 7) and the corresponding therapeutically relevant plasma concentration.

	Analytes	Minimum detectable concentration (μM)	Linear detection range (μM)	Therapeutically relevant plasma concentration (μ M)
IDA	MEM	0.05 (1.0)	1 – 6 (0 – 11)	~1 [213]
	ADA	0.07 (0.8)	0 – 6 (0 – 20)	0.6 – 29 [196]
	RMD	0.05 (1.0)	2 – 8 (0 – 20)	0.5 – 3 [217]
ABA	PC	0.02 (1.6)	1 – 10 (4 – 40)	1283 – 2199* [223]
	TYP	0.02 (1.2)	2 – 24 (4 – 33)	40 – 80 [232]
	TR	0.05 (0.8)	1 – 19 (2 – 40)	5 – 151 [300]

* Dosage when it used as a local anaesthetic in human.

5.5 Interference tolerance of CB8-MV^{2+} electrochemical assay

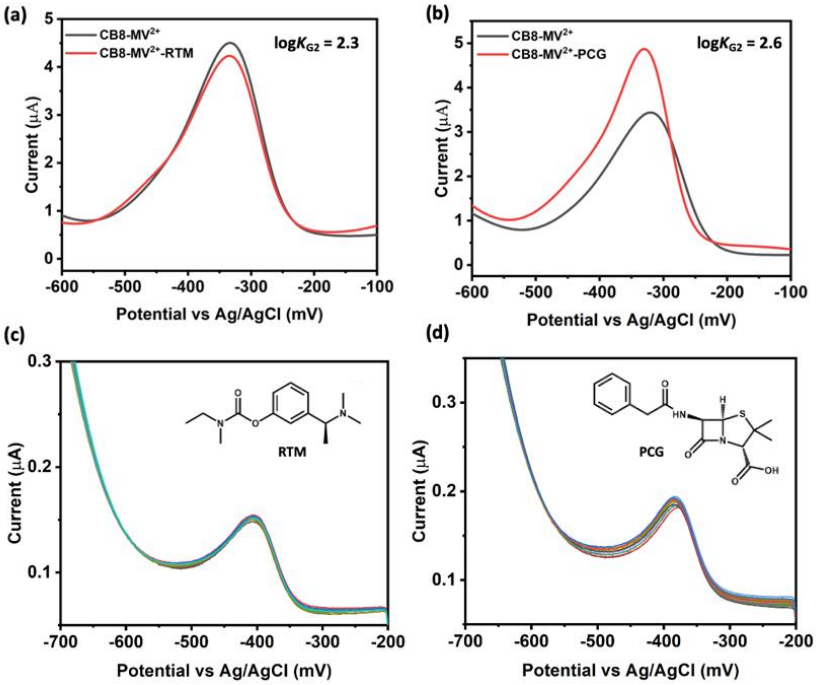

Fig. 5.13 SWV curves of 1 mM of CB8-MV^{2+} in absence (grey line) and presence (red line) of 1 equimolar of **(a)** rivastigmine (RTM) and **(b)** penicillin G Na (PCG) for the estimation of their binding constants (logK_{G2}) with CB8-MV^{2+} utilizing the correlation proposed in **Fig. 4.7b** in *Chapter 4* [269]. SWV curves of 20 μM of CB8-MV^{2+} with successive addition of **(c)** RTM and **(d)** PCG up to 10 equivalents. Insets are the chemical structures of **(c)** RTM and **(d)** PCG.

From the viewpoint of real applications, the target analyte is highly likely to coexist with multiple molecules as a mixture, thus making it important and necessary for sensing assay to tolerant interferents and generate selective sensing signals. We here chose MEM and PC as representative analyte corresponding to IDA and ABA working format of CB8-MV^{2+}, respectively. Both MEM and RTM are drugs for the treatment of Alzheimer's disease. It is of certain possibility for dementia patient to consume medicine repeatedly and exceed prescribed dose, thus it is probably for MEM and RTM to coexist in one test sample in real cases. Therefore, we here selected RTM as the interferent for MEM sensing. In clinical cases, PC is often used to mitigate the muscle pain caused by the injection of PCG, and moreover, PCG is an antibiotic drug for the treatment of the bacterial infections, being of high possibility to be prescribed after the patient finished dental operation that utilized local anaesthetic drug of PC. Hence, PCG is of great chance to present with PC at the same time and of reasonability to be chosen as the interferent for PC detection. Prior to the closer inspection on the interferent tolerance, the binding properties of PCG and RTM with CB8-MV^{2+} were investigation first following the proposed electrochemical scheme in *Chapter 4* [269]. As indicated by the SWV results measured at the concentration of 1 mM, the binding constants (logK_{G2}) of PCG and RTM were estimated as 2.6 and 2.3, respectively (**Fig. 5.13a-b**). For further investigation, SWV titration measurements of PCG and RTM based on 20 μM of CB8-MV^{2+} assay were performed (**Fig. 5.13c-d**). Neither the appearance of displaced MV^{2+} reduction peak nor pronounced peak potential shift was observed even with considerably excessive addition of PCG/RTM, *e.g.* 10 equivalents of CB8-MV^{2+}.

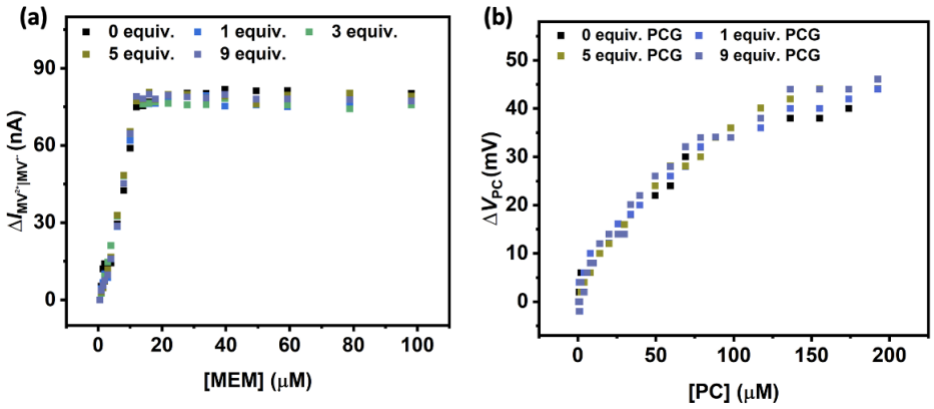

Fig. 5.14 (a) Overlaid scatter plots of $MV^{2+/}MV^{+\bullet}$ reduction peak current change ($\Delta I_{MV2+|MV+\bullet}$) against the concentration of memantine (MEM) in presence of 0, 1, 3, 5, and 9 equivalents of rivastigmine (RTM) based on 20 μM of CB8-MV^{2+}. **(b)** Overlaid scatter plots of peak potential shift (ΔV_{PC}) against the concentration of procaine hydrochloride (PC) in presence of 0, 1, 5, and 9 equivalents of penicillin G Na (PCG) based on 20 μM of CB8-MV^{2+}. Electrolyte: 6.25 mM PB solution (pH 7).

After exploring the binding features of interferents, the ability of CB8-MV^{2+} assay to avoid influence from interferents during the molecular detection was inspected by performing SWV titration experiments of target analyte (*e.g.* MEM and PC) in the presence of multiple equivalents of interferents (*e.g.* RTM and PCG). When CB8-MV^{2+} works as IDA, the SWV titration measurements of MEM were carried out in the presence of 0, 1, 3, 5 and 9 equivalents of RTM interferent (**Fig. 5.14a**). As expected, the key features and overall changing trend of MEM titration figure plotted between displaced MV^{2+} reduction peak current change ($\Delta I_{MV2+|MV+\bullet}$) and the concentration of MEM were still there regardless of the presence of multiple equivalents of RTM interferent, allowing for CB8-MV^{2+} IDA to avoid interferent substances for biosensing. In addition to the IDA mode, the interferent tolerance of CB8-MV^{2+}

ABA was also monitored by performing SWV titration experiments of PC in the presence of various equivalents of PCG interferent. As comparison among the overlaid scatter diagrams plotting between the reduction potential shift of CB8-MV^{2+}(ΔV_{PC}) and the concentration of PC in **Fig. 5.14b**, no predominant difference in PC titration scatter diagrams was observed with the introduction of multiple equivalents of PCG interferent into system, implying that CB8-MV^{2+} ABA possesses satisfactory tolerance towards PCG interferent and maintains desired sensing features (*e.g.* sensitivity and selectivity).

In a nutshell, CB8-MV^{2+} possesses great specificity and selectivity towards the target analyte by resisting the interference from potentially co-existing interferents in the system, which is of promising meanings for practical sensing applications. Encouraged by these findings, we then moved our attention to explore new possibilities in other biologically most relevant media, such as urine, serum and even animal blood.

5.6 Binding constants estimation and biosensing using CB8-MV^{2+} electrochemical assay in complex bio-media

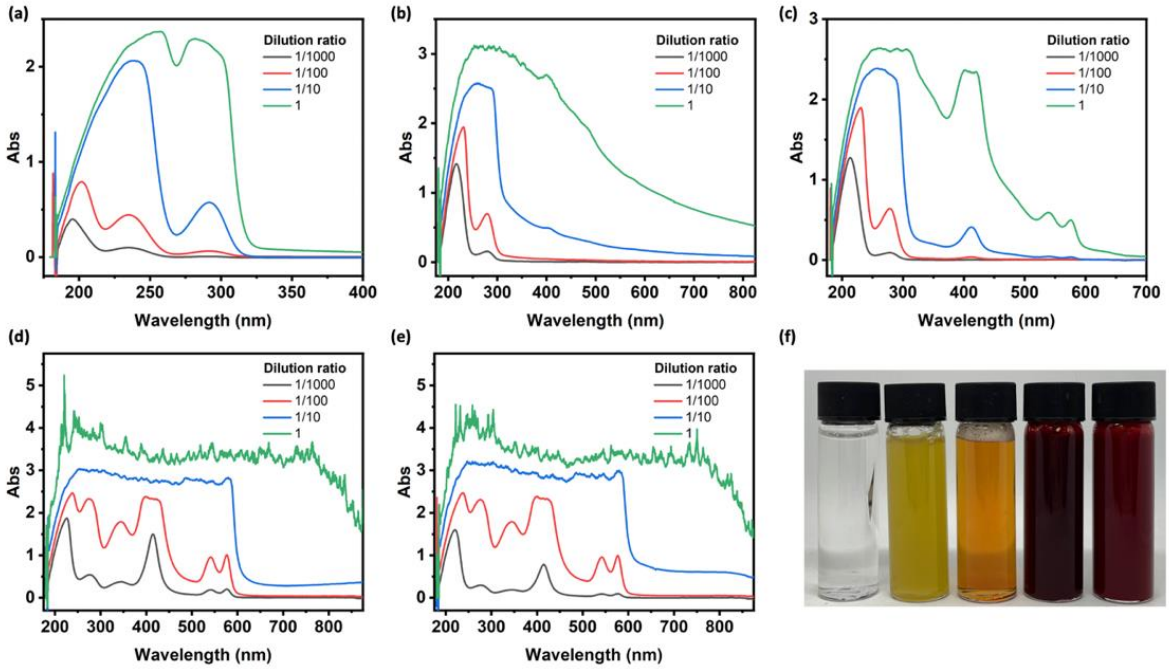

Fig. 5.15 UV-vis spectra of **(a)** SU, **(b)** HS, **(c)** FBS, **(d)** SB and **(e)** HB at a range of dilutions. 6.25 mM PB solution (pH 7) was employed to dilute these biological matrices. **(f)** From left to right: photo of whole SU, HS, FBS, SB and HB.

Bio-media, such as urine, serum and blood, are more physiologically and clinically relevant with respect to simple buffer solution for biosensing in real cases but the precedent research in this filed is still limited since complex substances in these bio-media can cause strong background spectra shielding the target detection signals and/or generate competitive binding with supramolecular-based assays interfering the binding of target analytes, for example, the UV-vis spectra of five different bio-media, including synthetic urine (SU), fetal bovine serum (FBS), human serum (HS), sheep blood (SB) and horse blood (HB) at different dilutions in **Fig. 5.15** shown strong and noisy absorbance. Although the Biedermann group have reported sensing in SU, FBS and HS, these biofluids were required to be diluted by more than 100 times before sensing [161,301,302]. Thus, research regarding biosensing in concentrated and even native bio-media without the introduction of biomolecules, such as antibody, enzyme,

aptamers, *etc*, is still relatively blank and needs to be further developed. Compared to biosensing, it is even more tough to estimate binding constants of host-guest complexes in complex bio-media, which is of particular importance and interests in supramolecular chemistry area but has never been exploited yet to the best of our knowledge.

5.6.1 Synthetic urine

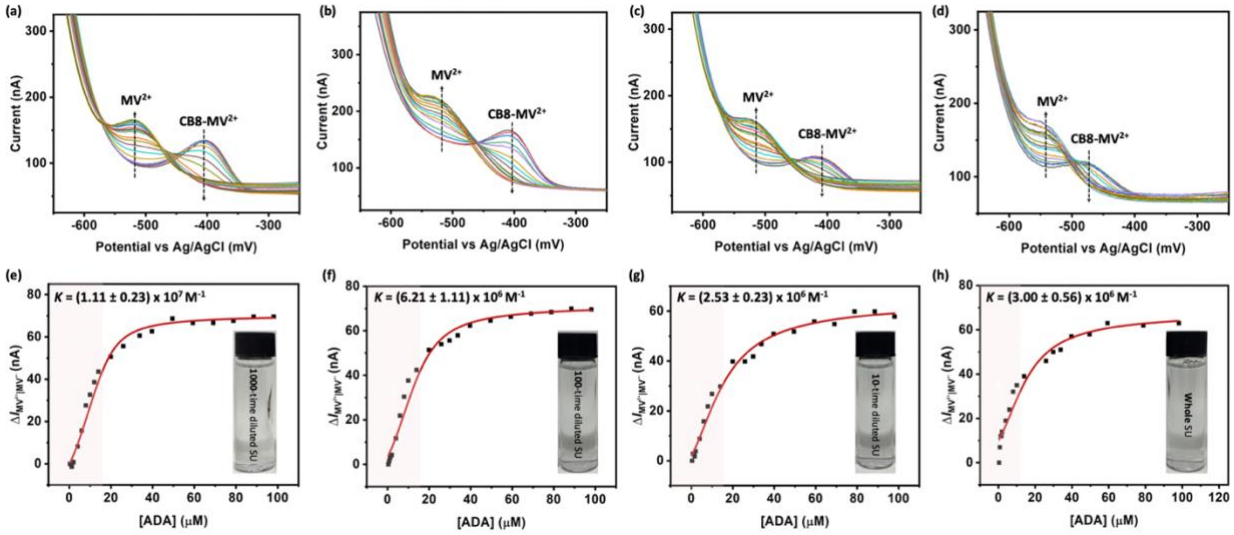

Fig. 5.16 SWV titration curves of adamantylamine (ADA) based on 20 μM CB8-MV^{2+} in **(a)** 1000x, **(b)** 100x, **(c)** 10x diluted and **(d)** whole synthetic urine (SU). Arrows indicate the peak changing trend with increasing amount of ADA. Binding constants of CB8-ADA estimated by fitting the peak current change corresponding to the reduction of displaced MV^{2+} ($\Delta I_{MV2+|MV+\bullet}$) over the titration in **(e)** 1000x, **(f)** 100x, **(g)** 10x diluted and **(h)** whole SU into 'one host-one guest–one competitor' model. Light red shadow indicates the linear detection range for ADA in SU at different dilutions. Insets are the photo of SU at different dilutions where the SWV titration performed.

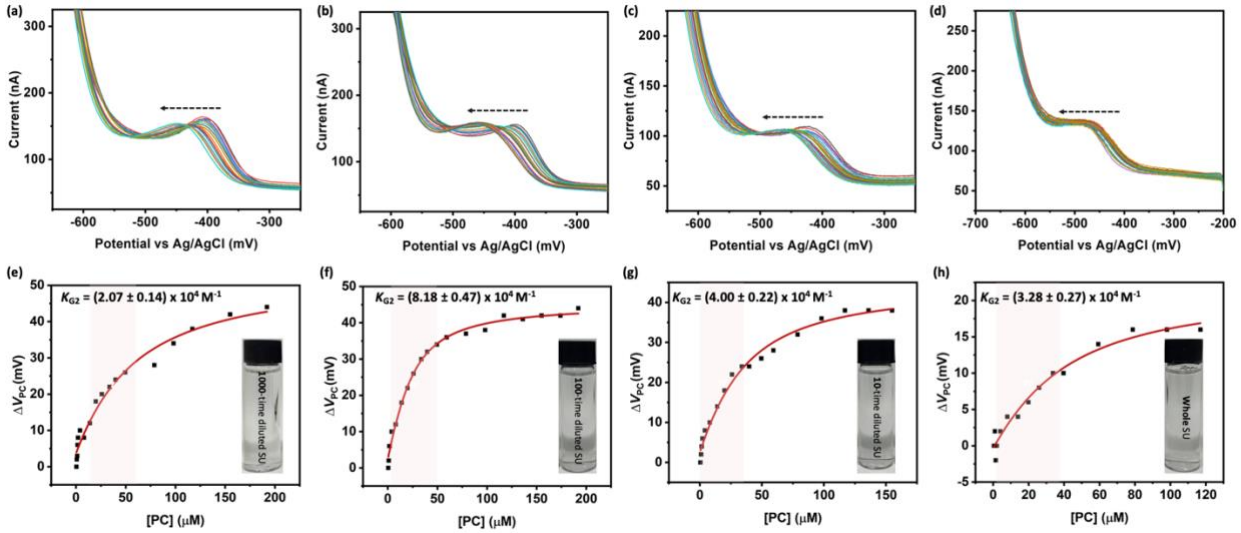

Fig. 5.17 SWV titration curves of procaine hydrochloride (PC) based on 20 μM CB8-MV^{2+} in **(a)** 1000x, **(b)** 100x, **(c)** 10x diluted and **(d)** whole SU. Arrows indicate the peak shifting trend with increasing amount of PC. Binding constants of CB8-MV^{2+}-PC estimated by fitting the peak potential shift amount (ΔV_{PC}) over the titration in SU at dilution ratios of **(e)** 1000x, **(f)**

100x, **(g)** 10x diluted and **(h)** whole SU into 'one host-one guest' model by taking CB8-MV^{2+} as a host for PC. Light red shadow indicates the linear detection range for PC in SU at different dilutions. Insets are the photo of SU at different dilutions where the SWV titration performed.

Compared to buffer solution like PB, synthetic urine (SU) is more physiologically relevant. Although SU consists of multiple concentrated species, such as NaCl, KCl, NaH_2PO_4, creatinine, urea, uric acid and albumin, it is relatively less complicated than other bio-media, such as serum and blood, thus being chosen as the starting point to explore the possibilities of sensing and binding constant estimation of CB8-MV^{2+} electrochemical assay in complex biofluids. We employed ADA and PC as the example target analytes to be analysed via IDA and ABA formats of CB8-MV^{2+} electrochemical assay, respectively. We performed SWV titration measurements for ADA and PC based on 20 μM CB8-MV^{2+} in SU at different dilutions, ranging from the 1000x, 100x, 10x diluted till native SU. It was observed that the intensity of CB8-MV^{2+} reduction peak reduced and became less sharp and clear as the concentration of SU increased (**Fig. 5.16-5.17**), which could be resulted from the competitive binding of concentrated salt ions like Na^+ in SU with CB8. Nevertheless, the key SWV features of CB8-MV^{2+} were still there even in native SU, allowing for CB8-MV^{2+} to maintain its functions of sensing and binding constant estimation in such concentrated SU. Notably, sub-micromolar minimum detectable concentration and physiologically relevant micromolar linear detection range for ADA and PC were achieved by CB8-MV^{2+} in SU without any dilutions and pre-treatment steps, and more surprisingly, the binding constants of CB8-ADA and CB8-MV^{2+}-PC were determined in native SU (see detail values in **Fig. 5.16-5.17**).

5.6.2 Fetal bovine serum and human serum

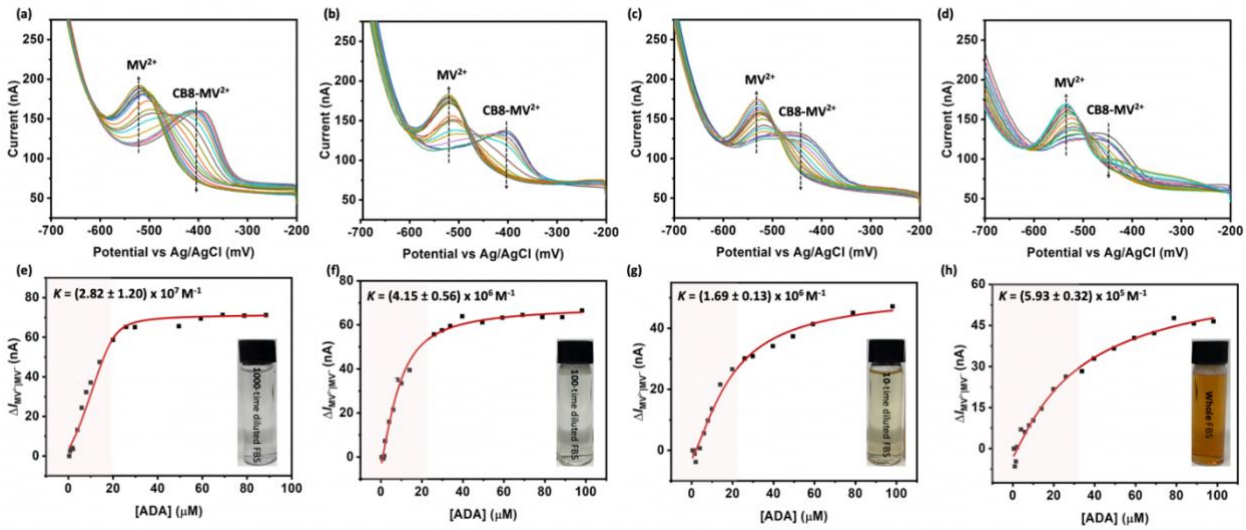

Fig. 5.18 SWV titration curves of adamantylamine (ADA) based on 20 μM CB8-MV^{2+} in **(a)** 1000x, **(b)** 100x, **(c)** 10x diluted and **(d)** whole fetal bovine serum (FBS). Arrows indicate the peak changing trend with increasing amount of ADA. Binding constants of CB8-ADA estimated by fitting the peak current change corresponding to the reduction of displaced MV^{2+} ($\Delta I_{MV2+|MV+\bullet}$) over the titration in **(e)** 1000x, **(f)** 100x, **(g)** 10x diluted and **(h)** whole FBS into 'one host-one guest–one competitor' model. Light red shadow indicates the linear detection range for ADA in FBS at different dilutions. Insets are the photo of FBS at different dilutions where the SWV titration performed.

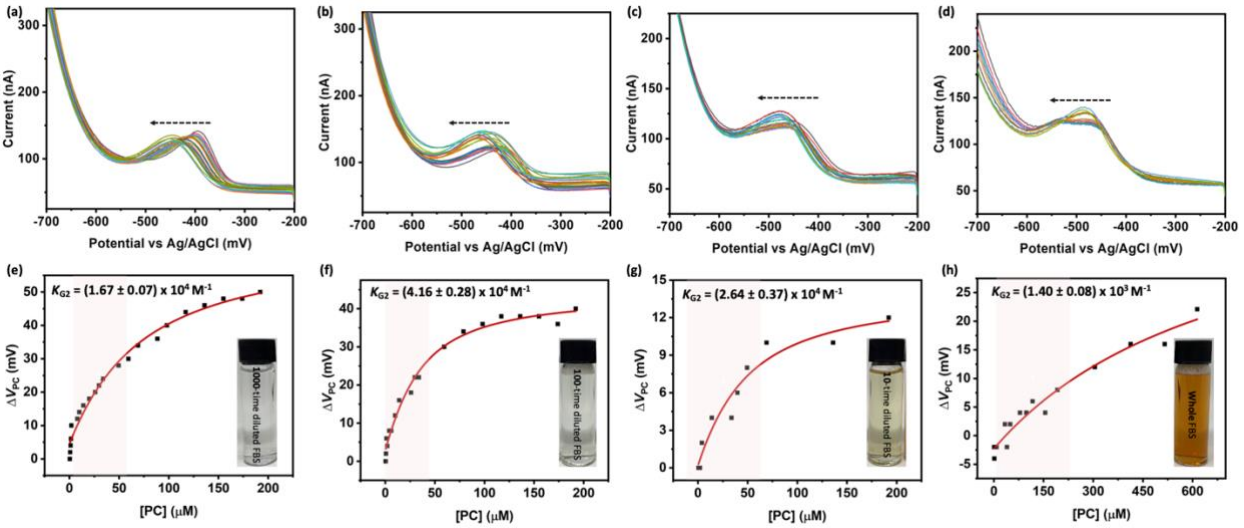

Fig. 5.19 SWV titration curves of procaine hydrochloride (PC) based on 20 μM CB8-MV^{2+} in **(a)** 1000x, **(b)** 100x, **(c)** 10x diluted and **(d)** whole FBS. Arrows indicate the peak shifting trend with increasing amount of PC. Binding constants of CB8-MV^{2+}-PC estimated by fitting the peak potential shift amount (ΔV_{PC}) over the titration in **(e)** 1000x, **(f)** 100x, **(g)** 10x diluted and **(h)** whole FBS into 'one host-one guest' model by taking CB8-MV^{2+} as a host for PC. Light red shadow indicates the linear detection range for PC in FBS at different dilutions. Insets are the photo of FBS at different dilutions where the SWV titration performed.

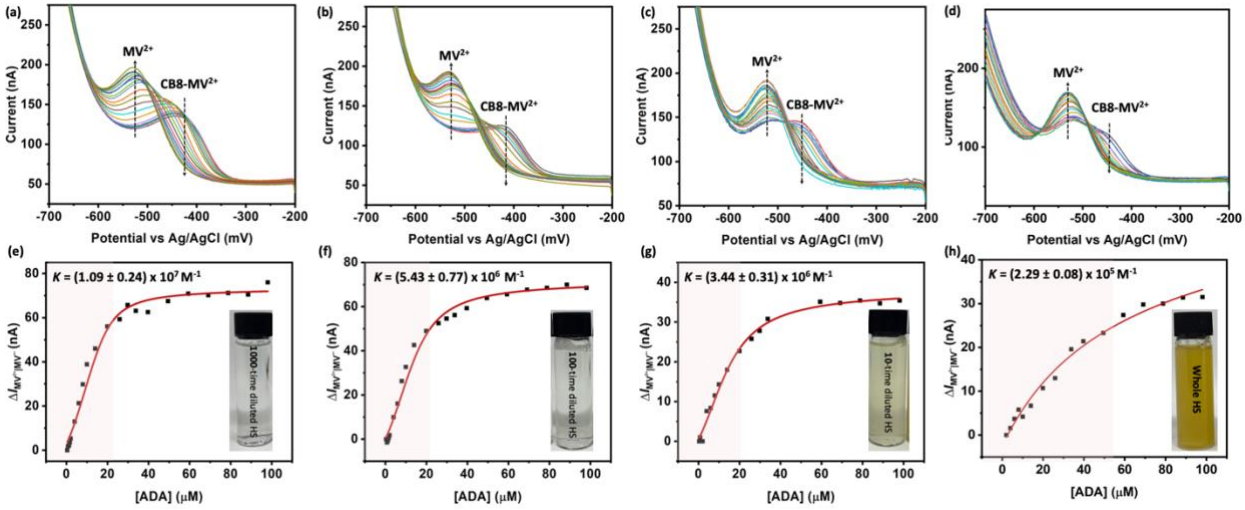

Fig. 5.20 SWV titration curves of adamantylamine (ADA) based on 20 $\boldsymbol{\mu}$M CB8-MV^{2+} in **(a)** 1000x, **(b)** 100x, **(c)** 10x diluted and **(d)** whole human serum (HS). Arrows indicate the peak changing trend with increasing amount of ADA. Binding constants of CB8-ADA estimated by fitting the peak current change corresponding to the reduction of displaced MV^{2+} ($\Delta I_{MV2+|MV+\bullet}$) over the titration in **(e)** 1000x, **(f)** 100x, **(g)** 10x diluted and **(h)** whole HS into 'one host-one guest–one competitor' model. Light red shadow indicates the linear detection range for ADA in HS at different dilutions. Insets are the photo of HS at different dilutions where the SWV titration performed.

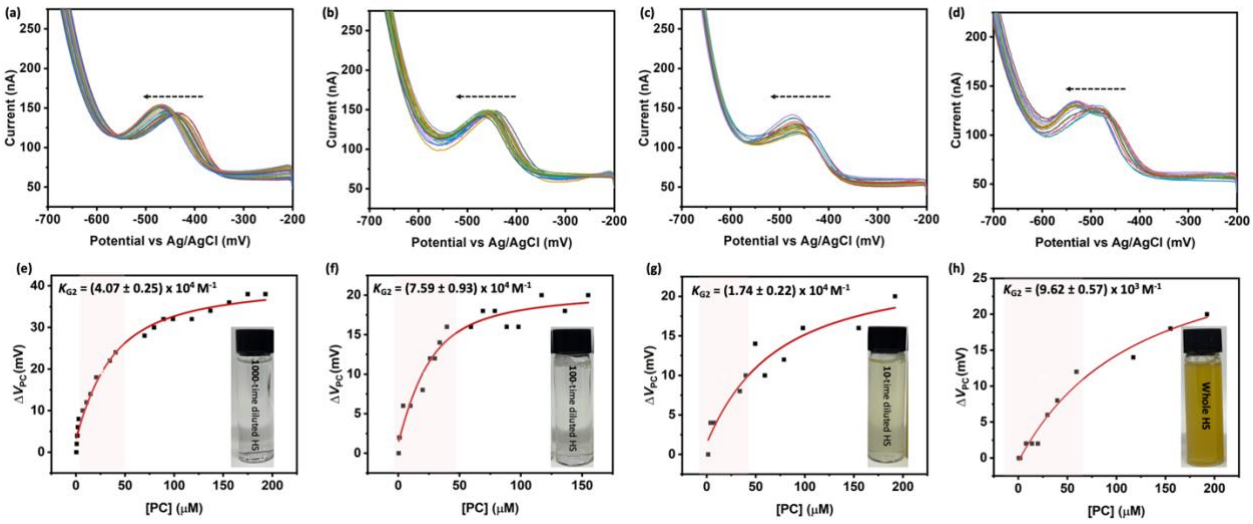

Fig. 5.21 SWV titration curves of procaine hydrochloride (PC) based on 20 μM CB8-MV^{2+} in **(a)** 1000x, **(b)** 100x, **(c)** 10x diluted and **(d)** whole HS. Arrows indicate the peak shifting trend with increasing amount of PC. Binding constants of CB8-MV^{2+}-PC estimated by fitting the peak potential shift amount (ΔV_{PC}) over the titration in **(e)** 1000x, **(f)** 100x, **(g)** 10x diluted and **(h)** whole HS into 'one host-one guest' model by taking CB8-MV^{2+} as a host for PC. Light red shadow indicates the linear detection range for PC in HS at different dilutions. Insets are the photo of HS at different dilutions where the SWV titration performed.

Following the SU research, we then took it a step further to explore possibilities of sensing and binding constant estimation in serum, *e.g.* fetal bovine serum (FBS) and human serum (HS), by CB8-MV^{2+} electrochemical assay. As known, serum is normally composed of multiple proteins, carbohydrates, hormones, fats, exogeneous species, antibodies, antigens and so on, appearing more complicated but more physiologically relevant compared to SU. In an analogous fashion, we performed SWV titration measurements of ADA and PC based on 20 μM CB8-MV^{2+} in serum diluted by different times and its whole form without pre-treatment steps like deproteinization. It was pleasingly found that the major SWV characteristics of CB8-MV^{2+} were maintained in serum, especially when serum was diluted by more than 10 times (**Fig. 5.18-5.21**). Even when serum was not diluted at all, the appearance and increase of displaced $MV^{2+}/MV^{+\bullet}$ peak ($\Delta I_{MV2+|MV+\bullet}$) with the addition of ADA and the reduction potential shift of CB8-MV^{2+} peak (ΔV_{PC}) with the addition of PC were still observed (**Fig. 5.18-5.21**), thus enabling in-situ biosensing in serum samples, which is of promising practical application potentials.

Notably, the minimum detectable concentration and linear detection range of ADA and PC were kept at sub-micromolar to micromolar range in the presence of complicated interferents in serum. Moreover, the binding constants of ADA and PC were successfully estimated by fitting the SWV titration results into 'one host-one guest-one competitor' and 'one host-one-guest' models, respectively. Compared to SU, it was observed that the weaking effect on binding affinities caused by the interplay between assay and substances presented in FBS and HS were more obvious; in particular, the binding constant of CB8-ADA and CB8-MV^{2+}-PC were weakened by two and one order of magnitude, respectively, when the concentration of serum increased from 1000x diluted to native version (**Fig. 5.18-5.21**). Such increased weakening effect observed in the case of serum can be attributed to the fact that there are more types and more concentrated interferent species in serum with respect to SU, such as proteins.

5.6.3 Animal blood

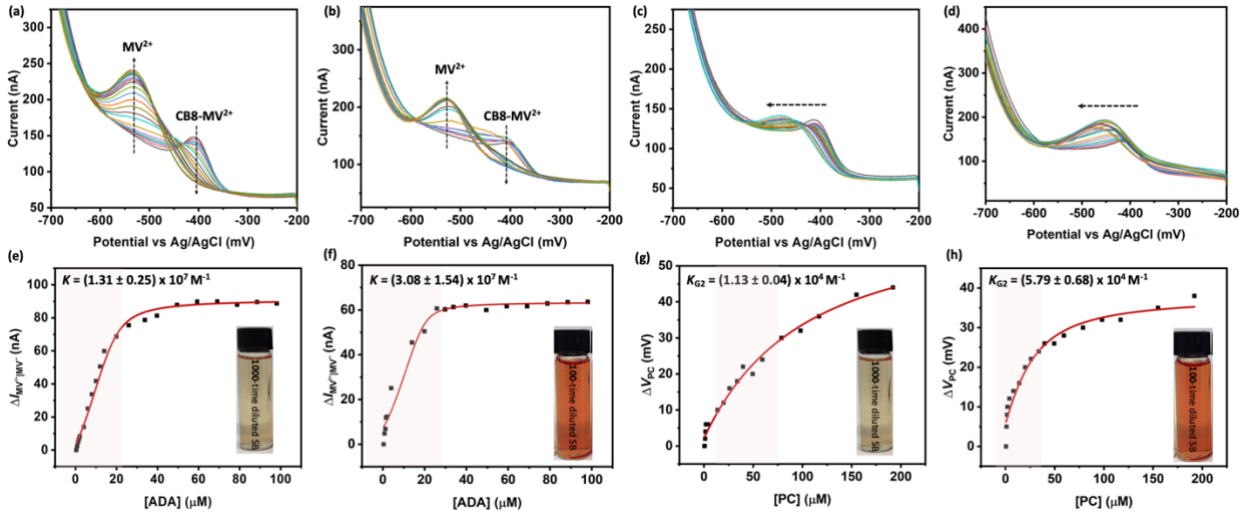

Fig. 5.22 SWV titration curves of adamantylamine (ADA) based on 20 μM CB8-MV^{2+} in **(a)** 1000x and **(b)** 100x diluted sheep blood (SB). SWV titration curves of procaine hydrochloride (PC) based on 20 μM CB8-MV^{2+} in **(c)** 1000x and **(d)** 100x diluted SB. Arrows indicate the peak changing trend with increasing addition of ADA or PC. Binding constants of CB8-ADA estimated by fitting the peak current change corresponding to the reduction of displaced MV^{2+} ($\Delta I_{MV2+|MV+\bullet}$) over the titration in **(e)** 1000x and **(f)** 100x diluted SB into 'one host-one guest–one competitor' model. Binding constants of CB8-MV^{2+}-PC estimated by fitting the peak potential shift amount (ΔV_{PC}) over the titration in **(g)** 1000x and **(h)** 100x diluted SB into 'one host-one guest' model by taking CB8-MV^{2+} as a host for PC. Light red shadow indicates the linear detection range for ADA or PC in SB at different dilutions. Insets are the photo of SB at different dilutions where the SWV titration performed.

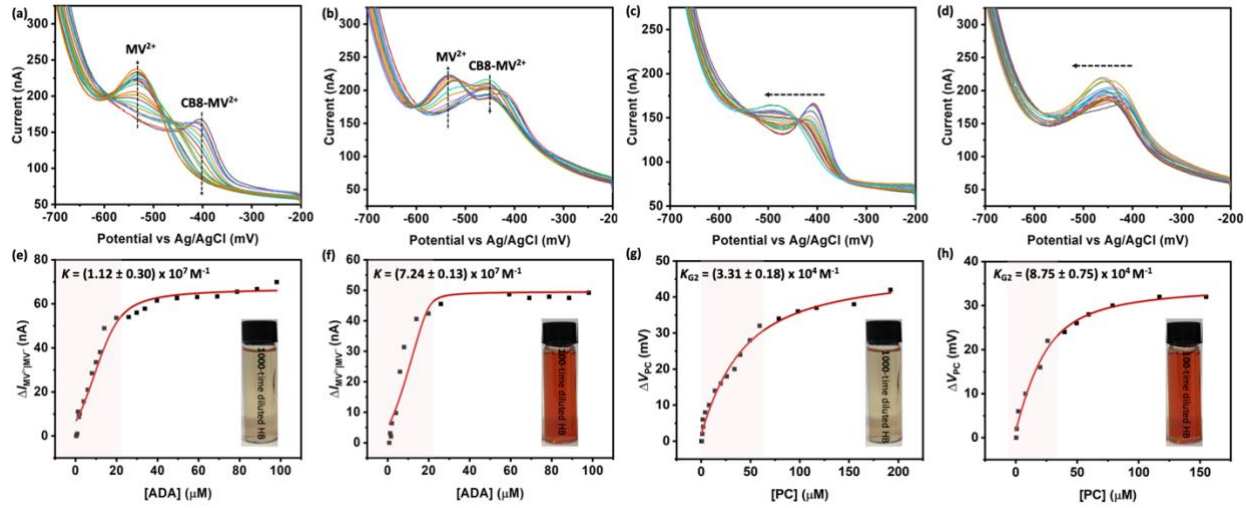

Fig. 5.23 SWV titration curves of adamantylamine (ADA) based on 20 μM CB8-MV^{2+} in **(a)** 1000x and **(b)** 100x diluted horse blood (HB). SWV titration curves of procaine hydrochloride (PC) based on 20 μM CB8-MV^{2+} in **(c)** 1000x and **(d)** 100x diluted HB. Arrows indicate the peak changing trend with increasing addition of ADA or PC. Binding constants of CB8-ADA estimated by fitting the peak current change corresponding to the reduction of displaced MV^{2+} ($\Delta I_{MV2+|MV+\bullet}$) over the titration in **(e)** 1000x and **(f)** 100x diluted HB into 'one host-one guest–one competitor' model. Binding constants of CB8-MV^{2+}-PC estimated by fitting the peak potential shift amount (ΔV_{PC}) over the titration in **(g)** 1000x and **(h)** 100x diluted HB into 'one

host-one guest' model by taking CB8-MV^{2+} as a host for PC. Light red shadow indicates the linear detection range for ADA or PC in HB at different dilutions. Insets are the photo of HB at different dilutions where the SWV titration performed.

With the satisfactory results obtained in urine and serums, we then turned our attention to an even more complex biofluid, *e.g.* animal blood, which presents highly challenging for sensing and extremely sever for binding constant estimation, and thus no research has been reported regarding binding constant estimation in blood yet. In addition to the compositions presented in serum, blood also includes blood cells, platelets, thereby making it considerably challenging to selectively detect the binding behaviours between supramolecular-based assays and the target analyst but not the interferents. To explore the applicability of CB8-MV^{2+} electrochemical assay in blood, we here employed sheep blood (SB) and horse blood (HB) and utilized them directly as received without any further treatments, we performed SWV titration experiments of ADA and PC in SB and HB at different dilutions.

We observed that the SWV curve of CB8-MV^{2+} appeared to be distorted when the concentration of blood increased from 100x to 10x diluted version, indicating that the capabilities of sensing and binding constant determination of CB8-MV^{2+} are hard to display in 10x diluted blood. The obtained SWV titration curves and corresponding scatter plots of ADA and PC in SB and HB were displayed in **Fig. 5.22** and **Fig. 5.23**, respectively. Surprisingly, although there are complicated biological interferents presented in SB and HB, down to sub-micromolar minimum detectable concentration, together with micromolar linear detection range for ADA and PC, were achieved by 20 μM CB8-MV^{2+}. Additionally, it is notably to see that the binding constants of CB8-ADA and CB8-MV^{2+}-PC were also successfully estimated in 100x diluted SB and HB. With these results, possibilities of sensing with desired properties and binding constant estimation with acceptable error bars in complicated animal blood sample were achieved by CB8-MV^{2+} electrochemical assay.

5.6.4 Comparison and discussion

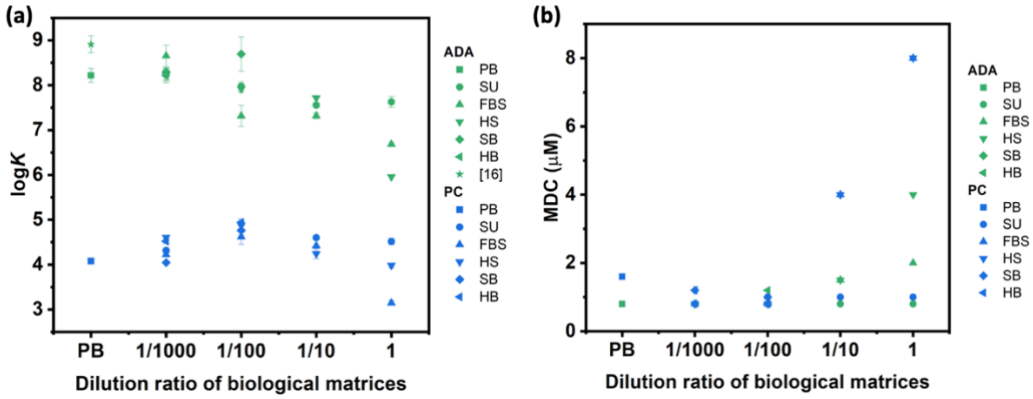

Fig. 5.24 The relationship of **(a)** estimated binding constants and **(b)** Minimum detectable concentration (MDC) of adamantylamine (ADA) and procaine hydrochloride (PC) against dilution ratio of biological matrices. Concentration of CB8-MV^{2+} assay: 20 μM. Asterisk represents the reported log*K* of CB8-ADA measured in 50 mM $NaCD_3CO_2$-buffered D_2O (pD=4.74) by NMR technique [71].

After exploring sensing and binding constants possibilities of CB8-MV^{2+} electrochemical assay in different biological matrices, including 6.25 mM PB solution (pH 7), SU (pH 6.94), FBS (pH 7.47), HS (pH 7.48), SB (pH 7.54) and HB (pH 7.58), we then analysed the influence of the type and concentration of bio-media on the binding constants by making comparison among the obtained binding constants of CB8-ADA and CB8-MV^{2+}-PC in

different biological matrices at different dilutions (**Fig. 5.24a**). Considering the electrochemical behaviours of CB8-MV^{2+} are not prone to pH values and the pH of six employed bio-media are not with huge differences, it is thus acceptable to ignore the effects on binding constants brought by different pH values. As found in the scatter plot in **Fig. 5.24a**, difference in binding constants caused by different types of bio-media are not significant when they are at the same dilution ratio. Nevertheless, the binding constants seemed to be more susceptible to the concentration of the bio-media, for instance, a general decreasing trend was observed in binding constants as the concentration of bio-media increased (**Fig. 5.24a**), attributed to the increasingly prominent competitive binding events taking place in concentrated biological matrices. With this information, we can read and understand the results obtained in real cases in a more clearly manner. In the concern of sensing sensitivity, **Fig. 5.24b** summarized the minimum detectable concentration (MDC) of ADA and PC achieved by CB8-MV^{2+} as IDA and ABA, respectively, in different bio-media with different times of dilutions. As can be seen, the LoD achieved in PB and SU were kept at a sub-micromolar level regardless how concentrated the SU is. In the case of serum and blood, the LoD tends to show obvious changing with the concentration of bio-media, which could be due to the fact that the interplay between substances presented in serum and blood is more intense with respect to that of PB and SU. Nevertheless, the LoD for ADA and PC detection in all bio-media achieved by CB8-MV^{2+} electrochemical assay are at least at micromolar scale, where is of most physiological interests in real cases.

Table 5.2 . Procaine hydrochloride (PC) detection in water, buffer and/or bio-media using different techniques reported in literatures

Sensor type		Matrix	LoD	Ref.
Electrochemical sensor	Electrochemical sensor	PBS	0.2 μM	[224]
		PB buffer	0.02 μM	
	Electrochemical supramolecular sensor	**Whole sythentic urine**	1 μM*	This work
		Whole fetal bovine serum	8 μM*	
		Whole human serum	8 μM*	
		100x diluted sheep blood	1 μM*	
		100x diluted horse blood	0.8 μM*	
	Electrochemical sensor	PBS	10 nM	[226]
	Electrochemical SERS sensor	KCl	0.1 pM	[303]
Optical sensor	SIA-chemiluminescence sensor	Aqueous sulphuric acid	1.1mM	[228]
	Spectrophotometric sensor	Glacial acetic acid	0.37 mM	[229]
	Colorimetric sensor	Aqueous solution	0.9 μM	[230]
	SERS sensor	H_2O	0.1 nM	[227]
Chromatographic sensor	HPLC sensor	**urine**	36.7 nM	[231]
		plasma	3.67 nM	
	GC–MS sensor	75% EtOH	0.37 μM	[225]
		PC spiked plasma sample	73 to 85% recovery	
		PC spiked urine sample	78 to 86% recovery	

* represents minimum detectable concentration

Table 5.3 . Adamantylamine (ADA) detection in water, buffer and/or bio-media using different techniques reported in literatures

Sensor type		Matrix	LoD	Ref.
Electrochemical sensors	Electrochemical sensor	BR buffer	90 μM	[198]
	Electrochemical sensor	PBS in EtOH/H_2O (10 % v/v)	80 μM	[199]
	FIA-potentiometric sensor	Deionized H_2O	50 μM	[304]
	Potentiometric sensor	Buffer	0.17 μM	[305]
	Electrochemical supramolecular sensor	PB buffer	0.07 μM	This work
		Whole sythentic urine	0.8 μM*	
		Whole fetal bovine serum	2 μM*	
		Whole human serum	4 μM*	
		100x diluted sheep blood	0.8 μM*	
		100x diluted horse blood	1.2 μM*	
Optical sensor	Electrochemical sensor	Buffer	3.06 nM	[306]
	UV-vis and fluorescence sensor	Chloroform	11.8 μM	[307]
	FRET sensor	Deionized H_2O	8.82 μM	[205]
	Fluorescence sensor	PBS	5 μM	[206]
	UV-vis and fluorescence sensor	**5x diluted human urine and saliva**	2 μM	[207]
Chromatographic sensor	FIA-fluorescence sensor	PBS	0.16 μM	[208]
	HPLC-MS sensor	**462x diluted serum**	0.13 mM	[200]
	HPLC sensor	**Rat plasma**	0.17 μM	[195]
NMR sensor	NMR sensor	dimethyl sulfoxide (DMSO-d6)	0.24 mM	[202]
ELISA	Magnetic-assisted ELISA	PBS	4.2 nM	[203]
	Indirect competitive ELISA	PBS	4.1 nM	[204]
	ELISA	Buffer	2.1 nM	[308]
	Fenton reaction and AuNPs aggregation-based indirect competitive ELISA	10% methanol in PBS	0.51 nM	[201]
	Indirect competitive fluorescence ELISA	PBS	0.23 nM	[209]
	Fluorescent ELISA	PBS	0.13 nM	[210]
Immunosensor	Multi-wavelength fluorescence polarization immunosensor	**20x diluted human serum**	0.12 μM	[211]
	Immunochromatographic sensor	Buffer	11.9 nM	[212]
	Piezoelectric QCM immunosensor	PBS	8.6 nM	[197]
	Magnetic separation-assisted SERS immunosensor	PBS	0.03 nM	[309]
	SERS immunosensor	PBS	0.03 nM	[310]

* represents minimum detectable concentration

In addition to the comparison made among the LoD achieved by CB8-MV^{2+} in different bio-media at different dilutions, LoD values of PC and ADA detection based on different sensing assays and measuring techniques reported in literatures were reviewed in **Table 5.2** and **Table 5.3**. As can be seen, only limited number of sensors are able to perform in-situ sensing of ADA/PC in complex biofluids, and most of them need to dilute the biofluids before sensing. It can be found that the reported LoD values in literatures achieved in biofluids are comparable to ours, but the majority of precedent research was limited to urine and serum but not included blood.

5.7 Real-time monitoring of continuous biological process by CB8-MV^{2+} electrochemical assay

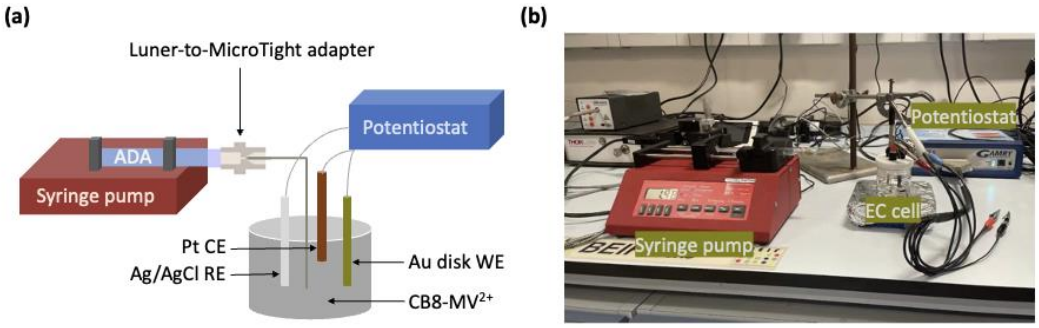

Fig. 5.25 (a) Schematic representation of SWV real-time monitoring of adamantylamine (ADA) continuous injection from syringe pump into 20 μM of CB8-MV^{2+} solution. Electrolyte: 6.25 mM PB solution (pH 7). **(b)** Photo of the setup.

Driven by the excellent sensing performances achieved by self-assembly CB8-MV^{2+} electrochemical assay, its capability of real-time monitoring the continuous processes of biomolecules, such as drug loading/releasing events, is of particular interest to be further explored. We employed syringe pump to simulate the continuous ADA drug releasing process and performed real-time investigation on it utilizing CB8-MV^{2+} electrochemical assay. The overall setup is schematically illustrated in **Fig. 5.25a**, corresponding to the photo in **Fig. 5.25b**. In particular, the stock solution of target drug at a specific concentration (*i.e.* we here used 2 mM) was filled in the syringe and mounted onto the syringe pump prior to flowing through the tubing into the electrochemical cell, and on the other hand, 20 μM of CB8-MV^{2+} solution was stocked in the electrochemical cell and connected to Gamry Potentiostat for measurement. Ahead of the continuous recording of SWV, the injection speed and overall injection amount of solution were set up as a fixed value to facilitate the data quantitative analysis.

Here, ADA and PC drugs were selected as representative analytes to be detected via IDA and ABA working formats of CB8-MV^{2+} electrochemical assay. SWV curves of 20 μM CB8-MV^{2+} during the injection of ADA or PC at a variety of injection speeds, ranging from 2 μL/min to 20 μL/min, were recorded at specific time intervals. The time intervals of measurement were accordingly adjusted to a value at which the recorded frequency was neither too lose to miss the characteristic SWV curves nor too dense to figure out the difference between two adjacent SWV curves. For example, the time interval between each measurement in the case of 20 μL/min was around 2 mins, which was wider than that of 2 μL/min (*e.g.* ~10 mins). The concentration of analyte injected into the electrochemical cell at each SWV measurement point was estimated via the equation of 'injection speed × injection time × the concentration of stock solution stored in the syringe'. Considering the injection speed was constant over the entire injection, thus the overall changing trends of $\Delta I_{MV2+|MV+\bullet}$ and ΔV_{PC}

against the concentration of ADA and PC are expected to be comparable to the ones obtained in titration experiments illustrated in *Chapter 5.4.1* and *Chapter 5.4.2*. For the sake of easy comparison, we overlaid scatter plots recorded at different injection speeds in **Fig. 5.26**. Compared between the SWV titration scatter plots obtained at different injection speeds of ADA and PC in **Fig. 5.26a,c**, no huge difference was observed, and the range of offset was acceptable from practical viewpoint. On the other hand, $\Delta I_{MV2+|MV+\bullet}$ or ΔV_{PC} was also plotted against the injection time in **Fig. 5.26b,d**, which indicates that the faster the injection speed, the quicker the indicative signal (*i.e.* $\Delta I_{MV2+|MV+\bullet}$ or ΔV_{PC}) changed, in line with expectation. With these obtained results, CB8-MV^{2+} electrochemical assay is expected to work as an effective platform for in-situ monitoring of biological continuous processes, where the target bio-analytes can either be strong binders or aromatic derivatives corresponding to two working formats of CB8-MV^{2+} assay.

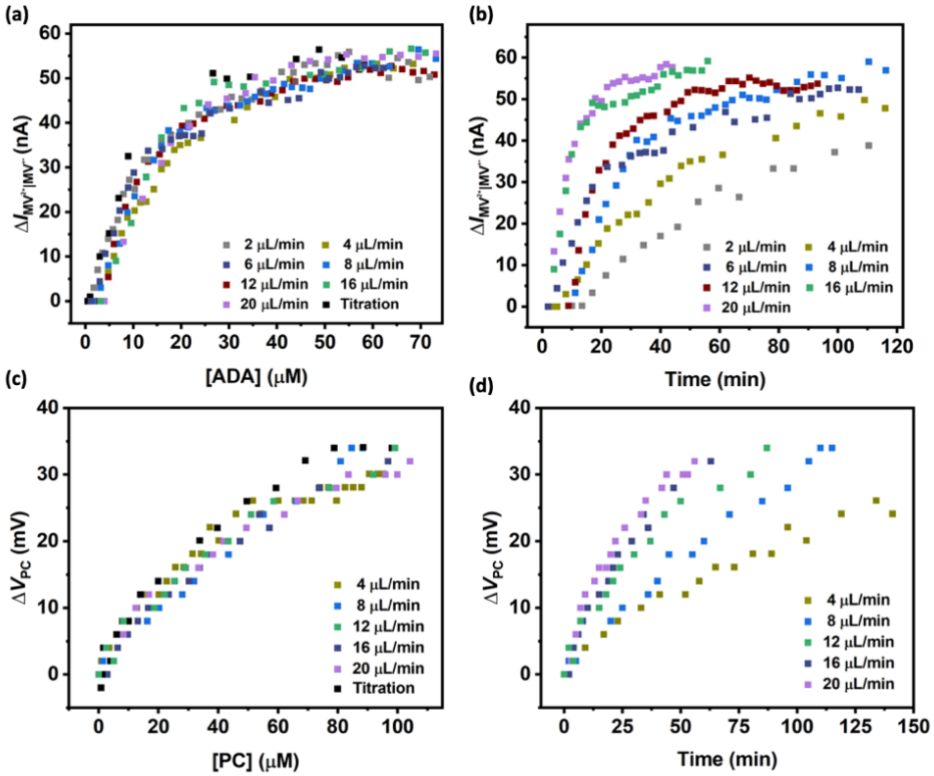

Fig. 5.26 Overlaid scatter plots of peak current change corresponding to the reduction of displaced MV^{2+} ($\Delta I_{MV2+|MV+\bullet}$) under continuous injection of adamantylamine (ADA) at different speeds **(a)** against the concentration of ADA and **(b)** against the overall injection time. Overlaid scatter plots of peak potential shift (ΔV_{PC}) under continuous injection of procaine hydrochloride (PC) at different speeds **(c)** against the concentration of PC and **(d)** against the overall injection time. Stock solution in pump: 2 mM ADA or PC sample prepared in 6.25 mM PB solution (pH 7).

The present results are still at a conceptual stage, suggesting the possibility for CB8-MV^{2+} electrochemical assay to be utilized for real-time monitoring of continuous biological processes. Optimization on recording intervals and parameters are necessary when studying different dynamic processes. For example, if the kinetics of the target biological event is quick, the time intervals for SWV recording should be shortened to avoid missing the point where the key changes take place.

5.8 Conclusions

This Chapter has discovered new possibilities of sensing, and especially, binding constant determination, in complex bio-media, ranging from simple buffer solution, urine, serum even to blood, by using CB8-MV^{2+} as multi-functional electrochemical assay with the aid of SWV titration approach. Redox active, environment sensitive and commercially available MV^{2+} was employed as indicator to generate characteristic responsive signals towards the competitive binding and associative binding events, enabling CB8-MV^{2+} to work in dual-functional way, *e.g.* IDA and ABA. Gratifying to note that down to 10^{-8} M^{-1} minimum detectable concentration and linear detection range located within physiologically relevant micromolar range have been achieved, and moreover, both minimum detectable concentration and linear detection range showed adjustability upon easily changing the concentration of CB8-MV^{2+} assay, thus being able to better cater for different requirements in real cases. In addition to sensing, CB8-MV^{2+} assay demonstrated binding constant determination capability in complex bio-media (*e.g.* SU, FBS, HS, SB and HB) by taking advantage of its promising interferent tolerance ability benefited from its superior binding specificity and selectivity, which has never been achieved by conventional supramolecular titration methodologies to the best of our knowledge and is of interests in the area of supramolecular chemistry. Moreover, CB8-MV^{2+} assay also showed ability to real-time monitor continuous injection of drug molecules from syringe pump, indicating it possess promising potentials to be utilized for in-situ monitoring of other continuous biological events, such as drug loading and releasing process. In conclusion, the proposed self-assembly and multi-functional CB8-MV^{2+} electrochemical assay can greatly inspire the design of other versatile supramolecular-based assays for a wide range of practical applications in biological and pharmaceutical fields.

Chapter 6. Conclusions, limitations and outlook

This Chapter concluded what have been done and achieved by our research, what are the major limitations of current research findings, and discussed what can be further investigated based on present research outcomes in future.

6.1 Conclusions

Electrochemistry is known to be a powerful tool to provide information-rich features when probing redox-active analytes, and supramolecular chemistry is a burgeoning area investigating unique properties of free molecules imparted via molecular interactions between host and guest molecules during complexation. Thus, combing supramolecular chemistry with electrochemistry is expected to provide exceptional functions in the fields of analytical chemistry and sensing, thus being of our research interest.

In this research, we have reported rigid macrocycles of cucurbit[*n*]urils (CB*n*, *n* = 7, 8) are amenable to modulate the electrochemical reactivity of redox-active resazurin guest upon complexation. Notably, the modulation effect exerted by CB7 and CB8 were reverse, *i.e.* CB8 facilitated the irreversible reduction process of resazurin while CB7 hindered it, which was rationalized by their different binding tightness. However, flexible hosts β-cyclodextrin (βCD) and γ-cyclodextrin (γCD) did not show any significant modulation effects on the electrochemical reactivity of resazurin although their cavity size are comparable to CB7 and CB8, respectively. The observed supramolecular modulation effect is expected to be extended for studying other redox-active molecules to cater for different end applications.

Quantitative analysis of molecular interactions between host and guest is indispensable for comprehensive understanding of host-guest complexes. Binding constant is a generally utilized indicator to represent the thermodynamic stability of host-guest complexes. Diverse methodologies have been proposed for the estimation of binding constants of supramolecular complexes, among which titration approaches present most prevailing. However, titration experiments suffer from several inherent limitations such as long experiment period, specific requirement regarding the solubility and complicated data analysis, which were overcame by our proposed electrochemical scheme. In particular, we reported a simple electrochemical approach for estimation of binding constants ($\log K_{G2}$) of CB8-MV^{2+}-based ternary complexes by uncovering the linear correlation with $R^2 = 0.85$ between ITC determined binding constants and the electrochemically (*e.g.* cyclic voltammetry and square wave voltammetry) measured reduction potential shift of CB8-MV^{2+}-based ternary complexes with respect to CB8-MV^{2+} (ΔV_{G2}). The rich information provided by electrochemistry help us to figure out which species exactly exist in the system and avoid false-positive binding results. The precision and practical accuracy in $\log K_{G2}$ of our scheme achieved ± 0.03 and ± 0.32, respectively, and the measurement time was reduced to less than 10 mins by one-point measurement instead of titration steps. Inspection regarding the mechanism underlying such linear correlation was achieved by the convergence of experimental and computational results. It has been found that the linear correlation tends to be rooted from the host-guest exchange scene taking place after the electron transfer process. With this rapid electrochemical scheme, screening guest molecules based on binding constants to meet the requirement for specific application is achievable, providing a powerful premise for exploring the application of supramolecular electrochemistry in multiple real cases. Ultimately, we demonstrated the wide applicability and robustness of our scheme by estimating binding constants of a group of volatile and sparsely soluble hydrocarbons, which are hard to be directly measured by conventional titration methodologies otherwise, thus considerably broadening the range of quantitative analysis and application potentials of host-guest systems. These findings are expected to inspire the

application of electrochemistry in supramolecular analytical field to study other redox active species involved systems, which can then be utilized in different scenarios. For example, a redox active species with proper binding affinity can be selected among multiple candidates using this scheme to work as sensing probe in electrochemical sensor.

Take it a step further from the rapid electrochemical scheme enabling estimate binding constant in high-throughput fashion, with the aid of CB8-MV^{2+} assay and electrochemical titration protocol, we have brought binding constant estimation to a new era, *e.g.* determine the binding constant in physiologically most relevant but highly complex matrices, such as urine, serum and even blood, which has never been achieved yet to the best of our knowledge. With this achievement, we could gain an understanding of how host and guest molecules interact with each other in bio-media in the presence of multiple complex biofluid species like salts, proteins, blood cells, *etc*, which could provide guidance on biological applications of supramolecular electrochemistry.

Encouraged by this finding, the application potentials of CB8-MV^{2+} in sensing area were also explored. Other than the binding constant determination, the self-assembled CB8-MV^{2+} assay demonstrates powerful biosensing ability. In particular, by employing redox active and environmental sensitive MV^{2+} as probe, CB8-MV^{2+} electrochemical assay is capable of integrating two working formats of IDA and ABA in one, allowing for the detection of analytes with a wide range of binding affinities (10^8 M^{-1} to 10^3 M^{-1}) achieving down to 10^{-8} M minimum detectable concentration and linear detection range within physiologically relevant micromolar range. Compared to conventional electrochemical sensors, this assay eliminated the need of laborious electrode modification steps but did not sacrifice sensing sensitivity and selectivity. To widen the application scope of CB8-MV^{2+} assay from buffer solution to complex bio-media, we tested its interferent tolerance by performing sensing for MEM and PC in the presence of multiple equivalents of potential interferent biomolecules, *e.g.* RTM and PCG. Gratifying to see that CB8-MV^{2+} was able to maintain its major characteristic electrochemical profile for sensing in the presence of interferent molecules. Encouraged by the desired interference tolerance of CB8-MV^{2+} assay, its ability of sensing in complex biological matrices were then explored; in particular, it was investigated that CB8-MV^{2+} held its great sensing properties in both IDA and ABA modes in a group of different biofluids, including native synthetic urine, whole fetal bovine serum, whole human serum and even animal blood, which was rarely or never reported to the best of our knowledge, opening up a new venue for supramolecular electrochemistry to apply in bio-sensing field. Moreover, the establishment of simple yet multi-functional and robust CB8-MV^{2+} electrochemical assay is expected to inspire the design of diverse powerful molecular platforms with the aid of supramolecule and redox active species.

Furthermore, the potential of CB8-MV^{2+} electrochemical assay to real-time monitor continuous dynamic processes was also investigated by performing conceptual measurements using syringe pump to mimic drug release event by continuously injecting drug molecules. Inspired by the preliminary results obtained with the aid of syringe pump, application capabilities of supramolecular-based electrochemical assay in real-time studying dynamic processes, such as enzymatic reactions, drug loading and releasing processes, *etc*, were confirmed, and future works can be done towards this direction.

The findings in terms of reactivity modulation, quantitative analysis of host-guest interactions, and bio-sensing achieved with the aid of supramolecular-based electrochemical platform in this work spark new possibilities in future development and practical applications of supramolecular electrochemistry.

6.2 Limitations of current research

Research in *Chapter 3* demonstrated the supramolecular modulation effect on electrochemical reactivity of resazurin, which was rationalized by the ease for water molecules to approach the reaction centre on supramolecule encapsulated resazurin in photo transfer step. Although the present mechanistic analysis was supported by computational simulations and calculations, it would be better to gain supplemental evidence from experiments for in-deep explanation. Moreover, the application potentials of such supramolecular widened redox active window have not been investigated in this chapter, which deserve further research.

The application range of rapid electrochemical protocol for binding constant estimation proposed in *Chapter 4* is mainly limited to the CB8-MV^{2+}-based ternary complexes and cannot be directly utilized for other supramolecular systems. Although it is ready to be extended to study other CB8-based hetero-ternary complexes with one redox active guest as first guest upon performing similar electrochemical measurements to obtain corresponding linear correlation functions, one redox active guest molecule is necessarily required in this protocol. Whether such electrochemical approach is applicable for determining binding constants of supramolecular ternary complexes based on different host molecules, *e.g.* cyclodextrins (CDs), remains unclear, which deserves following studies. This should depend on whether an obvious change in electrochemical features of the first redox active guest can be observed upon supramolecular binding with second guest molecule.

CB8-MV^{2+} electrochemical assay implemented in *Chapter 5* is predominately for the detection of the molecules which are required to be able to either from ternary complex with CB8-MV^{2+} or displace MV^{2+} out of CB8 cavity, showing relatively limited application scope. On the other hand, as CB8-MV^{2+} assay is capable of detecting a group of molecules but not exclusively designed for one specific target analyte, its sensing specificity and selectivity appear to be less desirable compared to other biomolecule-based sensors, such as enzyme-linked immunosorbent assay (ELISA) and immunosensors, which could hinder its diagnostic applications. Moreover, although the minimum detection concentration of CB8-MV^{2+} electrochemical assay towards target drug molecules is located within physiologically relevant micromolar range, it can still be not enough for clinical tests in real-world cases. In addition to minimum detectable concentration, the recovery rate of CB8-MV^{2+} bioassay has not been evaluated in this work, which could be supplemented in the future. There are still limitations need to be overcame if we would like to turn the established CB8-MV^{2+} electrochemical assay into a real commercial product for practical applications. Different practical application scenarios often require different properties of sensor, which cannot be fully met by the present CB8-MV^{2+} electrochemical assay. For example, point-of-caring testing (POCT) often required high specificity and sensitivity, real-time connectivity, quick measurements, portable devices, ease of sample preparation; chip-based sensors for on-site detection often requires miniatured devices performing localized detection with small sample volume and superior sensitivity and selectivity; multiplexed detection often requires differential selectivity towards a group of analytes with similar chemical structures. Generally, certain modification and optimization steps are necessary to be taken to enhance the possibility of CB8-MV^{2+} electrochemical assay for real-world applications.

As for the ability of real-time monitoring of continuous biological processes, the results achieved with the aid of syringe pump in *Chapter 5* are still at preliminary stage, more work needs to be done to verify whether the CB8-MV^{2+} electrochemical assay is indeed capable of monitoring real biological processes but not the mimic drug releasing process demonstrated by syringe pump. Meanwhile, the design of the set-up and corresponding test parameters could be

further optimized to increase the sensitivity and selectivity to better cater for different proceeding speeds and rates of different real continuous biological processes.

6.3 Future work

Application of supramolecular electrochemistry in the areas of analytical chemistry and molecular detection have been explored in this research. However, this research mainly focused on using cucurbit[*n*]uril (CB*n*) as supramolecular host and methyl viologen as redox active reporter. Generally, potentials provided by other kinds of supramolecular hosts [124] and redox active guests remain unexplored and worth to be further studied. For example, inspired by the findings achieved by MV^{2+} in this work, other redox active species like viologen derivatives which are of planar structures present as proper electrochemical probe for CB*n*-based systems, and additionally, redox active ferrocene and cobaltocenium derivatives are also ready to be encapsulated by CB*n* as electrochemical probe [67]. Upon using redox probes with different binding properties, the obtained supramolecular sensing assay can thus provide different sensing specificity and selectivity towards different analytes, allowing for a wide application range. In the concern of hosts, other synthetic hosts like calixarenes (CXs) and cyclodextrins (CDs) demonstrating different binding properties towards analytes compared to CBs also show promising application potentials in sensing and analytical chemistry [16-19]. In addition to one single host, diverse mechanically interlocked molecular architectures based on several kinds of hosts have been designed and utilized for sensing [132], *i.e.* rotaxane formed based on CB8 and βCD reported by the Biedermann group shows ability of optical sensing in complex bio-media [311], which can achieve improved sensing features by combining advantages of multiple hosts with different geometries.

With the investigated electrochemical activity modulation effect of CB7 and CB8 imposed on redox process of resazruin ($[RZ\text{-}H]^-$ at pH 7) in *Chapter 3*, supramolecular modulation effects on other photo transfer involved electrochemical reactions can be investigated. Although the investigation of underlying mechanism has been discussed in *Chapter 3*, more supportive experiments could be followed up to provide more evidence on the conclusions draw from the computational simulations and offer more comprehensive knowledge of such supramolecular-based reverse modulation effects. Such information can better pave the way for investigations on other supramolecular-based redox active system. For example, apart from this group of reaction, we can further widen our research scope to other supramolecular modulation on electrochemical reactivity of encapsulated molecules based on different mechanisms. Most of precedent examples regarding supramolecular modulation effects on redox species are rooted from supramolecular preferable complexation between reactants and products caused by the charge difference after electron transfer steps in electrochemical reactions. Inspired by the reported mechanism of binding tightness and the ease for water molecule to approach the reaction centre in this work, other possible mechanisms, such as the supramolecular pre-organization effect, that can cause different modulation effects are attractive to be explored, and meanwhile, mechanistic study is helpful to gain full understanding and deep insight of the electrochemical reaction, facilitating applying it to practical cases in a more proper way. In addition to the mechanistic analysis, the application aspect of these supramolecular modulation effects can be explored. For example, the widened redox window of the redox active indicator, *e.g.* $[RZ\text{-}H]^-$, could make its detection range shift to a different group of analytes when it works as tracer for biological sensors by using either redox potential or redox-related fluorescent properties as indicative signals. Moreover, based on such modulation, sensing platforms targeting redox active analytes could be implemented by using supramolecule as the receptor and the reactivity changes as the responsive signals.

With the proposed electrochemical scheme for rapid estimation of cucurbit[*8*]uril-methyl viologen (CB8-MV^{2+})-based ternary complexes in *Chapter 4*, diverse practical applications of supramolecular electrochemistry can be achieved. For instance, this scheme can be utilized to screen multiple candidate probe molecules to select the one which can bind to supramolecular host with a suitable binding affinity when designing a supramolecular-based sensor for enzymatic reaction monitoring or supramolecular-based indicator displacement assays (IDAs). Additionally, this scheme can be employed to identify a group of analytes which possess binding affinities with certain degree of difference for supramolecular sensors to perform multiplexing sensing. On the other hand, beyond the scope of CB8-MV^{2+}-based ternary complexes, future works can be done along this direction to design rapid and simple binding constant estimation approach for other host-guest complexes, which can revolutionize the quantitative analysis of host-guest interactions in supramolecular chemistry area and bring new possibilities for the application of supramolecular-based systems. For example, similar electrochemical measurements can be performed for other ternary complexes formed by different host molecules (*e.g.* CB8, γCD, *etc*) and two guest molecules, of which one is fixed and redox active, to see if any correlation can be observed between the change in redox peak potential of the redox active guest and the binding constants of ternary complexes with different second guest molecules. In addition to utilizing redox peak potential as indicative factor, other electrochemical features are probably also suitable as tracing signals, such as the peak current, when the target supramolecular systems are based on different working principles or using different testing techniques (*e.g.* amperometry) instead of voltametric techniques.

Encouraged by the findings regarding the biosensing in complex biological matrices enabled by CB8-MV^{2+} electrochemical assay in *Chapter 5*, new possibilities of sensing small molecules without complicated laboratory synthetic steps in complex bio-media emerged. With such simple assay design strategy, a series of supramolecular-based electrochemical sensing assay with improved sensing properties and multiple working modes, *e.g.* associative binding assay (ABA) and indicator displacement assay (IDA), can be formed by using different kinds of supramolecular hosts and electrochemical active reporters to detect target analytes that are of different chemical and physical properties. Taking advantage of the design concept of such electrochemical active ABA and IDA sensors, analytes which are electrochemical and spectroscopic transparent can be sensitively detected. Although electrochemical detection of small molecules in native serum have been achieved by this work, sensing in untreated and undiluted blood sample remains challenging as multiple concentrated complex species, such as salts, proteins and blood cells, presented in blood tend to interplay with sensing assay and blur sensing signals. Hence, designing strategies for establishing sensing assays that can address this remained biofluid challenge are of certain interests. For example, molecular engineering can be employed to modify and/or fabricate unique hosts and/or redox active indicators to effectively avoid biofouling and biofluids effects, enabling in-situ detection of small molecules in real complex blood environment; electrode modification strategies are worthwhile to explore to enhance the sensitivity and selectivity of electrode. Considering the practical applications of biosensors, such as point-of-care-testing (POCT), chip-based devices, commercialized home used product, there are lots of works need to be carried out to investigate and explore the possibilities of the established CB8-MV^{2+} sensor. Sensitivity and specificity are often of crucial importance for diagnostic sensor, and short and easy measurement are also required for POCT, which can be future optimization direction for our CB8-MV^{2+} biosensor. For example, modifying electrode surface by receptor molecules could be helpful to enhance the sensing specificity; modifying electrode by nanomaterials can effectively improve sensitivity by taking advantages of the large surface of nanomaterials. The possibility of CB8-MV^{2+} electrochemical assay to be miniaturized as chip-based devices for on-site detection could be explored by

employing portable measuring potentiostat and screen-printed electrodes instead of Au disk electrode in the future.

New possibilities of binding constant estimation in complex bio-media explored in *Chapter 5* could offer more in-situ information regarding the non-covalent molecular interactions of the supramolecular system, providing more specific guidance for designing supramolecular systems for applications involved with complex bio-media. Thus, more work can be followed up to take advantage of such capability to design different supramolecular-based systems catering for diverse applications.

Inspired by the preliminary results regarding real-time monitoring of continuous adamantylamine (ADA) injection process achieved by CB8-MV^{2+} electrochemical assay in *Chapter 5*, application potentials of supramolecular-based electrochemical assays in continuous monitoring of dynamic biological processes such as drug loading and releasing processes as well as enzymatic reactions are attractive to be further studied. For instance, the amount of loaded/released drug can be traced by the degree of increase/decrease in electrochemical signals of supramolecular-based electrochemical assay upon capturing drug molecule released into bulk solution to form inclusion complexes; the degree of enzymatic reactions progress can be analysed when supramolecular-based electrochemical assay can preferably bind with substrate molecule or reaction product molecule. Research regarding the application possibilities of supramolecular-based electrochemical assay in real-time monitoring of continuous chemical progresses done by this work remains in conceptual stage, and proof-of-concept experiments are worthwhile to be performed in future. Along this direction, drug loading/releasing systems such as nano-capsules, that are compatible with supramolecular electrochemical platform are worthwhile to be designed in future work.

References

[1] Ruiz-Hitzky, E.; Casal, B. Crown ether intercalations with phyllosilicates. *Nature*. **1978**, *276*, 596-597.

[2] Rebek Jr, J. Host–guest chemistry of calixarene capsules. *Chem. Comm.* **2000**, 637-643.

[3] Pedersen, C. J. Cyclic polyethers and their complexes with metal salts. *J. Am. Chem. Soc.* **1967**, *89*, 7017-7036.

[4] Chen, L.; Zhang, H. Y.; Liu, Y. High affinity crown ether complexes in water: thermodynamic analysis, evidence of crystallography and binding of NAD+. *J. Org. Chem. Res.* **2012**, *77*, 9766-9773.

[5] van Maarschalkerwaart, D. A.; Willard, N. P.; Pandit, U. K. Synthesis of carbohydrate containing crown ethers and their application as catalysts in asymmetric Michael additions. *Tetrahedron* **1992**, *48*, 8825-8840.

[6] Chehardoli, G.; Bahmani, A., The role of crown ethers in drug delivery. *Supramol. Chem.* **2019**, *31*, 221-238.

[7] Tso, W.-W.; Fung, W.-P.; Tso, M.-Y. W. Variability of crown ether toxicity. *J. Inorg. Biochem*. **1981**, *14*, 237-244.

[8] Gutsche, C. D. Calixarenes Cambridge. *R. Soc. Chem.* **1989**.

[9] De Namor, A. D.; Cleverley, R. M.; Zapata-Ormachea, M. L. Thermodynamics of calixarene chemistry. *Chem. Rev*. **1998**, *98*, 2495-2525.

[10] Ludwig, R.; Dzung, N. T. K. Calixarene-based molecules for cation recognition. *Sens.* **2002**, *2*, 397-416.

[11] Yousaf, A.; Abd Hamid, S.; Bunnori, N. M.; Ishola, A. Applications of calixarenes in cancer chemotherapy: facts and perspectives. *Drug Des. Devel. Ther*. **2015**, *9*, 2831.

[12] Kim, J. S.; Quang, D. T. Calixarene-derived fluorescent probes. *Chem. Rev.* **2007**, *107*, 3780-3799.

[13] Crini, G.; Fourmentin, S.; Fenyvesi, É.; Torri, G.; Fourmentin, M.; Morin-Crini, N. Cyclodextrins, from molecules to applications. *Environ. Chem. Lett.* **2018**, *16*, 1361-1375.

[14] Crini, G. A history of cyclodextrins. *Chem. Rev.* **2014**, *114*, 10940-10975.

[15] Del Valle, E. M. Cyclodextrins and their uses: a review. *Process Biochem.* **2004**, *39*, 1033-1046.

[16] Haimhoffer, Á.; Rusznyák, Á.; Réti-Nagy, K.; Vasvári, G.; Váradi, J.; Vecsernyés, M.; Bácskay, I.; Fehér, P.; Ujhelyi, Z.; Fenyvesi, F. Cyclodextrins in drug delivery systems and their effects on biological barriers. *Sci. Pharm.* **2019**, *87*, 33.

[17] Zhang, Y.-M.; Xu, Q.-Y.; Liu, Y. Molecular recognition and biological application of modified β-cyclodextrins. *Sci. China Chem*. **2019**, *62*, 549-560.

[18] Liu, Y.; Chen, Y.; Gao, X.; Fu, J.; Hu, L. Application of cyclodextrin in food industry. *Crit. Rev. Food Sci. Nutr.* **2022**, *62*, 2627-2640.

[19] Tian, B.; Hua, S.; Tian, Y.; Liu, J. Cyclodextrin-based adsorbents for the removal of pollutants from wastewater: a review. *Environ. Sci. Pollut. Res.* **2021**, *28*, 1317-1340.

[20] Barrow, S. J.; Kasera, S.; Rowland, M. J.; Del Barrio, J.; Scherman, O. A. Cucurbituril-based molecular recognition. *Chem. Rev.* **2015**, *115*, 12320-12406.

[21] Nau, W. M.; Florea, M.; Assaf, K. I. Deep inside cucurbiturils: physical properties and volumes of their inner cavity determine the hydrophobic driving force for host–guest complexation. *Isr. J. Chem.* **2011**, *51*, 559-577.

[22] Kim, K.; Selvapalam, N.; Ko, Y. H.; Park, K. M.; Kim, D.; Kim, J. Functionalized cucurbiturils and their applications. *Chem. Soc. Rev.* **2007**, *36*, 267-279.

[23] Tan, L. L.; Wei, M.; Shang, L.; Yang, Y. W. Cucurbiturils-mediated noble metal nanoparticles for applications in sensing, sers, theranostics, and catalysis. *Adv. Funct. Mater.* **2021**, *31*, 2007277.

[24] Funk, S.; Schatz, J. Cucurbiturils in supramolecular catalysis. *J. Incl. Phenom. Macrocycl. Chem.* **2020**, *96*, 1-27.

[25] Cicolani, R. S.; Souza, L. R. R.; de Santana Dias, G. B.; Gonçalves, J. M. R.; Abrahao, I. d. S.; Silva, V. M.; Demets, G. J.-F. Cucurbiturils for environmental and analytical chemistry. *J. Incl. Phenom. Macrocycl. Chem.* **2021**, *99*, 1-12.

[26] Behrend, R.; Meyer, E.; Rusche, F. I. Ueber condensationsproducte aus glycoluril und formaldehyd. *Justus Liebigs Ann. Chem*. **1905**, *339*, 1-37.

[27] Freeman, W.; Mock, W.; Shih, N. Cucurbituril. *J. Am. Chem. Soc.* **1981**, *103*, 7367.

[28] Assaf, K. I.; Nau, W. M. Cucurbiturils: from synthesis to high-affinity binding and catalysis. *Chem. Soc. Rev*. **2015**, *44*, 394-418.

[29] Lagona, J.; Mukhopadhyay, P.; Chakrabarti, S.; Isaacs, L. The cucurbit [n] uril family. *Angew. Chem. Int. Ed.* **2005**, *44*, 4844-4870.

[30] Kim, J.; Jung, I.-S.; Kim, S.-Y.; Lee, E.; Kang, J.-K.; Sakamoto, S.; Yamaguchi, K.; Kim, K. New cucurbituril homologues: syntheses, isolation, characterization, and X-ray crystal structures of cucurbit [n] uril (n= 5, 7, and 8). *J. Am. Chem. Soc.* **2000**, *122*, 540-541.

[31] Day, A.; Arnold, A. P.; Blanch, R. J.; Snushall, B. Controlling factors in the synthesis of cucurbituril and its homologues. *J. Org. Chem. Res.* **2001**, *66*, 8094-8100.

[32] Masson, E.; Ling, X.; Joseph, R.; Kyeremeh-Mensah, L.; Lu, X. Cucurbituril chemistry: a tale of supramolecular success. *RSC Adv.* **2012**, *2*, 1213-1247.

[33] Isaacs, L. Cucurbit [n] urils: from mechanism to structure and function. *Chem. Comm.* **2009**, 619-629.

[34] Isaacs, L. The mechanism of cucurbituril formation. *Isr. J. Chem.* **2011**, *51*, 578-591.

[35] Huang, W.-H.; Zavalij, P. Y.; Isaacs, L. Cucurbit [n] uril formation proceeds by step-growth cyclo-oligomerization. *J. Am. Chem. Soc.* **2008**, *130*, 8446-8454.

[36] Pisani, M. J.; Zhao, Y.; Wallace, L.; Woodward, C. E.; Keene, F. R.; Day, A. I.; Collins, J. G. Cucurbit [10] uril binding of dinuclear platinum (II) and ruthenium (II) complexes: association/dissociation rates from seconds to hours. *Dalton Trans*. **2010**, *39*, 2078-2086.

[37] Nau, W. M. Mohanty, J., Taming fluorescent dyes with cucurbituril. *Int. J. Photoenergy.* **2005**, *7*, 133-141.

[38] Mecozzi, S.; Rebek, J. Julius. The 55% solution: a formula for molecular recognition in the liquid state. *Eur. J. Chem.* **1998**, *4*, 1016-1022.

[39] Garel, L.; Dutasta, J. P.; Collet, A. Complexation of methane and chlorofluorocarbons by cryptophane-A in organic solution. *Angew.Chem. Int. Ed*. **1993**, *32*, 1169-1171.

[40] Yang, G.; Xu, Y. Probing chiral solute-water hydrogen bonding networks by chirality transfer effects: a vibrational circular dichroism study of glycidol in water. *J. Chem. Phys.* **2009**, *130*, 164506.

[41] Biedermann, F.; Uzunova, V. D.; Scherman, O. A.; Nau, W. M.; De Simone, A. Release of high-energy water as an essential driving force for the high-affinity binding of cucurbit [n] urils. *J. Am. Chem. Soc.* **2012**, *134*, 15318-15323.

[42] Romero-Vargas Castrillón, S.; Giovambattista, N.; Aksay, I. A.; Debenedetti, P. G. Effect of surface polarity on the structure and dynamics of water in nanoscale confinement. *J. Phys. Chem. B* **2009**, *113*, 1438-1446

[43] Giovambattista, N.; Rossky, P. J.; Debenedetti, P. G. Phase transitions induced by nanoconfinement in liquid water. *Phys. Rev. Lett.* **2009**, *102*, 050603.

[44] Sharma, S.; Debenedetti, P. G. Evaporation rate of water in hydrophobic confinement. *Proc. Natl. Acad. Sci. U.S.A.* **2012**, *109*, 4365-4370.

[45] Biedermann, F.; Nau, W. M.; Schneider, H. J. The Hydrophobic Effect Revisited—Studies with Supramolecular Complexes Imply High-Energy Water as a Noncovalent Driving Force. *Angew. Chem. Int. Ed.* **2014**, *53*, 11158-11171.

[46] Chio, W. I. K.; Peveler, W. J.; Assaf, K. I.; Moorthy, S.; Nau, W. M.; Parkin, I. P.; Olivo, M.; Lee, T. C. Selective detection of nitroexplosives using molecular recognition within self-assembled plasmonic nanojunctions. *J. Phys. Chem. C* **2019**, *123*, 15769-15776.

[47] Chio, W.-I. K.; Liu, J.; Jones, T.; Perumal, J.; Dinish, U.; Parkin, I. P.; Olivo, M.; Lee, T.-C. SERS multiplexing of methylxanthine drug isomers via host–guest size matching and machine learning. *J. Phys. Chem. C* **2021**, *9*, 12624-12632.

[48] Chio, W.-I. K.; Moorthy, S.; Perumal, J.; Dinish, U.; Parkin, I. P.; Olivo, M.; Lee, T.-C. Dual-triggered nanoaggregates of cucurbit [7] uril and gold nanoparticles for multi-spectroscopic quantification of creatinine in urinalysis. *J. Mater. Chem. C* **2020**, *8*, 7051-7058.

[49] Peveler, W. J.; Jia, H.; Jeen, T.; Rees, K.; Macdonald, T. J.; Xia, Z.; Chio, W.-I. K.; Moorthy, S.; Parkin, I. P.; Carmalt, C. J. Cucurbituril-mediated quantum dot aggregates formed by aqueous self-assembly for sensing applications. *Chem. Comm.* **2019**, *55*, 5495-5498.

[50] Thomas, C. R.; Ferris, D. P.; Lee, J.-H.; Choi, E.; Cho, M. H.; Kim, E. S.; Stoddart, J. F.; Shin, J.-S.; Cheon, J.; Zink, J. I. Noninvasive remote-controlled release of drug molecules in vitro using magnetic actuation of mechanized nanoparticles. *J. Am. Chem. Soc.* **2010**, *132*, 10623-10625.

[51] Walker, S.; Oun, R.; McInnes, F. J.; Wheate, N. J. The potential of cucurbit [n] urils in drug delivery. *Isr. J. Chem.* **2011**, *51*, 616-624.

[52] Saleh, N. i.; Ghosh, I.; Nau, W. M. Cucurbiturils in drug delivery and for biomedical applications. *Supram. Sys. Biome. Fi.* **2013**, *13*, 164.

[53] Day, A. I.; Collins, J. G. Cucurbituril receptors and drug delivery. *Supram. Chem. Mol. Nanom.* **2012**.

[54] Saleh, N. i.; Koner, A. L.; Nau, W. M. Activation and Stabilization of Drugs by Supramolecular pKa Shifts: Drug-Delivery Applications Tailored for Cucurbiturils. *Angew. Chem. Int. Ed.* **2008**, *120*, 5478-5481.

[55] Lambert, H.; Zhang, Y.-W.; Lee, T.-C. Supramolecular catalysis of m-xylene isomerization by cucurbiturils: transition state stabilization, vibrational coupling, and dynamic binding equilibrium. *J. Phys. Chem. C* **2020**, *124*, 11469-11479.

[56] Tonga, G. Y.; Jeong, Y.; Duncan, B.; Mizuhara, T.; Mout, R.; Das, R.; Kim, S. T.; Yeh, Y.-C.; Yan, B.; Hou, S. Supramolecular regulation of bioorthogonal catalysis in cells using nanoparticle-embedded transition metal catalysts. *Nat. Chem.* **2015**, *7*, 597-603.

[57] Ellis, E.; Moorthy, S.; Chio, W.-I. K.; Lee, T.-C. Artificial molecular and nanostructures for advanced nanomachinery. *Chem. Comm.* **2018**, *54*, 4075-4090.

[58] Gürbüz, S.; Idris, M.; Tuncel, D. Cucurbituril-based supramolecular engineered nanostructured materials. *Org. Biomol. Chem.* **2015**, *13*, 330-347.

[59] Tuncel, D. Cucurbituril-based Functional Materials. *R. Soc. Chem.* **2019.**

[60] Mock, W. L.; Shih, N. Y. Host-Guest Binding Capacity of Cucurbituril. *J. Org. Chem.* **1983**, *48*, 3618–3619.

[61] Zhang, S.; Grimm, L.; Miskolczy, Z.; Biczók, L.; Biedermann, F.; Nau, W. M. Binding affinities of cucurbit [n] urils with cations. *Chem. Comm.* **2019**, *55*, 14131-14134.

[62] Buschmann, H.-J.; Cleve, E.; Jansen, K.; Schollmeyer, E. Determination of complex stabilities with nearly insoluble host molecules: cucurbit [5] uril, decamethylcucurbit [5] uril and cucurbit [6] uril as ligands for the complexation of some multicharged cations in aqueous solution. *Anal. Chim. Acta* **2001**, *437*, 157-163.

[63] Buschmann, H.-J.; Cleve, E.; Jansen, K.; Wego, A.; Schollmeyer, E. Complex formation between cucurbit [n] urils and alkali, alkaline earth and ammonium ions in aqueous solution. J. *Incl. Phenom. Macrocycl. Chem.* **2001**, *40*, 117-120.

[64] Kellersberger, K. A.; Anderson, J. D.; Ward, S. M.; Krakowiak, K. E.; Dearden, D. V. Encapsulation of N2, O2, methanol, or acetonitrile by decamethylcucurbit [5] uril (NH4+) 2 complexes in the gas phase: influence of the guest on “lid” tightness. *J. Am. Chem. Soc.* **2001**, *123*, 11316-11317.

[65] Rekharsky, M. V.; Ko, Y. H.; Selvapalam, N.; Kim, K.; Inoue, Y. Complexation thermodynamics of cucurbit [6] uril with aliphatic alcohols, amines, and diamines. *Supram. Chem.* **2007,** *19*, 39-46.

[66] Mukhopadhyay, P.; Zavalij, P. Y.; Isaacs, L. High fidelity kinetic self-sorting in multi-component systems based on guests with multiple binding epitopes. *J. Am. Soc. Chem.* **2006**, *128*, 14093-14102.

[67] Gadde, S.; E Kaifer, A. Cucurbituril complexes of redox active guests. *Curr. Org. Chem.* **2011**, *15*, 27-38.

[68] Ong, W.; Kaifer, A. E. Unusual electrochemical properties of the inclusion complexes of ferrocenium and cobaltocenium with cucurbit [7] uril. *Organometallics* **2003**, *22*, 4181-4183.

[69] Jeon, W. S.; Moon, K.; Park, S. H.; Chun, H.; Ko, Y. H.; Lee, J. Y.; Lee, E. S.; Samal, S.; Selvapalam, N.; Rekharsky, M. V. Complexation of ferrocene derivatives by the cucurbit [7] uril host: a comparative study of the cucurbituril and cyclodextrin host families. *J. Am. Soc. Chem.* **2005**, *127*, 12984-12989.

[70] Lee, J. W.; Samal, S.; Selvapalam, N.; Kim, H.-J.; Kim, K. Cucurbituril homologues and derivatives: new opportunities in supramolecular chemistry. *Acc. Chem. Res.* **2003**, *36*, 621-630.

[71] Liu, S.; Ruspic, C.; Mukhopadhyay, P.; Chakrabarti, S.; Zavalij, P. Y.; Isaacs, L. The cucurbit [n] uril family: prime components for self-sorting systems. *J. Am. Soc. Chem.* **2005**, *127*, 15959-15967.

[72] Sigwalt, D.; Sekutor, M.; Cao, L.; Zavalij, P. Y.; Hostas, J.; Ajani, H.; Hobza, P.; Mlinaric-Majerski, K.; Glaser, R.; Isaacs, L. Unraveling the structure–affinity relationship between cucurbit [n] urils (n= 7, 8) and cationic diamondoids. *J. Am. Soc. Chem.* **2017**, *139*, 3249-3258.

[73] Cao, L.; Šekutor, M.; Zavalij, P. Y.; Mlinarić-Majerski, K.; Glaser, R.; Isaacs, L. Cucurbit [7] uril· guest pair with an attomolar dissociation constant. *Angew. Chem. Int. Ed.* **2014**, *126*, 1006-1011

[74] Ol'ga, A.; Samsonenko, D. G.; Fedin, V. P. Supramolecular chemistry of cucurbiturils. *Russ. Chem. Rev.* **2002**, *71*, 741-760.

[75] Yi, S.; Captain, B.; Kaifer, A. E. The importance of methylation in the binding of (ferrocenylmethyl) tempammonium guests by cucurbit [n] uril (n= 7, 8) hosts. *Chem. Comm.* **2011**, *47*, 5500-5502

[76] Ko, Y. H.; Kim, Y.; Kim, H.; Kim, K. U-Shaped Conformation of Alkyl Chains Bound to a Synthetic Receptor Cucurbit [8] uril. *Chem. Asian J.* **2011**, *6*, 652-657.

[77] Porel, M.; Jockusch, S.; Ottaviani, M. F.; Turro, N.; Ramamurthy, V. Interaction between encapsulated excited organic molecules and free nitroxides: communication across a molecular wall. *Langmuir* **2011**, *27*, 10548-10555.

[78] Rinkevicius, Z.; Frecus, B.; Murugan, N. A.; Vahtras, O.; Kongsted, J.; Ågren, H. Encapsulation influence on EPR parameters of spin-labels: 2, 2, 6, 6-tetramethyl-4-methoxypiperidine-1-oxyl in cucurbit [8] uril. *J. Chem. Theory Comput.* **2012**, *8*, 257-263.

[79] Peresypkina, E. V.; Fedin, V. P.; Maurel, V.; Grand, A.; Rey, P.; Vostrikova, K. E. Inclusion of a nitronyl nitroxyl radical and its hydrochloride in cucurbit [8] uril. *Eur. J. Chem.* **2010**, *16*, 12481-12487.

[80] Yi, S.; Captain, B.; Ottaviani, M. F.; Kaifer, A. E. Controlling the extent of spin exchange coupling in 2, 2, 6, 6-tetramethylpiperidine-1-oxyl (TEMPO) biradicals via molecular recognition with cucurbit [n] uril hosts. *Langmuir* **2011**, *27*, 5624-5632.

[81] Bardelang, D.; Banaszak, K.; Karoui, H.; Rockenbauer, A.; Waite, M.; Udachin, K.; Ripmeester, J. A.; Ratcliffe, C. I.; Ouari, O.; Tordo, P. Probing cucurbituril assemblies in water with TEMPO-like nitroxides: a trinitroxide supraradical with spin− spin interactions. *J. Am. Chem. Soc.* **2009**, *131*, 5402-5404.

[82] Mileo, E.; Mezzina, E.; Grepioni, F.; Pedulli, G. F.; Lucarini, M. Preparation and Characterisation of a New Inclusion Compound of Cucurbit [8] uril with a Nitroxide Radical. *Eur. J. Chem.* **2009,** *15*, 7859

[83] Kasera, S.; Biedermann, F.; Baumberg, J. J.; Scherman, O. A.; Mahajan, S. Quantitative SERS Using the Sequestration of Small Molecules Inside Precise Plasmonic Nanoconstructs. *Nano Lett.* **2012**, *12*, 5924−5928.

[84] Bush, M. E.; Bouley, N. D.; Urbach, A. R. Charge-mediated recognition of N-terminal tryptophan in aqueous solution by a synthetic host. *J. Am. Chem. Soc.* **2005**, *127*, 14511-14517.

[85] Taylor, R. W.; Coulston, R. J.; Biedermann, F.; Mahajan, S.; Baumberg, J. J.; Scherman, O. A. In situ SERS monitoring of photochemistry within a nanojunction reactor. *Nano Lett.* **2013**, *13*, 5985-5990.

[86] Biedermann, F.; Scherman, O. A. Cucurbit [8] uril mediated donor–acceptor ternary complexes: a model system for studying charge-transfer interactions. *J. Phys. Chem. B* **2012,** *116*, 2842-2849.

[87] Rauwald, U.; Biedermann, F.; Deroo, S.; Robinson, C. V.; Scherman, O. A. Correlating Solution Binding and ESI-MS Stabilities by Incorporating Solvation Effects in a Confined Cucurbit[8]uril System. *J. Phys. Chem. B* **2010**, *114*, 8606−8615.

[88] Shaikh, M.; Choudhury, S. D.; Mohanty, J.; Bhasikuttan, A. C.; Pal, H. Contrasting guest binding interaction of cucurbit [7-8] urils with neutral red dye: controlled exchange of multiple guests. *Phys. Chem. Chem. Phys.* **2010**, *12*, 7050-7055.

[89] Carvalho, C. P.; Dominguez, Z.; Da Silva, J. P.; Pischel, U. A Supramolecular Keypad Lock. *Chem. Comm.* **2015**, *51*, 2698−2701

[90] Biedermann, F.; Ross, I.; Scherman, O. A. Host–guest accelerated photodimerisation of anthracene-labeled macromolecules in water. *Polym. Chem.* **2014**, *5*, 5375-538.

[92] 1ang, R.; Yuan, L.; Ihmels, H.; Macartney, D. H. Cucurbit[8]uril/Cucurbit[7]uril Controlled Off/On Fluorescence of the Acridizinium and 9-Aminoacridizinium Cations in Aqueous Solution. *Chem. Eur. J.* **2007**, *13*, 6468−6473.

[92] Wu, X.; Meng, X.; Cheng, G. A novel 1:2 Cucurbit[8]uril Inclusion Complex with N-phenylpiperazine Hydrochloride. *J. Inclusion Phenom. Mol. Recognit. Chem.* **2009**, *64*, 325−329

[93] Wang, R.; Bardelang, D.; Waite, M.; Udachin, K. A.; Leek, D. M.; Yu, K.; Ratcliffe, C. I.; Ripmeester, J. A. Inclusion complexes of coumarin in cucurbiturils. *Org. Biomol. Chem.* **2009**, *7*, 2435-2439.

[94] Jeon, W. S.; Kim, H. J.; Lee, C.; Kim, K. Control of the Stoichiometry in Host-Guest Complexation by Redox Chemistry of Guests: Inclusion of Methylviologen in Cucurbit[8]uril. *Chem. Comm.* **2002**, 1828−1829.

[95] Ling, Y.; Mague, J. T.; Kaifer, A. E. Inclusion complexation of diquat and paraquat by the hosts cucurbit [7] uril and cucurbit [8] uril. *Eur. J. Chem.* **2007**, *13*, 7908-7914.

[96] Kim, H.-J.; Jeon, W. S.; Ko, Y. H.; Kim, K. Inclusion of methylviologen in cucurbit [7] uril. *Proc. Natl. Acad. Sci. U.S.A.* **2002**, *99*, 5007-5011.

[97] Jiang, G.; Li, G. Preparation and biological activity of novel cucurbit [8] uril–fullerene complex. *J. Photochem. Photobiol. B* **2006**, *85*, 223-227.

[98] Stojek, Z. The electrical double layer and its structure. *Electroanal. Methods*, **2010**, *Springer. p.* 3-9.

[99] Damaskin, B. B.; Petrii, O. A. Historical development of theories of the electrochemical double layer. *J. Solid State Electrochem.* **2011**, *15*, 1317-1334.

[100] Stock, J. T.; Orna, M. V. Electrochemistry, past and present. *ACS Publications.* **1989**, *Vol. 390.*

[101] Wahl, D. A Short History of Electrochemistry- Part I. *Galvanotechnik*. **2005**, *96*, 1600-1610.

[102] Scholz, F. *Electroanal. Methods*. **2010,** *Springer. Vol. 1.*

[103] Uslu, B.; Aboul-Enein, H. Y.; Ozkan, S. A. Modern analytical electrochemistry: fundamentals, experimental techniques, and applications. *Int. J. Electrochem.* **2011**. *Hindawi.*

[104] Elgrishi, N.; Rountree, K. J.; McCarthy, B. D.; Rountree, E. S.; Eisenhart, T. T.; Dempsey, J. L. A practical beginner's guide to cyclic voltammetry. *J. Chem. Educ.* **2018**, *95*, 197-206.

[105] Noel, M.; Vasu, K. Cyclic Voítammetry and the Frontiers of Electrochemistry. Aspect Pubi. Ltd., London. **1990**, *223*.

[106] Compton, R. G.; Banks, C. E. Understanding voltammetry. *World Sci. Res.* **2018**.

[107] Oldham, K.; Myland, J. Fundamentals of electrochemical science. *Elsevier*. **2012**.

[108] Osteryoung, J. G.; Osteryoung, R. A. Square wave voltammetry. *Anal. Chem.* **1985**, *57*, 101-110.

[109] O'Dea, J. J.; Osteryoung, J. G. Characterization of quasi-reversible surface processes by square-wave voltammetry. *Anal. Chem.* **1993**, *65*, 3090-3097.

[110] Krause, M. S.; Ramaley, L. Analytical application of square wave voltammetry. *Anal. Chem.* **1969**, *41*, 1365-1369.

[111] Ramaley, L.; Krause, M. S. Theory of square wave voltammetry. *Anal. Chem.* **1969**, *41*, 1362-1365.

[112] Ashwin, B. C. M. A.; Shanmugavelan, P.; Muthu Mareeswaran, P. Electrochemical aspects of cyclodextrin, calixarene and cucurbituril inclusion complexes. J. *Incl. Phenom. Macrocycl. Chem.* **2020**, *98*, 149-170.

[113] Mei, C. J.; Ahmad, S. A. A. A review on the determination heavy metals ions using calixarene-based electrochemical sensors. *Arab. J. Chem.* **2021**, *14*, 103303.

[114] Zhu, G.; Yi, Y.; Chen, J. Recent advances for cyclodextrin-based materials in electrochemical sensing. *TrAC Trends Anal. Chem.* **2016**, *80*, 232-241.

[115] Hein, R.; Beer, P. D.; Davis, J. J. Electrochemical anion sensing: supramolecular approaches. *Chem. Rev.* **2020,** *120*, 1888-1935.

[116] Nijhuis, C. A.; Ravoo, B. J.; Huskens, J.; Reinhoudt, D. N. Electrochemically controlled supramolecular systems. *Coord. Chem. Rev.* **2007,** *251*, 1761-1780.

[117] Boulas, P. L.; Gómez-Kaifer, M.; Echegoyen, L. Electrochemistry of supramolecular systems. *Angew. Chem. Int. Ed.* **1998**, *37*, 216-247.

[118] Bakker, E.; Telting-Diaz, M. Electrochemical sensors. *Anal. Chem.* **2002,** *74*, 2781-2800.

[119] Niu, X.; Mo, Z.; Yang, X.; Sun, M.; Zhao, P.; Li, Z.; Ouyang, M.; Liu, Z.; Gao, H.; Guo, R. Advances in the use of functional composites of β-cyclodextrin in electrochemical sensors. *Microchim. Acta* **2018,** *185*, 1-17.

[120] Agnihotri, N.; Chowdhury, A. D.; De, A. Non-enzymatic electrochemical detection of cholesterol using β-cyclodextrin functionalized graphene. *Biosens. Bioelectron.* **2015,** *63*, 212-217

[121] Fu, L.; Lai, G.; Yu, A. Preparation of β-cyclodextrin functionalized reduced graphene oxide: application for electrochemical determination of paracetamol. *RSC Adv.* **2015,** *5*, 76973-76978.

[122] Guo, Y.; Guo, S.; Ren, J.; Zhai, Y.; Dong, S.; Wang, E. Cyclodextrin functionalized graphene nanosheets with high supramolecular recognition capability: synthesis and host− guest inclusion for enhanced electrochemical performance. *ACS Nano* **2010,** *4*, 4001-4010.

[123] Ai, Q.; Jin, L.; Gong, Z.; Liang, F. Observing Host–Guest Interactions at Molecular Interfaces by Monitoring the Electrochemical Current. *ACS Omega* **2020,** *5*, 10581-10585.

[124] Luo, H.; Chen, L.-X.; Ge, Q.-M.; Liu, M.; Tao, Z.; Zhou, Y.-H.; Cong, H. Applications of macrocyclic compounds for electrochemical sensors to improve selectivity and sensitivity. *J. Incl. Phenom. Macrocycl. Chem.* **2019,** *95*, 171-198.

[125] del Pozo, M.; Mejías, J.; Hernández, P.; Quintana, C. Cucurbit [8] uril-based electrochemical sensors as detectors in flow injection analysis. Application to dopamine determination in serum samples. *Sens Actuators B Chem.* **2014,** *193*, 62-69.

[126] Wei, T.; Dong, T.; Xing, H.; Liu, Y.; Dai, Z. Cucurbituril and azide cofunctionalized graphene oxide for ultrasensitive electro-click biosensing. *Anal. Chem.* **2017,** *89*, 12237-12243.

[127] Tadini, M. C.; Balbino, M. A.; Eleoterio, I. C.; de Oliveira, L. S.; Dias, L. G.; Demets, G. J.-F.; de Oliveira, M. F. Developing electrodes chemically modified with cucurbit [6] uril to detect 3, 4-methylenedioxymethamphetamine (MDMA) by voltammetry. *Electrochim. Acta* **2014,** *121*, 188-193.

[128] Liu, Q.; Yue, X.; Li, Y.; Wu, F.; Meng, M.; Yin, Y.; Xi, R. A novel electrochemical aptasensor for exosomes determination and release based on specific host-guest interactions between cucurbit [7] uril and ferrocene. *Talanta* **2021,** *232*, 122451.

[129] Jeon, W. S.; Kim, E.; Ko, Y. H.; Hwang, I.; Lee, J. W.; Kim, S. Y.; Kim, H. J.; Kim, K. Molecular loop lock: a redox-driven molecular machine based on a host-stabilized charge-transfer complex. *Angew. Chem. Int. Ed.* **2005,** *117*, 89-93.

[130] Kaifer, A. E. Toward reversible control of cucurbit [n] uril complexes. *Acc. Chem. Res.* **2014,** *47*, 2160-2167.

[131] Jeon, W. S.; Ziganshina, A. Y.; Lee, J. W.; Ko, Y. H.; Kang, J. K.; Lee, C.; Kim, K. A [2] Pseudorotaxane-Based Molecular Machine: Reversible Formation of a Molecular Loop Driven by Electrochemical and Photochemical Stimuli. *Angew. Chem. Int. Ed.* **2003,** *42*, 4097-4100.

[132] Kim, K. Mechanically interlocked molecules incorporating cucurbituril and their supramolecular assemblies. *Chem. Soc. Rev.* **2002,** *31*, 96-107.

[133] Le Poul, N.; Colasson, B. Electrochemically and chemically induced redox processes in molecular machines. *ChemElectroChem.* **2015,** *2*, 475-496.

[134] Hirose, K. A practical guide for the determination of binding constants. *J. Incl. Phenom. Macrocycl. Chem.* **2001**, *39*, 193-2

[135] Hirose, K. Determination of binding constants. *Anal. Methods Supramol. Chem.* **2007**, *2*, 2-7.

[136] Rodrigues, C. H.; Hernández-González, J. E.; Pedrina, N. J.; Leite, V. B.; Bruni, A. T., In silico Evaluation of Cucurbit [6] uril as a Potential Detector for Cocaine and Its Adulterants Lidocaine, Caffeine, and Procaine. *J. Braz. Chem. Soc.* **2021,** *32*, 800-810.

[137] Chio, W.-I. K.; Xie, H.; Zhang, Y.; Lan, Y.; Lee, T.-C. SERS biosensors based on cucurbituril-mediated nanoaggregates for wastewater-based epidemiology. *TrAC Trends Anal. Chem.* **2022,** *146*, 116485.

[138] Liebau, M.; Hildebrand, A.; Neubert, R. H. Bioadhesion of supramolecular structures at supported planar bilayers as studied by the quartz crystal microbalance. *Eur. Biophys. J.* **2001,** *30*, 42-52.

[139] Wu, Y.; Ma, H.; Gu, D. A quartz crystal microbalance as a tool for biomolecular interaction studies. *RSC Adv.* **2015,** *5*, 64520-64525.

[140] EP Souto, D.; R Faria, A.; M de Andrade, H.; T Kubota, L. Using QCM and SPR for the kinetic evaluation of the binding between a new recombinant chimeric protein and specific antibodies of the visceral leishmaniasis. *Curr. Protein Pept. Sci.* **2015,** *16*, 782-790.

[141] Jecklin, M. C.; Schauer, S.; Dumelin, C. E.; Zenobi, R. Label-free determination of protein–ligand binding constants using mass spectrometry and validation using surface plasmon resonance and isothermal titration calorimetry. *J. Mol. Recognit.* **2009,** *22*, 319-329.

[142] Kempen, E. C.; Brodbelt, J. S. A method for the determination of binding constants by electrospray ionization mass spectrometry. *Anal. Chem.* **2000,** *72*, 5411-5416.

[143] Chen, Z.; Weber, S. G. Determination of binding constants by affinity capillary electrophoresis, electrospray ionization mass spectrometry and phase-distribution methods. *TrAC Trends Anal. Chem.* **2008,** *27*, 738-748.

[144] Dotsikas, Y.; Loukas, Y. L. Efficient determination and evaluation of model cyclodextrin complex binding constants by electrospray mass spectrometry. *J. Am. Soc. Mass Spectrom.* **2003,** *14*, 1123-1129

[145] Ho, C. S.; Lam, C.; Chan, M.; Cheung, R.; Law, L.; Lit, L.; Ng, K.; Suen, M.; Tai, H. Electrospray ionisation mass spectrometry: principles and clinical applications. *The Clinical Biochem. Rev.* **2003,** *24*, 3.

[146] Rosu, F.; De Pauw, E.; Gabelica, V. Electrospray mass spectrometry to study drug-nucleic acids interactions. *Biochimie* **2008,** *90*, 1074-1087.

[147] Rundlett, K. L.; Armstrong, D. W. Methods for the determination of binding constants by capillary electrophoresis. *Electrophoresis* **2001,** *22*, 1419-1427.

[148] Jiang, C.; Armstrong, D. W. Use of CE for the determination of binding constants. *Electrophoresis* **2010,** *31*, 17-27.

[149] Rudnev, A. V.; Aleksenko, S. S.; Semenova, O.; Hartinger, C. G.; Timerbaev, A. R.; Keppler, B. K. Determination of binding constants and stoichiometries for platinum anticancer drugs and serum transport proteins by capillary electrophoresis using the Hummel-Dreyer method. *J. Sep. Sci.* **2005,** *28*, 121-127.

[150] Leavitt, S.; Freire, E. Direct measurement of protein binding energetics by isothermal titration calorimetry. *Curr. Opin. Struct. Biol.* **2001,** *11*, 560-566.

[151] Freyer, M. W.; Lewis, E. A. Isothermal titration calorimetry: experimental design, data analysis, and probing macromolecule/ligand binding and kinetic interactions. *Methods Cell Biol.* **2008,** *84*, 79-113.

[152] Wilcox, D. E. Isothermal titration calorimetry of metal ions binding to proteins: An overview of recent studies. *Inorg. Chim. Acta.* **2008,** *361*, 857-867.

[153] Fenley, A. T.; Henriksen, N. M.; Muddana, H. S.; Gilson, M. K. Bridging calorimetry and simulation through precise calculations of cucurbituril–guest binding enthalpies. *J. Chem. Theory Comput.* **2014,** *10*, 4069-4078.

[154] Zhang, J.; Chen, L.; Zeng, B.; Kang, Q.; Dai, L. Study on the binding of chloroamphenicol with bovine serum albumin by fluorescence and UV–vis spectroscopy. *Spectrochim. Acta A Mol. Biomol. Spectrosc.* **2013,** *105*, 74-79.

[155] Naik, P. N.; Nandibewoor, S. T.; Chimatadar, S. A. Non-covalent binding analysis of sulfamethoxazole to human serum albumin: Fluorescence spectroscopy, UV–vis, FT-IR, voltammetric and molecular modeling. *J. Pharm. Anal.* **2015,** *5*, 143-152.

[156] Li, Y.; Griend, D. A. V.; Flood, A. H. Modelling triazolophane–halide binding equilibria using Sivvu analysis of UV–vis titration data recorded under medium binding conditions. *Supram. Chem.* **2009,** *21*, 111-117.

[157] Gamov, G.; Zavalishin, M.; Sharnin, V. Comment on the frequently used method of the metal complex-DNA binding constant determination from UV–Vis data. *Spectrochim. Acta A Mol. Biomol. Spectrosc.* **2019,** *206*, 160-164.

[158] Ma, D.; Zavalij, P. Y.; Isaacs, L. Acyclic cucurbit [n] uril congeners are high affinity hosts. *J. Org. Chem. Res.* **2010,** *75*, 4786-4795.

[159] Sinn, S.; Spuling, E.; Bräse, S.; Biedermann, F. Rational design and implementation of a cucurbit [8] uril-based indicator-displacement assay for application in blood serum. *Chem. Sci.* **2019,** *10*, 6584-6593.

[160] Lazar, A. I.; Biedermann, F.; Mustafina, K. R.; Assaf, K. I.; Hennig, A.; Nau, W. M. Nanomolar binding of steroids to cucurbit [n] urils: selectivity and applications. *J. Am. Chem. Soc.* **2016,** *138*, 13022-13029.

[161] Liu, Y.; Li, C.-J.; Guo, D.-S.; Pan, Z.-H.; Li, Z. A comparative study of complexation of β-cyclodextrin, calix [4] arenesulfonate and cucurbit [7] uril with dye guests: fluorescence behavior and binding ability. *Supram. Chem.* **2007,** *19*, 517-523.

[162] Hennig, A.; Bakirci, H.; Nau, W. M. Label-free continuous enzyme assays with macrocycle-fluorescent dye complexes. *Nat. Methods.* **2007,** *4*, 629-632.

[163] Praetorius, A.; Bailey, D. M.; Schwarzlose, T.; Nau, W. M. Design of a fluorescent dye for indicator displacement from cucurbiturils: A macrocycle-responsive fluorescent switch operating through ap K a shift. *Org. Lett.* **2008,** *10*, 4089-4092.

[164] Zhu, L.; Zhao, Z.; Zhang, X.; Zhang, H.; Liang, F.; Liu, S. A Highly Selective and Strong Anti-Interference Host-Guest Complex as Fluorescent Probe for Detection of Amantadine by Indicator Displacement Assay. *Molecules* **2018,** *23*, 947.

[165] Xu, W.; Feng, H.; Zhao, W.; Huang, C.; Redshaw, C.; Tao, Z.; Xiao, X. Amino acid recognition by a fluorescent chemosensor based on cucurbit [8] uril and acridine hydrochloride. *Anal. Chim. Acta* **2020,** *1135*, 142-149.

[166] Geng, W. C.; Ye, Z.; Zheng, Z.; Gao, J.; Li, J. J.; Shah, M. R.; Xiao, L.; Guo, D. S. Supramolecular Bioimaging through Signal Amplification by Combining Indicator Displacement Assay with Förster Resonance Energy Transfer. *Angew. Chem. Int. Ed.* **2021,** *60*, 19614-19619.

[167] Tan, Z.; Zhu, X.; Brown, G. Formation of inclusion complexes of cyclodextrins with bile salt anions as determined by NMR titration studies. *Langmuir* **1994,** *10*, 1034-1039.

[168] Xie, J.; Dong, H.; Yu, Y.; Cao, S. Inhibitory effect of synthetic aromatic heterocycle thiosemicarbazone derivatives on mushroom tyrosinase: Insights from fluorescence, 1H NMR titration and molecular docking studies. *Food Chem.* **2016,** *190*, 709-716.

[169] Lamm, J. H.; Niermeier, P.; Mix, A.; Chmiel, J.; Neumann, B.; Stammler, H. G.; Mitzel, N. W. Mechanism of Host–Guest Complex Formation and Identification of Intermediates through NMR Titration and Diffusion NMR Spectroscopy. *Angew. Chem. Int. Ed.* **2014,** *53*, 7938-7942.

[170] Akita, T.; Matsui, Y.; Yamamoto, T. A ^{1}H NMR titration study on the binding constants for D-and l-tryptophan inclusion complexes with 6-O-α-D-glucosyl-β-cyclodextrin. Formation of 1: 1 and 2: 1 (host: guest) complexes. *J. Mol. Struct.* **2014,** *1060*, 138-141.

[171] Fielding, L. NMR methods for the determination of protein–ligand dissociation constants. *Prog. Nucl. Magn. Reson* **2007,** *51*, 219-242.

[172] Labuta, J.; Ishihara, S.; Šikorský, T.; Futera, Z.; Shundo, A.; Hanyková, L.; Burda, J. V.; Ariga, K.; Hill, J. P. NMR spectroscopic detection of chirality and enantiopurity in referenced systems without formation of diastereomers. *Nat. Commun.* **2013,** *4*, 1-8.

[173] Brachvogel, R.-C.; Maid, H.; Von Delius, M. NMR Studies on Li+, Na+ and K+ Complexes of Orthoester Cryptand o-Me2-1.1. 1. *Int. J. Mol. Sci.* **2015,** *16*, 20641-20656.

[174] Johnson, J. A.; Olson, N. M.; Tooker, M. J.; Bur, S. K.; Pomerantz, W. C. Combined Protein-and Ligand-Observed NMR Workflow to Screen Fragment Cocktails against Multiple Proteins: A Case Study Using Bromodomains. *Molecules* **2020,** *25*, 3949.

[175] Sinn, S.; Biedermann, F. Chemical sensors based on cucurbit [n] uril macrocycles. *Isr. J. Chem.* **2018,** *58*, 357-412.

[176] Minami, T.; Esipenko, N. A.; Akdeniz, A.; Zhang, B.; Isaacs, L.; Anzenbacher Jr, P. Multianalyte sensing of addictive over-the-counter (OTC) drugs. *J. Am. Chem. Soc.* **2013,** *135*, 15238-15243.

[177] Bockus, A. T.; Smith, L. C.; Grice, A. G.; Ali, O. A.; Young, C. C.; Mobley, W.; Leek, A.; Roberts, J. L.; Vinciguerra, B.; Isaacs, L. Cucurbit [7] uril–Tetramethylrhodamine conjugate for direct sensing and cellular imaging. *J. Am. Chem. Soc.* **2016,** *138*, 16549-16552.

[178] Bailey, D. M.; Hennig, A.; Uzunova, V. D.; Nau, W. M. Supramolecular tandem enzyme assays for multiparameter sensor arrays and enantiomeric excess determination of amino acids. *Eur. J. Chem.* **2008,** *14*, 6069-6077.

[179] Zhong, C.; Hu, C.; Kumar, R.; Trouillet, V.; Biedermann, F.; Hirtz, M. Cucurbit [n] uril-immobilized sensor arrays for indicator-displacement assays of small bioactive metabolites. *ACS Appl. Nano Mater.* **2021,** *4*, 4676-4687.

[180] Ghale, G.; Nau, W. M. Dynamically analyte-responsive macrocyclic host–fluorophore systems. *Acc. Chem. Res.* **2014,** *47*, 2150-2159.

[181] Dsouza, R. N.; Hennig, A.; Nau, W. M. Supramolecular tandem enzyme assays. *Eur. J. Chem.* **2012,** *18*, 3444-3459.

[182] Karimvand, S. K.; Abdollahi, H. A new strategy for calibrating indicator displacement assay (IDA)-based sensor systems. *Anal. Chim. Acta* **2020,** *1127*, 174-181.

[183] Sedgwick, A. C.; Brewster, J. T.; Wu, T.; Feng, X.; Bull, S. D.; Qian, X.; Sessler, J. L.; James, T. D.; Anslyn, E. V.; Sun, X. Indicator displacement assays (IDAs): the past, present and future. *Chem. Soc. Rev.* **2021,** *50*, 9-38.

[184] Hennig, A.; Nau, W. M. Interaction of Cucurbit [7] uril With Protease Substrates: Application to Nanosecond Time-Resolved Fluorescence Assays. *Front. Chem.* **2020,** *8*, 806.

[185] Miskolczy, Z.; Megyesi, M.; Sinn, S.; Biedermann, F.; Biczók, L. Simultaneous analyte indicator binding assay (SBA) for the monitoring of reversible host–guest complexation kinetics. *Chem. Comm.* **2021,** *57*, 12663-12666.

[186] Florea, M.; Nau, W. M. Strong Binding of Hydrocarbons to Cucurbituril Probed by Fluorescent Dye Displacement: A Supramolecular Gas-Sensing Ensemble. *Angew. Chem. Int. Ed.* **2011,** *123*, 9510-9514.

[187] Ghale, G.; Ramalingam, V.; Urbach, A. R.; Nau, W. M. Determining protease substrate selectivity and inhibition by label-free supramolecular tandem enzyme assays. *J. Am. Chem. Soc.* **2011,** *133*, 7528-7535.

[188] Nau, W. M.; Ghale, G.; Hennig, A.; Bakirci, H. s.; Bailey, D. M. Substrate-selective supramolecular tandem assays: monitoring enzyme inhibition of arginase and diamine oxidase by fluorescent dye displacement from calixarene and cucurbituril macrocycles. *J. Am. Chem. Soc.* **2009,** *131*, 11558-11570.

[189] Biedermann, F.; Hathazi, D.; Nau, W. M. Associative chemosensing by fluorescent macrocycle–dye complexes–a versatile enzyme assay platform beyond indicator displacement. *Chem. Comm.* **2015,** *51*, 4977-4980.

[190] Biedermann, F.; Rauwald, U.; Cziferszky, M.; Williams, K. A.; Gann, L. D.; Guo, B. Y.; Urbach, A. R.; Bielawski, C. W.; Scherman, O. A. Benzobis (imidazolium)–cucurbit [8] uril complexes for binding and sensing aromatic compounds in aqueous solution. *Eur. J. Chem.* **2010,** *16*, 13716-13722.

[191] Biedermann, F.; Nau, W. M. Noncovalent chirality sensing ensembles for the detection and reaction monitoring of amino acids, peptides, proteins, and aromatic drugs. *Angew. Chem. Int. Ed.* **2014,** *53*, 5694-5699.

[192] Prabodh, A.; Sinn, S.; Grimm, L.; Miskolczy, Z.; Megyesi, M.; Biczók, L.; Bräse, S.; Biedermann, F. Teaching indicators to unravel the kinetic features of host–guest inclusion complexes. *Chem. Comm.* **2020,** *56*, 12327-12330.

[193] Ling, Y.; Wang, W.; Kaifer, A. E. A new cucurbit [8] uril-based fluorescent receptor for indole derivatives. *Chem. Comm.* **2007**, 610-612.

[194] Sindelar, V.; Cejas, M. A.; Raymo, F. M.; Chen, W.; Parker, S. E.; Kaifer, A. E. Supramolecular assembly of 2, 7-dimethyldiazapyrenium and cucurbit [8] uril: A new fluorescent host for detection of catechol and dopamine. *Eur. J. Chem.* **2005,** *11*, 7054-7059.

[195] Higashi, Y.; Uemori, I.; Fujii, Y. Simultaneous determination of amantadine and rimantadine by HPLC in rat plasma with pre-column derivatization and fluorescence detection for pharmacokinetic studies. *Biomed. Chromatogr.* **2005,** *19*, 655-662.

[196] Nishikawa, N.; Nagai, M.; Moritoyo, T.; Yabe, H.; Nomoto, M. Plasma amantadine concentrations in patients with Parkinson's disease. *Park. Relat. Disord.* **2009,** *15*, 351-353.

[197] Yun, Y.; Pan, M.; Wang, L.; Li, S.; Wang, Y.; Gu, Y.; Yang, J.; Wang, S. Fabrication and evaluation of a label-free piezoelectric immunosensor for sensitive and selective detection of amantadine in foods of animal origin. *Anal. Bioanal. Chem.* **2019,** *411*, 5745-5753.

[198] Hao, X.; Li, N.; Xu, Z.; Li, N. B.; Luo, H. Q. An Electrochemical Sensing Strategy for Amantadine Detection Based on Competitive Host-guest Interaction of Methylene Blue/β-cyclodextrin/Poly (N-acetylaniline) Modified Electrode. *Electroanalysis* **2016,** *28*, 1489-1494.

[199] Jalali, F.; Riahi, S. Surface-confined amantadine–β-cyclodextrin inclusion complex: voltammetric study and application. *J. Incl. Phenom.* **2015,** *81*, 153-160.

[200] Arndt, T.; Guessregen, B.; Hohl, A.; Reis, J. Determination of serum amantadine by liquid chromatography-tandem mass spectrometry. *Clin. Chim. Acta* **2005,** *359*, 125-131.

[201] Yu, W.; Zhang, T.; Ma, M.; Chen, C.; Liang, X.; Wen, K.; Wang, Z.; Shen, J. Highly sensitive visual detection of amantadine residues in poultry at the ppb level: A colorimetric immunoassay based on a Fenton reaction and gold nanoparticles aggregation. *Anal. Chim. Acta* **2018,** *1027*, 130-136.

[202] Salem, A. A.; Abdou, I. M.; Saleh, H. A. Application of quantitative nuclear magnetic resonance spectroscopy for the determination of amantadine and acyclovir in plasma and pharmaceutical samples. *J. AOAC Int.* **2012,** *95*, 1644-1651.

[203] Xie, S.; Wen, K.; Xie, J.; Zheng, Y.; Peng, T.; Wang, J.; Yao, K.; Ding, S.; Jiang, H. Magnetic-assisted biotinylated single-chain variable fragment antibody-based immunoassay for amantadine detection in chicken. *Anal. Bioanal. Chem.* **2018,** *410*, 6197-6205.

[204] Xu, L.; Peng, S.; Liu, L.; Song, S.; Kuang, H.; Xu, C. Development of sensitive and fast immunoassays for amantadine detection. *Food Agric Immunol* **2016,** *27*, 678-688.

[205] Ai, X.; Niu, L.; Li, Y.; Yang, F.; Su, X. A novel β-Cyclodextrin-QDs optical biosensor for the determination of amantadine and its application in cell imaging. *Talanta* **2012,** *99*, 409-414.

[206] Li, Y.; Gao, Y.; Li, Y.; Liu, S.; Zhang, H.; Su, X. A novel fluorescence probing strategy based on mono-[6-(2-aminoethylamino)-6-deoxy]-β-cyclodextin functionalized graphene oxide for the detection of amantadine. *Sens. Actuators B Chem.* **2014,** *202*, 323-329.

[207] Hu, C.; Grimm, L.; Prabodh, A.; Baksi, A.; Siennicka, A.; Levkin, P. A.; Kappes, M. M.; Biedermann, F. Covalent cucurbit [7] uril–dye conjugates for sensing in aqueous saline media and biofluids. *Chem. Sci* **2020,** *11*, 11142-11153.

[208] Del Pozo, M.; Fernández, Á.; Quintana, C. On-line competitive host-guest interactions in a turn-on fluorometric method to amantadine determination in human serum and pharmaceutical formulations. *Talanta* **2018,** *179*, 124-130.

[209] Dong, B.; Li, H.; Sun, J.; Mari, G. M.; Yu, X.; Ke, Y.; Li, J.; Wang, Z.; Yu, W.; Wen, K. Development of a fluorescence immunoassay for highly sensitive detection of amantadine using the nanoassembly of carbon dots and MnO2 nanosheets as the signal probe. *Sens. Actuators B Chem.* **2019,** *286*, 214-221.

[210] Dong, B.; Li, H.; Mari, G. M.; Yu, X.; Yu, W.; Wen, K.; Ke, Y.; Shen, J.; Wang, Z. Fluorescence immunoassay based on the inner-filter effect of carbon dots for highly sensitive amantadine detection in foodstuffs. *Food Chem.* **2019,** *294*, 347-354.

[211] Guo, L.; Liu, M.; Zhang, S.; Wang, Z.; Yu, X. Multi-wavelength fluorescence polarization immunoassays for simultaneous detection of amantadine and ribavirin in chicken and human serum. *Food Agric Immunol* **2021,** *32*, 321-335.

[212] Wu, S.; Zhu, F.; Hu, L.; Xia, J.; Xu, G.; Liu, D.; Guo, Q.; Luo, K.; Lai, W. Development of a competitive immunochromatographic assay for the sensitive detection of amantadine in chicken muscle. *Food Chem* **2017,** *232*, 770-776.

[213] Parsons, C.; Rammes, G.; Danysz, W. Pharmacodynamics of memantine: an update. *Curr. Neuropharmacol* **2008,** *6*, 55-78.

[214] Toker, S. E.; Sağırlı, O.; Çetin, S. M.; Önal, A. A new HPLC method with fluorescence detection for the determination of memantine in human plasma. *J. Sep. Sci.* **2011,** *34*, 2645-2649.

[215] Xie, M. F.; Zhou, W.; Tong, X. Y.; Chen, Y. L.; Cai, Y.; Li, Y.; Duan, G. L. High-performance liquid chromatographic determination of memantine hydrochloride in rat plasma using sensitive fluorometric derivatization. *J. Sep. Sci.* **2011,** *34*, 241-246.

[216] Michail, K.; Daabees, H.; Beltagy, Y.; Elkhalek, M. A.; Khamis, M. High-performance liquid chromatographic determination of memantine in human urine following solid-phase extraction and precolumn derivatization. *J. AOAC Int.* **2013,** *96*, 1302-1307.

[217] Nahata, M.; Brady, M. T. Serum concentrations and safety of rimantadine in paediatric patients. *Eur. J. Clin. Pharmacol.* **1986,** *30*, 719-722.

[218] Wintermeyer, S. M.; Nahata, M. C. Rimantadine: a clinical perspective. *Ann Pharmacother* **1995**, *29*, 299-310.

[219] Higashi, Y.; Uemori, I.; Fujii, Y. Simultaneous determination of amantadine and rimantadine by HPLC in rat plasma with pre-column derivatization and fluorescence detection for pharmacokinetic studies. *Biomed. Chromatogr.* **2005,** *19*, 655-662.

[220] Zhao, S.; Li, D.; Qiu, J.; Wang, M.; Yang, S.; Chen, D. Simultaneous determination of amantadine, rimantadine and chlorpheniramine in animal-derived food by liquid chromatography-tandem mass spectrometry after fast sample preparation. *Anal. Methods* **2014,** *6*, 7062-7067.

[221] Yan, H.; Liu, X.; Cui, F.; Yun, H.; Li, J.; Ding, S.; Yang, D.; Zhang, Z. Determination of amantadine and rimantadine in chicken muscle by QuEChERS pretreatment method and UHPLC coupled with LTQ Orbitrap mass spectrometry. *J. Chromatogr. B* **2013,** *938*, 8-13.

[222] Fukuda, E. K.; Rodriguez, L. C.; Choma, N.; Keigher, N.; De Grazia, F.; Garland, W. A. Quantitative determination of rimantadine in human plasma and urine by GC–MS. *Biomed. Environ. Mass Spectom* **1987,** *14*, 549-553.

[223] Deupree, J. Procaine. *xPharm: The Comprehensive Pharmacology Reference*. **2007**, 1-5.

[224] Wu, K.; Wang, H.; Chen, F.; Hu, S. Electrochemistry and voltammetry of procaine using a carbon nanotube film coated electrode. *Bioelectrochemistry* **2006,** *68*, 144-149.

[225] Ohshima, T.; Takayasu, T. Simultaneous determination of local anesthetics including ester-type anesthetics in human plasma and urine by gas chromatography–mass spectrometry with solid-phase extraction. *J. Chromatogr. B Biomed. Appl.* **1999,** *726*, 185-194.

[226] Guan, X.; Li, X.; Chai, S.; Zhang, X.; Zou, Q.; Zhang, J. A sensitive electrochemical sensor based on solution polymerized molecularly imprinted polymers for procaine detection. *Electroanalysis* **2016,** *28*, 2007-2015.

[227] Al-Saadi, A. A.; Haroon, M.; Popoola, S. A.; Saleh, T. A. Sensitive SERS detection and characterization of procaine in aqueous media by reduced gold nanoparticles. *Sens. Actuators B Chem.* **2020,** *304*, 127057.

[228] Paseková, H.; Polášek, M. Determination of procaine, benzocaine and tetracaine by sequential injection analysis with permanganate-induced chemiluminescence detection. *Talanta* **2000,** *52*, 67-75.

[229] Liu, L. D.; Liu, Y.; Wang, H. Y.; Sun, Y.; Ma, L.; Tang, B. Use of p-dimethylaminobenzalhyde as a colored reagent for determination of procaine hydrochloride by spectrophotometry. *Talanta* **2000,** *52*, 991-999.

[230] Silva, T. G.; de Araujo, W. R.; Munoz, R. A.; Richter, E. M.; Santana, M. H.; Coltro, W. K.; Paixao, T. R. Simple and sensitive paper-based device coupling electrochemical sample pretreatment and colorimetric detection. *Anal. Chem.* **2016,** *88*, 5145-5151.

[231] Stevenson, A.; Weber, M.; Todi, F.; Mendonca, M.; Fenwick, J.; Young, L.; Kwong, E.; Chen, F.; Beaumier, P.; Timmings, S. Determination of procaine in equine plasma and urine by high-performance liquid chromatography. *J. Anal. Toxicol.* **1992,** *16*, 93-96.

[232] Dolšak, A.; Gobec, S.; Sova, M. Indoleamine and tryptophan 2, 3-dioxygenases as important future therapeutic targets. *Pharmacol. Ther.* **2021,** *221*, 107746.

[233] Zhang, L.; Sun, M.; Jing, T.; Li, S.; Ma, H. A facile electrochemical sensor based on green synthesis of Cs/Ce-MOF for detection of tryptophan in human serum. *Colloids Surf. A Physicochem. Eng. Asp.* **2022,** *648*, 129225.

[234] Krämer, J.; Grimm, L. M.; Zhong, C.; Hirtz, M.; Biedermann, F. A supramolecular cucurbit [8] uril-based rotaxane chemosensor for the optical tryptophan detection in human serum and urine. *Nat. Commun* **2023,** *14*, 518.

[235] R.; Liu, B.; Qiu, M.-M.; Miao, W.-N.; Xu, L. A Europium MOF-based turn-off fluorescent sensor for tryptophan detection in human serum, urine and lake water. *J. Solid State Chem.* **2022,** *311*, 123138.

[236] Zhu, D.; Bai, Z.; Ma, H.; Tan, L.; Pang, H.; Wang, X. High performance simultaneous detection of β-nicotinamide adenine dinucleotide and l-tryptophan in human serum based on a novel nanocomposite of ferroferric oxide-functionalized polyoxometalates. *Sens. Actuators B: Chem.* **2020,** *309*, 127787.

[237] Herve, C.; Beyne, P.; Jamault, H.; Delacoux, E. Determination of tryptophan and its kynurenine pathway metabolites in human serum by high-performance liquid chromatography with simultaneous ultraviolet and fluorimetric detection. *J. Chromatogr. B Biomed. Appl* **1996,**

[238] Pautova, A.; Khesina, Z.; Getsina, M.; Sobolev, P.; Revelsky, A.; Beloborodova, N. Determination of tryptophan metabolites in serum and cerebrospinal fluid samples using microextraction by packed Sorbent, Silylation and GC–MS detection. *Molecules* **2020,** *25*, 3258.

[239] Fan, M.; Lu, D.; You, R.; Chen, C.; Lu, Y.; Wu, Y.; Shen, H.; Feng, S. Highly sensitive detection of tryptophan (Trp) in serum based on diazo-reaction coupling with Surface-Enhanced Raman Scattering and colorimetric assay. *Anal. Chim. Acta* **2020,** *1119*, 52-59.

[240] Ford, J. M.; Truman, C. A.; Wilcock, G. K.; Roberts, C. J. Serum concentrations of tacrine hydrochloride predict its adverse effects in Alzheimer's disease. *Clin. Pharmacol. Ther.* **1993,** *53*, 691-695.

[241] Park, T. H.; Tachiki, K. H.; Summers, W. K.; Kling, D.; Fitten, J.; Perryman, K.; Spidell, K.; Kling, A. S. Isolation and the fluorometric, high-performance liquid chromatographic determination of tacrine. *Anal. Biochem.* **1986,** *159*, 358-362.

[242] Aparico, I.; Jiménez, J. C. Spectrofluorimetric determination of tacrine in pharmaceuticals and spiked human serum. *Analyst* **1998,** *123*, 1575-1576.

[243] Huang, L.; Li, Z.; Guo, L. Colorimetric assay of acetylcholinesterase inhibitor tacrine based on MoO2 nanoparticles as peroxidase mimetics. *Spectrochim. Acta A Mol. Biomol. Spectrosc.* **2020,** *224*, 117412.

[244] Yan, B.; Liu, W.; Duan, G.; Ni, P.; Jiang, Y.; Zhang, C.; Wang, B.; Lu, Y.; Chen, C. Colorimetric detection of acetylcholinesterase and its inhibitor based on thiol-regulated

oxidase-like activity of 2D palladium square nanoplates on reduced graphene oxide. *Mikrochim. Acta* **2021,** *188*, 1-9.

[245] Chen, Y.; Zhang, X.; Luo, X. Enzyme colorimetric cellulose membrane bioactivity strips based on acetylcholinesterase immobilization for inhibitors preliminary screening. *Colloids Surf. B* **2023,** *223*, 113184.

[246] Dong-Dong, L.; Zhang, F.-F.; Ming, G.; Jun-Chen, Z.; Ye-Fei, W.; Yi-Zhong, L. Pt nanoparticle/N-doped graphene nanozymes for colorimetric detection of acetylcholinesterase activity and inhibition. *Chinese J. Anal. Chem.* **2022,** *50*, 100177.

[247] Liu, D.-M.; Xu, B.; Dong, C. Recent advances in colorimetric strategies for acetylcholinesterase assay and their applications. *TrAC, Trends Anal. Chem.* **2021,** *142*, 116320.

[248] Mock, W. L.; Irra, T. A.; Wepsiec, J. P.; Adhya, M. Catalysis by cucurbituril. The significance of bound-substrate destabilization for induced triazole formation. *J. Org. Chem. Res.* **1989,** *54*, 5302-5308.

[249] Klöck, C.; Dsouza, R. N.; Nau, W. M. Cucurbituril-mediated supramolecular acid catalysis. *Org. Lett.* **2009,** *11*, 2595-2598.

[250] Ren, S.; Zeng, J.; Zheng, Z.; Shi, H. Perspective and application of modified electrode material technology in electrochemical voltammetric sensors for analysis and detection of illicit drugs. *Sens. Actuators A: Phys.* **2021,** *329*, 112821.

[251] Grimme, S. Supramolecular binding thermodynamics by dispersion-corrected density functional theory. *Eur. J. Chem.* **2012,** *18*, 9955-9964.

[252] Stewart, J. J. Optimization of parameters for semiempirical methods V: Modification of NDDO approximations and application to 70 elements. *J. Mol. Model.* **2007,** *13*, 1173-1213.

[253] Kolafa, J. Time-reversible always stable predictor–corrector method for molecular dynamics of polarizable molecules. *J. Comput. Chem.* **2004,** *25*, 335-342.

[254] Schlitter, J.; Massarczyk, M. Estimating configurational entropy and energy of molecular systems from computed spectral density. *arXiv preprint arXiv:1909.04726* **2019**.

[255] O'brien, J.; Wilson, I.; Orton, T.; Pognan, F. Investigation of the Alamar Blue (resazurin) fluorescent dye for the assessment of mammalian cell cytotoxicity. *Eur. J. Biochem.* **2000,** *267*, 5421-5426.

[256] Rodríguez-Corrales, J. Á.; Josan, J. S., Resazurin live cell assay: Setup and fine-tuning for reliable cytotoxicity results. *In Proteomics Drug. Discov*. **2017**, *Springer. p. 207-219*.

[257] Emter, R.; Natsch, A. A fast Resazurin-based live viability assay is equivalent to the MTT-test in the KeratinoSens assay. *Toxicol. In Vitro* **2015,** *29*, 688-693.

[258] Präbst, K.; Engelhardt, H.; Ringgeler, S.; Hübner, H., Basic colorimetric proliferation assays: MTT, WST, and resazurin. *In Cell viability assays*. **2017**, *Springer. p. 1-17.*

[259] Chen, J. L.; Steele, T. W.; Stuckey, D. C. Modeling and application of a rapid fluorescence-based assay for biotoxicity in anaerobic digestion. *Environ. Sci. Technol.* **2015,** *49*, 13463-13471.

[260] Mishra, P.; Singh, D.; Mishra, K.; Kaur, G.; Dhull, N.; Tomar, M.; Gupta, V.; Kumar, B.; Ganju, L. Rapid antibiotic susceptibility testing by resazurin using thin film platinum as a bio-electrode. *J. Microbiol. Methods* **2019,** *162*, 69-76.

[261] Ibáñez, D.; Izquierdo-Bote, D.; Pérez-Junquera, A.; González-García, M. B.; Hernandez-Santos, D.; Fanjul-Bolado, P. Raman and fluorescence spectroelectrochemical monitoring of resazurin-resorufin fluorogenic system. *Dyes Pigm.* **2020,** *172*, 107848.

[262] Danchuk, A. I.; Komova, N. S.; Mobarez, S. N.; Doronin, S. Y.; Burmistrova, N. A.; Markin, A. V.; Duerkop, A. Optical sensors for determination of biogenic amines in food. *Anal. Bioanal. Chem.* **2020,** *412*, 4023-4036.

[263] Ong, W.; Gómez-Kaifer, M.; Kaifer, A. E. Cucurbit [7] uril: a very effective host for viologens and their cation radicals. *Org. Lett.* **2002,** *4*, 1791-1794.

[264] Gadde, S.; Batchelor, E. K.; Kaifer, A. E. Electrochemistry of redox active centres encapsulated by non-covalent methods. *Aust. J. Chem.* **2010,** *63*, 184-194.

[265] Paul, B. K. Classical vs. nonclassical hydrophobic interactions underlying various interaction processes: Application of isothermal titration calorimetry. *Chem. Phys. Impact* **2022**, 100104.

[266] Khazalpour, S.; Nematollahi, D. Electrochemical study of Alamar Blue (resazurin) in aqueous solutions and room-temperature ionic liquid 1-butyl-3-methylimidazolium tetrafluoroborate at a glassy carbon electrode. *RSC Adv.* **2014,** *4*, 8431-8438.

[267] Han, X.-L.; Mei, P.; Liu, Y.; Xiao, Q.; Jiang, F.-L.; Li, R., Binding interaction of quinclorac with bovine serum albumin: a biophysical study. *Spectrochim. Acta A* **2009**, *74*, 781-787.

[268] Präbst, K.; Engelhardt, H.; Ringgeler, S.; Hübner, H. Basic colorimetric proliferation assays: MTT, WST, and resazurin. *In Cell viability assays*. **2017**, *Springer. p. 1-17.*

[269] Liu, J.; Lambert, H.; Zhang, Y.-W.; Lee, T.-C. Rapid estimation of binding constants for cucurbit [8] uril ternary complexes using electrochemistry. *Anal. Chem.* **2021,** *93*, 4223-4230.

[270] Çakir, S.; Arslan, E. Y. Voltammetry of resazurin at a mercury electrode. *Chem. Pap.* **2010,** *64*, 386-394.

[271] Taylor, R. W.; Lee, T.-C.; Scherman, O. A.; Esteban, R.; Aizpurua, J.; Huang, F. M.; Baumberg, J. J.; Mahajan, S. Precise subnanometer plasmonic junctions for SERS within gold nanoparticle assemblies using cucurbit [n] uril "glue". *ACS Nano* **2011,** *5*, 3878-3887.

[272] Jiao, D.; Geng, J.; Loh, X. J.; Das, D.; Lee, T. C.; Scherman, O. A. Supramolecular peptide amphiphile vesicles through host–guest complexation. *Angew. Chem. Int. Ed.* **2012,** *51*, 9633-9637.

[273] Kim, C.; Agasti, S. S.; Zhu, Z.; Isaacs, L.; Rotello, V. M. Recognition-mediated activation of therapeutic gold nanoparticles inside living cells. *Nat. Chem.* **2010,** *2*, 962-966.

[274] Appel, E. A.; Biedermann, F.; Rauwald, U.; Jones, S. T.; Zayed, J. M.; Scherman, O. A. Supramolecular cross-linked networks via host− guest complexation with cucurbit [8] uril. *J. Am. Chem. Soc.* **2010,** *132*, 14251-14260.

[275] Walsh, Z.; Janeček, E.-R.; Hodgkinson, J. T.; Sedlmair, J.; Koutsioubas, A.; Spring, D. R.; Welch, M.; Hirschmugl, C. J.; Toprakcioglu, C.; Nitschke, J. R. Multifunctional supramolecular polymer networks as next-generation consolidants for archaeological wood conservation. *Proc. Natl. Acad. Sci. U.S.A.* **2014,** *111*, 17743-17748.

[276] Rowland, M. J.; Appel, E. A.; Coulston, R. J.; Scherman, O. A. Dynamically crosslinked materials via recognition of amino acids by cucurbit [8] uril. *J. Mater. Chem. B* **2013,** *1*, 2904-2910.

[277] Appel, E. A.; Loh, X. J.; Jones, S. T.; Biedermann, F.; Dreiss, C. A.; Scherman, O. A. Ultrahigh-water-content supramolecular hydrogels exhibiting multistimuli responsiveness. *J. Am. Chem. Soc.* **2012,** *134*, 11767-11773.

[278] Coulston, R. J.; Jones, S. T.; Lee, T.-C.; Appel, E. A.; Scherman, O. A. Supramolecular gold nanoparticle–polymer composites formed in water with cucurbit [8] uril. *Chem. Comm.* **2011,** *47*, 164-166.

[279] Appel, E. A.; Loh, X. J.; Jones, S. T.; Dreiss, C. A.; Scherman, O. A. Sustained release of proteins from high water content supramolecular polymer hydrogels. *Biomaterials* **2012,** *33*, 4646-4652.

[280] Maddipatla, M. V.; Kaanumalle, L. S.; Natarajan, A.; Pattabiraman, M.; Ramamurthy, V. Preorientation of olefins toward a single photodimer: Cucurbituril-mediated photodimerization of protonated azastilbenes in water. *Langmuir* **2007,** *23*, 7545-7554.

[281] Lee, T.-C.; Kalenius, E.; Lazar, A. I.; Assaf, K. I.; Kuhnert, N.; Grün, C. H.; Jänis, J.; Scherman, O. A.; Nau, W. M. Chemistry inside molecular containers in the gas phase. *Nat. Chem.* **2013,** *5*, 376-382.

[282] Zhang, W.; Gan, S.; Vezzoli, A.; Davidson, R. J.; Milan, D. C.; Luzyanin, K. V.; Higgins, S. J.; Nichols, R. J.; Beeby, A.; Low, P. J. Single-molecule conductance of viologen–cucurbit [8] uril host–guest complexes. *ACS Nano* **2016,** *10*, 5212-5220.

[283] Thordarson, P. Determining association constants from titration experiments in supramolecular chemistry. *Chem. Soc. Rev.* **2011,** *40*, 1305-1323.

[284] Kim, H. J.; Heo, J.; Jeon, W. S.; Lee, E.; Kim, J.; Sakamoto, S.; Yamaguchi, K.; Kim, K. Selective inclusion of a hetero-guest pair in a molecular host: formation of stable charge-transfer complexes in cucurbit [8] uril. *Angew. Chem.Int. Ed.* **2001,** *40*, 1526-1529.

[285] Wang, W.; Kaifer, A. E. Electrochemical switching and size selection in cucurbit [8] uril-mediated dendrimer self-assembly. *Angew. Chem. Int. Ed.* **2006,** *45*, 7042-7046.

[286] Bard, A. J.; Faulkner, L. R. Fundamentals and applications. *Electrochem. Methods* **2001,** *2*, 580-632.

[287] Lee, T. C.; Scherman, O. A. A facile synthesis of dynamic supramolecular aggregates of cucurbit [n] uril (n= 5–8) capped with gold nanoparticles in aqueous media. *Eur. J. Chem.* **2012,** *18*, 1628-1633.

[288] Suhail, M.; Ali, I. Gas chromatography: A tool for drug analysis in biological samples. *Chem Int.* **2020,** *6*, 277-294.

[289] Gumbi, B. P.; Moodley, B.; Birungi, G.; Ndungu, P. G. Detection and quantification of acidic drug residues in South African surface water using gas chromatography-mass spectrometry. *Chemosphere* **2017,** *168*, 1042-1050.

[290] Hewitt, E. F.; Lukulay, P.; Galushko, S. Implementation of a rapid and automated high performance liquid chromatography method development strategy for pharmaceutical drug candidates. *J. Chromatogr. A* **2006,** *1107*, 79-87.

[291] Shabir, G. A. Validation of high-performance liquid chromatography methods for pharmaceutical analysis: Understanding the differences and similarities between validation requirements of the US Food and Drug Administration, the US Pharmacopeia and the International Conference on Harmonization. *J. Chromatogr. A* **2003,** *987*, 57-66.

[292] Das, D.; Assaf, K. I.; Nau, W. M. Applications of cucurbiturils in medicinal chemistry and chemical biology. *Front. Chem.* **2019,** *7*, 619.

[293] Koner, A. L.; Ghosh, I.; Saleh, N. i.; Nau, W. M. Supramolecular encapsulation of benzimidazole-derived drugs by cucurbit [7] uril. *Can. J. Chem.* **2011,** *89*, 139-147.

[294] Zhou, J.; Yu, G.; Huang, F. Supramolecular chemotherapy based on host–guest molecular recognition: a novel strategy in the battle against cancer with a bright future. *Chem. Soc. Rev.* **2017,** *46*, 7021-7053.

[295] Ferreira, P.; Ventura, B.; Barbieri, A.; Da Silva, J. P.; Laia, C. A.; Parola, A. J.; Basílio, N. A Visible–Near-Infrared Light-Responsive Host–Guest Pair with Nanomolar Affinity in Water. *Eur. J. Chem.* **2019,** *25*, 3477-3482.

[296] Biedermann, F.; Ghale, G.; Hennig, A.; Nau, W. M. Fluorescent artificial receptor-based membrane assay (FARMA) for spatiotemporally resolved monitoring of biomembrane permeability. *Commun. Biol.* **2010**, *3*, 1-10.

[297] Nguyen, B. T.; Anslyn, E. V. Indicator–displacement assays. *Coord. Chem. Rev.* **2006,** *250*, 3118-3127.

[298] Rather, I. A.; Ali, R. Indicator displacement assays: from concept to recent developments. *Org. Biomol. Chem.* **2021,** *19*, 5926-5981.

[299] Sedgwick, A. C.; Brewster, J. T.; Wu, T.; Feng, X.; Bull, S. D.; Qian, X.; Sessler, J. L.; James, T. D.; Anslyn, E. V.; Sun, X. Indicator displacement assays (IDAs): the past, present and future. *Chem. Soc. Rev.* **2021,** *50*, 9-38.

[300] Johansson, M.; Hellström-Lindahl, E.; Nordberg, A. Steady-state pharmacokinetics of tacrine in long-term treatment of Alzheimer patients. *Dement Geriatr Cogn Disord* **1996,** *7*, 111-117.

[301] Kumar, N.M.; Picchetti, P.; Hu, C.; Grimm, L.M.; Biedermann, F. Chemiluminescent Cucurbit [n] uril-Based Chemosensor for the Detection of Drugs in Biofluids. *ACS Sens.* **2022**, *7,* 2312-2319.

[302] Hu, C.; Jochmann, T.; Chakraborty, P.; Neumaier, M.; Levkin, P. A.; Kappes, M. M.; Biedermann, F. Further Dimensions for Sensing in Biofluids: Distinguishing Bioorganic Analytes by the Salt-Induced Adaptation of a Cucurbit [7] uril-Based Chemosensor. *J. Am. Chem. Soc.* **2022**, *144*(29), 13084-13095.

[303] Haroon, M.; Abdulazeez, I.; Saleh, T. A.; Al-Saadi, A. A. Electrochemically modulated SERS detection of procaine using FTO electrodes modified with silver-decorated carbon nanosphere. *Electrochim. Acta* **2021,** *387*, 138463.

[304] Abdel-Ghani, N. T.; Shoukry, A. F.; Hussein, S. H. Flow injection potentiometric determination of amantadine HCl. *J. Pharm. Biomed. Anal.* **2002,** *30*, 601-611.

[305] Elzanfaly, E. S.; Saad, A. S. Green in-line ion selective electrode potentiometric method for determination of amantadine in dissolution media and in pharmaceutical formulations. *ACS Sustain. Chem. Eng.* **2017,** *5*, 4381-4387.

[306] Yun, Y.; Pan, M.; Fang, G.; Yang, Y.; Guo, T.; Deng, J.; Liu, B.; Wang, S. Molecularly imprinted electrodeposition o-aminothiophenol sensor for selective and sensitive determination of amantadine in animal-derived foods. *Sens. Actuators B Chem.* **2017,** *238*, 32-39.

[307] Yan, X. Q.; Wang, H.; Di Chen, W.; Jin, W. J. The halogen bond between amantadine and iodine and its application in the determination of amantadine hydrochloride in pharmaceuticals. *Anal Sci* **2014,** *30*, 365-370.

[308] Wang, Z.; Wen, K.; Zhang, X.; Li, X.; Wang, Z.; Shen, J.; Ding, S. New hapten synthesis, antibody production, and indirect competitive enzyme-linked immnunosorbent assay for amantadine in chicken muscle. *Food Anal. Methods* **2018,** *11*, 302-308.

[309] Yang, J.; Pan, M.; Liu, K.; Xie, X.; Wang, S.; Hong, L.; Wang, S. Core-shell AuNRs@ Ag-enhanced and magnetic separation-assisted SERS immunosensing platform for amantadine detection in animal-derived foods. *Sens. Actuators B Chem.* **2021,** *349*, 130783.

[310] Ma, M.; Sun, J.; Chen, Y.; Wen, K.; Wang, Z.; Shen, J.; Zhang, S.; Ke, Y.; Wang, Z. Highly sensitive SERS immunosensor for the detection of amantadine in chicken based on flower-like gold nanoparticles and magnetic bead separation. *Food Chem. Toxicol.* **2018,** *118*, 589-594.

[311] Krämer, J.; Grimm, L. M.; Zhong, C.; Hirtz, M.; Biedermann, F. A supramolecular cucurbit [8] uril-based rotaxane chemosensor for the optical tryptophan detection in human serum and urine. *Nat. Commun.* **2023**, *14*(1), 518.